

INFORMATION TO USERS

This manuscript has been reproduced from the microfilm master. UMI films the text directly from the original or copy submitted. Thus, some thesis and dissertation copies are in typewriter face, while others may be from any type of computer printer.

The quality of this reproduction is dependent upon the quality of the copy submitted. Broken or indistinct print, colored or poor quality illustrations and photographs, print bleedthrough, substandard margins, and improper alignment can adversely affect reproduction.

In the unlikely event that the author did not send UMI a complete manuscript and there are missing pages, these will be noted. Also, if unauthorized copyright material had to be removed, a note will indicate the deletion.

Oversize materials (e.g., maps, drawings, charts) are reproduced by sectioning the original, beginning at the upper left-hand corner and continuing from left to right in equal sections with small overlaps.

ProQuest Information and Learning
300 North Zeeb Road, Ann Arbor, MI 48106-1346 USA
800-521-0600

UMI[®]

Control of ITH Percussive Longhole Drilling in Hard Rock

Muhammad Amjad

B.Sc.Eng. UET, M.Eng. McGill



Department of Mining and Metallurgical Engineering, McGill University,
Montreal, Quebec, Canada

A thesis submitted to the Faculty of Graduate Studies and Research in partial
fulfilment of the requirements for the degree of Doctor of Philosophy

©Muhammad Amjad, 1996



**National Library
of Canada**

**Acquisitions and
Bibliographic Services**

**385 Wellington Street
Ottawa ON K1A 0N4
Canada**

**Bibliothèque nationale
du Canada**

**Acquisitions et
services bibliographiques**

**385, rue Wellington
Ottawa ON K1A 0N4
Canada**

Your file Votre référence

Our file Notre référence

The author has granted a non-exclusive licence allowing the National Library of Canada to reproduce, loan, distribute or sell copies of this thesis in microform, paper or electronic formats.

The author retains ownership of the copyright in this thesis. Neither the thesis nor substantial extracts from it may be printed or otherwise reproduced without the author's permission.

L'auteur a accordé une licence non exclusive permettant à la Bibliothèque nationale du Canada de reproduire, prêter, distribuer ou vendre des copies de cette thèse sous la forme de microfiche/film, de reproduction sur papier ou sur format électronique.

L'auteur conserve la propriété du droit d'auteur qui protège cette thèse. Ni la thèse ni des extraits substantiels de celle-ci ne doivent être imprimés ou autrement reproduits sans son autorisation.

0-612-70176-X

Canada

To my little daughter
SHANZAY

Abstract

This thesis aims to develop a comprehensive strategy for automatic control of the ITH percussive drilling process. Such automation would provide the benefits of improved productivity and quality in terms of penetration rate and hole deviation, as well as enhanced hole quality and machine life.

Analysis of field data acquired from drilling experiments performed at INCO's Little Stobie Mine is presented. As a result of this analysis, a control algorithm is formulated to enhance the drilling process efficiency. This algorithm calculates the specific energy (SE) of the rock and adjusts the applied feed force based on this SE value, using a relationship obtained from the field data analysis.

A model of the percussive drilling process is developed and simulated in software. The proposed control algorithm is tested through simulations on this simulated drilling process. The results of the simulation show a significant increase in efficiency of the drilling process.

As a result of vibration data analysis it is concluded that vibration should be controlled through an improved design of the shock-absorber, rather than through drilling variables. A detailed shock-absorber test data analysis is therefore presented. Recommendations for design changes in the shock-absorber are also given.

Deviation analysis is also presented in the thesis, which shows a poor correlation between the machine variables and the hole deviation data. Hence, it is recommended that deviation be controlled by steering. An innovative guided drilling mechanism for controlling the hole deviation is also proposed. This mechanism consists of an eccentric ITH percussive hammer with controlled rotational speed, which can be employed as an actuator to steer the drill string in a desired direction without using any down hole instrumentation. Modelling and simulation analysis of this system is also presented.

Résumé

Cette thèse a comme objectif le développement d'une stratégie de commande automatique du procédé de forage à percussion ITH. L'automatisation de ce procédé peut améliorer la productivité et la qualité en ce qui a trait au taux de pénétration et à l'écart du trou tout en améliorant la qualité du trou et en augmentant la longévité de la machine.

Des expériences de forage à la mine Little Stobie de la compagnie INCO ont produit des données dont l'analyse permet la formulation d'un algorithme de commande visant à augmenter l'efficacité du procédé de forage. L'algorithme calcule l'énergie spécifique (SE) du minerais et ajuste la force d'application en fonction de cette énergie spécifique.

Nous avons développé et simulé un modèle du procédé de forage sur lequel nous avons testé la stratégie de commande proposée par des simulations. Les simulations ont démontré une nette augmentation de l'efficacité du procédé de forage.

L'analyse des données de vibration nous mène à conclure que les vibrations devraient être contrôllées par un meilleur design de l'amortisseur plutôt que par l'ajustment des variables de forage. Une analyse détaillée de donnée d'essai de l'amortisseur est présentée. De cette analyse nous formulons des recommandations.

La thèse présente aussi une analyse des données d'écart. Cette analyse montre qu'il existe une faible corrélation entre les variables de la machine et les données d'écart. Nous recommandons donc de contrôler l'écart par le mécanisme de direction. De plus, nous proposons un nouveau mécanisme de forage guidé pour contrôler l'écart. Ce mécanisme comprend un marteau à percussion ITH excentrique avec vitesse de rotation contrôllée qui utilise un actuateur pour diriger la foreuse dans une direction désirée sans avoir à insérer d'instrument dans le trou. La modélisation et la simulation de ce système est présentée.

Acknowledgements

I am indebted to my thesis supervisor, Prof. Laeeque Khan Daneshmend, for his guidance and personal involvement during the course of this research. His enthusiasm, friendship, and encouragement during the periods of despair have greatly contributed to my understanding of the research process and helped me persevere over the past years.

I initially started work on this thesis topic under the auspices of CCARM (the Canadian Centre for Automation and Robotics in Mining). I would like to thank Dr. Jonathan Peck, former Manager of CCARM, and Dr. Deyi Jiao, former Researcher at CCARM, for their help in introducing me to ITH drilling and the practicalities of such experimentation.

Financial support for the first half of my thesis research was provided by INCO Mines Research, Copper Cliff, Ontario. I am very grateful to INCO for this initial funding, as well as to the personnel at Mines Research for the exposure to underground mining provided during many weeks spent underground at Little Stobie.

Funding for the latter part of my thesis research was provided under an IRIS Centre of Excellence grant (IRIS Project ISDE-1). This funding enabled me to explore new avenues in my thesis research, specifically the CRE-hammer mechanism.

The computer simulations found herein would not have been possible without the support of the McGill Centre for Intelligent Machines (CIM). The facilities and consultation they have provided are gratefully acknowledged.

The students, staff, and professors in Mining Engineering at McGill provided an environment where I could learn about many disciplines and research areas in a positive atmosphere. In particular, I am happy to acknowledge my friend Ayman Bedair for his support and discussions on technical matters. Special thanks go Moe

Momayez, Jian Ming and Arshad Khan. Thanks to Sylvain Gendron for French translation of the abstract of this thesis.

I wish to extend my gratitude to my parents for the greatest gift I have received so far - my education, and to my brother Muhammad Saleem for his support.

Finally, I would like to thank my wife for her moral support and encouragement throughout this research process and for her understanding of the nature of my work.

Contents

1	Introduction	1
1.1	Research Objectives	1
1.2	Percussive Drilling	2
1.3	In-the-hole (ITH) percussive drill	3
1.4	Problems Associated with ITH Percussive Drilling	6
1.4.1	Poor Machine Operation	6
1.4.2	Hole Deviation	7
1.5	Generic Control Methodology	9
1.6	Modelling	10
1.7	Scope of the Thesis	11
1.8	Overview of the Thesis	12
2	Literature Survey	14
2.1	Introduction	14
2.2	Percussive Drilling: Motivatives and Constraints	15
2.3	Parameter Interaction Studies	17

2.4	Guided Drilling	19
2.4.1	Sensing	20
2.4.2	Steering	21
2.5	Drilling Process Modeling	23
2.6	Drilling Control	25
2.7	Drill Deviation	26
2.8	Summary of Key Results and Concepts	30
2.9	Conclusion	32
3	Machine Monitoring	34
3.1	Introduction	34
3.2	Experimental Setup	35
3.2.1	Percussive Drill CD90B	35
3.2.2	TEAC RD-200 Data Recorder	36
3.2.3	Signal Conditioning Hardware	36
3.2.4	Pre-filtering Hardware	37
3.3	Field Experiments	37
3.3.1	Variables Analysed in the Research	41
3.4	Geological Context of Little Stobie	43
3.5	Preliminary Observations	43
3.5.1	Effect of Feed on Drilling Performance	44
3.5.2	Effect of Torque on Performance	46

Table of Contents

iii

3.5.3	Effect of Feed on Vibration	47
3.6	Conclusion	51
4	Drilling Performance Modelling	52
4.1	Introduction	52
4.2	Parameter Correlations Study	53
4.2.1	Correlation between feed and penetration rate	53
4.2.2	Correlation Between Feed Force and Torque	54
4.2.3	Feed and Vibration	54
4.3	Specific Energy of the Rock	58
4.3.1	Comparison of Specific Energy with Uniaxial Compressive Strength of the Rock	61
4.4	Investigation of Effect of SE on Machine Performance	64
4.5	Conclusion	71
5	Development of Drilling Process Simulation Model	72
5.1	Introduction	72
5.2	Drilling Process Model	73
5.3	Machine Model	73
5.3.1	Feed System	74
5.3.2	Percussive Hammer	81
5.3.3	Rotary Motor Applied Torque	83
5.4	Bit-Rock Interaction	85

Table of Contents

iv

5.4.1	Prediction of Penetration Rate	85
5.4.2	Load Torque	86
5.5	Conclusion	90
6	Drilling Rate Control	91
6.1	Introduction	91
6.2	Process Controller: Pre-Design Considerations	92
6.2.1	Control Objective	92
6.2.2	Choice of Variables	92
6.2.3	Selection of Controller Type	93
6.3	Simulation Model of Controlled System	94
6.3.1	Process Model	94
6.3.2	Disturbance Model	96
6.3.3	The Controller Blocks	96
6.3.4	Brief Description of the Simulator Operation	97
6.4	The Control Algorithm	97
6.4.1	Estimation of Specific Energy	99
6.4.2	Estimation of Optimal Feed Value	99
6.4.3	Torque Monitoring	100
6.5	Simulation Results	103
6.6	Conclusions	113

7 Shock-absorber Tests and Analysis	114
7.1 Introduction	114
7.2 Shock Absorber Field Test	115
7.2.1 Digitization	116
7.3 Vibration Analysis	116
7.3.1 Without Shock Absorber	116
7.3.2 With Shock Absorber	117
7.3.3 Statistical Comparison	121
7.4 Determination of Natural Frequency and Damping	123
7.4.1 System Identification	123
7.4.2 Natural Frequency by Graphical Method	126
7.5 Static Test	127
7.5.1 Implication of Static Test Results for Shock Absorber	130
7.6 Conclusions and Recommendations	131
8 Investigation of Machine Dependent Hole Deviation	132
8.1 Introduction	132
8.1.1 Deviation in the Blast Hole	133
8.2 Hole Trajectory and Deviation Analysis	134
8.3 Study of Correlation between Deviation and Machine Parameters	140
8.3.1 Applied Feed Force and Drill Deviation	141
8.3.2 Study of Torque at Bit Direction Change	143

8.3.3	Observation of Vibration at Bit Direction Change	143
8.4	Quantitative Correlation between Deviation and Machine Variables .	146
8.5	Conclusions	149
9	Design Concept for an ITH Guided Drill	150
9.1	Introduction	150
9.2	Guided Drilling System	151
9.3	Bit Location Measurement	152
9.3.1	Bit Location Measurement by Down-Hole Sensor	153
9.3.2	Bit Location Measurement with Top-Hole Sensor	154
9.4	Steering Concept	155
9.5	The Closed-loop Guided System	159
9.6	Conclusion	160
10	Modelling and Simulation of Proposed Hammer Mechanism	161
10.1	Introduction	161
10.2	Trajectory of Hole drilled with Conventional ITH Percussive Hammer	162
10.3	Trajectory of Hole drilled with CRE-Hammer with no rotation	163
10.4	Addition of Rotation	167
10.5	Steering the CRE-Hammer through Speed Control	173
10.6	Compensation for Torsional Twist in the Drill String	177
10.6.1	Analytical Compensation	179

10.6.2 Compensation by Closed-loop System	180
10.7 Conclusions	182
11 Conclusions	183
11.1 Original Contributions	183
11.2 Practical Relevance and Implications	186
11.2.1 Usage	186
11.2.2 Limitations	187
11.3 Future Work	188
Bibliography	189
A Modelling of Electro-Hydraulic Servo Valve	200
B SIMULINK Programs for drilling process simulator	208
B.1 Introduction	208
C Test Hole Trajectories and Deviation	217
D Table of Conversion	227

List of Figures

1.1	ITH percussive drill CD90B	4
1.2	ITH percussive hammer	5
1.3	Poor fragmentation caused by the deviated hole blasting	8
1.4	Blockage cause by improper fragmentation	9
3.1	Experimental setup for drilling process monitoring	35
3.2	Laboratory setup for digitizing the data	36
3.3	Site location map	38
3.4	Plan and cross-sectional view of underground holes	40
3.5	Observatory result of feed vs penetration rate	45
3.6	Feed and Penetration rate (from hole 4)	46
3.7	Jamming due to excessive torque	48
3.8	Effect of feed on head vibration part 1	49
3.9	Effect of feed on head vibration part 2	50
3.10	Effect of feed on head vibration part 3	50
4.1	Correlation between feed and penetration rate	53

4.2	Correlation between feed and torque	55
4.3	Effect of hole length on the motor speed	55
4.4	Correlation between feed and vibration	56
4.5	Specific Energy for hole 1	60
4.6	Comparison of SE and UCS	62
4.7	Feed vs penetration rate group 1 to 4	66
4.8	Feed vs penetration rate group 5 to 8	67
4.9	Feed vs penetration rate group 9 and 10	68
4.10	Feed vs penetration rate fitted curves	69
4.11	Maximum penetration rate line	69
4.12	Optimal feed curve	70
5.1	Drilling process model	74
5.2	Schematic of feed system	75
5.3	Electro-Hydraulic servo valve dynamics	77
5.4	Set-point tracking of feed system	80
5.5	Comparison of predicted and original torque	89
6.1	Passive controller	95
6.2	Disturbance Model	96
6.3	Feed vs penetration rate curves	98
6.4	Controller signal flow diagram	101
6.5	Control system flow chart	102

6.6	Comparison of penetration rate field and simulated data	103
6.7	Simulator results without controller	105
6.8	Simulation results with controller	107
6.9	Penetration rate	108
6.10	Results of simulation without controller at different feed values	109
6.11	Controller reaction to torque perturbation	111
6.12	Simulation of Hole 4	112
7.1	Vibration without shock absorber	118
7.2	Frequency spectrum of vibration signal without shock absorber	118
7.3	Vibration with shock absorber	119
7.4	Frequency spectrum of vibration signal with shock absorber	119
7.5	Cumulative signal power without shock absorber	120
7.6	Cumulative signal power with shock absorber	120
7.7	ARX model output	124
7.8	ARX model input	124
7.9	One cycle of vibration on head signal	126
7.10	Static Test: feed vs displacement	128
7.11	Working range straight line fit for feed vs displacement	129
7.12	Full range curve fit for feed vs displacement of shock absorber	129
8.1	Sources of hole deviation	134
8.2	Trajectory of hole 1	136

8.3	Deviation of hole 1	136
8.4	Trajectory of hole 5	138
8.5	Deviation in hole 5	138
8.6	Deviation and drilling data for hole 5	142
8.7	Dip angle and feed force from hole 1	144
8.8	Dip angle and feed force from hole 3	144
8.9	Dip angle and Torque at bit from hole 2	145
8.10	Dip angle and bit Torque from hole 7	145
8.11	Dip angle and head vibration from hole 1	147
8.12	Dip angle and head vibration from hole 4	147
9.1	Close loop guided system	152
9.2	Bit position representation	153
9.3	Proposed layout of Bit location measurement technique by triaxial detector, and signal processing diagram	156
9.4	Possible bit configurations for CRE-Hammer	157
9.5	Hole trajectory by and CRE-hammer	158
9.6	Closed-loop guided system with CRE-Hammer and Triaxial detector .	159
10.1	Penetration cause by a single blow	164
10.2	Simulation of CRE-Hammer without rotation when $\theta_d = 0.96^\circ$	168
10.3	Simulation of CRE-Hammer without rotation at $\theta = .47^\circ$	168
10.4	Rotating vector representing the CRE-Hammer with rotation	169

10.5	Trajectory of hole drilled with CRE-Hammer when it is rotated at constant speed for vertical drilling	171
10.6	Simulation of CRE-Hammer drilling with constant rotation inclined drilling	172
10.7	Result of simulation when CRE-Hammer with speed control for $\theta_d = 0.47^\circ$	176
10.8	Result of simulation when CRE-Hammer with speed control for $\theta_d = 0.96^\circ$	176
10.9	Result of simulation of CRE-Hammer with two rotation speeds	178
10.10	Result of simulation of CRE-Hammer with two rotation speeds	178
A.1	Schematic of electro hydraulic control valve	201
A.2	Block diagram of electro hydraulic differential pressure control valve	206
B.1	Simulink block diagram of drilling process simulator	209
B.2	Drilling process controller	210
B.3	Electro-Hydraulic Control Valve	211
B.4	Bit-rock interaction	212
B.5	Torque Predictor	213
B.6	Randomly varying rock property generator	214
B.7	SE estimator	215
B.8	Percussive Hammer Model	216
C.1	Trajectory of hole 1	219

C.2 Deviation for hole 1 219

C.3 Trajectory of hole 2 220

C.4 Deviation for hole 2 220

C.5 Trajectory of hole 3 221

C.6 Deviation for hole 3 221

C.7 Trajectory of hole 4 222

C.8 Deviation for hole 4 222

C.9 Trajectory of hole 5 223

C.10 Deviation for hole 5 223

C.11 Trajectory of hole 7 224

C.12 Deviation for hole 7 224

C.13 Trajectory of hole 8 225

C.14 Deviation for hole 8 225

C.15 Trajectory of hole 9 226

C.16 Deviation for hole 9 226

List of Tables

3.1	An overview of test holes drilled at Little Stobie	42
4.1	An overview of drilling performance analysis.	57
4.2	Comparison of SE and UCS	63
4.3	Groups of Specific Energy	65
5.1	Estimated parameters for torque model	88
7.1	Statistics of Vibration without shock absorber	122
7.2	Statistics of Vibration with shock absorber	122
8.1	Table to compare deviations due to misalignment and machine/rock .	139
8.2	Table to show correlation coefficient between individual parameters .	148
A.1	Parameter value for the electro-hydraulic control valve use in the simulation	207

Chapter 1

Introduction

1.1 Research Objectives

This thesis investigates the possibility of controlling and automating one of the most important production processes in mining, i.e. percussive rock drilling, and in particular ITH drilling.

ITH percussive drilling is typically used in hard-rock. We have focused our research objectives towards this type of drill due to involvement in contractual work by McGill University for Inco Mines Research into ITH drill analysis. The objectives of this thesis are to:

- **Increase Productivity**

A substantial part of mine production cost is incurred in drilling of blast holes. More footage drilled per hour will save both time and labour. One objective of this study is therefore to develop an automatic control system to enhance the drilling rate hence increasing the productivity of the drilling process.

- **Minimize Wear and Tear on Machine**

It is also intended to minimize the machine wear and tear, hence reducing maintenance cost and increasing machine availability. This would indirectly lead to improved hole quality such as smoothness of the hole.

- **Control Hole Deviation**

Deviation of drilled holes from their intended path adversely affects the fragmentation process during blasting. Control of hole deviation would help in improving fragmentation, leading to save time and secondary blasting.

1.2 Percussive Drilling

The percussive fragmentation of rock is very old as an art and well established as a technology. Yet fundamental understanding of many phenomena involved is quite young. Thus, for many centuries it has been possible to break rock by means of simple percussive tools and for more than one century pneumatic percussive rock drills have been used. In contrast to this, fundamental knowledge about the basic mechanics of percussive rock destruction was not significantly improved until recently [42].

If the various types of percussive rock fragmentation are studied, it is found that they are often based upon one of the three basic methods briefly described below.

In the first method a hammer with a bit attached to its front impacts the rock, which is thereby crushed and chipped. In the second method a hammer impacts a bit, which before impact rests against the rock. In the third method a hammer impacts a rod, which is long in comparison to the hammer. During impact a stress wave is generated in the rod. This stress wave propagates towards the bit at the end of the rod, where it is partly reflected; under the combined action of the incident and reflected stress wave the bit is forced into the rock, which is thereby crushed

and chipped [42].

All three methods may be looked upon as methods of force transformation: the low level long duration force accelerating the hammer is transformed by impact into a higher level short duration force which facilitates destruction of rock [21].

Three main fields of application of these basic methods of percussive rock destruction are churn drilling, down-the-hole percussive drilling (otherwise known as in-the-hole percussive drilling) and top hammer drilling respectively. Therefore, the methods are referred to as the “churn drilling method”, the “in-the-hole drilling method (ITH)” and the “top hammer drilling method” respectively. The three methods are also frequently applied in different types of drop-hammers in rock drilling and rock mechanics research.

1.3 In-the-hole (ITH) percussive drill

The most important of the applications mentioned is in-the-hole drilling, which is extensively utilised in drilling of blast holes in medium hard and hard rock. Therefore, a brief description of in-the-hole drilling is given below. A schematic of such a percussive drill rig (CD90B by CMS Ltd.) is also shown in Figure 1.1.

An in-the-hole drilling system consists of a cylinder with a reciprocating hammer, a drill bit that rests in front of the hammer and the drill rods which are coupled at the rear of the hammer. These rods serve as a link between the hammer and the rest of the machine. Figure 1.2 is a schematic representation of this drilling system. The source of energy is usually compressed air, but other fluids are also used. Through impact, the kinetic energy of the accelerated hammer is transformed into stress wave energy in the drill bit, which is rotated at a certain angle between each blow. When deep holes are drilled there may be several rods joined together with the hammer. Compressed air, in such a case, is fed through the central hole in the drill rods. The

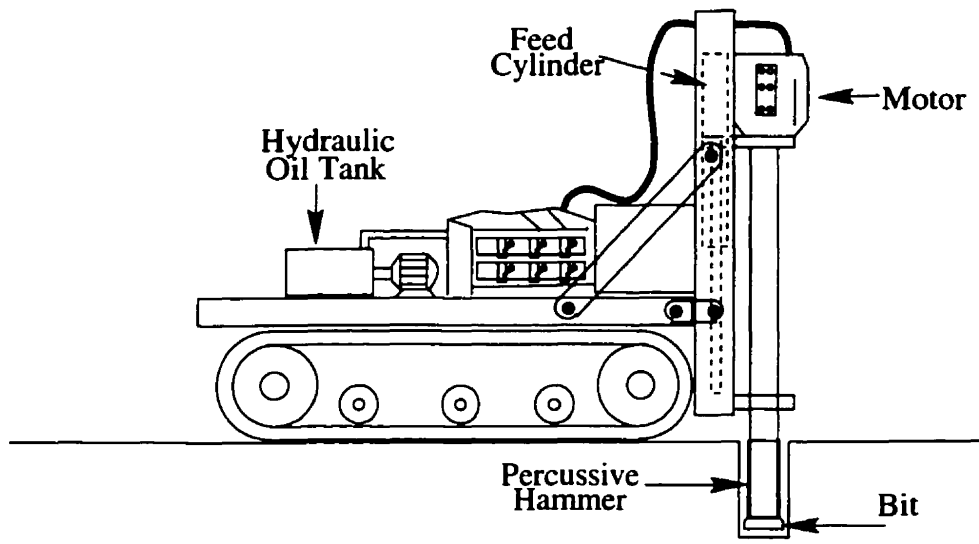


Figure 1.1: *ITH percussive drill CD90B by CMS used in experiments*

stress wave reaches the bit and impacts on several cutter elements to break the rock through a combination of compressive failure and fracture propagation. The stress wave reflected from the bit gives rise to another stress wave, which is regenerated in the upper end of the drill rod. This reflected stress wave may cause further rock breakage when it arrives back at the bit rock interface.

To make drilling efficient it is important that the fragments of rock be continuously conveyed away from the hole bottom. This is done with the aid of a flushing fluid (usually air or water). In the case of an ITH hammer, the exhaust air of the hammer is used for flushing. It is supplied through one or several holes in the front face of the bit. The fragments are then transported to the hole opening via space between the drill rod and the wall of the bore hole to the rock surface.

To keep the drill bit in contact with the rock it is necessary to exert a thrust force upon it. The thrust is also important in forcing the bit towards the rock and thus making transfer of energy to rock efficient.

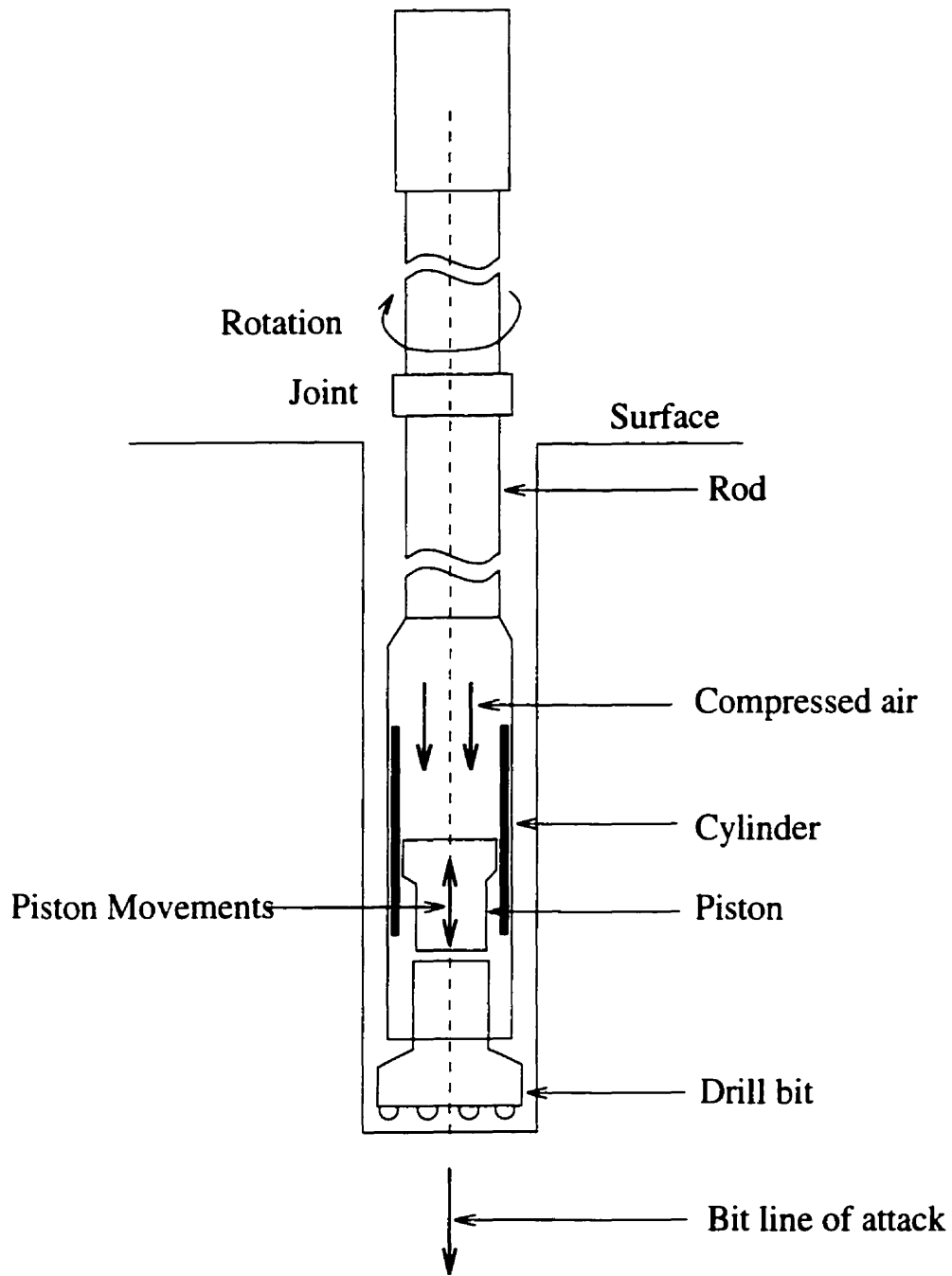


Figure 1.2: A schematic representation of a drilling system with ITH percussive hammer

1.4 Problems Associated with ITH Percussive Drilling

1.4.1 Poor Machine Operation

The drilling cycle of an ITH percussive drill consists of the following manual operations.

- a. Positioning the entire drill at the designed location of the hole.
- b. Levelling the machine by lowering four independently controlled jacks.
- c. Anchoring the machine by raising the upper anchoring jack or stringer.
- d. Adjusting the machine head along the angle of inclination desired for that hole.
- e. The operator first starts the rotation of the hammer, then he lowers the hammer by applying feed until the bit touches the ground. The percussion is then started by supplying compressed air to the hammer.
- f. A suitable low feed pressure is applied during the initial drilling (collaring) to set the hole in the fractured ground present at the opening.
- g. Feed is then increased after collaring the hole. New rods are added when needed. This operation is continued till completion of the hole.

This procedure requires continuous involvement of the operator. Hence human factors can greatly affect drilling performance such as:

1. To adjust the feed force, the operator follows a prescribed chart provided by the manufacturer. He has to keep varying the applied feed pressure with the depth of drilling to compensate for weight of the drill rods. This adds a precision error.

2. The feed force also requires adjustment if there is change in the rock hardness causing excessive vibration etc. which must be avoided.
3. Sometimes hammer jamming occurs due to excessive rock hardness or improper hole cleaning. This requires stopping the hammer, purging the hole with compressed air and restarting the machine.

Hence, it is apparent that there is significant potential for machine performance to be improved with the addition of automatic control.

1.4.2 Hole Deviation

Another problem in rock drilling is the hole deviation. ITH percussive drills are mostly used in production hence, the problem of hole deviation in percussive drilling is associated with the blast hole drilled for production.

During the ore production process, blast holes are drilled in vertical, horizontal and inclined directions depending upon the type of mine and mining method. These parallel holes are then charged with explosives for rock breaking. The proper fragmentation is only possible if all the holes are successfully drilled according to the design (see figure 1.3*a*).

However if these holes are changing their direction unknowingly, the spacing between parallel holes varies and causes improper fragmentation. Figure 1.3*a* and *b* illustrates these two situations. The uneven breakage of rock sometimes causes severe consequences: e.g. it can cause blockage of the whole channel see figure 1.4. These situations are extremely dangerous to handle especially when the blockage is not within easy access of a drill rig for secondary drilling. Deviation control would therefore solve these complex problems.

In other applications, holes are intentionally deviated in a desired trajectory. For

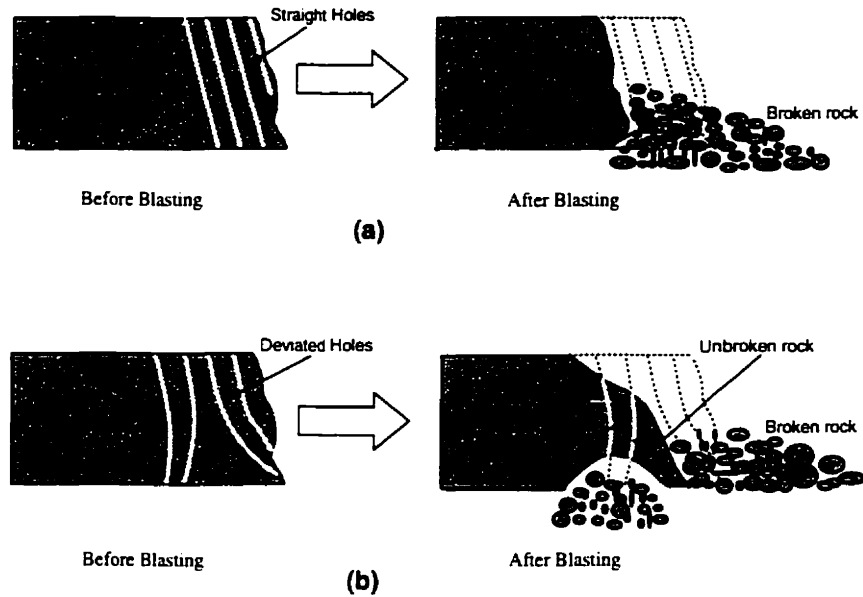


Figure 1.3: An example to illustrate the effect of hole deviation on rock fragmentation
 (a) Straight holes results in better fragmentation (b) Deviations in production drilling may cause improper fragmentation and incomplete breaking

example. in off shore drilling to target a petroleum source the drilling is performed from the same site in different required directions. Deviation of the drill string from the designed direction can be guided with the use of wedges. In some cases these deviated holes are abandoned and new holes are planned. Hence the accuracy in long hole drilling is a factor that has a significant influence on the production operation. Large deviations lead to bad fragmentation and hence to poor mining efficiency.

In light of the above it is evident that an automatic control of the drilling process could have significant benefits and that deviation control should be an integral part of such a control system.

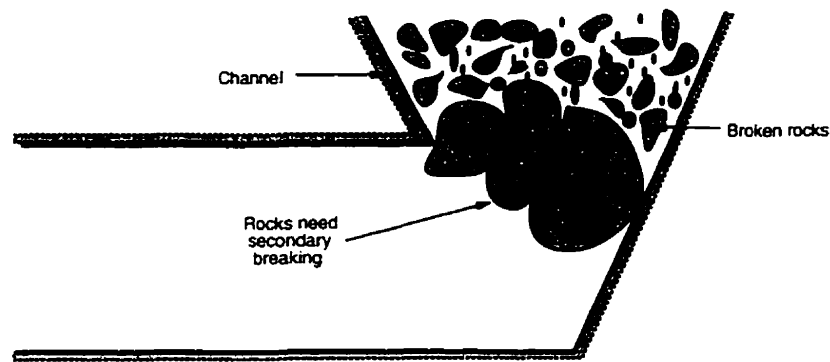


Figure 1.4: *Blockage caused by improper rock fragmentation*

1.5 Generic Control Methodology

Automatic control has played a vital role in the advance of engineering and science. In addition to its extreme importance in space-vehicle systems, missile-guidance, aircraft auto-pilot, robotics, and the like, automatic control has become an important and integral part of modern manufacturing and industrial processes. A general approach to designing a control system includes the following:

- Setting of input-output variables:

The first step in the development of a control system is defining the input and output variables. i.e. to investigate which parameter is to be controlled, and which variable can be manipulated to vary the output quantity.

- Developing the input-output model:

A model should define the relationship between input-output variables, and should adequately represent the process being controlled.

- Designing a suitable controller:

After modelling is completed a controller can be designed. The choice of

controller type depends upon the process model and on the desired output behaviour e.g. response time etc.

- **Analysis of the controller and validation through simulations:**

Through computer simulations, the analysis of the controlled closed-loop system can be conducted. This includes frequency response and stability analysis of the system.

- **Implementation of the controller in real time:**

After validation, the controller is applied to the actual plant.

1.6 Modelling

Modelling of the process is one of the most important and essential requirement for a controller design and analysis. Until the process to be controlled is not properly represented mathematically, the subsequent step described in the control methodology cannot be followed.

There are two approaches to obtain an input-output model of a system

- **By Physical Laws (Analytically)**
- **Empirical Modelling/ System Identification:**

A mixed approach to obtain the model is most commonly used. That is: establish the basic structure of the input-output model by basic physical laws and estimate the parameter values of the mathematical model from experiments. An empirical study of machine performance is adopted in this thesis.

1.7 Scope of the Thesis

To achieve the above objective it was necessary to investigate through experiments the basic inter-relationships of the drilling parameters. This investigation process constitutes the scope of this thesis and includes the following:

1. **Field Experiments**

Acquisition of drilling process data for the ITH percussive drill CD90B through field experiments.

2. **Performance Modelling**

Analysis of collected data to establish the relationship between machine variables and formulation of recommendations for controller design.

3. **Machine Modelling**

This includes the development of actuator input output model necessary for control system design. It does not include the structural modelling of the drilling machine. It does however, include the shock-absorber model for analysis purpose.

4. **Controller Design and Simulation**

Based on the results of field data analysis, formulation of a suitable control strategy. Design of a drilling process controller. Simulation of the percussive drilling process and evaluation of the control algorithm.

5. **Deviation Analysis and Control**

Investigation of correlation of hole deviation with drilling parameters. Formulation of recommendations for deviation control system design. Propose the prospective mechanism required to develop guided drilling for percussive system. Develop simulator for the proposed mechanism.

1.8 Overview of the Thesis

Chapter 2 surveys state of the art research on the subject of percussive drilling. We have organised this chapter according to different subject areas related to the design of the control system for the drilling process.

Chapter 3 presents details of the field experiments and shows some preliminary results from the acquired data.

A detailed discussion on data analysis is given in chapter 4. Modelling of the drilling process and correlation among the drilling parameters is established in this chapter.

Chapter 5 develops a simulation model of the percussive drilling process. We have adopted a mixed approach, analytical and empirical, to achieve the simulation model. Both machine and the bit-rock interaction models are developed.

In chapter 6 we have formulated a control algorithm for the percussive drilling process to improve drilling performance. The control algorithm is tested through simulations. The simulation results are also presented.

In chapter 7 vibration analysis is presented. The purpose of this analysis is to evaluate the existing shock-absorber installed on the CD90B drill and formulate recommendations to improve the design to minimize transmission of the vibration from the hammer to other parts of the machine.

Chapter 8 looks into the hole deviation results obtained from the field experiments. We have tried to correlate the drilling parameters to the drilling deviation. Unfortunately, very little success in this respect is achieved. This chapter is, however, included to provide a guidelines for future experiment designs when investigating the deviation in percussive drilling.

Chapter 9 discusses the prospects of development of future guided drilling systems. A novel approach for designing a hammer mechanism that could be employed for

steering in the guided drilling system without downhole instruments is also described in this chapter.

Chapter 10 develops a model for the hammer mechanism explained in chapter 9. The model has been simulated in Matlab and the simulation results are provided.

Finally, chapter 11 concludes the thesis with recommendations for further research.

Chapter 2

Literature Survey

2.1 Introduction

The literature survey was focused on various subjects such as percussive drilling, drilling deviation, drilling system modelling from a control perspective, and control systems developed for such systems. It served to establish the foundations on which prospective research could proceed.

Most literature available on rock drilling deals with rotary drilling. At present, very little scientific literature appears to have been published on the subject of percussive drilling especially in respect of drilling process control and hole deviation. Existing literature on percussion drilling consists of either a brief reference to field observations in mining equipment manufacturer's brochures (e. g. [83]), or of relatively systematic experimental and statistical field studies performed on various equipment and drilling techniques (for example Medda [49], Sinkala [78]).

The results of the literature survey are organised below by subjects area.

2.2 Percussive Drilling: Motivatives and Constraints

Some literature is of an introductory level on the percussive drilling, which addresses the merits of percussive drills or compares the percussive and rotary drills.

Auranen [6] writes that the bench drilling equipment for quarries and open pits has traditionally fallen into two main groups depending on the drilling technology employed i.e. rotary or percussive. The percussive group is further subdivided into top hammer rigs and ITH machines. The ITH are used for mostly inclined holes. In the modern mining methods inclined holes are preferred for their merits over the vertical holes.

Auranen [6] has also compared these two type of holes. In the inclined holes: the energy of the explosive is utilised more efficiently in blast holes than in vertical holes and geometry of the toe makes more efficient use of the reflected shock waves. Vertical holes also produce “stumps” which tend to accumulate as the bench is worked back. Inclined blast holes also allow better control of the bottom of the bench. Other benefits are the decreased backbreak and improved pit wall stability. Most of the drawbacks of inclined drilling are associated with the rotary drilling. These are: increased wear on drill rig, diminished penetration, drilling accuracy (i.e. more precision is required in alignment for accuracy), and hole deviation.

When rotary drills are used to drill inclined holes and smaller holes sizes (below 9 in.) drilling costs (\$/ton) tend to increase dramatically due to rig stability problems and diminished rotary drill bit life, as the rock breaking force produced by a rotary drill derives entirely from the weight of the rig. With the percussive drills on the other hand, the main breaking force is provided by the percussion mechanism in the drill, and a relatively small feed motor is sufficient to produce the required feed force. Therefore the rotary machines are used in vertical blast holes but seldom

used in inclined holes.

In [89] the advantages of percussive drilling ITH over top head drifter are given. It says ITH offers continued advantages against top head drifter providing clean straight easily charged blast holes to produce good fragmentation, well defined face profiler and with high degree of safety. Another advantage with ITH is that it can drill the hardest rock with ease. It is also pointed out [4] that in the field of drilling the most significant advance has been the development of the hydraulic rotary percussive rock drill.

A pioneering research project on percussive drilling was conducted in the late 1950s at the Colorado School of Mines to establish the correlations among the key parameters. The review by Hartman [25] concluded that the energy of blow, frequency of blows and plan area of the bit are the principal variables on which rate of penetration depends. Similar results were also obtained by Rubia [69], i.e. "The optimum thrust in percussive drilling is a function of impulsive loading, frequency, bit diameter and rock hardness". Hartman also derived a linear relation between *energy verses penetration rate*. The model assumptions were tested in experiments with good results. The experiments were conducted in the laboratory and a number of constraints like no change of rock type, uniform rock structure, single blow per test etc., were imposed in order to reduce the variables. Therefore, it is quite difficult to generalize the concept. However, these basic concepts can be useful in deriving more complicated models for penetration rate, especially with the addition of two more parameters; the vibration and the torque.

Lundberg [44] studied the efficiency of a percussive process for fragmentation of rock and similar materials analytically. He concluded through computer simulations that in percussive drilling the bit mass is a far more important parameter than the shape of the bit.

Rabia [69] comments that percussive breakage of rock is a result of the interaction

between the compression waves and the rock matrix. In case of percussive drifters, the strain waves have to travel from the surface to the rock, energy losses take place and penetration rate decreases with hole depth.

After comparing various equations for predicting the performance of percussive and oil well rotary drilling machines, and based on one dimensional strain wave theory, a unified model, which is applicable to both types of drilling (rotary and percussive), was proposed [69], which states that "The penetration rate is directly proportional to some power of energy input and inversely proportional to some power of product of strength properties". Some simple analytical models have been derived to predict the penetration rate for different types rocks.

2.3 Parameter Interaction Studies

Hustrulid [30] carried out field experiments at two different sites. In which drilling was performed at different thrust F_c levels for various fixed percussion pressure magnitudes, using three different hand-held jack hammer rifle-bar rock drills. The drill string length used was approximately 2m, and maximum thrust applied was 2722N (600 lb).

The variation of penetration rate (r_a) with thrust (F_c) and hole length was studied. It was observed that the shape of penetration rate-thrust curves were virtually independent of rock drill type and the values of the percussion pressure (p), and were only weakly dependent on the different rock type at the two sites.

For a given air pressure, the penetration rate (R_a) increased with thrust (F_c) until a peak penetration rate (R_{pr}) value was reached. As the thrust increased further, the penetration rate decreased and the drill finally stalled. The optimum thrust was defined to be the thrust at which near-peak penetration rate is obtained without excessive bit wear. The decrease in penetration rates at high thrust levels were

attributed largely to bit wear. There was no mention of buckling effects possibly because the drill was assumed to be "short".

He also showed that a low thrust results in free rotation of the bit and poor chip formation occurs. Also, the piston may impact the drill rod while the bit is not in contact with rock, and energy is then wasted. A higher thrust will reduce rotation even though bit rotation occurs during the back stroke of the piston. A higher thrust will also increase the torque required for bit rotation; when this increases to a critical value, the drill will stall. Each drill has a characteristic optimum thrust for the maximum penetration which corresponds to good contact at the bit rock interface and to optimum indexing.

Unger and Fumanti [85] performed laboratory tests using percussive drilling with independent (controlled) rotation. They observed that for a constant rotation speed (n) to be maintained, the pressure (P_1) to the rotation motor must be increased with the applied thrust (F_c). For some rocks at the low thrust values and at 70psi (about 5 bar) drill operating air pressure, penetration rates were higher than the rates at 100psi (about 7 bar). This reverse trend is thought to have been due to inadequate thrust, which permits bouncing of the bit and rod. This in turn prevented effective bit rock contact. The form of penetration rate-thrust curve obtained was in agreement with results by Hustrulid [30]. To maintain rotation speed, torque pressure (P_1) was observed to increase with increasing applied thrust.

Pearse [65] reports drilling tests conducted by Montabert using hydraulic rock drills with independent rotation. Montabert investigated the sensitivity of penetration rate to applied feed pressure (thrust). It was found that insufficient pressure causes vibration and heating effects, especially at rod connections. Excessive feed pressure in jointed ground causes deflection and rod jamming, and in weak rock the bit action cannot break the rock sufficiently for removal by flushing, and jamming and slow penetration will result.

The torque exerted by the rotation motor will be directly affected by the feed pressure, and there exists a definite relationship between feed pressure and the torque when the penetration rate is maximized. From the plots given in [65] it seems that this relationship is almost linear at maximum penetration rate. The slope of this linear curve increases at higher thrust values. Montabert found that when drills are used in variable rock conditions and for variable hole sizes, a compromise must be reached concerning maximum torque. In their results it is observed that the penetration rate decreases with an increase in bit (hole) diameter. The penetration rate-thrust relationship is similar to experimental observations by Hustrulid [30].

Using computer simulation, Nordlund [60] studied the effect of thrust on the performance of percussive rock drills. The following results were obtained:

- An increase in thrust increases the efficiency of the drilling processes, the contact time and the contact force at the bit/rock interface.
- The disadvantages of applied thrusts of large magnitudes include drill string buckling, increased drill bit wear and large torques required to rotate the drill string.

2.4 Guided Drilling

Guided drilling can be defined in two different ways. One type is drilling a hole to reach the desired target regardless of the trajectory as, for example, when drilling a number of holes into a submarine reservoir from a single on-shore location. The other type is drilling a hole in a desired trajectory or in a desired rock type an example of this is coal mining in-seam drilling

The coal industry has undertaken significant work in guided drilling, with major contribution by MRDE (Mining Research and Development Establishment) under

the National Coal Board, UK, where certain research projects were started to build a guided drill (see for instance, Morris [54, 10], Rees [71] etc.).

2.4.1 Sensing

In the paper by Morris & Wykes [54] it was stated that the best way to measure coal thickness between the drill head position and the coal-stone interface was via natural gamma counts, using a gamma logger for this measurement. This idea was used as the major sensing system for drilling guidance. They developed a special instrument for borehole monitoring. This experimental system could make off line measurements in the first phase of the project. This consists of a pump-in survey probe, which took measurements during a pause in the drilling operation and transmitted them back to control units. The probe took three measurements: local gamma field, from which the distance from the nearest edge of the seam may be obtained; the probe attitude, i.e. the angle w.r.t. gravitational vertical; the probe roll orientation, i.e. the angle of rotation about the probe axis of a reference plane through the probe axis from vertical direction (tool face angle). The attitude and roll measurements were by liquid electrolyte sensor. Both angles are measured by placing two such sensors at right angle to each other. These sensors have very small range of ± 12 degree and high accuracy upto 10^{-2} degree.

In addition to these measurements was the provision of magnetic azimuth sensing. By measuring the strength of the earth magnetic field in three mutually orthogonal directions, using magnetic compass. There is an inaccuracy because of fluctuation in earth's field of ± 0.5 . Other sensors for these measurements are flux-gate magnetometers and commercial Linear Variable Differential Transformers (LVDT) displacement sensors.

A proposed technique for signal communication between down hole sensors and the top hole control units of an electromagnetic wave traveling along the outside of

the drill string has been pioneered in the USA [71]. Initial feasibility studies on the signal communication on several techniques performed by [54], it appeared that the use of UHF (electromagnetic)–or audio/ultrasonic (acoustic)– waves in ground probing radar modes offer the most promising. But these were never used by them.

In microtunnelling project “FlowMole”[51], the position of the drill bit was determined by a locator system consisting of radio transmission/detection devices, a part of which was installed on the bit. These holes were drilled horizontally at small depths, it was convenient to use the radio transmission/detection system to locate bit position from the surface. However use of this technique is difficult for underground mining holes, especially in magnetic rocks.

The tracking and detection system used in the Guided Piercing Tool [38] was the magnetic field attitude sensing and rotation system (i.e. magnetic fields generated by energized coil on board the boring tool are detected by sensing coil located in the launching or retrieval pits, or both). They also considered an alternative approach for tracking the boring tool using conventional electromagnetic conduction pipe and cable locators.

2.4.2 Steering

Morris [92] has given the detail of the instrument development for the steering system for their project Mark I and the Mark II.

Rees [71] has reported of using simple steering device for the drills, called “kick-off-sub”, which are used to offset the bit slightly from the axis of drilling string. This technique involved a down-hole-motor without drill string rotation. The important feature of this technique is that steering direction can be changed easily by merely rotating the drill string. Other techniques used were the use of stabilizers or fulcrums in the hole. The steering was done by positioning of these stabilizers.

However in this technique the operator has to withdraw the drill string for positioning the stabilizers. The field trials indicated that down-hole motors were essential for steering adequately. However this improved steering characteristics of the down-hole motor tended to be negated by the effect of measuring natural radiation at a point further back from the bit (5m) than in the case of rotary drilling. Surface and underground trials with the pump up survey probe to measure the hole trajectories are also described.

Mercer [51] explained that FlowMole corporation designed a microtunnelling equipment for small diameter utility installation, called GuideDrill. This system bores its way through the soil by extremely high pressure jets of bentonite slurry. It was steered into required directions by controlling the jet orientation.

Other steering technique used in the FlowMoles, which have pressure jets for drilling, is achieved by remotely biasing the direction of the cutting jets at the nose of the boring tool [4]. The pressure of drilling fluid (bentonite slurry) in these jets is in the range of 1000psi to 4350psi.

Distribution technology's Guided Piercing Tool, as reported in [38], used a different technique for steering. It was accomplished by mechanically shifting an eccentric cam (pad) mounted on the rear of the propulsion section against the side of the borehole. The theoretical turning radius of the steering device was 1 ft. per 5 ft of travel.

Woods & Hopley, [91] used method of steering during the horizontal long hole drilling with the help of a *reaming shell* using the conventional drilling equipments. They have successfully used this method at Boulby Mine.

Terra Tek developed a new concept for a self-contained downhole tool in 1979, Green [23]. This tool could both sense borehole deviation (from a straight path) and tend to correct the drill so as to drill ahead along a straight path. The drilling fluid was used both for the sensing and to operate side thrust pads for corrections.

A groups of three nozzles –at four radial locations– installed at the rear of the tools worked as sensing elements. Whereas the four push-off side thrust pads were used as actuators for correcting the drilling direction. These were installed on an outer sleeve of the tool which did not rotate. Some of the drilling fluid was allowed to exit the rotating torque tube through holes, and proceed through venturi (one for each nozzle group) and then return in the hole by exiting the tool through the nozzles. As the nozzles come close to the borehole wall –if the borehole begins to deviate from a straight path for example– the nozzle in that group tend to become plugged and flow is reduced; the converse happens to nozzle group diametrically opposite. This produced relatively high and low pressure across the venturis in the low and high nozzles flow groups, respectively. The difference in venturi pressures activates a rotary valve with correct porting to allow the correct side-thrust push-off pads to be activated. Feasibility of this project was done by Terra Tek, however no report on its implementation is found in the literature.

2.5 Drilling Process Modeling

To date, considerable effort has been devoted to the development of relationships between various drilling parameters. Such investigations range from purely theoretical to field activities.

Many investigations, for example Lundberg [42], Rabia [68] and Nordlund [60], regarding bit/rock interaction are concerned mainly with the prediction of drilling penetration rates. The intended applications of the results include equipment design and planning of drilling and blasting operations.

Some formulae contain the physical/mechanical properties of the rock considered, while other are centered around specific energy (the energy required to excavate a unit volume of rock). Limitations of many of the current studies have been listed in

various publications, for example by Paithankar and Misra [62], [61] and Rabia [69].

The concept of Specific Energy, SE, was proposed by Teale [84] as a quick means of assessing rock drillability. Teale defined SE as the energy required to remove a unit volume of rock. Since then, however, another definition of SE, in terms of new surface area created has appeared in the literature [61]. The two definitions appear to produce uncorrelated values. Teale showed also that the minimum value of SE is approximately equal to the compressive strength of the rock while Mellor [50] showed SE to be the approximately equal to the value of compressive strength divided by 1000.

It was therefore concluded that the value of specific energy for a particular rock varies with drill type. For instance, Rabia has found that the specific energy for rotary drilling is higher than that for percussive drilling.

An empirical formula given by James Paone *et al.* [66] can be used to calculate the specific energy of the rock from drilling data. These calculated values were also employed by Hustrulid [29] for prediction of drilling rate.

The specific energy (E_v) is not a fundamental property of a rock Rabia [69]. In full scale drilling, it also depends on parameters of the drilling system such as bit geometry, indexing angle, thrust, breakage system (percussive, rotary, etc), rock properties and also hole length. The prediction of drill performance using specific energy alone cannot therefore be accurate Rubia [69], Paithanker and Misra [62].

An attempt has also been made to predict penetration rate by incorporating the compressive strength of a rock and relating the results to the specific energy (E_v), Paithanker and Misra [62]. They found that correlation of penetration rate with individual rock properties is poor. However, a good correlation between penetration rate and a set of rock properties was established [62].

Since no one rock property alone completely defines rock breakage characteristics

due to large number of variables (Rabia [69], Howarth and Rowlands [27]) theoretical treatment of drilling has not been very successful. In the prediction of penetration rate a number of parameters must be related in an empirical manner.

Lundberg [42, 43, 44, 46, 45], Nordlund [60] and Karlsson [35] have worked extensively on the computer simulation of percussive drilling. Much of this work has been directed towards drilling efficiencies and machine design. The computer programs, developed at Lulea University of Technology, are also reported [45] to be in use by Sandvik Rock Tools. Laboratory and field experiments have been performed to test the models. The results obtained here have been reported to give good agreement between field and model results, and these models are being developed further [45].

Regarding possible limitation of these models, most relevant for our discussion is that almost all drilling rate theories developed in the past have not included interaction between thrust, torque, and rock inhomogeneity, despite their strong effects on drilling rates.

2.6 Drilling Control

Ho & Jianchi [26] studied the technique of using a micro-computer to control a rock drilling machine. They developed a simulator which used the kinematic techniques for positioning at a given geometrical configuration. The actual drilling process was not controlled.

Hancke [24], Designed a control system for controlling the parameters which determine the performance of a deep hole diamond drill, which is a rotary type machine. Two algorithm were formulated "Bit force control" and "Bit power control". In the former, force on the bit (WOB) is maintained by the controller. On line calculation of WOB is made by the load cell on the elevator. In the latter case power on the bit is maintained. The bit power is calculated form on line measured parameters; the

rotation speed, input torque, and the in-hole friction torque (measured, frequently by rotating at various speeds within the operating speed range of the equipment with the bit just off bottom). A rough dynamic model (two spring a mass and a damper) is used to analyze the control system. This rough model is based on the assumption that the dynamics of the drill machine would be dominated by the drill string.

Dahl [15] concludes from drilling experience that penetration rate of the drill depends very much on the adjustment of parameters like percussive energy, feed pressure, rotation speed etc. He described the design of the first prototype jumbo at Furuholmen, Norway.

Changming & Sinkala [11] choose thrust as the key controlling parameter to drill hole with small deviation and high penetration rate. An automatic thrust control system was developed and tested successfully. In this control the rotation torque was measured and thrust was adjusted to keep torque in a certain operating range. The setting of minimum thrusts for the control system were obtained from the field experience and empirically derived formula. Comparison of drilling results from both automatic and ordinary control system shows that higher penetration rate, less drill string jamming, and smaller hole deviations were obtained with the automatic control system.

2.7 Drill Deviation

Karfakis & Evers [34] have mentioned three main causes of the rotary drill deviation these include:

1. The lamination or the foliations in the rock effects borehole deviation.

2. The mechanical behavior of drill string, as it buckles causing the resultant thrust on the drill bit to deviate from the axis of the wellbore.
3. The rock-bit interaction which creates unbalance lateral forces on the tooth.

Based on rock-bit interaction theory of anisotropic rock strength and a the possible effect of these anisotropies on the rate of penetration and hole deviation (see McLamore [48]), a model was proposed for prediction of lateral force acting on the bit.

McLamore concluded that anisotropic rocks will fail preferentially on one side of a bit tooth with resultant horizontal thrust and hole deviation toward the side of chip formation. Models have been defined to predict chip formation and direction of the deviation.

Brown & Green [8] in 1981 did a review on the hole deviation and has compared the theories available on hole deviations. They concluded that rock anisotropy plays a major role in hole deviation, and that bit-rock interaction is not well understood and is affected by rock anisotropy. The theories given so far were not considered satisfactory. They believed that boreholes are deviated by anisotropy in a rock mass (i.e. by schistosity, lamination or bedding), and by sudden change in rock properties as at an unconformity, a fault or some other geological boundary.

McLamore [48], found that generally, in the first general class of anisotropic or laminated rocks, vertical holes will tend to deviate up-dip, i.e. towards the perpendicular to the laminations, if the laminations are not steeply dipped. In steeply dipping strata, hole deviation tends to be down-dip, i.e. parallel to the laminations. Closely bedded, laminated or schistose strata will generally deviate a hole towards the perpendicular to the lamination for angles of incidence to the borehole to the lamination of from 90° to about 30° , and parallel to the laminations for shallower angles of incidence.

It is widely reported that, when drilling across an inclined boundary from a softer to a harder rock, deviation is up-dip. Conversely, when drilling from a harder to a softer rock, the deviation tends to be down-dip.[8]. Dog legging is caused by sudden changes in bit thrust, irrespective of geological conditions.

Brown & Green [8] also stated that the deviation increased with decreasing water circulation rate and with decreasing bit clearance angle. The drilling rate in both stronger and weaker 'rock' decreased to differing degrees with increasing bit wear, and the drift of the borehole increased as the ratio of the drilling rates in the two materials increased. No theoretical explanation of the results was offered other than a qualitative one. In other experiments an attempt was made to determine the lateral deviation forces on acting on the bit by using a strain-gauged aluminium load cell to measure the bending moment in the drill string. From the simple beam bending theory, the value of the lateral force could be estimated at each stage of a given drilling test from the recorded values of bending moment and thrust. It was found that all holes drilled in the Dworshsk gneiss deviated up-dip towards the perpendicular to the foliation dip direction.

Murphey [56] suggests that as the bit drill through each lamination, a point is reached at which the rock can no longer support the applied stresses and so it fractures through to the next lamination along a path perpendicular to the bedding plane. This produces easily removed wedges of rock on the upper side of the hole and small wedges on lower side which act like miniature whipstock creating lateral forces that tend to deflect the up-dip.

Sultanov [82] gives argument that hole direction changes because, in crossing the interface, the bit will drill more slowly in the harder of the two rocks. Deviation will be up-dip when drilling from a softer into a harder rock, and down-dip when drilling from a harder into a softer rock.

Murphey [56] pointed out that the moment generated at a stratum change will alter the pendulum length to the point of tangency of the drill-string with the hole, as well as the side force on the bit. Because of this, the variation in side force and the consequent change in hole direction, will not be the same when drill from soft to hard rock as when grilling from hard to soft rock.

Knapp [37] argued that when drilling from harder to softer rock, the bit would be unable to ream the hard stratum to gauge as quickly as it could drill the softer stratum and so would be deflected towards the softer stratum.

McLamore [48], the removal of larger amounts of material from one side of the hole than from the other will cause the hole to deviate from its original direction. Preferential chip formation also results in the creation of a lateral force on the bit which causes it to deviate in the direction of greater material removal.

Lubinski & Woods [41] suggest that anisotropic rocks will have slightly lower drillabilities parallel than perpendicular to the bedding, lamination or schistosity. They defined the index h whose values varies between zero and 0.075

McLamore-Bradley [48] deviation force theory: McLamore developed an analysis of the chipping mechanism of a single wedge-shaped tooth in dipping anisotropic rock. He calculated the magnitude of the wedge penetration force, F , required to produce chipping on either side of the wedge. The experiments showed that the maximum deviation forces were measured for dips in the region of 30° (up-dip deviation) and 60° (down-dip deviation). Deviation forces were close to zero at 0° to 90° and in the region of 45° . The measured deviation forces were in fair agreement with those calculated from the equation they gave.

Pariseau [63] presented the results of experiments, performed in order to investigate the effects of anisotropy on the deviation force acting on single wedges during static penetration of plastically deforming rock. He found that the deviation force always acted down-dip and attained a 60° in both the transversely isotropic and the

orthotropic cases.

Brown [8] suggests that further research will be required to understand rock-bit action. He suggested some down-hole measurements, like measurement of bending moment in the drill string at a location between the bit and the tangent point and to attempt to isolate anisotropy induced components from those resulting from drill-string flexure by using a computer program such as that developed by Walker & Friedman [87].

2.8 Summary of Key Results and Concepts

The following list summarizes the literature survey.

- Blow energy, blow frequency and area of the bit are the principal variables of percussive drilling on which penetration rate depends [25].
- In percussive drilling the bit mass is far more important than the shape of the bit [42].
- For a given percussive pressure, the penetration rate varies proportionally with thrust upto some upper value of thrust, above which it decreases and drill will finally stall [30].
- There exists minimum and maximum values of thrust, between these values the operation of the percussive drill is most efficient.
- Excessive feed pressure in jointed ground causes deflection and rod jamming.
- The torque exerted by the rotation motor is directly affected by the thrust, this relationship is almost linear at the maximum penetration rate. The slope of this linear curve however, increases at higher thrust values [65].

- Down Hole measurements by [92] used natural gamma counts for coal seam thickness measurements, and electrolyte sensors for attitude and roll orientation measurements.
- In microtunnelling, where horizontal holes are drilled at small depths, radio transmission detection system to locate bit position from the surface was successfully used by [51]
- Use of stabilizers in the holes is the most common way for steering of drill string. The steering is done by positioning the stabilizers.
- Offsetting the bit slightly from the axis of the drilling string is most suitable for hole steering methods. This scheme requires the ITH percussive drill without rotation. Steering direction is changed by merely rotating the drill string [71].
- Pressure jets steering is achieved by remotely biasing the direction of the cutting jets at the nose of the boring tool [4].
- Steering was also achieved by mechanically shifting an eccentric cam, mounted on the rear of the piercing tool against the side of the borehole [38].
- For control of a rotary drill [24] formulated two algorithms; “Bit Force Control” and “Bit Power Control”.
- [11] used thrust as a key parameter in drilling process control. The algorithm was “measure torque and adjust thrust”.
- Drilling process depends on rock specific energy, parameters of drilling system (e.g thrust, breaking system, rotary speed etc) and hole length [69].
- Three main causes of drill deviation are: the lamination or the foliation in the rock; the mechanical behavior of the drill string; and the bit-rock interaction [34].

- Bit-rock interaction, which varies largely in anisotropic rocks, is the major cause of drilling deviation [8]

2.9 Conclusion

Most literature on guided drilling deals with rotary drilling. It seems that less attention was given towards the automation of the drilling process especially for percussive drilling. However significant work relating to investigations of rock bit interaction has been found both for percussive and rotary drilling. This work has focused primarily on laboratory experiments and less attention was given to field experiments.

In a discussion of hole deviation a number of theories were discussed (Brown & Green [8]), but none of these are capable of fully explaining the bit-rock interaction, hence no perfect model has been designed so far. It should be possible to modify existing models of drill-string mechanics to allow for anisotropy induced deviation force acting on the bit.

The approach of Changming & Sinkala [11] for controlling the hole deviation is unique in its nature. However, it does not control the deviation but *avoids* conditions leading to deviation. A true controller for hole deviation would include the actuation for correcting the error.

The development of an economic means of overcoming borehole deviation in a wide range of percussive/rotary drilling applications requires an improved drilling theory based on a better understanding of rock-bit interaction, drill string and the machine effects in the rock. A series of field and laboratory experiments should be conducted. The results of such series of experiments could be used to evaluate previously advanced theories. As a result it will be possible to predict hole deviation in particular cases of drilling conditions of the rock, and to calculate the forces that would have

to be applied by control devices to produce a desired degree of direction control.

Chapter 3

Machine Monitoring

3.1 Introduction

Field experiments for drilling process monitoring and data acquisition were performed on the percussive drill (CD90B of CMS Ltd.) during the period of September 1991 to March 1992. These experiments were conducted at two different mining sites, at Little Stobie mine and at Copper Cliff North Mines in Ontario. In this chapter these experiments are briefly described, with a summary of the experimental setup for both field experiments and laboratory setup for data processing. Some preliminary observations of acquired data are also presented.

Results presented here include the data showing the effects of machine input variables on machine performance. An attempt was also made to obtain the optimal value of machine variable such as feed, bit torque and vibration for efficient machine operation from these observations.

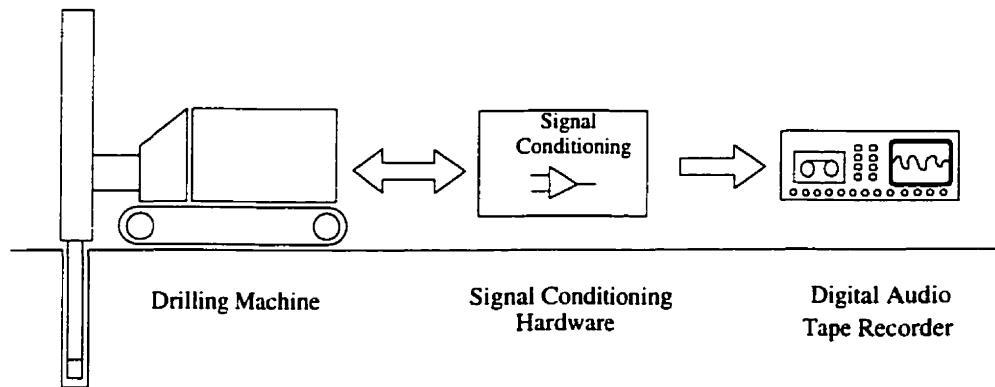


Figure 3.1: *Experimental setup for drilling process monitoring and data acquisitions*

3.2 Experimental Setup

For full range performance study of drilling process, the drill was instrumented so that all the measurable variables could be recorded. Instrumentation was installed at Pool Technology Ltd. A total of 16 variables could be recorded at the same time. On site data was recorded using a Digital Audio Tape Recorder (DAT). The data was later digitized by computer in the laboratory at a suitable sampling rate.

The field experiments setup is shown in the figure 3.1, and the laboratory digitization setup is illustrated in 3.2.

A brief description of components of these two setups is given below.

3.2.1 Percussive Drill CD90B

CD90B is a percussive drill with in-the-hole hammer developed by Continues Mining System (CMS), Sudbury, Ont. This rig is equipped with a pneumatic hammer, of type Halco Mach 80, which uses compressed air for percussive operation. A hydraulically powered piston cylinder mechanism provides force for weight-on-the-bit. Drill string rotation system employs a Sauer Sundstrand Series 40 M46 Axial piston fixed displacement motor, to provide bit rotation.

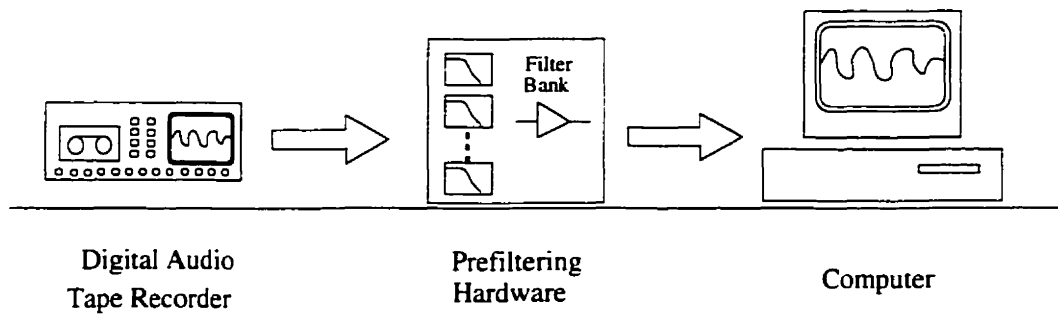


Figure 3.2: *Laboratory setup for digitizing the data acquired during drilling process monitoring*

The control panel of the machine provides the operator control over the feed force and the rotation speed through the joystick installed on it. For air supply to percussive hammer there is only a two state button for opening and closing of the air supply. It therefore, does not provide a precise control on the air supply pressure.

3.2.2 TEAC RD-200 Data Recorder

The recording system used was a Digital Audio Tape (DAT) recorder, Model RD-200 PCM from TEAC (Japan). The unit is capable of recording 16 analog channels of 2.5 kHz bandwidth each. An additional voice channel allows to record comments by the operator, using a hand held microphone. Each tape can store real time data for a period of two hours. In addition it stores the date and time of the experiments.

3.2.3 Signal Conditioning Hardware

This module was designed and fabricated at CCARM McGill. The function of this module is to supply input power to all the sensors installed on CD90B and amplify the sensors' signal so that they could be recorded at a reasonable voltage level.

3.2.4 Pre-filtering Hardware

The data collected was digitized at two different sampling frequencies depending on the type of analysis to be conducted. Data to be used for machine performance analysis was sampled at 1Hz. The vibration signal, on which a frequency domain analysis was required to be applied, was sampled at a higher sampling frequency of 1KHz.

The pre-filtering hardware, which consists of a set of analog low pass filters, was designed to filter the analog data before sampling. The purpose of pre-filtering was to avoid any possible aliasing that could occur in the sampled data. The corner frequency of the filters was set at half the sampling rate of the signal. Therefore, the corner frequency of all the filter was set at 0.5 Hz, except for the vibration data filter whose cutoff frequency was set at 500 Hz.

3.3 Field Experiments

The drilling experiments were conducted at Copper Cliff North Mine and Little Stobie Mine of INCO Ltd. These two sites can be located in Figure 3.3. The surface experiments which were performed at Copper Cliff North Mine were used for the instrumentation testing. The full range of data could not be recorded during the surface trials due to repeated failure of the instrumentation.

During the underground trials which were performed at Little Stobie mine, nine holes were drilled with the CD90B percussive drill. A total of 1022 feet of drilling was done. Most of the data analysis presented in this thesis was acquired from the Little Stobie Mine.

For rock analysis three holes were diamond drilled at the same site. The core collected from these holes was analysed at the Rock Mechanics Laboratory of McGill

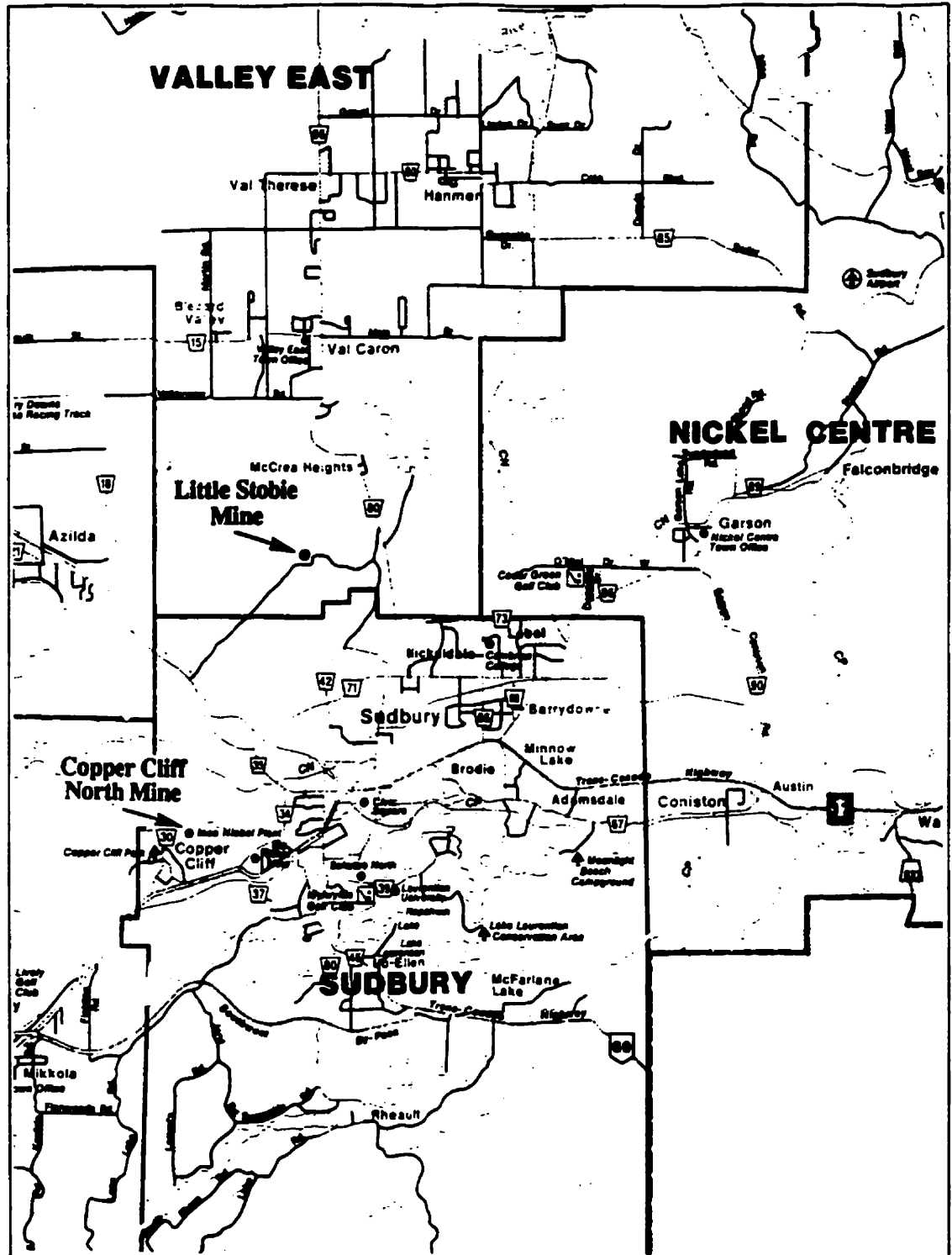


Figure 3.3: Site location map illustrating two mines, the Little Stobie Mine and the Copper Cliff North Mine, where the drilling experiments were performed.

University.

All these holes were surveyed later by three different logging companies, the IFG Corporation, Sperry-Sun Drilling Services, and GPR International Inc. Hole survey data was used for deviation analysis, whereas the results of laboratory analysis of the rock were used for comparison with calculated specific energy.

A layout of the underground holes drilled during the experiments are shown in the figure 3.4. The test holes drilled with the CD90B are marked as number 1 to 9 whereas the holes marked as A B and C represents the core holes.

These experiments were designed to investigate the effects of machine variables on drilling performance. It was therefore necessary to limit the variation of other parameters which were not recorded and effect machine performance. The following precautions were undertaken in this regard during the field experiments:

- To minimize the effect of bit wear a sharpened bit was used at the start of each hole. The bit was frequently changed at least twice for each hole.
- To keep machine stability during the drilling, the machine was properly anchored using lower and upper stringers of the machine before starting of drilling of each hole. The machine was frequently readjusted and aligned during the drilling.
- To limit the interaction among machine input variables, only one input variable of machine was changed at a time while keeping all other variables constant. For example, vary feed force and keep RPM and air pressure constant etc.
- Rock hardness is an uncontrollable variable. To limit the effects these variations, it was tried to conduct the machine variable tests only during the smooth running of the machine. If any variation in penetration rate, as a result in sudden variation in the rock hardness, was observed during a test the test was stopped and was repeated later.

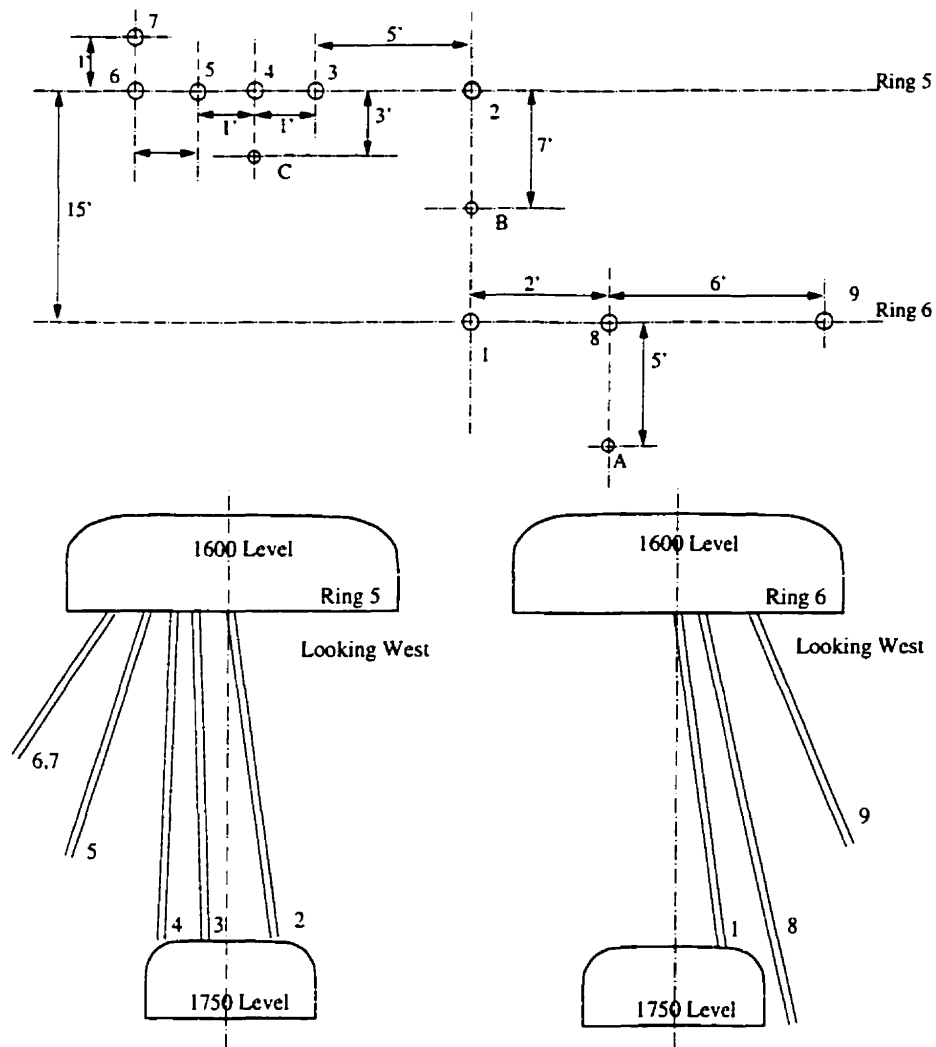


Figure 3.4: Plan and cross-sectional view of underground holes drilled at 1600 level of Little Stobie mine. Test holes drilled with CD90B are marked 1-9 and the core logging holes drilled with the diamond drill are marked as A B and C

Table 3.1 gives an overview of the underground holes drilled at 1600 level of Little Stobie mine.

3.3.1 Variables Analysed in the Research

A total 16 signals were recorded during data acquisition experiments. Analysis of all the recorded variable is beyond the scope of this thesis. The parameters that have been analysed in this thesis are listed below. A complete list of all the variables and their analysis can be found in [33].

- Thrust force applied by feed cylinder
- Torque exerted by the hydraulic rotary motor
- Vibration of drill head
- Drilling displacement
- Compressed air pressure & flow

The following variable from drilling survey and rock analysis data were also used in this thesis.

- Hole dip angle
- Hole azimuth angle
- Uniaxial compressive strength of the rock

Hole No	Length (feet)	Inclination (degree)	Deviation Observed (feet)	Average Penetration Rate (in/min)
1 (R6H15)	137	82	7.216	7.2364
2 (R5H15)	140	82	7.897	6.0776
3 (R5H16)	143	88	3.096	7.2314
4 (R5H17)	120	84	3.798	6.0208
5 (R5H18)	88	72	10.397	6.2152
6 (R5H19a)	34	56	—	6.2705
7 (R5H19b)	68	56	6.008	7.1459
8 (R6H14)	225	77	22.427	6.2705
9 (R6H12)	67	67	17.637	9.4701
Total Drilling	1022			
A	230	Hole for core logging		
B	128	Hole for core logging		
C	140	Hole for cored logging		

Table 3.1: An overview of underground holes drilled at Little Stobie mine, Ontario.

3.4 Geological Context of Little Stobie

The data presented in this thesis was acquired from field experiments at INCO's Little Stobie Mine. The geology of the mine [33] is briefly described in the following.

The Little Stobie Mine geology is characteristic of the Sudbury District South Range ore deposits. The South Range contact deposits occur in depressions within the Footwall of the Sudbury Igneous Complex or as protrusions into the Footwall immediately adjacent to this contact.

The Little Stobie Mine comprises two orebodies. The first orebody occurs in a shallow embayment on the norite contact within the Sublayer, and extends some 610 meters in length. The second orebody is related to a zone of Footwall Breccia which is controlled by a granite-greenstone contact.

The orebodies are composed of a regular sequence of sulphides, within the Sublayer and consists, from hanging wall to footwall, of interstitial sulphide, ragged disseminated sulphide, gabbro-peridotite inclusion sulphide, inclusion-bearing massive sulphide and massive sulphide. The sulphide minerals consist primarily of pyrrhotite, pentlandite and chalcopyrite.

3.5 Preliminary Observations

The CD90B was a newly designed percussive drill from CMS. Therefore, one of the objectives of drilling experiments was to test the machine performance. It was also intended to find the suitable values of process variables for an efficient operation of the machine. A number of attempts were made for determination of optimal values of these variables, by running the machine at a several values of one parameter while keeping the other parameters constant and observing the response variables.

3.5.1 Effect of Feed on Drilling Performance

Feed force for a percussive drill is required in order to ensure that the bit is in good contact with the rock. When the piston strikes the bit, energy transfer from bit to rock takes place. A part of energy reflects back and travel in the form of stress waves. The reflected stress wave will first cause the bit and hammer to rebound and whole system will vibrate. The amount of reflected stress energy will depend on the rock properties and the amount of applied feed force. The feed force causes the bit to move back in contact with the rock prior to the next piston blow occurs.

To see the feed and penetration rate interrelationship, plot for feed and corresponding penetration rate from the data of hole 2 is shown in figure 3.5. The figure shows that an increase of feed causes increase of penetration rate up to the feed value of 2500 Lbs. The penetration rate decreases after further increase of the feed. In the figure 3.5c both feed and penetration rate values are plotted after proper scaling to see their interrelationship more clearly. It can be noticed that a maximum penetration rate is achieved when the feed value is close to 2500 Lbs. This shows that the optimal feed for this setup is 2500 Lbs. This result validates a previously obtained [32] result for percussive drilling.

The optimal feed observed seems to be different for other holes probably due to difference in the rock hardness. For example plot of Figure 3.6 shows a different value of optimal to feed. The maximum penetration rate in this case is obtained at feed value between 3000 to 3500 Lbs which is in between 225 seconds to 275 seconds of the figure 3.6. The higher value of feed has given lower penetration rate. At about 400 second the feed was suddenly decreased to 2800 Lbs. The penetration rate at this time increased to higher value. This shows that the optimal value of feed varies between 2500to 3500 Lbs.

The average penetration rate observed at both sites was in the range of 6 to 10 in/min.

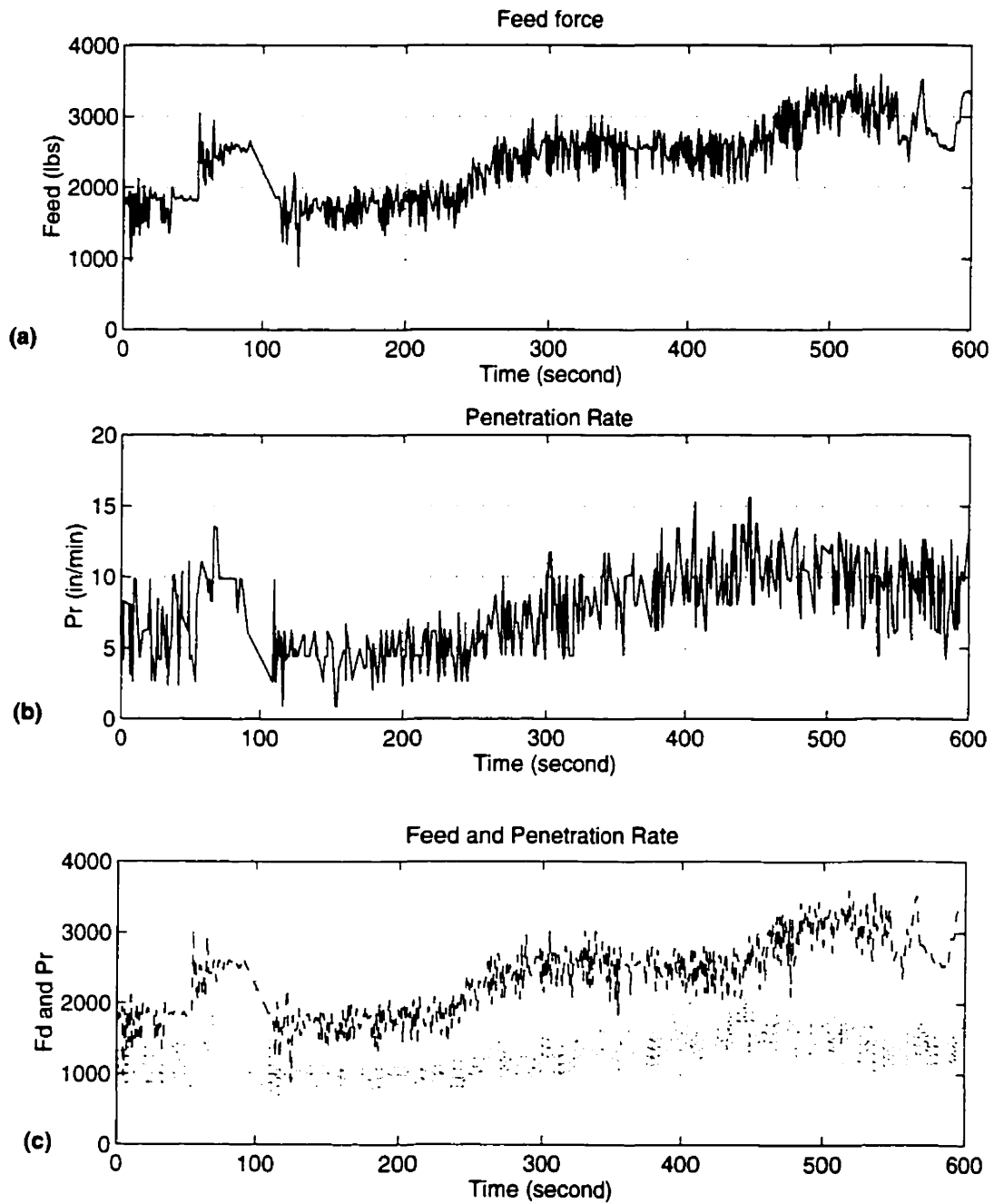


Figure 3.5: Feed and penetration rate from hole 2, (a) Feed force applied by the cylinder, (b) Corresponding penetration rate and (c) Two values are plotted together after suitable scaling to observe their interrelationship

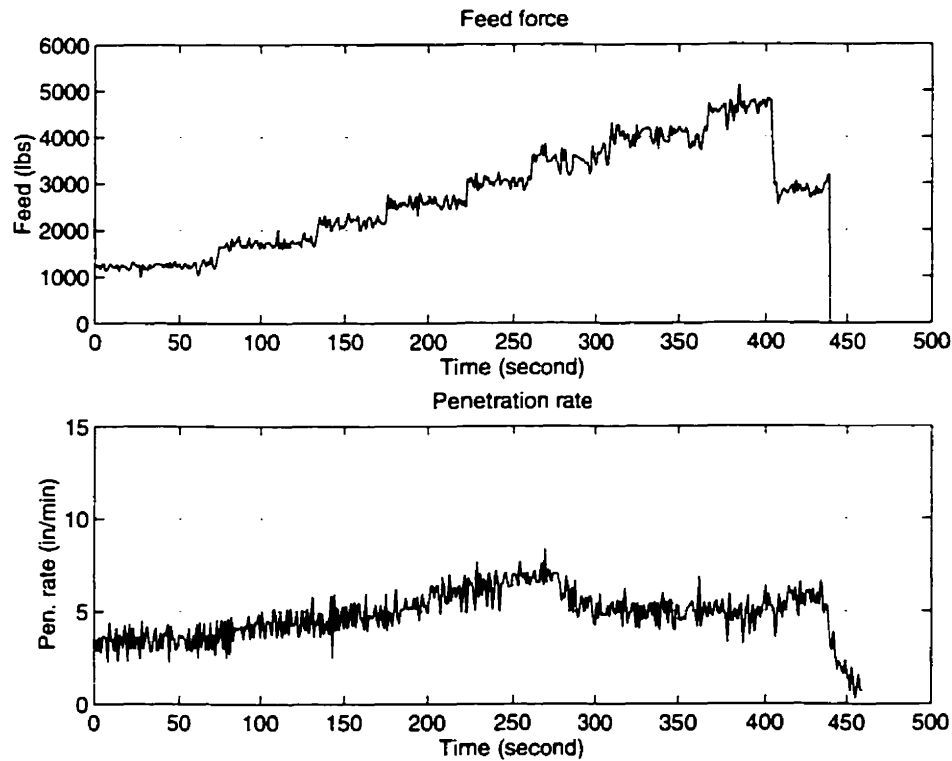


Figure 3.6: *Feed and Penetration rate (from hole 4)*

3.5.2 Effect of Torque on Performance

An excessive torque generated by the drilling process results in heavy loading of the rotary motor. If the load is so high that the required torque is beyond the power of the motor, the machine will stall and the drilling process will be interrupted. There are three possible sources of this loading, excessive feed force; hardness of the rock and improper cleaning condition of the hole. Whatever is the source of the high torque it will affect the machine performance. In order to study the machine behaviour at different torque values and to find the maximum value of torque that the motor could produce, several torque tests were performed. In these tests the feed was varied and the torque was observed while keeping all other machine variable constant. Plot of Figure 3.7 illustrates the result of one of these tests. Jamming was noticed at torque values higher than 3900 in-lbs. The corresponding feed was

equal or higher than 4800 Lbs.

During this test, feed was slowly increased (at 57th second in the figure 3.7), this resulted in a corresponding increase in the value of the torque, until a maximum value of torque was reached causing machine jamming at the 86th second. As can be seen from the figure at 86th second there is a sudden increase in the torque value as motor tried to avoid jamming by producing a higher torque. Correspondingly rotation stops as can be seen on the RPM plot (Figure 3.7c where speed drops to zero. At 99th seconds it comes out of jamming due to operator's interruption by reducing the applied feed value.

The feed was increased again slowly thereafter at 110th second. It was noticed that after 120th second machine rotation was at stick-slip. This can be seen by two torque spikes at 127 and 139th seconds. At these points machine stuck and rotation approached to zero. This gave an upper limit of torque value (close to 2500 in-lbs) which should be avoided for efficient drilling operation.

3.5.3 Effect of Feed on Vibration

The CD90B employs a shock absorber installed at the top of the percussive hammer in order to minimize transmission of hammer vibration to other parts of the machine. Some experiments were also performed to test the efficiency of the shock absorber. The vibration obtained at the head of CD90B was recorded. A detailed analysis and discussion on this vibration data is given in the chapter 7 of this thesis.

The data recorded during these tests showed that the vibration on the head is also a function of feed force. Figure 3.8 shows the feed and the average vertical vibration on the head of the drill. It can be seen that the average vertical vibration is less than 0.5g. The decrease of feed value causes an increase in the vibration. This result is expected since at lower feed the percussive energy has more tendency to

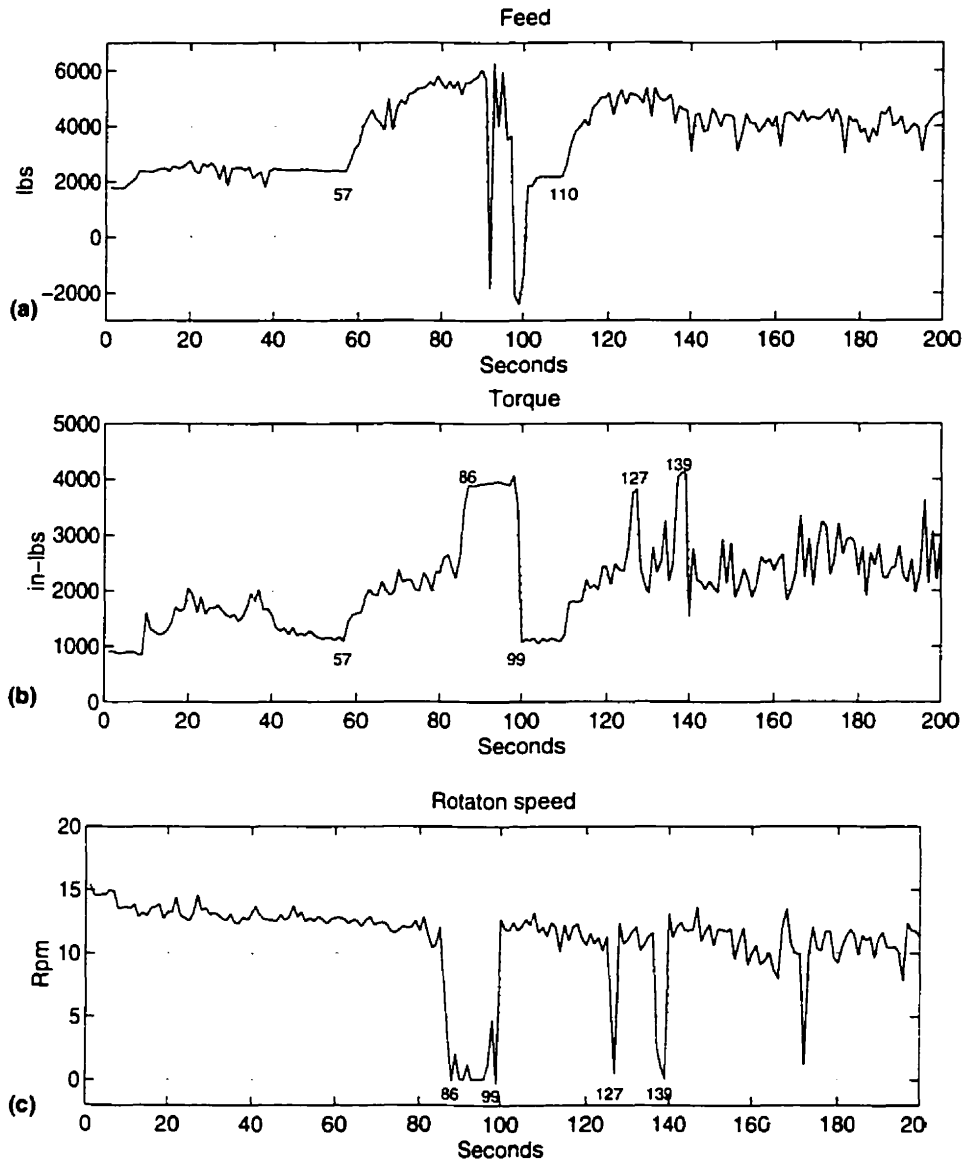


Figure 3.7: Torque on the bit and applied feed relationship: (a) the feed force, (b) corresponding torque on the bit and (c) rotation speed of the drill string. The numbers marked inside each plot indicates the time of corresponding value of the variable.

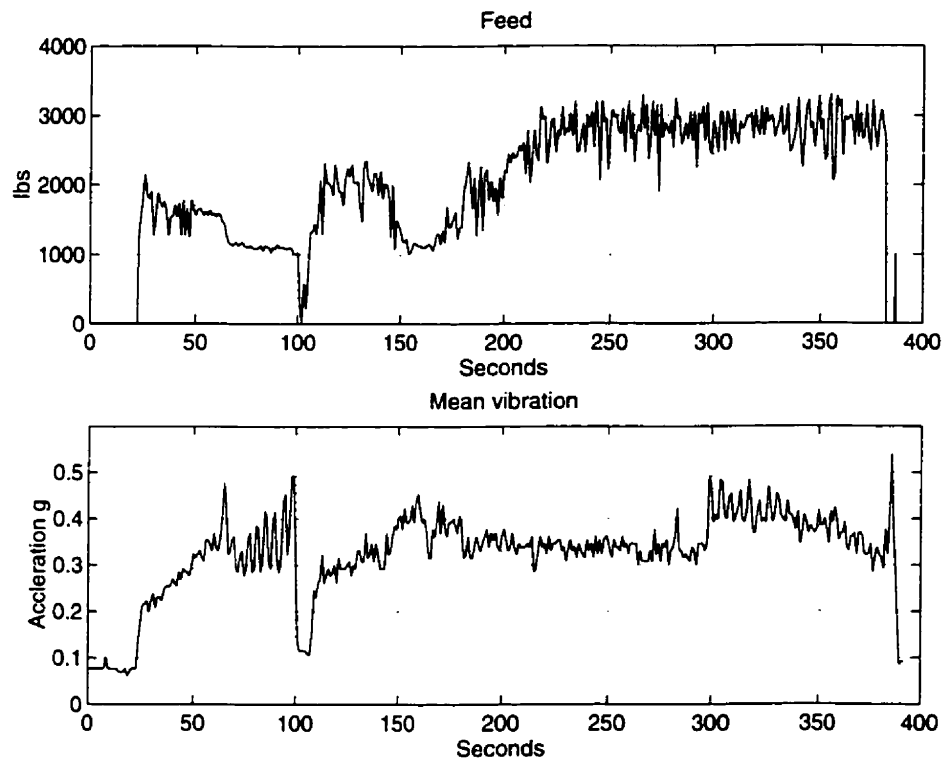


Figure 3.8: *Vibration level at drill head was noticed as increasing with decrease in applied feed value*

bounce back hence, a higher amplitude of vibration is transmitted. The inversely proportional relationship between the vibration and feed can more clearly be seen in the Figure 3.9 and Figure 3.10 in which portions of the data of the figure 3.8 has been plotted. In the figure 3.9 this data for 20-70th seconds is plotted and shows the effect of decrease in the feed on the vibration. While in figure 3.10 a data for 150-250 seconds is plotted and shows the effect of increase in feed on the vibration. It can be concluded from these results that for the feed values between 1200 to 3000 the vibration variations are approximately in the range of 0.5g to 0.3g with the shock-absorber installed on the hammer. This variation in the vibration is very small as compared to variation in the feed value, hence it is not advisable to control the vibration through feed. Instead, decrease in transmitted vibration should only be achieved by proper design of shock absorber.

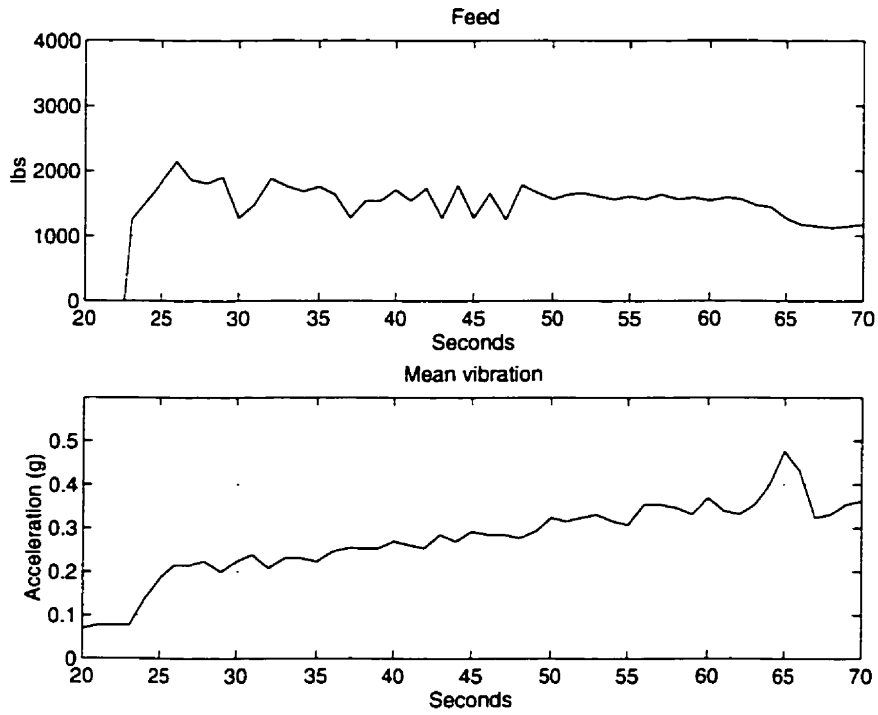


Figure 3.9: *Decrease in feed caused an increase in vibration*

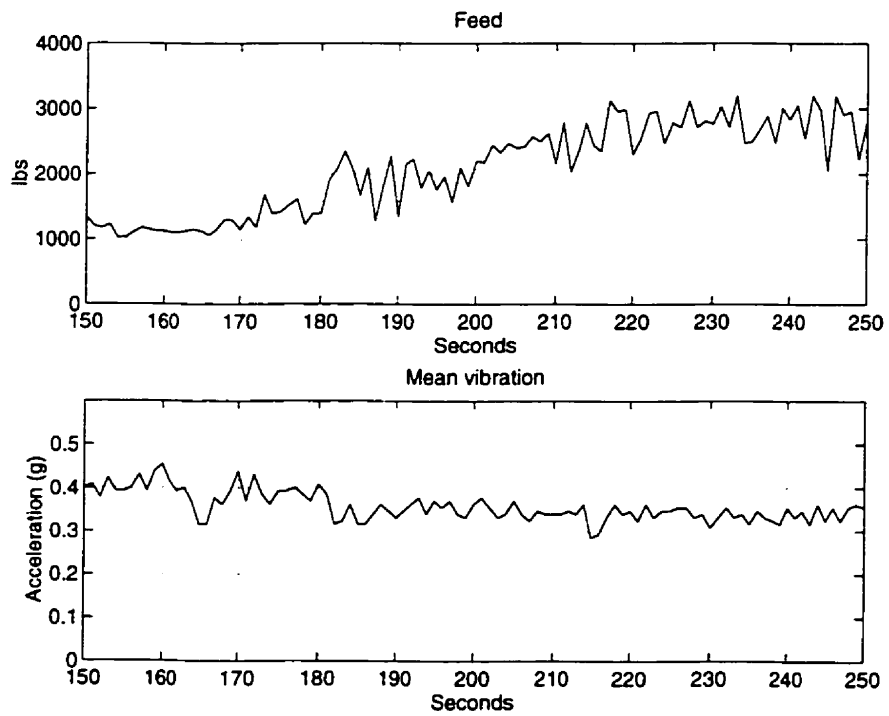


Figure 3.10: *Increase in feed caused decreased in vibration.*

3.6 Conclusion

In this chapter a brief explanation of data acquired from field experiments for percussive drilling process is given.

Preliminary observations show that there exists a correlation between the input variable, feed, and the output variables, penetration rate; torque; and vibration.

Average penetration measured for CD90B in hard rock (at Little Stobie Mine) varies between 6 to 9.4 in/min.

Drilling rate increases at an increase in applied feed until a optimal value of feed is reached. Further increase in feed value causes decrease in the penetration rate.

The maximum value of bit torque at which machine jamming was observed was 3900 in-lbs. Drill bit rotation at torque value above 2500 in-lbs is not smooth and tends to stall. The recommended torque value for smooth running is below 2500 lbs.

Vertical vibration transmitted from the percussive hammer through shock-absorber is a function of feed also. However there is only a slight variation in the vibration as a result of a wide variation in the feed. Maximum value of vibration observed was 0.5g.

Chapter 4

Drilling Performance Modelling

4.1 Introduction

Drilling process data acquired during the field experiments can be used for the purpose of developing a suitable model to represent the bit-rock interaction in the computer. The model obtained could be used for simulation of drilling process. A thorough analysis of the field data was conducted to achieve these results. In this chapter, we present the details of this data analysis.

Data analysis performed includes the study of the effects of machine input variables on machine performance and investigation of the optimal value of these variable for efficient machine operation.

To represent the rock hardness the specific energy of the rock was employed. Specific energy of the rock was calculated from the drilling data and its effect on drilling performance were studied. Comparison of specific energy with uniaxial compressive strength of the rock was also presented. Finally a correlation model to calculate an optimal feed value for a given rock hardness was also developed.

4.2 Parameter Correlations Study

4.2.1 Correlation between feed and penetration rate

Correlation between feed and penetration rate is shown in Figure 4.1. The data points for this plot are obtained by averaging the penetration and feed data around certain feed rates which vary gradually between 500 lbs to 5000 lbs.

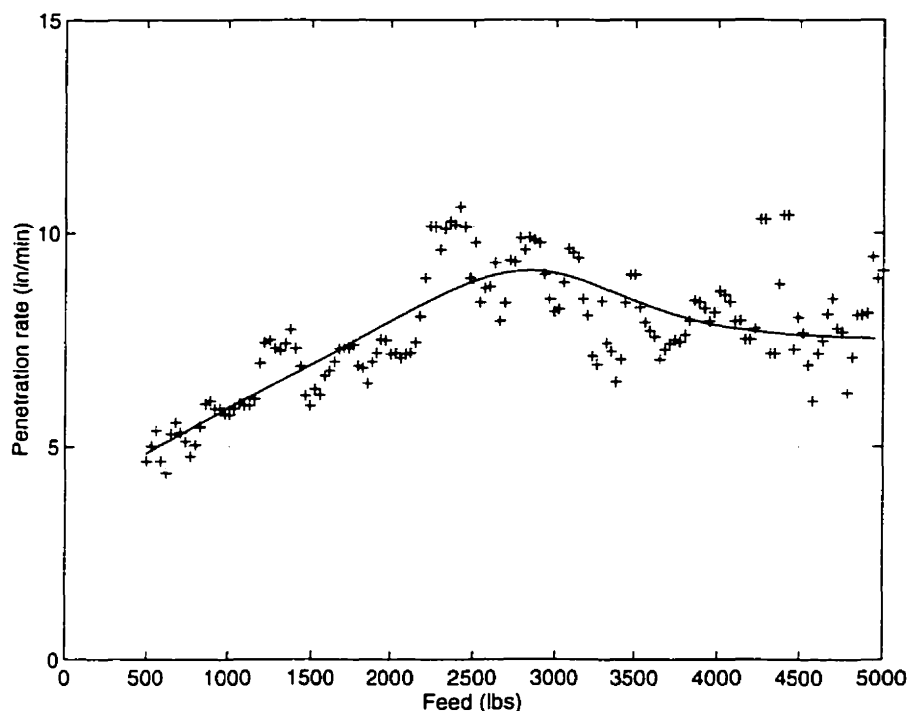


Figure 4.1: *Increasing of feed causes increase in penetration rate up to an optimal value of the feed, penetration rate decrease after that (result from hole 1)*

The plot shows reasonable correlation between the two parameters. There is a direct proportionality between feed and penetration rate for feed values of 500 lbs to 2400 lbs. The maximum value obtained is 11 *in/min* and is at the feed value of 2350 lbs. After the maximum value of penetration at an optimal feed value the penetration rate decreases. This implies that the optimal feed value for this setup is 2350 lbs. The solid line of the figure shows the fitted curve obtained for this data.

Similar results are obtained for other holes but with a different optimal feed force. This variation is probably due to variation in rock formation.

4.2.2 Correlation Between Feed Force and Torque

Variation in the torque has been found to be proportional to the feed force. This correlation is shown in Figure 4.2. This line fitting was done on the data of hole 1. Average values of the data were used for this curve fitting. The plot shows only the data for normal operation and does not include the jamming conditions. As can be seen that two parameters are directly related. The torque values for this results varies between 1200 to 2000 in-lbs.

The higher bit torque decreases the speed of the motor. As the torque increase with depth of the hole (due to increased loading) speed of motor slowly decrease with the depth. Figure 4.3 demonstrates this behaviour of the motor.

4.2.3 Feed and Vibration

Due to percussion of the bit, there is a continuous transmission of vibration from the bottom of the hole to the machine, which travels along the drill string. If this transmission is not reduced, it will cause the machine to vibrate may be up to a dangerous level. Generally, a shock absorber is installed on the hammer to minimize this transmission.

The data has shown a linear correlation between feed and vibration. The increase of feed has caused decrease in the vibration linearly see Figure 4.4. The average vibration observed in the drill head is 0.6g and the minimum is 0.15g. This variation in vibration was observed as a result of feed variation from 800 lbs to 5000 lbs.

A summary of the drilling performance analysis is given in the table 4.1. This table

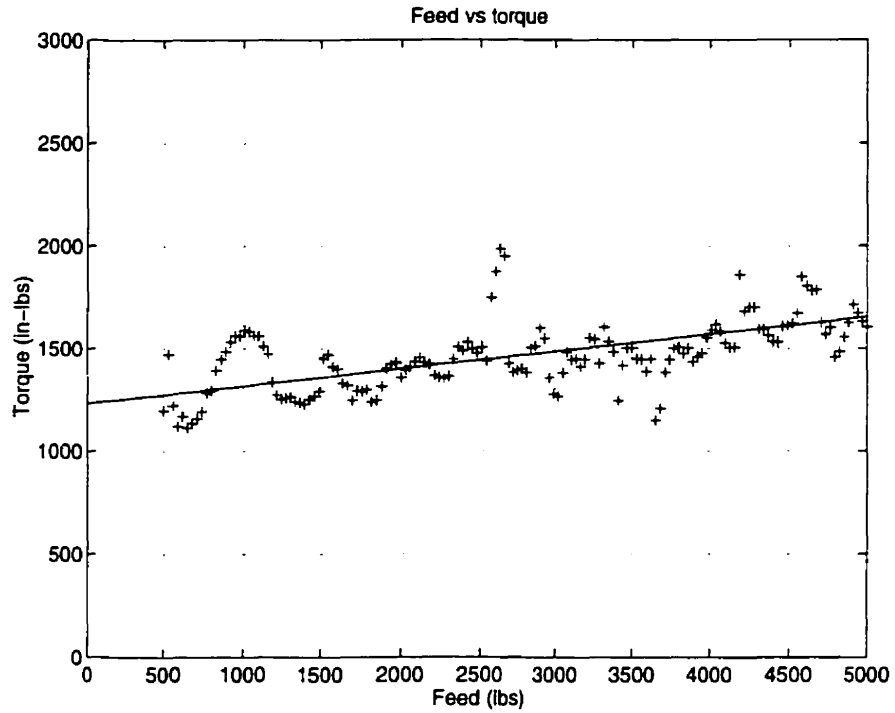


Figure 4.2: Increasing feed causes increased torque; the torque also increase with hole depth

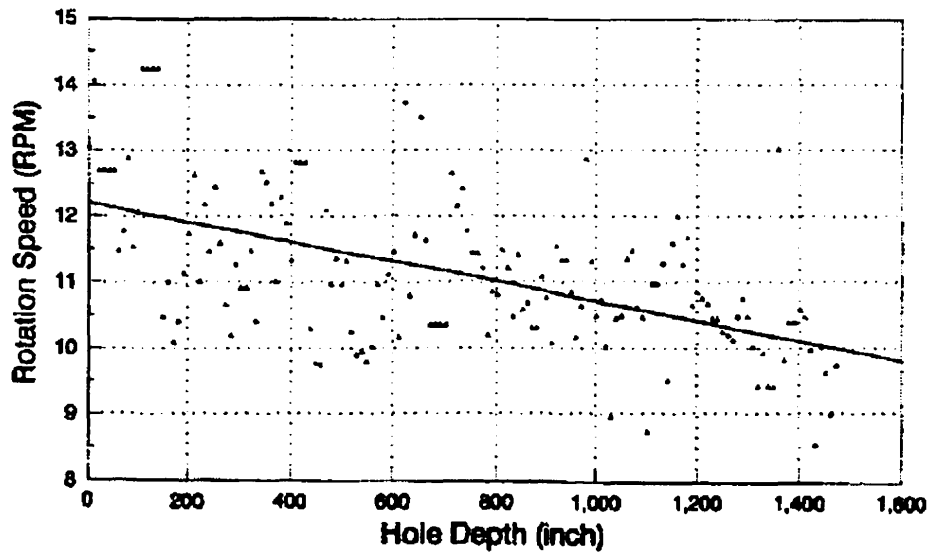


Figure 4.3: Effect of increasing of depth caused linearly decreases in the speed of the motor (This plot is taken from [33])

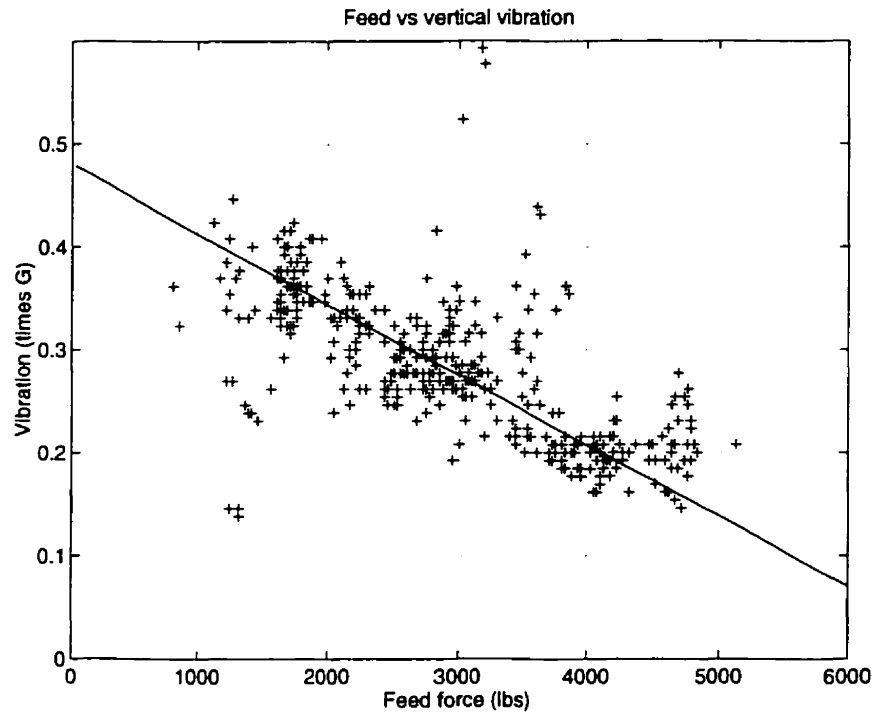


Figure 4.4: *Increasing of feed causes decrease in vibration.*

is prepared from the data of the hole 1. Similar results are obtained for other holes.

This table shows average values of torque, vibration and penetration rate of each applied feed. It can be concluded from the table listing that for an efficient operation feed values between 1600 lbs to 2000 lbs seems suitable. For this range of feed values the torque and the vibration are in their lower range whereas the penetration rate is in the higher range.

Feed force (lbs)	Torque range (lbs)	Vibration range times G	Penetration rate range (in/min)
800	833-1321(avg)	0.1-0.41(avg)	2.04-5.53(avg)
900	1250-1482(avg)	0.11-.41(avg)	5.83-9.16(avg)
1000	807-1980(avg)	0.18-0.41(avg)	6.82-13.60(avg)
1100	732-3688(avg)	0.16-0.54(avg)	5.07-13.50(avg)
1200	1026-4804(avg)	0.12-0.54(avg)	5.08-13.81(avg)
1300	1145-3881(avg)	0.19-0.59(avg)	5.16-14.28(avg)
1400	1159-4851(avg)	0.13-0.59(avg)	5.69-17.25(avg)
1500	1181-3999(avg)	0.12-0.61(avg)	5.04-13.88(avg)
1600	1116-4588(avg)	0.13-0.38(avg)	5.01-12.38(avg)
1700	1127-5057(avg)	0.17-0.25(avg)	5.37-14.97(avg)
1800	1174-3943(avg)	0.14-0.38(avg)	5.16-12.32(avg)
1900	1449-4046(avg)	0.12-0.35(avg)	5.32-16.94(avg)
2000	1733-5526(avg)	0.14-0.38(avg)	4.88-14.13(avg)
2100	1055-4858(avg)	0.14-0.33(avg)	4.84-10.34(avg)
2200	2087-5294(avg)	0.09-0.39(avg)	3.0-10.09(avg)

Table 4.1: An overview of drilling performance analysis. Variation of torque, vibration and penetration rate observed at different values of applied feed force in the data of hole No. 1

4.3 Specific Energy of the Rock

During a typical rock drilling process, hardness of the rock varies randomly. Drilling performance can significantly be improved if drilling parameters are continuously adjusted according to these changes. This requires an online measurement of the rock hardness. It is however, quite difficult to calculate this property during the drilling. Specific energy of the rock is one of the quantities that gives an approximate estimate of the rock hardness for a particular drill rig. The Specific Energy can be calculated on line during the drilling. It is therefore interesting to investigate its effects on performance.

In this section we use a conventional formula for calculation of the specific energy and modify it so that it could be used for machine performance analysis. The performance analysis is then presented in the subsequent section.

The concept of Specific Energy, SE, was proposed by Teale [84] as a quick means of assessing rock drillability. Teale defined SE as the energy required to remove a unit volume of rock. Since then, however, another definition of SE, in terms of new surface area created has appeared in the literature [61]. The two definitions appear to produce uncorrelated values. Teale showed also that the minimum value of SE is approximately equal to compressive strength of the rock.

The value of specific energy for a particular rock varies with drill type. e.g. Rabbia [69] has found that the specific energy for rotary drilling is higher than that for percussive drilling. Hence the value is associated with both the rock and drill type. It can therefore be more precisely referred to as Specific Fracture Energy.

Drilling data collected from the drilling experiments is employed to calculate the specific energy of the rock. Relationship between SE and other drilling parameters is also established. These results will be used in the design of the drilling control system.

An empirical formula given by Paone *et al.* [66] can be used to calculate the specific energy with minor modification. The specific energy SE was given by:

$$Se = \frac{4T_r P}{\pi d^2 P_r} \quad (4.1)$$

Where

Se is the energy required to produce a unit volume of rock ($in - lb/in^3$)

P is work rate ($in - lbs/min$) (total percussive energy)

P_r is penetration rate (in/min)

d is bit diameter and

T_r is the transfer ratio between energy transferred to the rock and the energy available for each blow.

Equation 4.1 does not include the effects of applied feed force on the specific energy. It assumes that a constant feed of optimal value at which a maximum energy transfer takes place was applied. The value of T_r was therefore, assumed as maximum equal to 0.8. If the applied feed varies it will effect the value of transfer ratio. The above equation will no longer be valid and needs modification to add the effect of thrust. The value of T_r assumes its maximum value at optimal feed force and lesser otherwise. For simplicity, it can be assumed that they are linearly related for feed value between zero and the optimal value. The value of T_r however, remains constant if applied feed is above the optimal value. i.e.

$$T_r = \begin{cases} aF + b & \text{for } 0 < F < F_{opt} \\ T_{rmax} & \text{for } F > F_{opt} \end{cases} \quad (4.2)$$

In the calculation we assumed maximum value of T_r as 0.8 at optimal feed value of 2500 lbs. The specific energy, after substitution of all the parameters is given by:

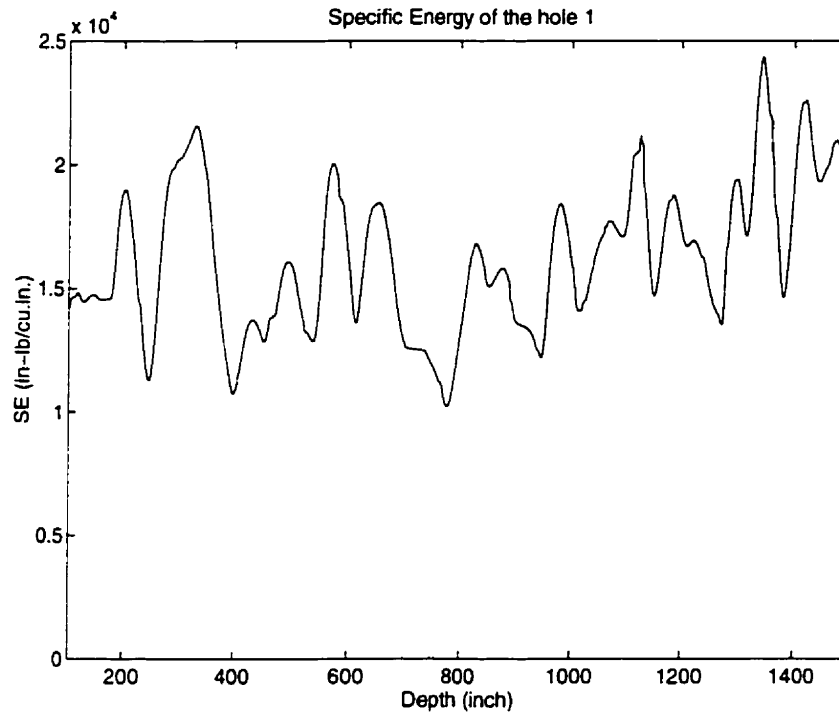


Figure 4.5: Plot of calculated specific energy for the hole 1

$$Se = \frac{T_r \times E_i \times f}{A_H P_r} \quad (4.3)$$

where

E_i is the input energy per blow supplied by the hammer

f is the blow frequency

d is diameter of the bit

A_H is the area of cross-section of the bit

The specific energy calculated using this equation for the hole no. 1 is plotted in the figure 4.5. The range of specific energy for this hole varies in between 1×10^4 to 2.5×10^4 in - lbs/in³

4.3.1 Comparison of Specific Energy with Uniaxial Compressive Strength of the Rock

The specific energy calculated from the drilling data depicts the strength of the rock being drilled. It can therefore be compared with the rock strength properties such as uniaxial compressive strength, tensile strength etc. Uniaxial compressive strength is more closely comparable to SE. The reason for this is that in percussive drilling the rock is broken by the action of crushing and chipping hence the breaking action is a work against the compressive strength of the rock.

During the drilling process monitoring experiments it was unfortunately not possible to measure the uniaxial compressive strength of the rock on line along the depth of the hole. In order to measure these properties three separate diamond drill holes were drilled. These are named A B and C in the figure 3.4. The core samples collected from these holes were analysed at the Rock Mechanics Laboratory of McGill University. The hole A was drilled closer to Hole 8 at a distance of 3 feet. Hole B closer to hole 2 with a distance of 5 feet and that the hole C is close to the holes 4 5 and 6. Data of only these adjacent holes can be compared. Rock strength analysis was not conducted at all lengths of the hole but only at selected lengths of the samples. Comparison can be made only at those selected lengths.

Figure 4.6 shows a comparison of SE of the hole 4 and the uniaxial compressive strength of hole C. The two plots agree with a reasonable accuracy. The SE plot of the figure is plotted after multiplying it with 1.4 for comparison purpose. Due to deviation of the holes it was not certain that the two equal depths of the two holes being compared represents the same rock formation. Therefore the UCS of a sample taken from a given depth was compared with the mean value of SE around the same depth of the test hole being compared.

Table 4.2 compares the calculated SE and the measure quantities of the rock UCS

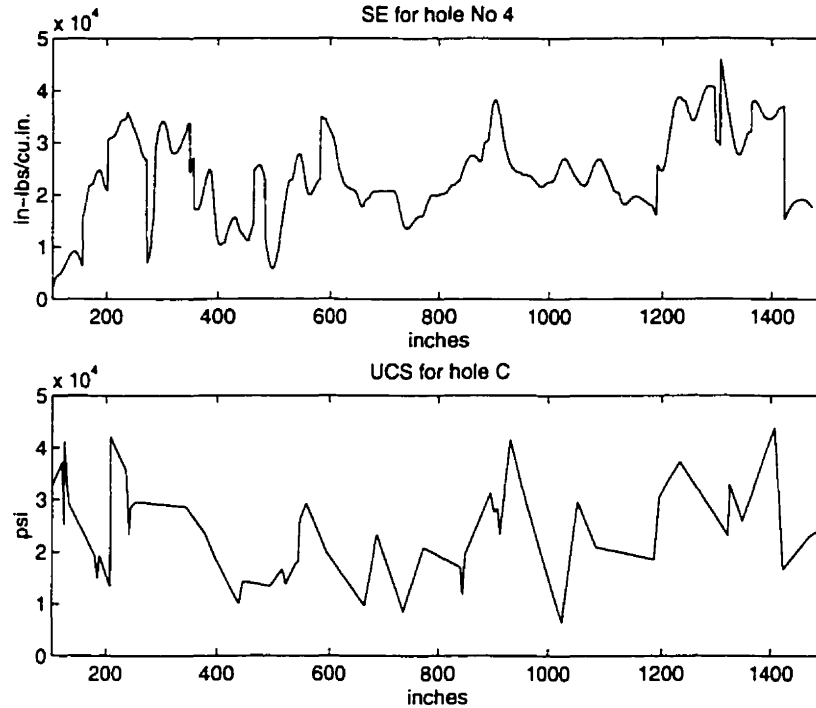


Figure 4.6: *Specific energy of hole 4 and the UCS for hole C. These holes were drilled at a distance of 3 feet. These quantities can therefore be compared. The comparison shows a small discrepancies between two plots.*

(uniaxial compressive strength) at some selected depths.

From the tables it can be noticed that the ratio of the uniaxial compressive strength and calculated specific is almost equal for all depths of the hole.

A linear relationship was established between compressive strength and the SE given by the following equation

$$UCS = K \times SE \quad (4.4)$$

where the value of K as estimated from the hole data varies between 1.3 to 1.5. This similar range of values of K were calculated in comparison of hole C with 3, as well as C with 4. However the value of K while comparing hole A with 8 varies between

Hole C		Hole 4		ratio K=UCS/SE
Depth	UCS	min-max	Average	
(feet)	(psi)	(in - lbs/in ³)		
5.18	23463	5752-22436	14848	1.44
10.17	25217	10276-12068	11226	1.70
20.17	23222	17544-21229	17081	1.36
31.60	23394	1304-21290	17891	1.30
41.08	13314	10061-12070	10178	1.31
49.51	19885	12642-24668	17240	1.15
64.42	20848	11014-24614	14701	1.42
74.38	31307	17172-25532	21568	1.45
75.79	23256	17084-18659	17800	1.31
90.56	20951	11991-18696	15533	1.35
99.64	30550	19941-25792	21273	1.44
109.95	22981	4902-20222	15128	1.52
122.28	22844	12793-15518	15621	1.46
134.09	17855	13846-13846	13846	1.29

Table 4.2: Comparison of calculated value of specific energy of rock of hole 4 and the uniaxial compressive strength of rock of adjacent diamond drilled hole C.

1.7 and 2.15. The reason for this is probably due to two reasons: firstly the distance between hole 8 and hole A is 5 feet whereas between C and 4 is only 1 foot, a less accurate comparison is therefore expected; and second the hole 8 was drilled in a different ring (ring 6) while hole 3, 4 and 5 are in ring 5. Hence, there is a possibility of different rock strength property.

4.4 Investigation of Effect of SE on Machine Performance

In order to study the machine performance with regards to change in the specific energy of the rock, a set of data was selected for analysis based on the following criteria:

- The data of only one mining site, Little Stobie mine, was used in this analysis.
- Data for the first ten rods only (55 feet) of each hole was included in this analysis since the penetration rate becomes less sensitive to the applied feed force at high rod weights.
- The data representing the stops and starts of machine was also discarded from the selected data.

This selected data was appended in one file. Then it was sorted in an ascending order of Specific energy. Other variables were sorted accordingly. The values of SE for the rock drilled at Little Stobie varies from 55 in-lbs/cu.in. to 5900 in-lbs/cu.in. Mean of SE is 15000 in-lbs/cu.in. This value of SE is approximately 1.4 times less than the uniaxial compressive strength of the rock.

The data of this calculated SE was then split in ten groups based on the specific energy. Each group was selected for a certain range of specific energy of the rock

Group No.	Specific Energy range	Average SE	mean Pr
	$(in - lbs/in^3)$	$(in - lbs/in^3)$	(in/min)
1	55–6899.9	5282.7	16.2
2	6808–9010	7912.0	12.4
3	9014–10926	10628.0	10.00
4	10934 –12629	11505	8.5
5	12630–13026	12540	7.50
6	13866–14765	14296	7.00
7	14705–15518	15416	6.50
8	15523–16541	16001	6.00
9	16565–17419	16984	5.50
10	19829–60630	----	4.50

Table 4.3: *Table of Specific energies selected for different groups*

as given in the table 4.3. The data length for each group was limited to 500 data points of each variable.

The plots of feed vs penetration rate of each group were drawn as given in Figures 4.7 to Figure 4.9 in order to investigate the relationship between two variables for different value of specific energy. A solid line in each plot of data set represents an average curve of the data set.

It was interesting to note that for each plot there existed a value of feed force which generated maximum penetration rate. In order to compare the fitted curves of each group these curves are plotted on a single graph shown in the figure 4.10. In this figure only selected eight curves are plotted the remaining being similar as compare to their adjacent group are not plotted. The '*' sign marked on each curve shows

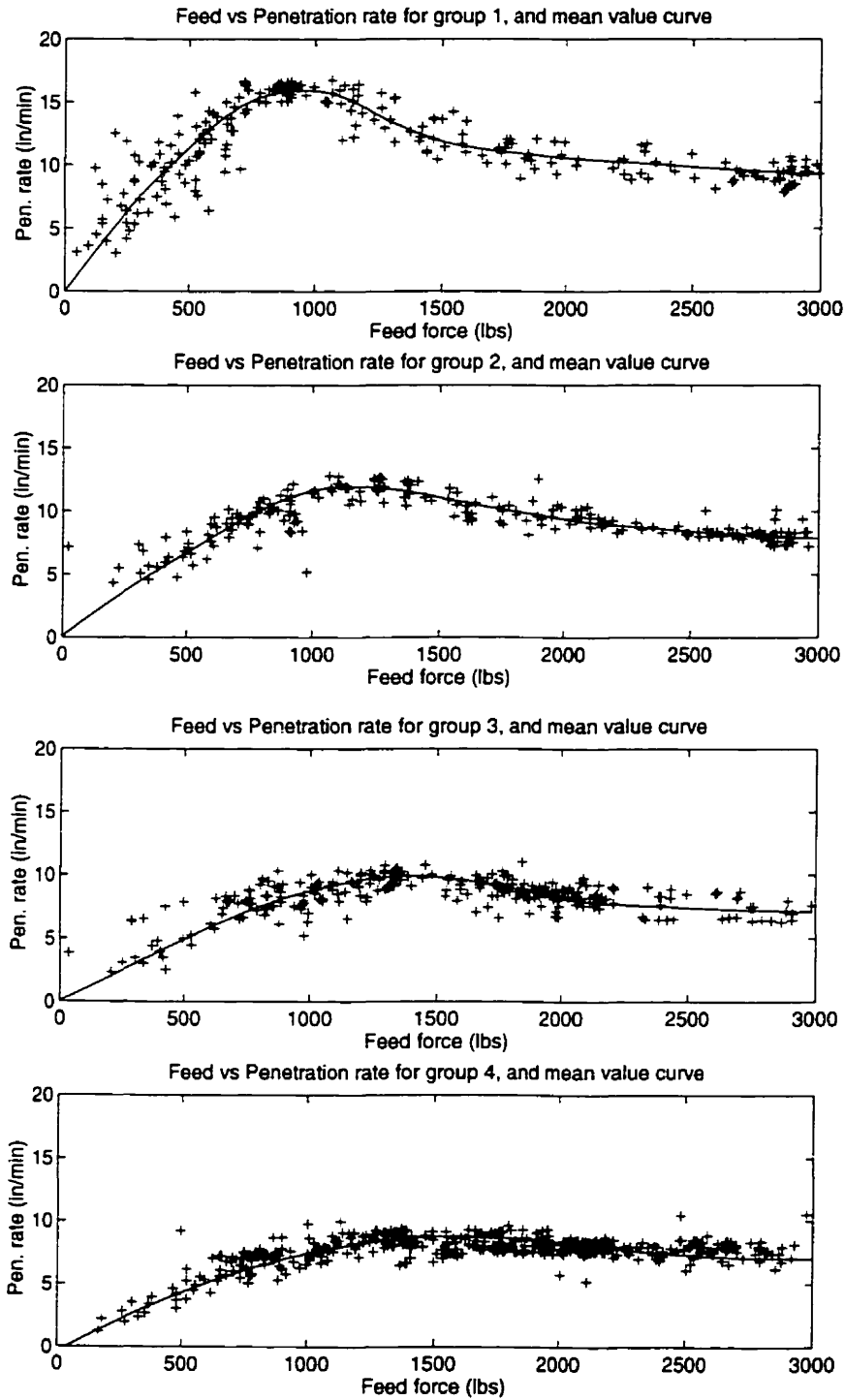


Figure 4.7: Feed vs penetration rate of data of group 1 to 4 with a average specific energy 5200, 7911, 10027 and 11505 in $-\text{lbs}/\text{in}^3$ respectively.

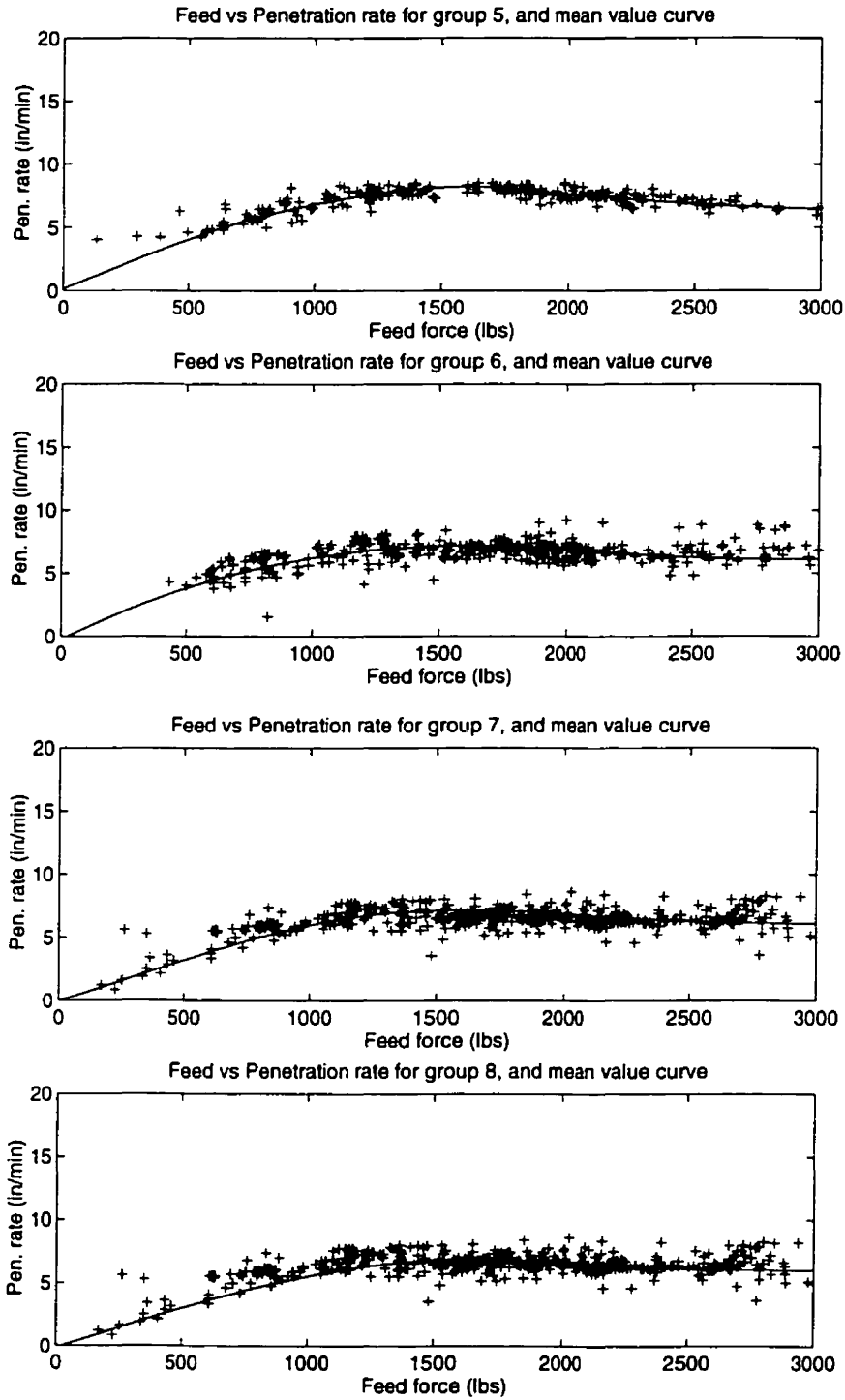


Figure 4.8: Feed vs penetration rate of data of group 5 to 8 with a average specific energy 12540, 14296, 15416 and 16001 in -- lbs/in^3 respectively

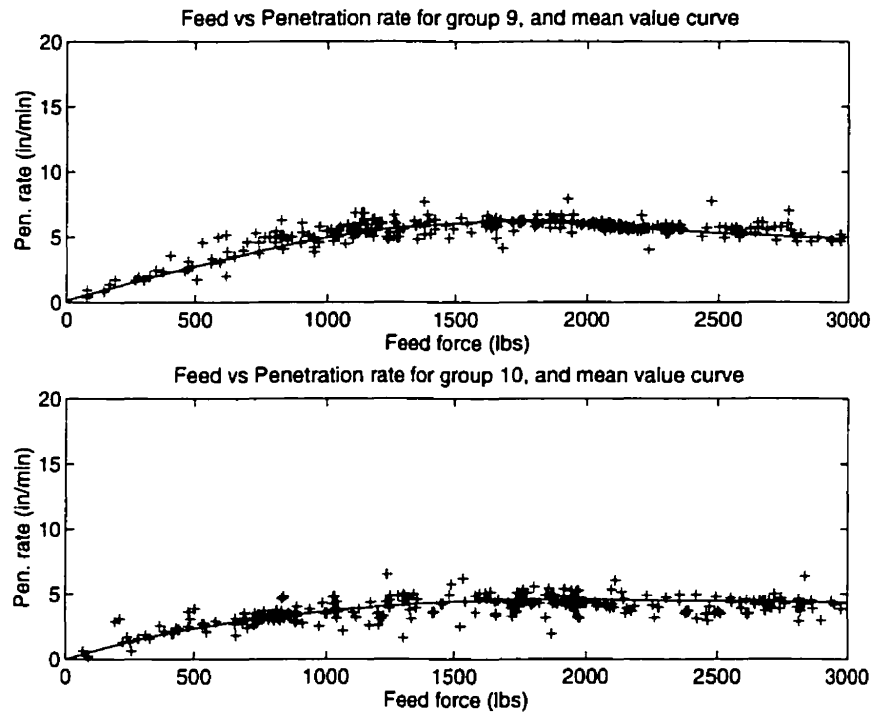


Figure 4.9: Feed vs penetration rate of data of group 9 and 10 with a average specific energy 16984 and 21668 $in - lbs/in^3$ respectively.

the maximum value of the penetration rate obtained. Joining these points for each set of data constitute a maximum penetration rate curve and is shown in the next figure 4.11. This curve gives an optimal value of the feed for a given SE to obtain a maximum penetration rate.

A correlation between specific energy of the rock for percussive drills and the optimal feed force required to achieve maximum penetration can be formulated for this result. The plot of figure 4.12 gives this correlation. Using nonlinear polynomial curve fitting technique a 3rd order polynomial was suitably fitted in these data points. The curve is good for the value of SE between 5000 $in - lbs/in^3$ and 50000 $in - lbs/in^3$. However it is not defined beyond these limits. In fact there was no drilling data available for a feed value less than 700 lbs. Similarly feed value for specific energy above 5000 $in - lbs/in^3$ remains its maximum value of F_{max} for maximum penetration rate. Therefore the optimal feed can be defined as follows:

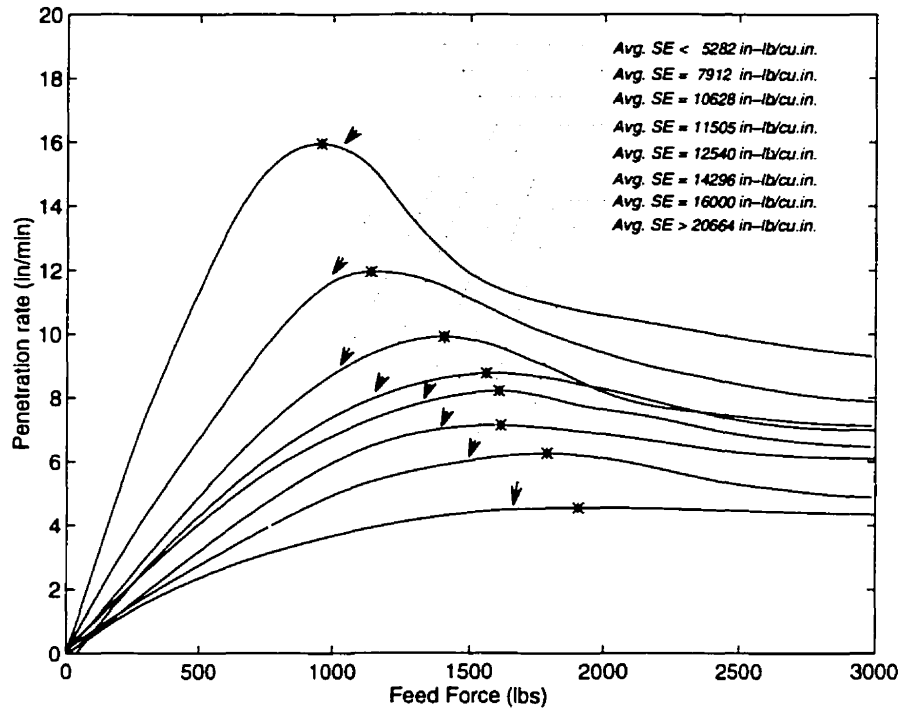


Figure 4.10: Comparison of Feed vs Penetration rate plots for different specific energies.

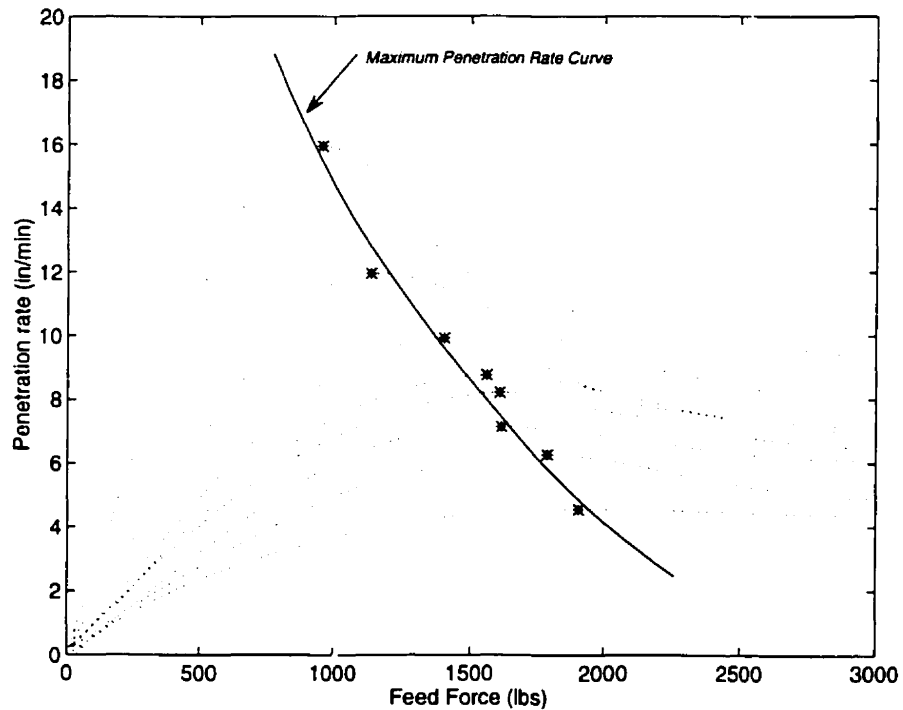


Figure 4.11: Maximum Penetration rate for different Specific energies

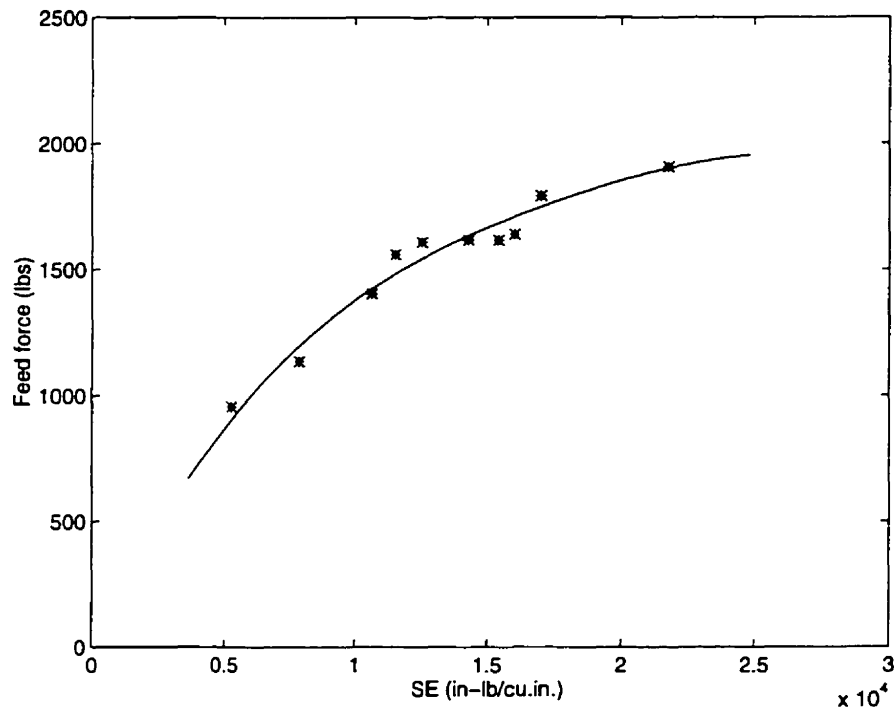


Figure 4.12: Optimal feed value curve for maximum production (Penetration rate).

$$F_{opt} = \begin{cases} aS_e^3 + bS_e^2 + cS_e + d & \text{for } SE_{min} < S_e < SE_{max} \\ F_{max} & \text{for } S_e > SE_{max} \end{cases} \quad (4.5)$$

As this relationship can be used to calculate a the optimal feed force require for a maximum penetration rate, we will use this as control strategy in the simulator for percussive drilling process discussed in the chapter 6. The estimated value of a b c and d for a 3rd order polynomial are 4.9968×10^{-11} , -5.0622×10^{-6} , 1.7244×10^{-1} and 2.5690 respectively.

4.5 Conclusion

The data acquired for percussive drilling process was analyzed in this chapter.

The relationship of feed with torque, penetration rate, and vibration was discussed. This reveals that there exists a correlation between the input variable, feed, and the output variables, penetration rate; torque; and vibration.

It can therefore be concluded that feed is an important input variable in percussive drilling and can be employed for controlling the percussive drilling process. The feed can be manipulated to control all the output variables and an optimal feed value can be obtained for an efficient operation of the process.

A detailed analysis was also conducted to correlate the specific energy of the rock with the drilling machine variables. It was found that there exists a feed value for each value of specific energy of the rock for which a maximum penetration rate can be achieved.

An empirical model to calculate the optimal feed value for a given specific energy of the rock was also formulated

Chapter 5

Development of Drilling Process Simulation Model

5.1 Introduction

We intend to formulate a strategy to control the drilling process for increasing drilling process efficiency in the next the chapter. The control algorithm obtained will be evaluated through computer simulations. In order to simulate the drilling process a simulation model will be required. This chapter concentrates on the development of the simulation model to be used in these simulation.

The simulation model developed in this chapter includes development of input-output models of only those sections of the drilling system which are necessary for the development a control system simulator. It therefore, does not include structural modelling of the drill rig.

In this regards we first develop analytical models of the feed system and percussive hammer. We then describe the modelling of bit-rock interaction to predict penetration rate and bit torque using experimental data.

5.2 Drilling Process Model

Drilling process can be divided into two parts as shown in the figure 5.1 the drilling machine model and the bit-rock interaction.

Model of the first block, the machine model, can be developed using basic physical laws and linear system theory. Due to linear nature of the response in the operation range. Conventional linear controller such as proportional, PI, and PID controller can easily be designed for all subsystems of this block. Among the subsystems of this block are rotation system, feed pressure system and the percussive hammer. Practically there are three physical inputs to this block, the compressed air for the percussive hammer, feed set-point (adjustable by the operator) and the rotation speed set-point (also adjustable).

The bit-rock interaction, on the other hand, is a complicated process due to the random variation in the rock property along the drill length and nonlinear response to its inputs. Outputs of the previous block (machine model) are the inputs to this block. Response to the inputs (outputs of the block) are the penetration rate, the vibrations and the load torque. Design of a control system will be incomplete without including the effect of this block on the drilling performance. Due to complexity of the process conventional linear system theory cannot be employed for developing the model of this process. An empirical approach with the help of field data to represent this interaction is therefore adapted.

5.3 Machine Model

A percussive drill (such as CD90B) consists of three systems. The percussive hammer, the rotation system and the feed system. The percussive hammer takes compressed air and responds with impacts on the rock at a certain blow rate causing

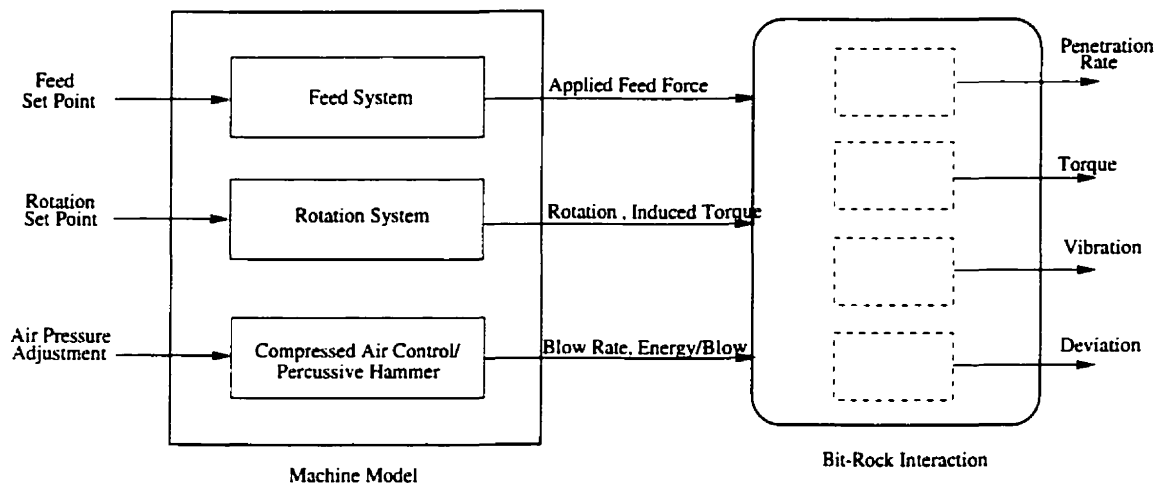


Figure 5.1: *Drilling system block model*

rock fragmentation. The feed system applies a force proportional to its input set-point, to the drill string to keep the bit in contact with the rock. The rotation system employs a hydraulic motor to rotate the bit between two consecutive impacts. Torque applied by this motor varies with the load. All these three systems are isolated from each other. Hence each can be modelled separately. They interact only in loading conditions when the complete system is taken into account, including bit-rock interaction.

5.3.1 Feed System

During the process of rock drilling a feed force is applied on the bit in order to keep the bit in contact with the rock. The feed system of the drill rig supplies this force. Figure 5.2 shows the schematic of the feed system. Power cylinder shown in the figure provides the feed force to the hammer as a result of differential pressure across the cylinder. This differential pressure is maintained by the differential pressure control valve.

The feed system is therefore consisted of the model of electro-hydraulic servo valve

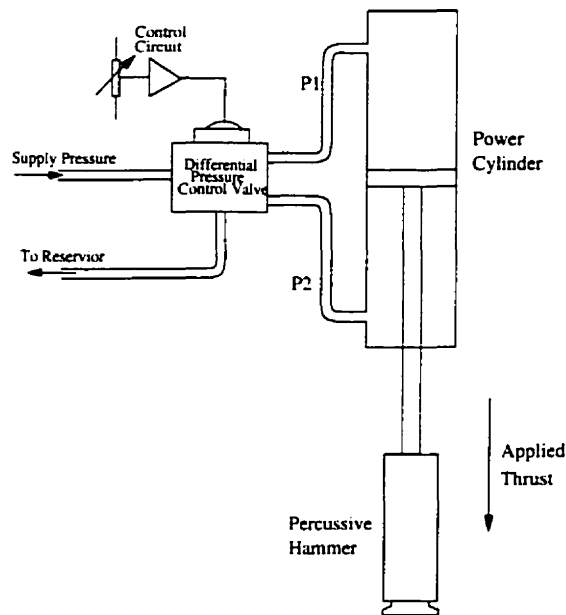


Figure 5.2: Schematic diagram of feed system

and the model of feed cylinder. The model of the electro-hydraulic valve is taken from Anderson [2] which is given in Appendix A of this thesis. It is also briefly described here in the following.

Diagram of the electro-hydraulic valve is shown in figure A.1 in appendix A. As clear from the figure there are two stages in the valves, the pilot stage and the boost stage. The pilot stage provides a differential pressure at small flow rate. The boost stage becomes a power amplifier so that it will reproduce the pilot pressures at much higher flow rate than the pilot stage alone could produce.

The pilot stage consists of a magnetic circuit and a hydraulic circuit. The magnetic circuit of the pilot stage provides movement of the flapper at the nozzles in order to activate the hydraulic circuit for a given electrical input signal. This circuit produces a torque in the armature to move it against the effective spring of the pivot plate. The resulting movement on the armature is reflected on the flapper through the pivot. This flapper movement, with respect to the nozzle, is the valve

input to the hydraulic circuit. The hydraulic circuit of the pilot stage uses the position created by an electro-magnetic circuit to create an unbalance. This results in building differential pressure across the nozzles and therefore across the output ports of the valve.

torque output (T) produced by the combination of the permanent magnet and the coil is proportional to the input current and the decentring spring rate given by:

$$T = K_{tm}I + K_m\alpha \quad (5.1)$$

where

K_{tm} = main torque motor gain (in-lb/mA)

K_m = magnetic decentring spring rate (in-lb/rad)

I = input current (mA)

α = angular position of armature

Torque motor's influence on the system takes place inside the close loop. The net torque is therefore given by:

$$\Sigma T = J\alpha = J\ddot{\theta} \quad (5.2)$$

This results in an equation A.3 (appendix A)

$$J\ddot{\theta} + f\dot{\theta} + K_x\theta = (T_i - T_{fb}) = Te \quad (5.3)$$

where

θ = armature and flapper rotation

J = polar inertia of armature and flapper

f = velocity coefficient of friction

$K_x = K_p - K_m + K_oL_o^2$

T_{fb} = feed back torque

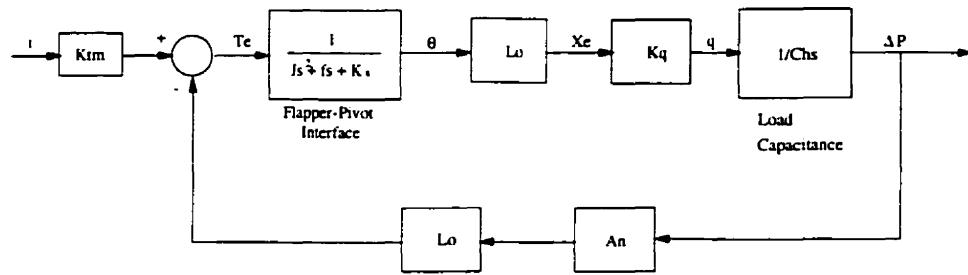


Figure 5.3: Block diagram of electro hydraulic differential pressure control valve for controlling the feed pressure across the feed cylinder

K_p = Stiffness of the torque armature pivot (in-lb/rad)

K_m = Magnetic decentring stiffness (in-lb/rad)

$K_p L_o^2$ = defective stiffness of the oil in its chamber.

L_o = Length of linkage

The Laplace transform of the equation 5.3 results in a transfer function of the magnetic circuit.

$$\frac{\theta(s)}{T_e} = \frac{1}{Js^2 + fs + K_x}$$

Transfer function for this hydraulic circuit of the servo valve is given by the equation A.13 of appendix A.

$$\frac{\Delta P(s)}{\theta(s)} = \frac{L_o K_q}{C_h s} \tag{5.4}$$

Figure 5.3 is the block diagram of the valve dynamics. In the diagram the feedback torque is represented by the $(T_{fb} = A_n L_o)$.

where

K_q = Flow gain

Ch = Hydraulic capacitance of main cylinder

A_n = Area of cross section of nozzle

K_{tm} = Torque motor gain

Transfer function of the system of the figure 5.3 is therefore:

$$\frac{\Delta P(s)}{I(s)} = \frac{K_q L_o}{C_h s^3 + C_h f s^2 + K_x C_h s + K_q L_o^2 A_n} \quad (5.5)$$

In the percussive drill rig CD90B, input current is supplied by a separate power control circuit that takes voltage as inputs. Assuming K_{pc} is gain of this power control circuit:

$$\frac{\Delta P(s)}{V(s)} = \frac{K_{pc} K_q L_o}{C_h s^3 + C_h f s^2 + K_x C_h s + K_q L_o^2 A_n} \quad (5.6)$$

The system of equation 5.6 represents the feed system model of the figure 5.2. Response to the set-point tracking of this system was compared with the real data in order to validate the model. A set of data recorded during rod pulling out shows a set-point tracking of the real machine this is shown in figure 5.4b. The response to the same inputs for set-point tracking of the servo model of the equation is in figure 5.4c. The two plots agrees with a reasonable accuracy. The values of the parameters used for this simulation are given in the table A.1 of appendix A.

To control the feed force output of this system a linear PID (Proportional plus Integral plus Derivative) type controller was designed. The transfer function of this controller is given by:

$$u(s) = K \left(1 + \frac{1}{T_I s} + \frac{T_D s}{1 + T_D s / N} \right) e(s) \quad (5.7)$$

Where $u(s)$ and $e(s)$ are the Laplace transform of the controller output and the error signal, respectively; K is the proportional gain; T_I is the integral, or reset time; and T_D is the derivative time, In the controller there is a filter, with time constant t_D/N , for the derivative part. This time constant is controlled by N which is often in the range of 3-10 and is usually fixed by the manufacturer of the controller [5].

The tuning of the PID controller for the simulator was done using rules set by Ziegler and Nichols. The values of the parameters such obtained are: $K = 11.73$; $T_I = 3.85$;

$$T_D = 0.238;$$

The response to set-point tracking of the model with PID is the figure 5.4d. The response shows damped system. This was intentionally designed to avoid overshooting in the response.

Drilling process simulator will be using discrete time data collected from the field experiments stored in a file. This field data was digitized at a sampling frequency of 1Hz. Transfer function of the equation 5.6 was sampled at the same frequency for obtaining its discrete time equivalent. Because of lower sampling frequency a faster dynamical parts of the servo valve, the flapper-pivot interface shown in the figure A.2 can be minimized to simply a gain of $1/K_x$. Replacing this value the equation 5.6 reduces to:

$$G(s) = \frac{K_{pc}L_oK_q}{K_xC_h s + K_qL_o^2A_n} \quad (5.8)$$

The discrete time equivalent of the model can be obtained by taking z-transform with zero order hold at T sampling period. This gives the following transfer function.

$$G(z) = \frac{K_{pc}L_oK_qT}{K_xC_h z + K_qTL_o^2A_n - 1} \quad (5.9)$$

Finally, the applied feed force by feed cylinder denoted by F_c (controlled feed) is the product of pressure across the piston of feed cylinder and the area the piston A_p .

$$F_c(t) = G(z).A_p V(t) \quad (5.10)$$

Equation 5.10 represents the feed system of percussive drilling rig and will be used in simulation of the process.

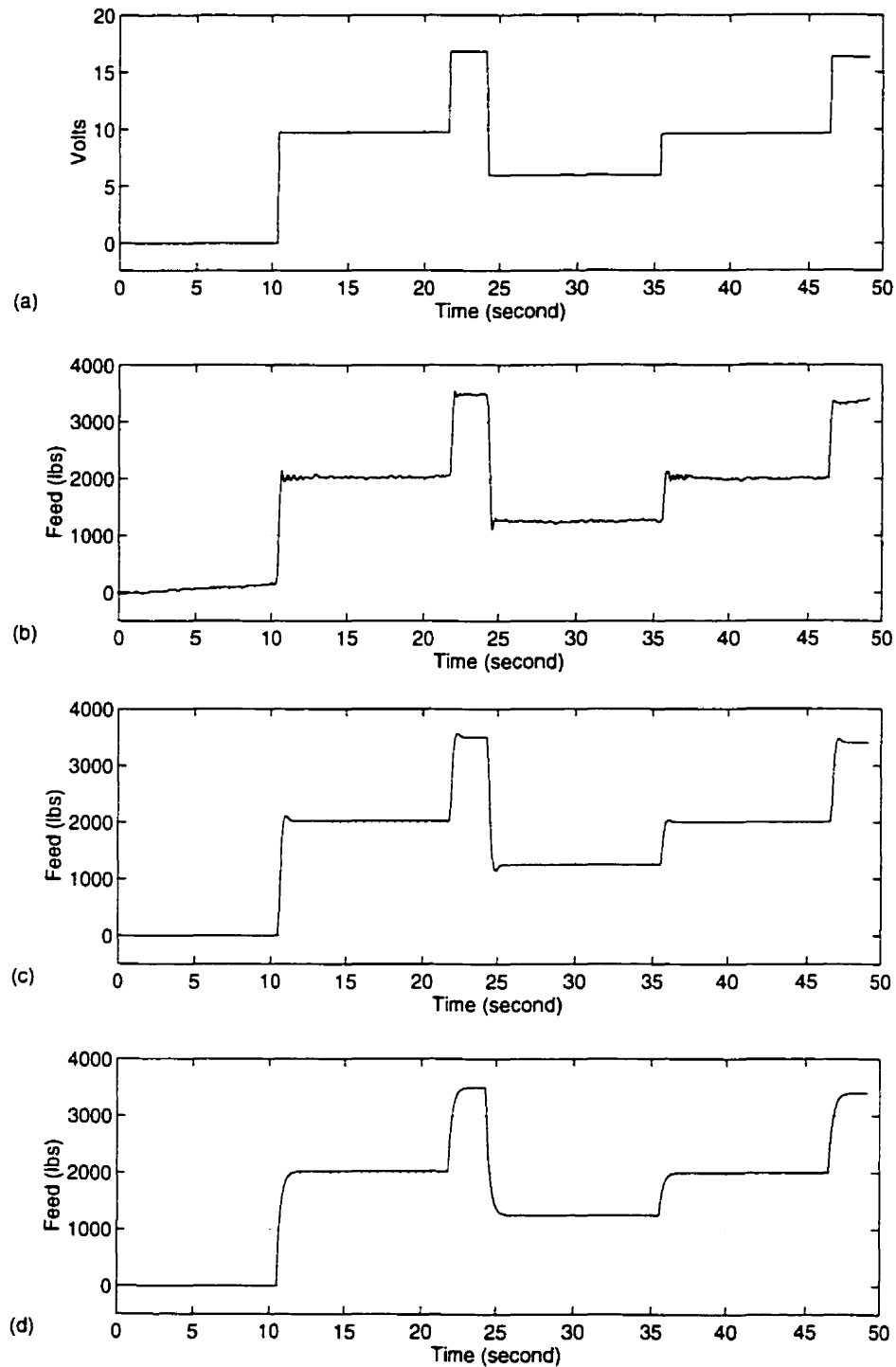


Figure 5.4: Set-point tracking of feed system (a) input voltage, (b) response of actual machine, (c) response of the model obtained for feed system and (d) response of model with PID controller.

5.3.2 Percussive Hammer

In a percussive drilling process it is the percussive action of the bit which causes breakage of the rock. The energy delivered to the rock by the percussive hammer is proportional to the rock fragmentation [29]. In a typical percussive cycle the piston is initially at rest when air with a pressure p is admitted to the cylinder. Assuming that the pressure remains constant during the whole cycle, the time t_1 required to move the piston for forward stroke

$$t_1 = \sqrt{\frac{SW}{6pAg}} \quad (5.11)$$

Where:

W=weight of piston (Lbs)

S=piston stroke (*in*)

A=Area of piston head (*in*²)

g=acceleration of gravity (*ft/sec*²)

t_1 =time of forward stroke (sec.)

If $K_1 t_1$ is the time for the backward stroke and $K_2 t_1$ the time it rests then the frequency of the stroke percussive action can be calculated as follows

$$f = \frac{60}{1 + K_1 + K_2} \sqrt{\frac{6pAg}{SW}} \quad \text{blows/min} \quad (5.12)$$

Piston rest time is too small as compared to travel time, hence the value of K_2 is assume equal to zero. Then the hammer frequency can be given by

$$f = \frac{60}{1 + K_1} \sqrt{\frac{6pAg}{SW}} \quad (5.13)$$

by assuming forward and backward strokes equal the above equation will be simplified as

$$f = 30\sqrt{\frac{6p.Ag}{SW}} \quad (5.14)$$

More general form of this equation is

$$f = K_o\sqrt{\frac{6p.Ag}{SW}} \quad (5.15)$$

where K_o varies with hammer configuration. Hustrulid assumed this variation between 20 and 30 in [29].

The velocity at which the piston impacts the end of the drill bit is given by:

$$V_s = \sqrt{\frac{Sp.Ag}{6W}} \quad (5.16)$$

where V_s is piston impact velocity (ft/sec).

In more general form equation 5.16 can be written as

$$V_s = \beta_o\sqrt{\frac{Sp.Ag}{6W}} \quad (5.17)$$

where β_o is constant.

Combining two equations we have

$$V_s = \frac{S\beta_o}{6K_o}f \quad (5.18)$$

and impact energy E_i is given by

$$E_i = \frac{1}{2}\frac{W}{g}V_s^2 \quad (5.19)$$

Substituting value of V_s form equation 5.17 we obtain

$$E_i = \frac{p \cdot A S \beta_o^2}{12} \quad (5.20)$$

This impact energy supplied to the rock by the hammer in each blow. If the frequency of the blows is f , the average energy delivered to the rock can be calculated as

$$E_{avg} = f E_i \quad ft - lbs/min. \quad (5.21)$$

This is main breaking energy delivered to the rock in the forms of impacts. This impacting energy transfers to the rock in the form of compression waves. The breakage of rock is a result of the interaction between these compression wave and the rock matrix [70].

5.3.3 Rotary Motor Applied Torque

Rotation to the bit of CD90B drill is provided by a hydraulic motor. It uses a Sauer Sundstrand Series 40 M46 Axial piston fixed displacement type motor. The purpose of rotation of the bit during drilling is to provide indexing to bit strokes and enabling the bit to break the rock in an efficient way. It can also provide some sheer force for the bit to chip away rock at the bottom of the hole with independent rotary action [33]. The motor produces a torque required to maintain the bit rotation. The value of this torque depends upon the bit loading conditions. The bit loading is caused by certain parameter s.a. applied feed force, hardness of the rock facing bit and the cleaning conditions of the hole. Among these factor the applied feed force is a variable that can be manipulated. The relationship between the applied feed force and the motor torque is proportional provided that all other parameters are kept constant [32]. This was illustrated in Figure 4.2, and will be discussed latter in the section of bit-rock interaction.

There always exists a maximum value of torque, M_{max} that a motor can produce. If the required value of the torque exceeds this point due to excessive loading, a jamming of drill string occurs causing an interruption in the drilling process. The control of this parameter is therefore important for an efficient control of drilling process. The drilling parameter should be adjusted so that torque does not exceed its maximum value.

The net torque generated by the motor is the sum of “no load” torque and the torque generated due to loading.

$$M_{net} = M_{nl} + M_{ld} \quad (5.22)$$

Conversely the torque generated due to the bit loading is equal to the total torque generated by motor minus the no load torque. This loading torque is due to rock-bit interaction.

$$M_{rb} = M_{ld} = M_{net} - M_{nl} \quad (5.23)$$

The no load torque is the minimum value of torque required to rotate the motor and was recorded for CD90B during a no load running tests of the machine. This value of the torque varies between 1000-1200 in-lbs. The torque is proportional to the differential pressure across the inlet and outlet ports of the rotary motor [33].

$$M = \frac{pq}{2\pi\eta} \quad \text{or} \quad M = \frac{(P_{in} - P_{out})q}{2\pi\eta} \quad (5.24)$$

where

M = torque produced by motor

p = differential pressure $p = P_{in} - P_{out}$

P_{in}, P_{out} = inlet and outlet pressures of the motor

q = geometrical displacement of the motor

η = efficiency of the motor

5.4 Bit-Rock Interaction

Machine model developed in the previous section supplies the breaking energy to rock. The bit-rock interaction is the actual process of rock breakage. There are three ways machine supplies its energy to the rock; the weight on bit; the percussive energy through hammer; and the bit rotation. These three inputs of the bit-rock interaction model interacts to exhibit penetration rate, vibration and loading torque.

5.4.1 Prediction of Penetration Rate

Penetration rate of in percussive drilling depends upon several parameters; most importantly on the rock hardness, average input percussive hammer energy and feed force. It is also slightly dependent on the rotation speed of the bit and gives best results on a speed which provides most suitable indexing.

The bit-rock interaction model uses a database for prediction penetration rate. A set of curves between SE vs feed force established in previous chapter constitutes this database shown in the Figure 4.10. To simulate the real situations where rock hardness varies randomly with drill depth, a random generator of specific energy is used. It picks up a random value of specific energy of the rock at certain time. It then selects a suitable curve from the set of curves of figure 4.10 and based on current feed value calculates the penetration rate according to the selected curve. In case the curve for a given specific energy value is not available in the database and is somewhere in between the two curves in the database a linear interpolation is used

to estimate the shape of feed vs penetration rate curve of that specific energy. For the SE value beyond the limits linear extrapolation is performed. For simulation, we have used a built in function of the Matlab which works exactly same ways as explained above.

5.4.2 Load Torque

The torque caused by bit loading is proportional the applied feed force provide the other parameters are constant. A correlation between bit torque and the other drilling parameter was introduced by Cunningham [13, 14] as a means of estimation the torque requirement for a bit. This empirical correlation is given by:

$$M = KD^mW^n \quad (5.25)$$

In this equation K being the variable formation constant and m and n are bit-related constants. W and D are applied weight on the bit and the diameter of the bit respectively. This result was produced for the rotary drills where most of the rock cutting is through rotation and the measured torque can be used to predict rock formation strength. In percussive drilling case a similar relationship can be used to estimate the torque for a given drilling conditions. The motor torque, in percussive drilling, cannot be used for prediction of rock formation strength, however gives an idea of hole cleaning condition.

We have employed this relationship to predict torque. The controller will be designed such that it will limit the torque in the simulation to avoid machine jamming.

The equation 5.25 can be modified by introducing the concept of specific energy. K being the formation constant varies randomly along the drilling depth. The specific energy of the rock is related to the formation strength. We assume the following nonlinear relations between the two variables

$$K = kS_e^a \quad (5.26)$$

where k and a are the constants. Combining two equations

$$M = kS_e^a D^b W^c \quad (5.27)$$

Taking logarithm of the equation 5.27 will linearize this non-linear relationship. A linear least square estimation technique can, therefore, be applied to estimate the values of the constants a b c and k for a given set of data. Taking logarithm of equation 5.27

$$\ln M = \ln k + a \ln S_e + b \ln D + c \ln W \quad (5.28)$$

$$Y = \Phi \Theta^T \quad (5.29)$$

where

$$Y = \ln M$$

$$\Phi = [1 \quad \ln S_e \quad \ln D \quad \ln W]$$

$$\Theta = [\ln k \quad a \quad b \quad c]$$

The estimate $\hat{\Theta}$ of Θ is given by

$$\hat{\Theta} = (\Phi \Phi^T)^{-1} \Phi^T Y \quad (5.30)$$

The estimated values of k , a , b and c for different holes are listed in the table 5.4.2. It should be noticed that there are slight variations in the values of each parameter estimated for different holes, especially in the values of k and a . The values of k varies between 0.0554 to 0.6511 and that of a varies between 0.0609 to 0.2160. These two parameters are related to the rock hardness (See equation 5.26). It can be seen from the equation that any variation in rock hardness will affect the value of K . Any

Hole No.	k	a	b	c
1	0.6511	0.1367	2.295	0.1846
2	0.0554	0.0609	1.5499	0.2835
3	0.2174	0.1779	3.2583	0.319
4	0.1939	0.1688	1.7025	0.2376
5	0.1302	0.2160	3.4556	0.1245
6	0.1868	0.1167	2.6076	0.1187
7	0.5880	0.2047	2.5663	0.6543
8	0.1943	0.1948	2.9063	0.3187
9	0.1703	0.2139	2.5281	0.2882
Average	0.2771	0.1656	2.5411	0.2810

Table 5.1: *Table for estimated parameters of Torque model*

change in hole cleaning conditions also reflects on the rock hardness and will lead to change in the values these parameters. The hole cleaning conditions therefore seems to be responsible factor for these variations in the estimated values. Unfortunately, this factor was beyond the control of operator in the field experiment. Variation in b and c are small as compared to the other parameters and are affected by the similar factors. Since we intended to use this model for simulations of all possible rock and hole cleaning conditions an average value of each estimated parameter was used in simulation as given in the last row of the table.

Comparison of original and estimated torque is shown in the Figure 5.5. This result shows a good approximation of the torque. There are few points where a departure from the original value can be noticed. This is only at the point where a sudden change of any of the input parameters such as of feed or of specific energy is noticed. The estimates of parameters of equation 5.27 are good only for smooth

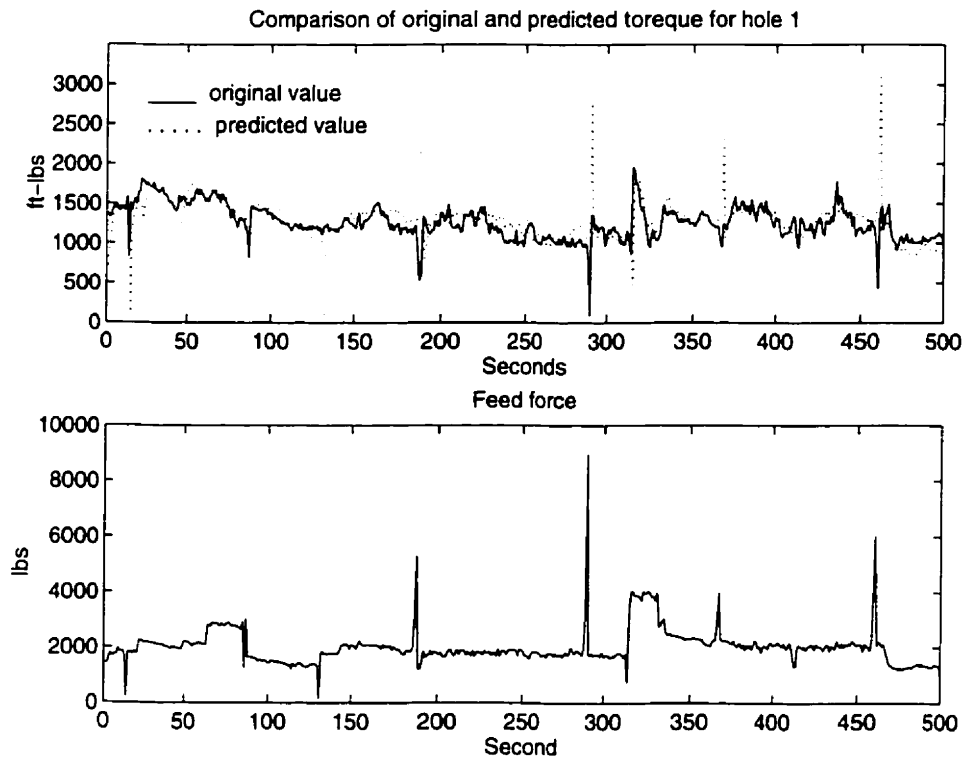


Figure 5.5: Comparison of predicted and original torque and applied feed value

data. Therefore at each sudden change in variable results in an error. Therefore, average predicted value of the torque should be considered as the true prediction in the simulation of drilling process simulator.

5.5 Conclusion

In this chapter we have developed a simulation model to represent percussive drilling process of CD90B drill. To achieve this, models of all necessary sections of percussive drilling system were developed.

Model of the feed system was developed analytically. A PID controller was also designed to control the applied feed force on the bit.

A percussive hammer model developed predicts the hammer energy per blow and the blow rate. It uses supplied air pressure as input.

To predict bit torque an empirical approach was adapted. The model structure obtained from the literature was modified to add the effect of specific energy of the rock. The parameters for the model were estimated using field data.

For prediction of penetration rate the correlation model derived in the previous chapter was employed. This model uses feed and specific energy of the rock to predict penetration rate.

Chapter 6

Drilling Rate Control

6.1 Introduction

Control of the percussive drilling process has the objective of achieving a maximum drilling rate with minimum hole deviations. Data analysis presented in the preceding chapters concludes that a control strategy to improve the drilling performance can be formulated. In this chapter we will concentrate on the development of a control algorithm in order to improve the drilling rate. This algorithm will however, not take into account the hole deviation. The problem of controlling hole deviation in percussive drilling will be discussed in the later chapters of this thesis.

The control algorithm developed in this chapter uses the specific energy of the rock being drilled to estimate the optimal feed to give maximum penetration rate. It also takes into consideration the bit torque and limits it at a maximum torque level for smooth running of the process.

6.2 Process Controller: Pre-Design Considerations

6.2.1 Control Objective

Drilling rate depends on how much drilling per hour can be achieved. Therefore we set the primary objective of this control system as maximization of the drilling rate. Jamming of bit rotation frequently interrupts the drilling process so the secondary objective is to avoid jamming. The controller is required to achieve these objectives by adjusting machine input variables.

6.2.2 Choice of Variables

The drilling process is a multi-input multi-output process as shown in the Figure 5.1 of previous chapter. It is not necessary that all these variable would take part in the controller design, instead the key variables can be selected according to system requirements. The following input and output variables are selected for the desired drilling process controller design:

Input Variables

There are three input variables for the percussive drilling process. These are feed force, rotation speed and hammer air pressure. Experimental data analysis showed that feed has a significant effect on the penetration rate. We have therefore selected feed as input variable for the controller.

Air pressure and bit rotation speed also play a role in the drilling efficiency. During the field experiments we did not have significant opportunity to manipulate these variables and were kept almost constant most of the time. Due to these reasons their effects on the drilling performance were not studied. These parameters will therefore be kept constant and the feed will be the only input to control the process.

Output Variables

There are four output variables for the drilling process: penetration rate, bit torque, vibration and deviation. As per the objectives of the control system, penetration rate and bit torque are selected as the output variables for this control system design.

The feed vs vibration relationship observed in chapter 4 showed that there is a very slight variation in vibration over a wide variation of feed. Hence this variable can't be properly controlled with feed only. Vibration can be minimized through the shock-absorber hence, with a proper design of the shock-absorber vibration can be reduced to minimum level. Similarly, deviation is not included in the design and can be controlled through an independent procedure to be discussed later.

6.2.3 Selection of Controller Type

Prior to the design of controller, it is important to decide the type of control scheme suitable for this application. The following point should be considered in this regard:

- The drilling process controller should adjust the input variable (Feed force) such that a maximum penetration rate is achieved. Optimal feed force is calculated using an empirical model developed from experimental data. The calculation procedure does not directly involve the control variable (penetration rate). This means that conventional feed back control is not suitable for this application.
- On the other hand the system model developed in the previous chapter consisted of a drill machine and a bit-rock interaction. The bit-rock interaction is a nonlinear process which makes the overall system nonlinear. This means linear control theory cannot be applied here and a control algorithm specific to the application should be developed.

As a result of the above issues, a passive type controller was selected for this system. Due to nonlinearity of the process a special algorithm would essentially be required. In the forthcoming discussion we will therefore focus on the development of a such a control strategy for controlling the percussive drilling process.

6.3 Simulation Model of Controlled System

The drilling process simulation model developed previously was used here for simulation purposes. In addition a disturbance model which randomly changes the rock hardness was also developed to simulate the real drilling situations. The block diagram of this complete controlled drilling system is shown in Figure 6.1. The controlled system contains the drilling process model, disturbance model and the controller blocks.

Computer simulation of this system were done using the simulation package “Simulink” which runs under the Matlab environment. The block diagrams of Simulink programs developed for this simulation are given in Appendix B.

6.3.1 Process Model

The drilling process model consists of the machine and the bit-rock interaction. Among the machine models shown in Figure 6.1 are the feed system and the percussive hammer model. These two machine models are represented by equation 5.6 and equation 5.21 respectively. The feed system is controlled by a local PID controller given by equation 5.7.

The bit-rock interaction model gives two outputs: the penetration rate and the torque. To predict penetration rate a data base scheme described in the section 5.4.1 was used. An empirical model predicts the bit torque given by the equation 5.25.

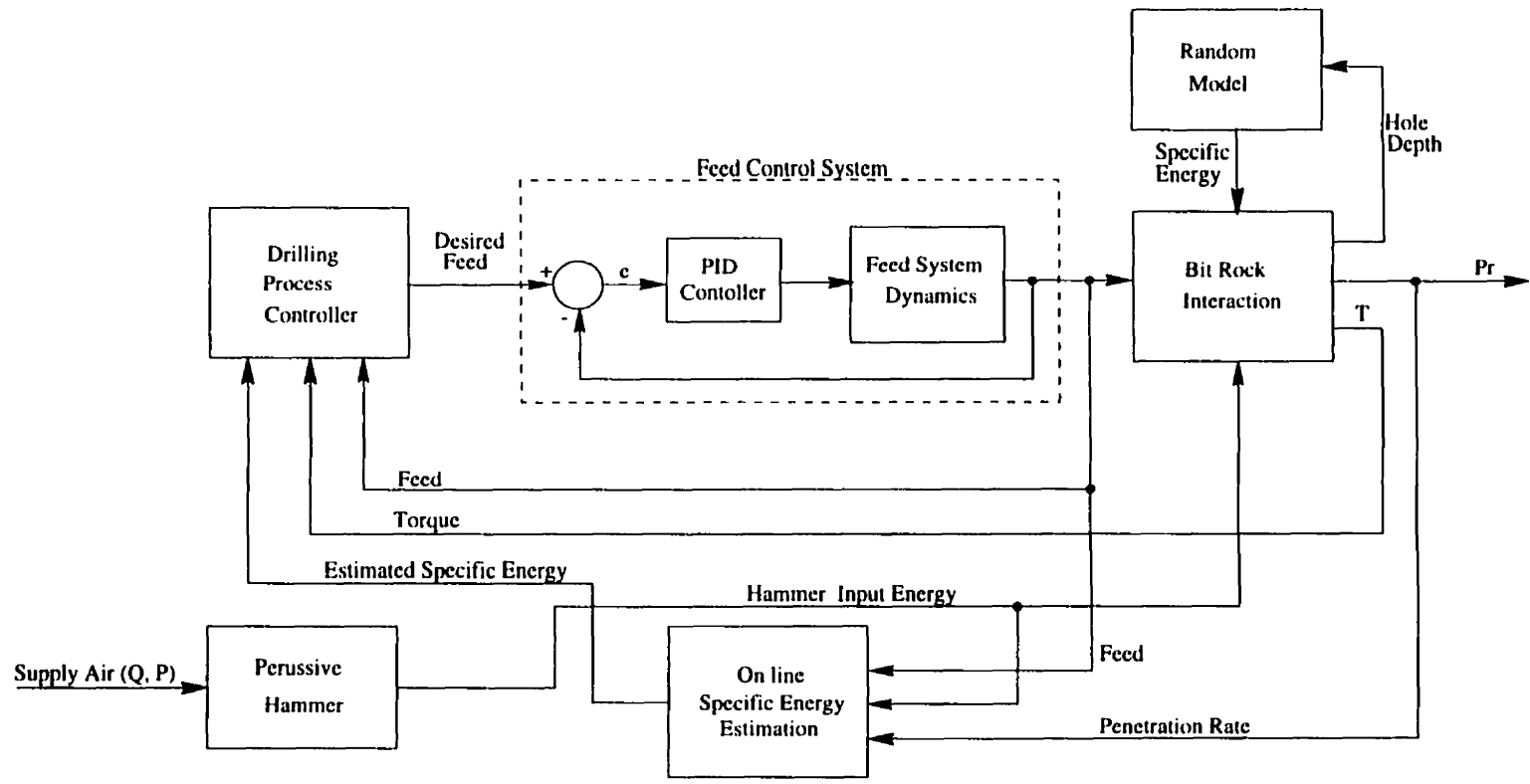


Figure 6.1: Block diagram of drilling process control system

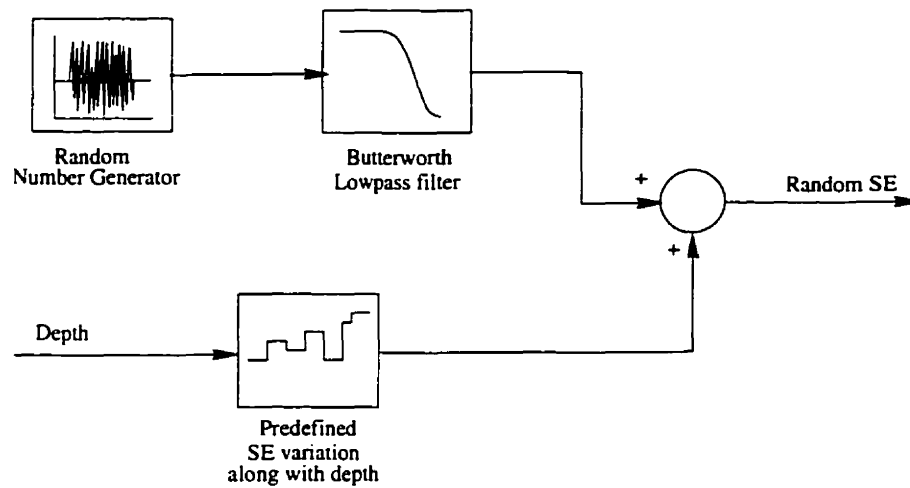


Figure 6.2: Block diagram of disturbance Model to generate randomly varying specific energy.

6.3.2 Disturbance Model

The variation in rock hardness along the drilled hole was simulated by the disturbance model. The output of this model is fed to the bit-rock interaction model as given in Figure 6.1. It perturbs the bit-rock interaction by randomly changing specific energy of the rock. Matlab's built-in random number generator along with a low-pass butterworth low-pass filter was used to develop this model. This configuration is shown in figure 6.2.

6.3.3 The Controller Blocks

Two blocks of Figure 6.1, the "Specific Energy Estimator" and the "Drilling Process Controller" implement the desired control strategy in the simulator. The SE-estimator estimates the specific energy of the the rock being drilled. The controller block employs this information to calculate the optimal value of the feed force to be applied.

A brief operation of the simulator is described in the following lines

6.3.4 Brief Description of the Simulator Operation

The machine controller is a feedback type PID controller that keeps a desired value of feed force maintained on the bit. The bit-rock interaction block predicts the penetration rate as a result of interaction between its input variables, the applied feed force, hammer input energy and the rock hardness property. It also estimates bit torque causing loading of the rotation system. The hammer energy is supplied by the percussive hammer block. The specific energy estimator block estimates the specific energy of the rock being drilled and provides this information to the drilling process controller. The drilling process controller calculates an optimal feed value. The output of the controller is fed as a set-point to the machine controller which maintains this optimal feed value on the bit.

The algorithm adapted by the drilling process controller to calculate the optimum feed value is described in the next section.

6.4 The Control Algorithm

During a typical rock drilling process, hardness of the rock varies independently. Drilling performance can significantly be improved if drilling parameters are continuously adjusted according to these changes. This requires an online measurement of the rock hardness. Specific energy of the rock is one of the quantities that gives an approximate estimate of the rock hardness for a particular drill rig. The Specific Energy can be calculated on line during the drilling. This gives some information about the hardness of the rock being drilled. The controller utilises information to improve the drilling performance by adjusting machine parameters to maximize the

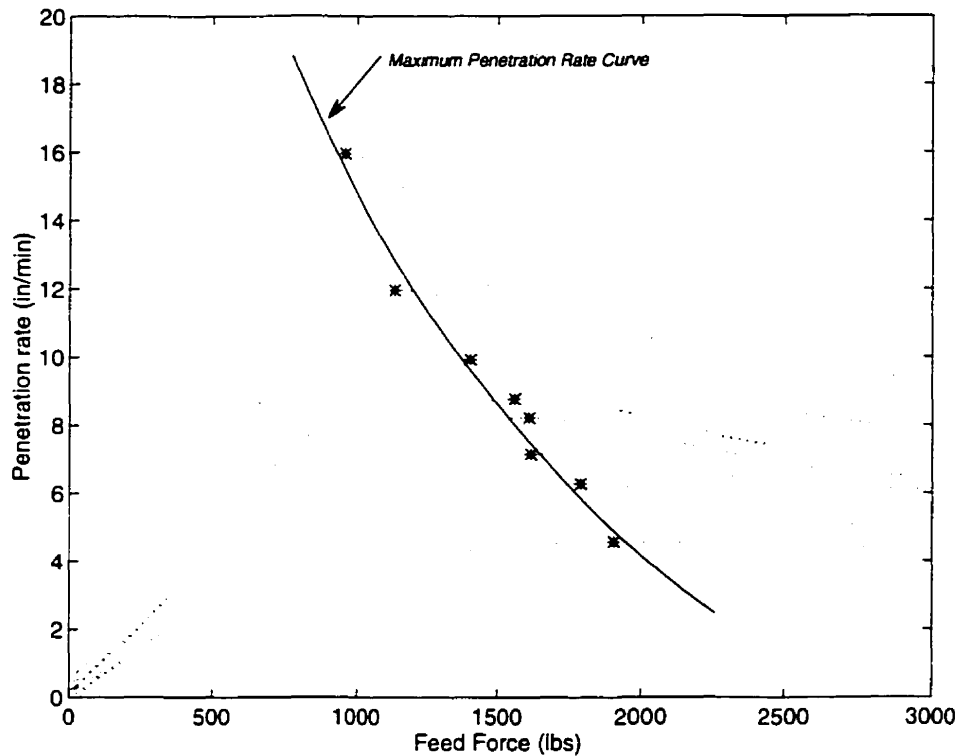


Figure 6.3: *Feed vs Penetration rate curves at different rock strengths and maximum penetration line*

drilling rate.

It was shown in chapter 4 during the data analysis that there exists a maximum value of penetration rate for each value of specific energy, at a certain value of applied feed force. This result was illustrated in the Figure 4.11 redrawn here in the Figure 6.3. The dotted lines in the figure are constant SE curves. The solid line was drawn through maximum penetration rate points for each SE. This controller will force the system to keep the operating point (feed value) along the maximum value curve of the figure.

The control law for the system is therefore stated as:

- Find an optimal feed value for maximum possible penetration rate for a given specific energy.

- Refine the optimal value to keep torque in the operating range.

6.4.1 Estimation of Specific Energy

The controller requires specific energy to estimate the optimal feed value. Equation 4.3 is employed to calculate the specific energy of the rock being drilled. The moving window averaging would take a mean value as the estimated value of the specific energy given by the equation.

$$S_e = \frac{1}{N} \sum_{j=1}^N \left(\frac{T_r \times E_i \times f}{A_H P_r} \right)_j \quad (6.1)$$

This equation include all measurable variables of the process, hence SE can be obtained on line with the above equation. The width of moving window (value of N) was taken to be 20 in the simulations.

6.4.2 Estimation of Optimal Feed Value

The optimum value of feed force required for maximum penetration rate is obtained from the lookup table of specific energy vs optimal feed.

Alternatively equation 4.5 developed in the previous chapter for obtaining the optimal feed value can also be used to estimate the optimal feed value, F_{opt} . i.e.

$$F_{opt}(t) = \begin{cases} aS_e^3 + bS_e^2 + cS_e + d & \text{for } SE_{min} < S_e < SE_{max} \\ F_{max} & \text{for } S_e > SE_{max} \end{cases} \quad (6.2)$$

where

F_{opt} = optimal feed value

F_{max} = maximum allowable feed value according to the lookup table.

SE_{min} , SE_{max} maximum and minimum limit of specific energy for which the data

base is available

a , b , c , and d are constants the estimated values of these constants are given on page 70 of chapter 4.

6.4.3 Torque Monitoring

Once the optimal feed value is obtained, the controller uses following logic in order to calculate the command signal:

Monitor if the current torque is in the normal range: then select the calculated optimal feed value otherwise re-optimize the feed value as follows:

$$F(t) = \begin{cases} F_{opt}(t) & \text{if } M(t-1) \leq M_{max} \\ F_p(t) & \text{otherwise} \end{cases} \quad (6.3)$$

Where F_p is the proportionally adjusted feed value and is calculated by the controller. This value is adjusted proportionally to the error $e(t)$ given by:

$$e(t) = M_{max} - M(t) \quad (6.4)$$

Hence the optimal feed value is

$$F_p(t) = F(t-1) + ke_n(t)F(t-1) \quad (6.5)$$

k is constant for the proportional controller where $e_n(t)$ is normalised torque error given by

$$e_n(t) = \frac{M_{max} - M(t)}{M_{max}} \quad (6.6)$$

It is clear from the above equation that the value of $e_n(t)$ will vary between -1 and 1, k is the proportional constant that controls the time constant of the controller. This constant was tuned using the simulations.

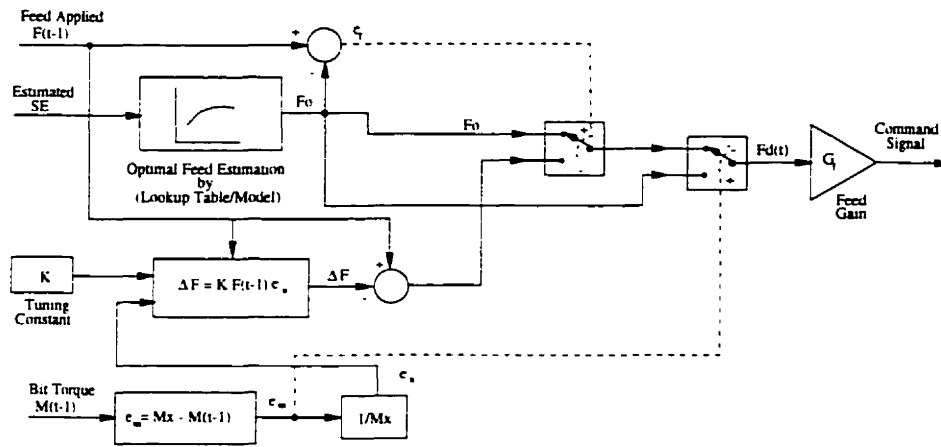


Figure 6.4: Drilling process controller schematic diagram.

The controller decision making logic and signal flow diagram is more explicitly illustrated in Figure 6.4. The flow chart of the controlled system is given Figure 6.5

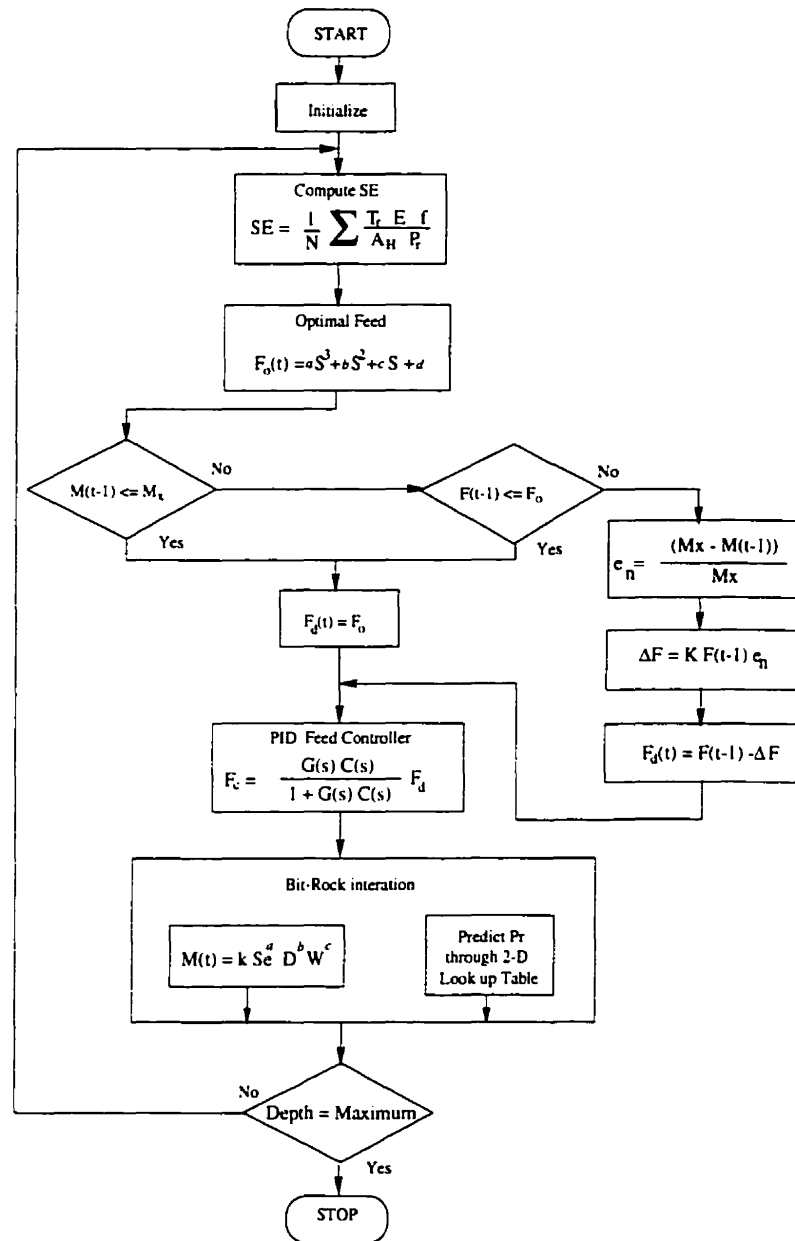


Figure 6.5: Flowchart of controlled percussive drilling system.

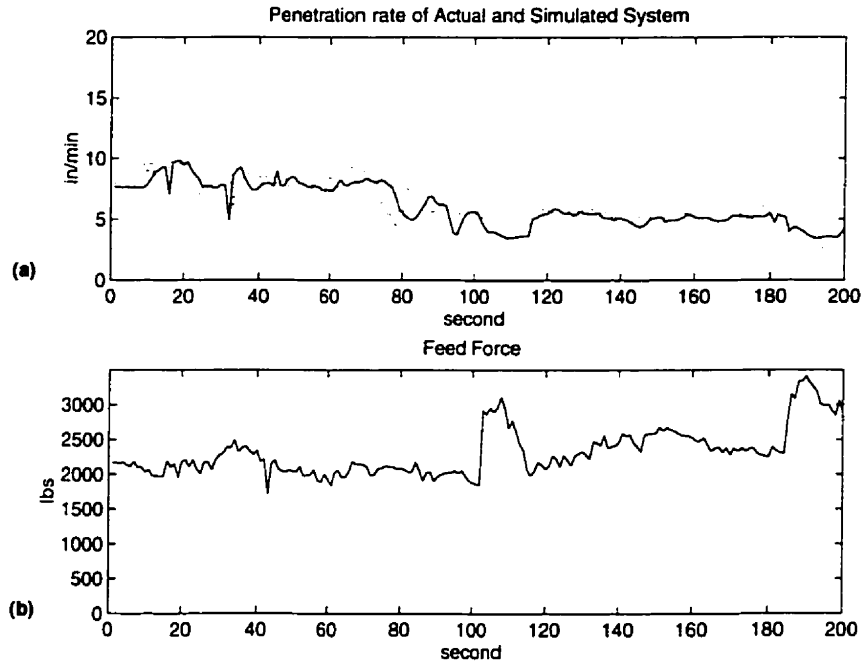


Figure 6.6: Comparison of Penetration rate in (a): dotted line is the actual penetration rate from hole 2, whereas solid line is the penetration rate given by the simulated system. This penetration rate was achieved when same feed force was applied to both systems given in (b).

6.5 Simulation Results

To validate the simulated drilling process the results of the simulated system and the actual data were compared for a same applied feed force. Figure 6.6 illustrates one of these results. The dotted line in the Figure 6.6a shows the penetration rate of actual data of hole 2 whereas the solid line is the penetration rate given by the simulated drilling system. This comparison shows a good agreement between two plots. For this simulation we applied same feed force which as applied to the actual system during the field experiments. The plot of the feed force is given in 6.6b. In addition we used calculated specific energy for the same hole as an rock hardness property.

For validation of the controller designed for this system, simulations of the process model were run in two different ways. First it was run as if the process was manually controlled by the operator i.e. setting the feed value at a constant level instead of automatically adjusted by controller. Secondly it was run while the process was automatically controlled i.e. the drilling process controller was controlling the process. Results of the two simulations were compared for validation of the controller. This comparison has shown that by inclusion of the controller, the efficiency of the drilling process can reasonably be improved.

Figure 6.7 *a* to *d* is the result of simulation when the process was not controlled by drilling process controller. Instead a constant feed is manually applied see Figure 6.7*b*. The rock hardness in the form of specific energy was deliberately changed at different depths in order to observe the controller response at different hardness levels. These changes in SE has been plotted in Figure 6.7*d*. These values are 10×10^3 , 14×10^3 , 18×10^3 , 12×20^3 , 22×10^3 and $10 \times 24^3 \text{ in} - \text{lbs}/\text{in}^3$. It is obvious that the change in SE has directly affected the penetration rate, Figure 6.7*a*, and hence, effecting the efficiency of the process.

In contrast to the above results obtained without controlling the feed value, the Figure 6.8 *a* to *d* shows the results of simulations when the process was being controlled by the controller. On each change in the rock hardness the controller adjusts the feed values at its optimal level where a maximum penetration rate can be obtained. Comparing the two figures (Figure 6.7 and 6.8), it is obvious that with adjusting the feed value according to rock hardness a higher penetration rate is obtained at lower torque values.

For SE $10 \times 10^3 \text{ in} - \text{lbs}/\text{in}^3$ the controller adjusts the feed value to 1207.80 Lbs, the penetration rate obtained with this feed value is 11.64 in/min the average torque level is 1233 in-lbs. At same SE value the penetration rate 8.72 in/min and the torque value of 1450 in-lbs is obtained when the process is running without controller.

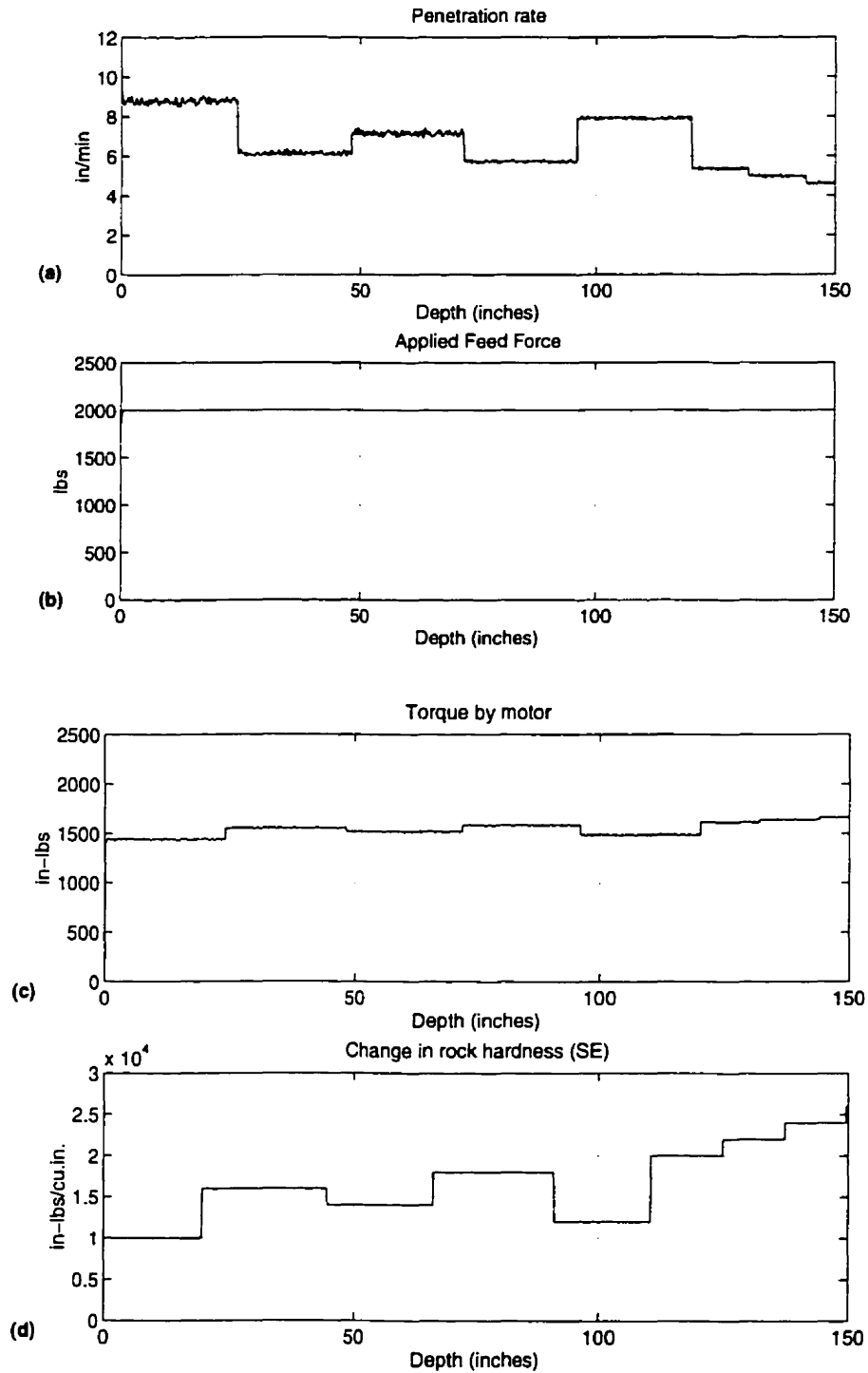


Figure 6.7: Run of simulator without controller (a) penetration rate (b) applied feed force, (c) resulting torque on the bit and (d) deliberate changes applied to rock hardness

For SE $14 \times 10^3 \text{ in} - \text{lbs}/\text{in}^3$ the controller adjusts the feed value to 1601.31 Lbs, the penetration rate obtained with this feed value 7.65 in/min the average torque level is 1407.09 in-lbs. At same SE value the penetration rate obtained without controller is 6.51 in/min and the torque is 1529.59 in-lbs. Obviously with controller a higher penetration rate at lower torque is achieved.

Similarly for SE $16 \times 10^3 \text{ in} - \text{lbs}/\text{in}^3$ the controller adjusts the feed value to 1807.18 Lbs, the penetration rate obtained with this feed value 6.52 *in/min* the average torque level is 1429.62 in-lbs. At the same hardness level the penetration rate obtained without the controller is 6.10 in/min and the torque is 1562.96 in-lbs. Ultimately a higher penetration rate at lower torque is still obtained with controller. The difference in penetration rate at this hardness level is very small, the reason for this is that the optimal feed value applied by the controller is very close to constant applied feed without controller.

For detailed comparison of results illustrated in these two figures the penetration rate curves obtained with and without controller are re-plotted figure 6.9. This shows that there is always a higher penetration rate when using controller except when the controller adjusted feed is same as manually applied feed value. In this comparison a drilling up to the hole depth of 150 inches (12.5 feed) is shown. This depth was bored in 1392 seconds (23.3 minutes) whereas it took 1158 seconds (19.3 minutes) which is 20.2% improvement in drilling rate.

In the above comparison, results of simulations with and without controller were compared for only one case when manually feed was set at 2000 Lbs. It is important that the comparison should be made at several manually fixed feed values. In order to compare the controlled outputs at other fix feed levels, the simulations were run repeatedly at different fix feed values without controller. Four of these results are given in the figure 6.10 *a*, *b*, *c* and *d* for a fix feed of 1000 Lbs, 1500 Lbs, 2500 Lbs and 3000 Lbs respectively. During all these simulations the rock hardness level

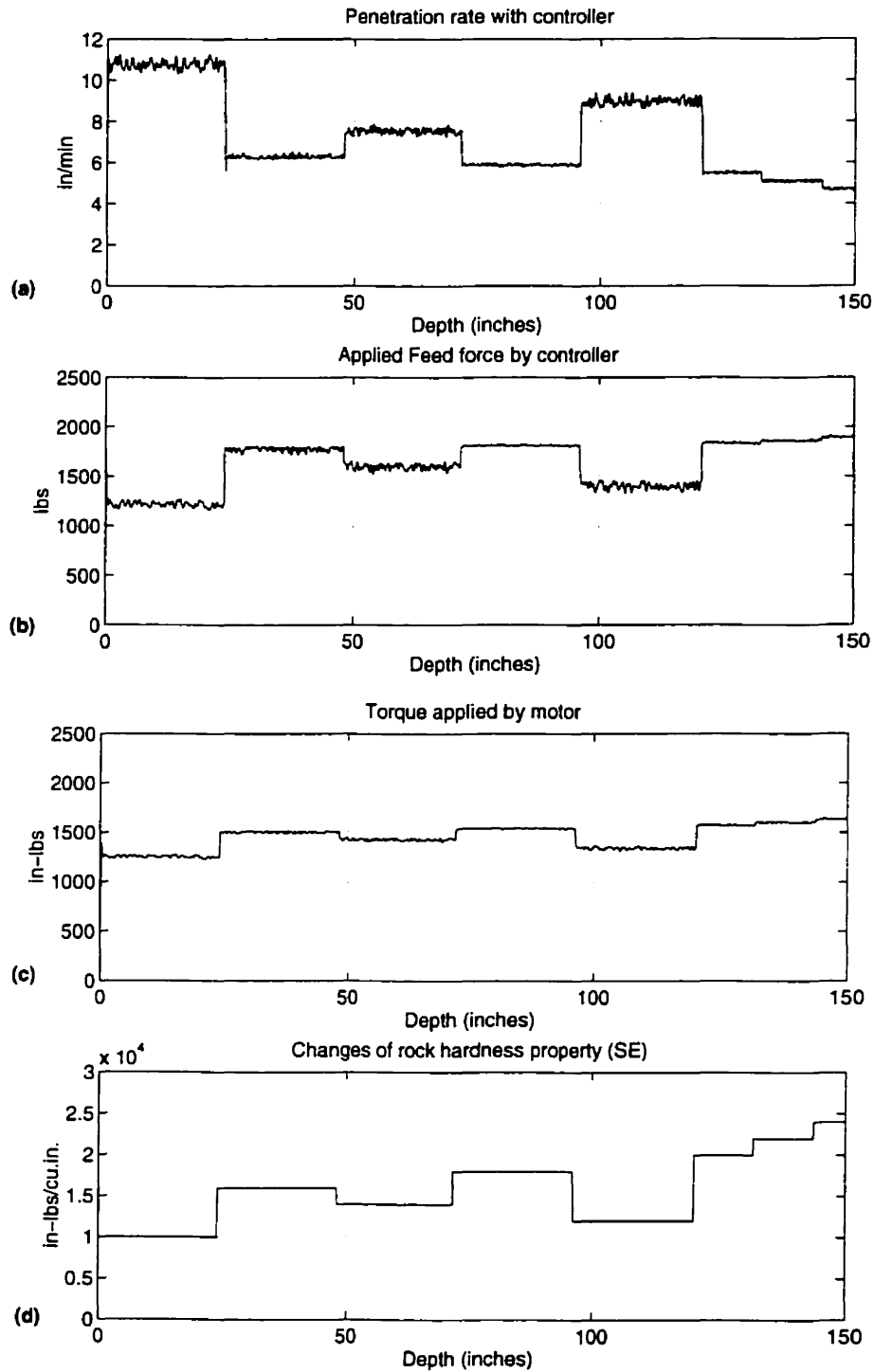


Figure 6.8: Run of simulator with controller (a) penetration rate (b) applied feed force, (c) resulting torque on the bit and (d) deliberately changes applied to rock hardness

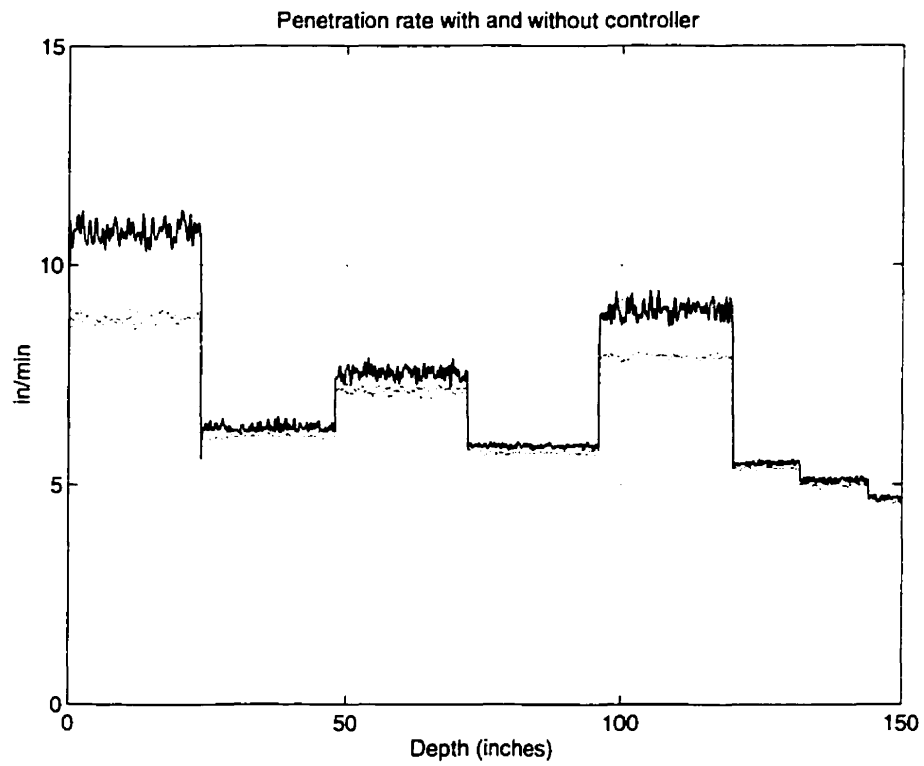


Figure 6.9: Comparison of penetration rate achieved when running simulator with and without controller. Solid line indicates penetration rate for simulator run with controller while dotted line is for the run without controller.

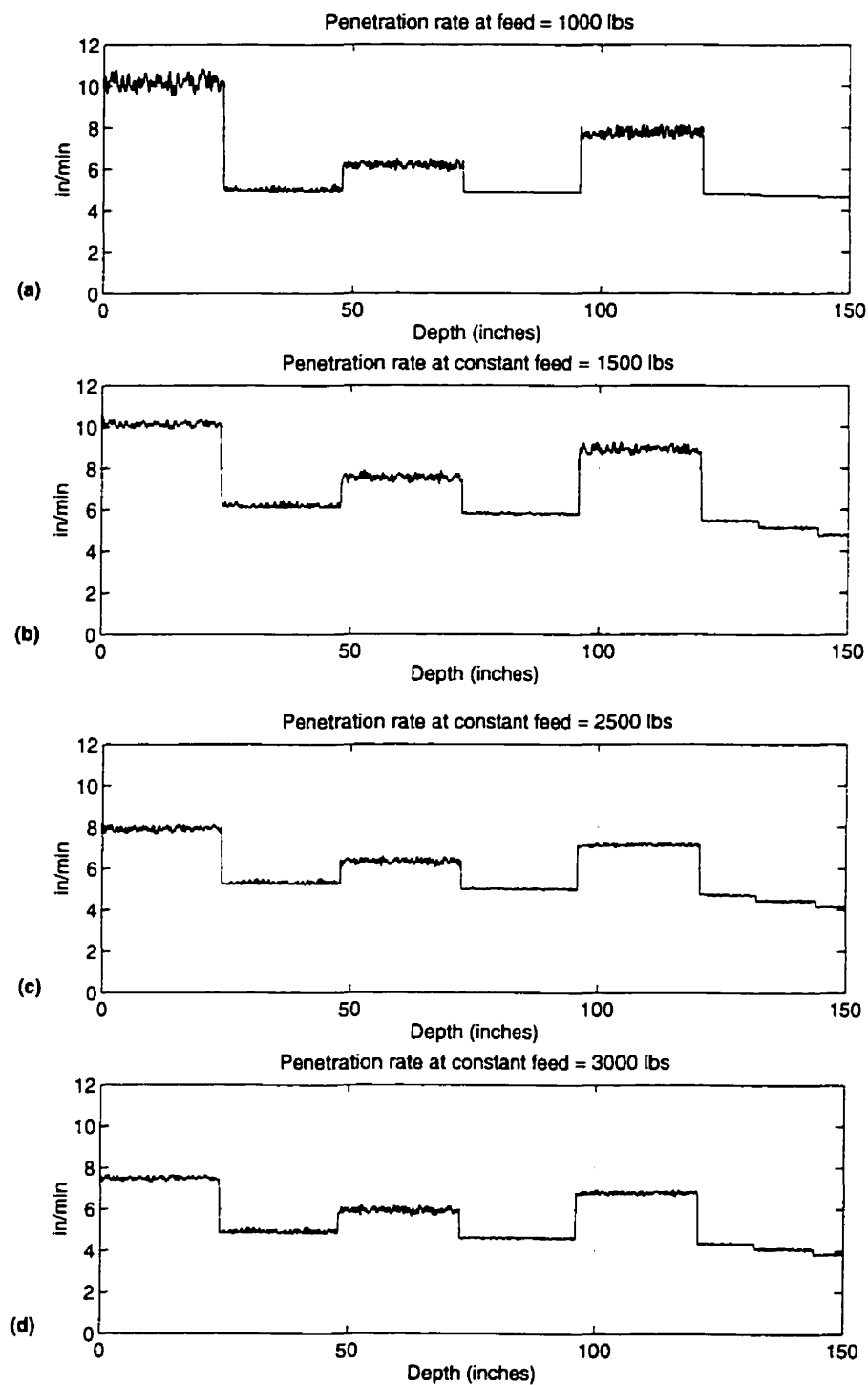


Figure 6.10: Result of simulations without controller at different feed force (a) when feed is 1000 Lbs., (b) when feed is 1500 Lbs., (c) when feed is 2500 Lbs and (d) when feed is 3000 Lbs.

was varied in the same manners as described before. Evidently, all these plots show lower penetration rate when compared with the penetration rate obtained in figure 6.8 except when the applied feed value matches.

Among the other features of the drilling process controller is that it continuously monitors the motor torque value and limits it at a value lower than maximum torque allowed. Hence avoiding the overloading of torque motor. The excessive torque can suddenly increase at machine in real situation when cutting is not properly blowed out or when the bit faces a harder rock. This cause the hammer jamming. To simulation this situation the system was perturbed by sudden increase in torque. The results of these simulations are shown in figure 6.11 *a b* and *c*. The maximum torque value was set as 2000 in-lbs. When the torque increases above this value the controller will automatically start reducing the applied feed value. This reduction applied to the feed value is proportional to the error in the torque. It continuously reduces the feed until the the torque reduces to its upper limit. This controller action is necessary to avoid jamming of the hammer which frequently occur in real situations.

Finally the simulation was tested for comparison with the field data. In order to do so, the simulation was run using field data. That is, instead of deliberately changing the rock hardness, the specific energy calculated from the data of different holes was used to perturb the bit-rock interaction. Figure 6.12*a* to *c* illustrates the results of these simulations for hole no. 4. Plot of figure 6.12*a* is the penetration rates achieved from actual drilling of hole no 4. While figure 6.12*b* penetration rate achieved from simulation of this hole. Comparison of two plots shows that a higher penetration rate of the simulated system is achieved. The average penetration rate of the real data plotted for 600 seconds is 5.87 in/min (29.35 ft/hr) whereas the penetration rate of the simulated hole 4 is calculated as 7.37 in/min (36.85 ft/hr) which is 26% higher than the field data. Figure 6.12*c* is the applied feed by the controller for this simulation.

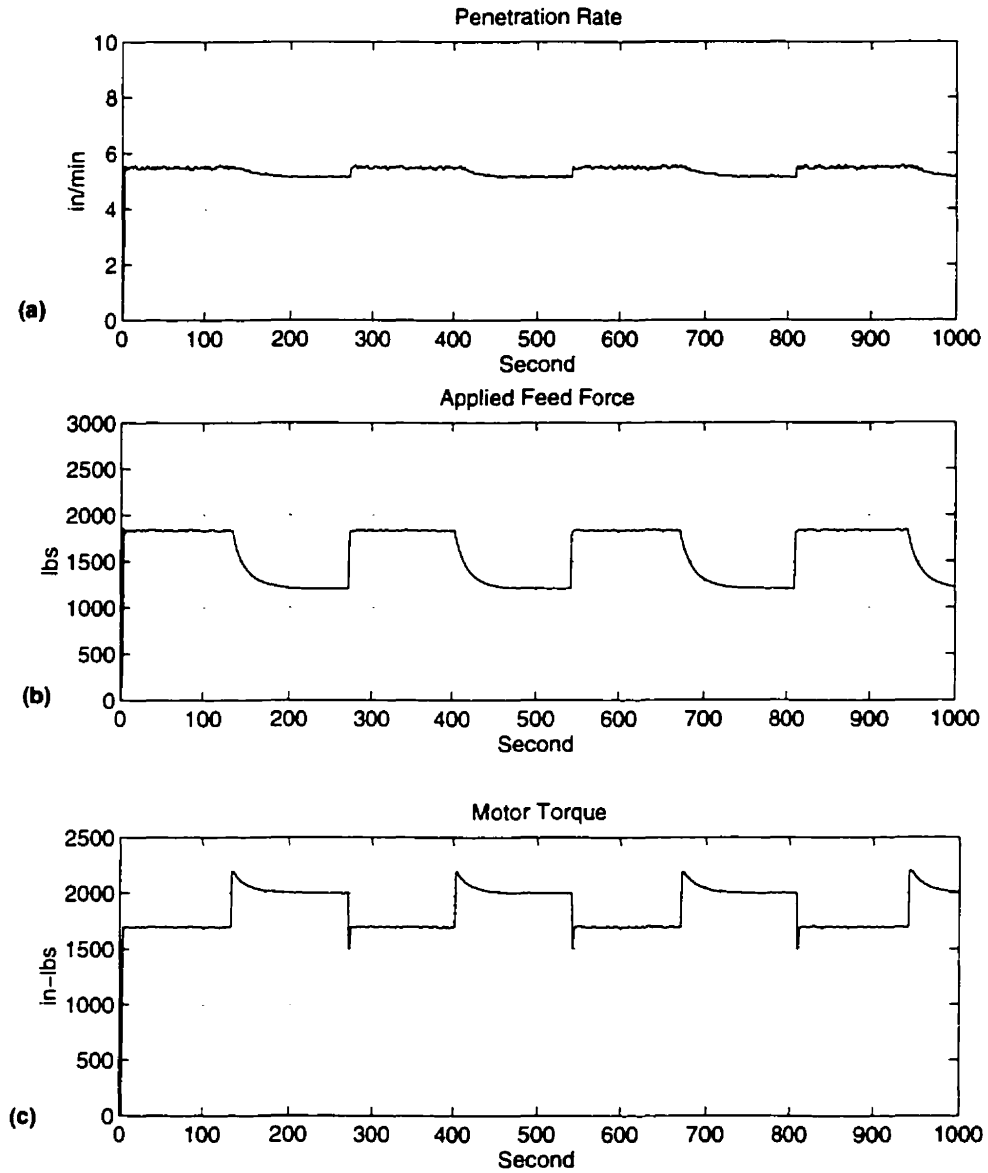


Figure 6.11: *Result of simulations with controller when the system was perturbed deliberately with a sudden change in bit torque value.*

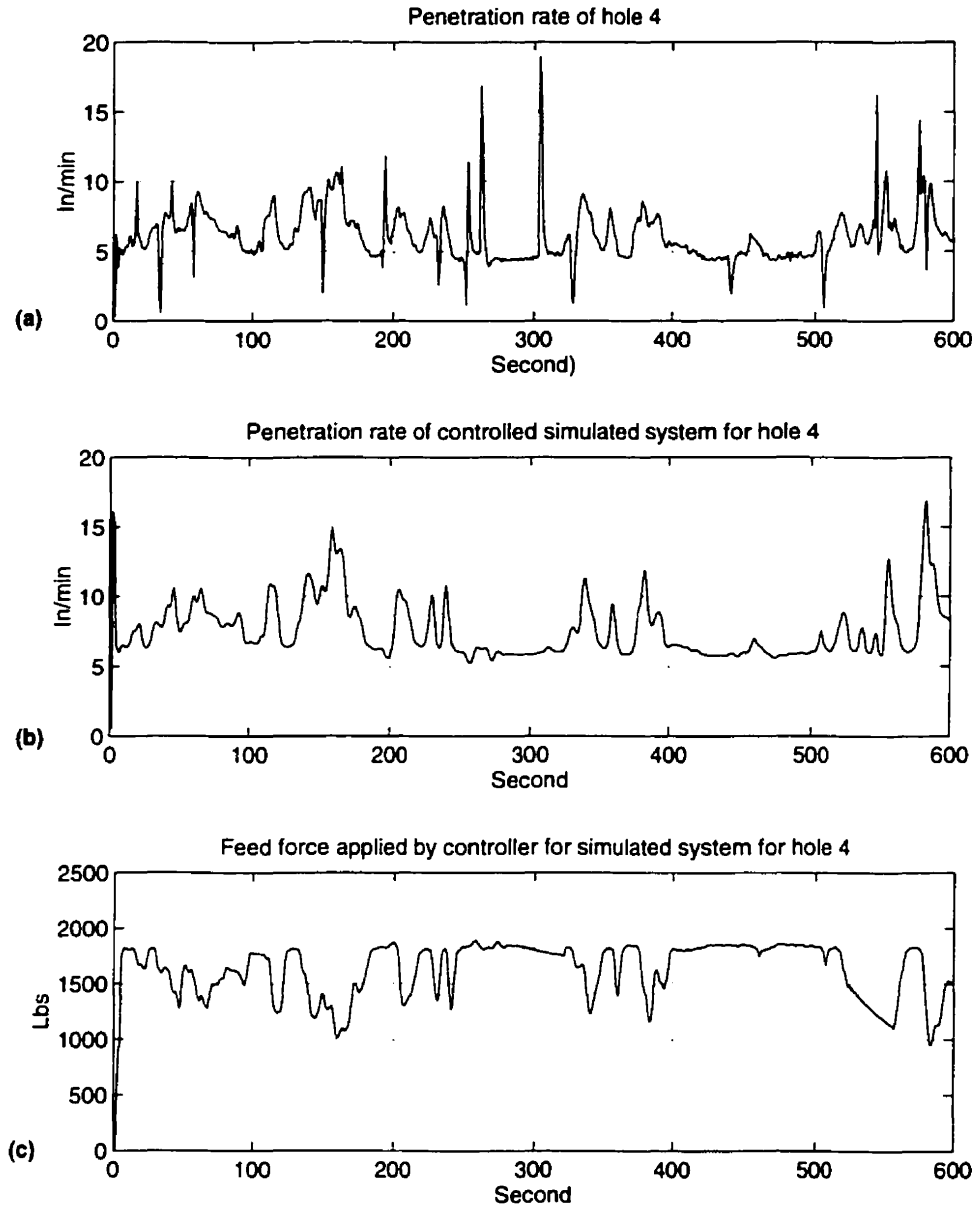


Figure 6.12: *Simulation of Hole 4. (a) Penetration rate of original data from hole 4, (b) Penetration rate of simulated system for hole 4, and (c) Corresponding feed force applied by the controller*

6.6 Conclusions

Based on the results of field data analysis, a passive drilling process controller was developed. This controller employs the specific energy of the rock being drilled to estimate the control signal. An empirical model developed from the field data was used for computing the optimal feed value.

The results of simulations have proved that the efficiency of the percussive drilling can considerably be improved with the controller.

The simulation was also run to compare the results with the actual data of hole 4 from field experiments. This comparison showed a 26% increase in the drilling rate when the drilling was controlled with controller.

It is important to mention here that an optimal feed calculation formula was developed from the data obtained from one mining site. More experimental data from different mining sites should be required to improve the accuracy of the prediction model.

Chapter 7

Shock-absorber Tests and Analysis

7.1 Introduction

The percussive drilling machine encounters severe vibrations due to the continuous percussion of the hammer. These vibrations, if transmitted to other parts of the machine, can effect its stability and decrease its life. It is therefore important that the vibrations be reduced to a minimum level.

The drilling data analysis presented in the section 4.2.3 has shown that vibrations are less sensitive to applied feed force in comparison to the other parameters such as penetration rate and torque. It is therefore not advisable to use feed force for controlling the vibration. The drilling process controller developed in the chapter 6, therefore, did not use vibration as a controllable variable. In contrast, attention should be given to a proper design of the shock absorber mechanism to reduce the transmission of vibration.

Generally, a shock absorber is installed on the top of the percussive hammer in

order to minimize transmission of vibrations from the bottom of the hole to the other parts of the machine. Field experiments were conducted in order to test the performance of the existing shock-absorber on the CD90B. In this chapter we present the analysis of the data for these shock absorber tests. The analysis shows a considerable decrease in vibration due to the shock-absorber. Design modifications are suggested to further reduce the vibration level and to increase its bandwidth for a wider range of applied feed force.

7.2 Shock Absorber Field Test

Field experiments for testing of a custom-designed shock absorber were conducted during September 1993 at INCO's North Mine in Copper Cliff, Ontario. The purpose of these experiments was to assess the performance of the shock absorber, and the results of its most recent design modifications.

During the September 1993 tests, five holes were drilled with a total depth of 110 feet. Total data collected was of three hours duration. Two types of tests were performed:

- 1. Static tests:** These were performed to determine the interaction between feed force and displacement of the shock absorber. In this test the machine was stopped, while the feed force was slowly increased and the displacement of the head was recorded.
- 2. Dynamic tests:** These were carried out during drilling of the holes. This data was collected under two drilling conditions:
 - a) When the shock absorber was installed on the machine.
 - b) When the shock absorber was not installed on the machine.

The purpose of these two types of dynamic test was to compare levels of vibration, feed force and torque with and without the shock absorber.

7.2.1 Digitization

The dynamics data was digitized at 500 Hz. This choice was a trade off between resolution and memory space available on the computer. A maximum of 10 seconds of data could be digitized at this sampling frequency in one shot because of memory limitations - each 10 second interval resulted in a data file of 0.5 Megabytes. Therefore only selected data was digitized and stored. A total of 61 sets of data, each of 10 second duration, were digitized, resulting in over 30 Megabytes of data files. The static data was, however, digitized at a much lower frequency of 1 Hz.

7.3 Vibration Analysis

The main purpose of the shock absorber is to minimize the transmitted vibration and shock from the percussive hammer to the machine head. Therefore the vibration signal has been focused on in this section.

7.3.1 Without Shock Absorber

Figure 7.1 is the plot of 2 seconds of data for the hole 3. This is the vibration observed at the rod when there is no shock absorber installed on the system. It can be seen that the signal contains a periodic signal with high peaks, which corresponds to the hammer blow rate (22 Hz). In between the high amplitude peaks, there are some higher frequency but lower amplitude signal components. This is presumably because of the natural damping action of the system, which attenuates high frequencies.

The signal in Figure 7.1 also contains some low frequencies, lower than the blow rate frequency, from sources other than the hammer e.g. rotary motor etc. The low frequency components act to modulate the overall vibration signal, at a modulation frequency of approximately 2 to 3 Hz.

To have a clearer picture of the frequency component contained in this signal, the FFT (Fast Fourier Transform) plot of the same vibration signal is shown in Figure 7.2. It shows a wide distribution of power throughout the frequency spectrum, with large contributions around 3, 25, 50, and 100 Hz. The contribution at around 25 Hz is evidently due to the hammer blow rate. The resonance at around 50Hz represents the resonant frequency of the rod.

7.3.2 With Shock Absorber

Figure 7.3 plots the vibration recorded for hole 4. This data was collected when the shock absorber was installed. Comparison of this figure with Figure 7.1 shows that vibration has decreased significantly: only the peaks at the blow rate frequency are still dominant, with other components significantly reduced.

The FFT of this signal is shown in Figure 7.4. This shows that the power at all the frequencies has been decreased, except at the blow rate frequency and its harmonics.

This can also be seen in the cumulative power of the two data sets. The cumulative power available in the spectrum of figure 7.2 is plotted in Figure 7.5, the total power is calculated as 17196. Whereas the cumulative power in the signal of figure 7.4 is plotted in figure 7.6, which shows that the cumulative power is 4012. Hence the shock absorber is effective in reducing the overall transmitted vibration by a factor of roughly one fourth.

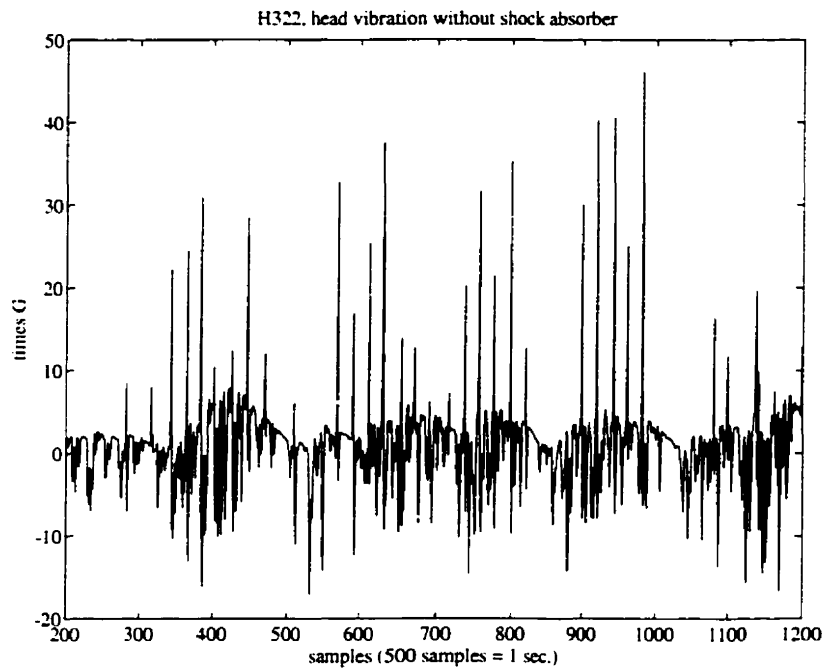


Figure 7.1: *Vibration signal at rod when no shock absorber installed*

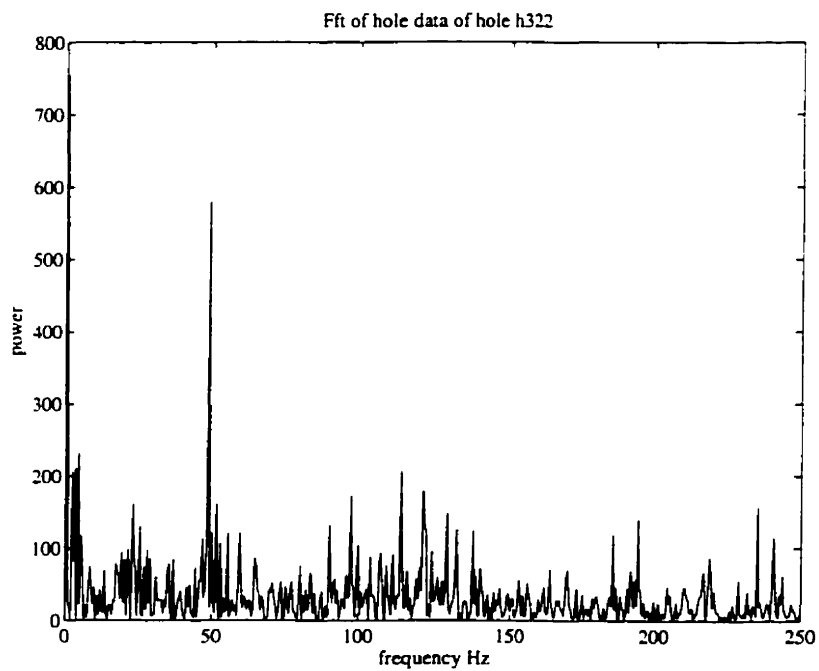


Figure 7.2: *Frequency spectrum of vibration of Figure 7.1*

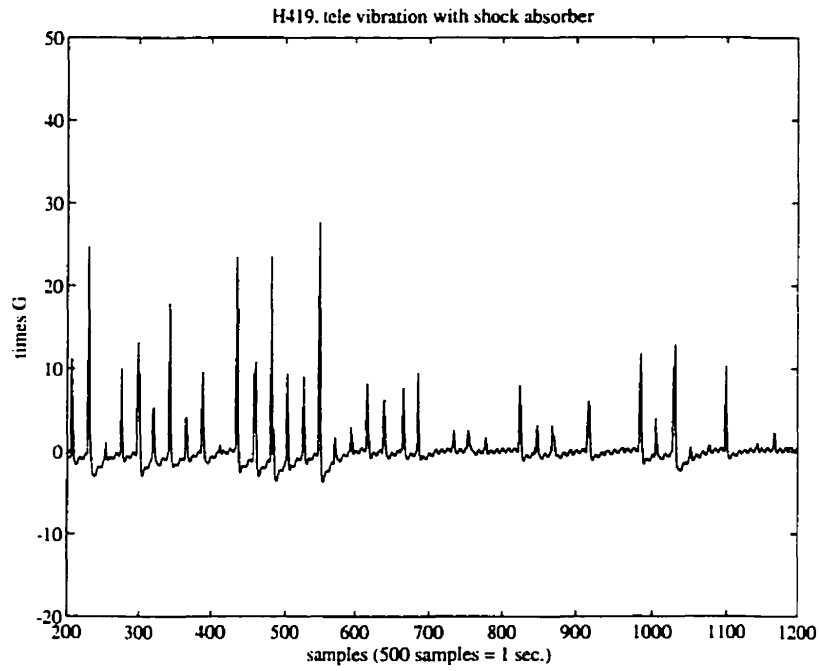


Figure 7.3: *Vibration at rod when shock absorber is installed*

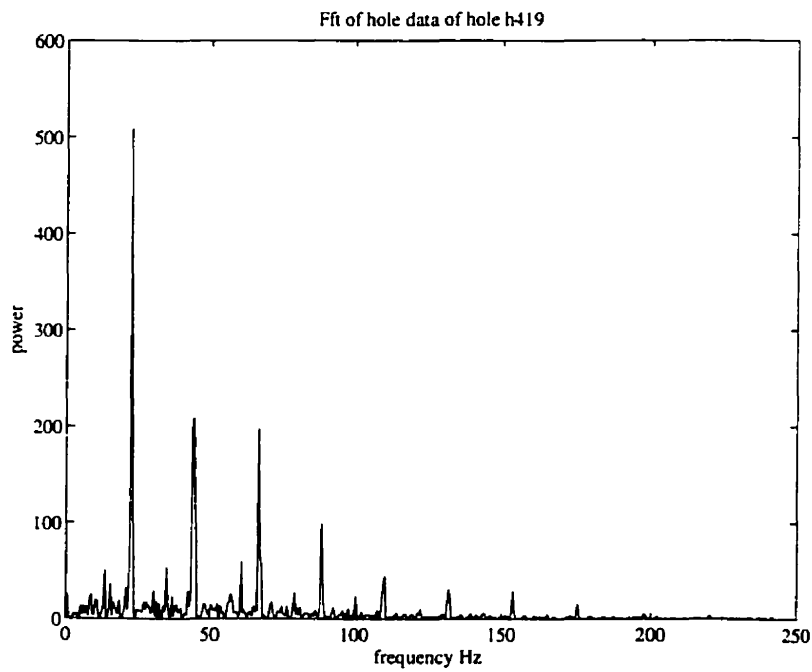


Figure 7.4: *Frequency spectrum of vibration of Figure 7.3*

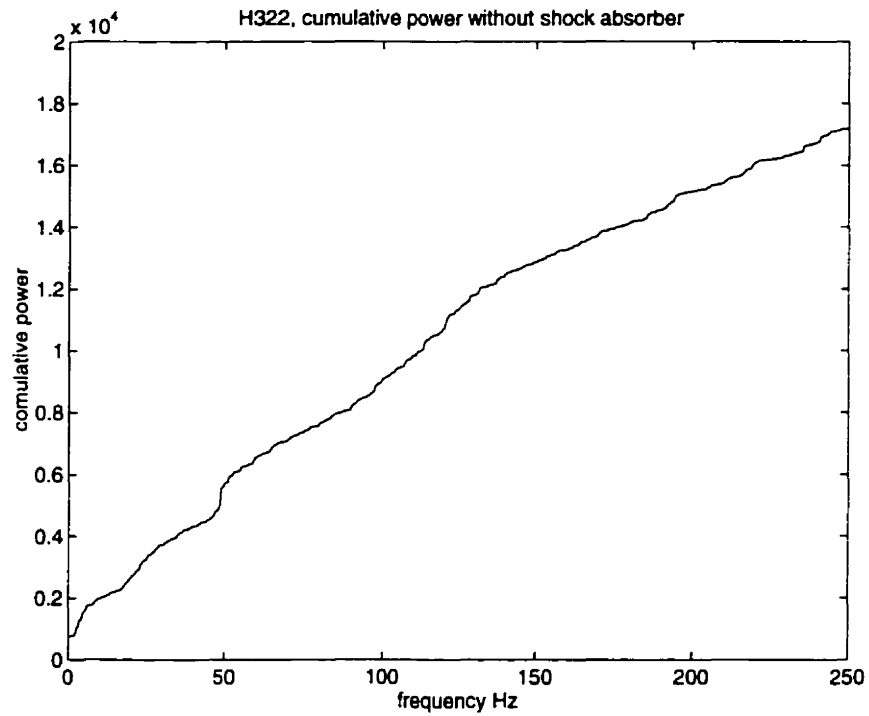


Figure 7.5: *Cumulative power of the vibration without shock absorber for hole H322*

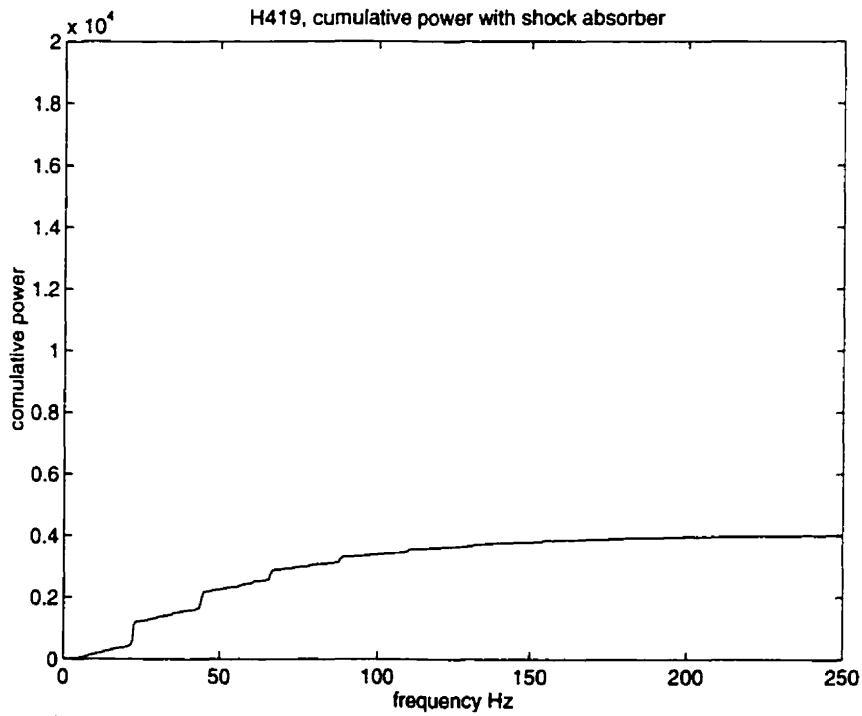


Figure 7.6: *Cumulative power of the vibration signal with shock absorber for hole H419*

7.3.3 Statistical Comparison

The data files which contain vibration data have been processed to calculate certain statistical properties of the vibration signal. These are listed in table 7.1 for data without shock absorber and in table 7.2 for data with shock absorber.

These statistics have been obtained in the following manner:

Average Vibration: This is the mean of the absolute value complete vibration signal.

Peaks Elimination: All those points which represents peaks in the data points have been eliminated. The resulting maximum and minimum and absolute mean are listed in the table. These are indicative of vibration performance.

Peaks: The points representing peaks in the data of vibration have been separated. The resulting maximum, minimum and absolute mean of the peaks is listed in the table. These are indicative of shock performance.

Comparison of the two tables highlights the performance of the shock absorber. The average vibration without shock absorber ranges between 2.671-5.116G, for a feed force range of 913-2465 lbs. In contrast, average vibration with the shock absorber ranges from 1.232-4.323 with a feed force range of 3392-5077 lbs. The mean values of vibration are further reduced after elimination of peaks (compare column 2 and 4). The highest mean peak vibration without the shock absorber is seen to be 25.84G, which is reduced by the shock absorber to 14.52G.

WITHOUT SHOCK ABSORBER

File	Average vib	Peaks Eliminated			Peaks			Feed
		Min	Max	Mean	Min	Max	Mean	
h321	4.445	-17.491	9.762	3.825	10.059	40.954	25.840	1117
h322	3.569	-17.096	10.456	3.001	11.819	46.133	23.931	1545
h323	2.671	-4.955	6.516	2.095	5.054	17.615	8.133	913
h324	3.588	-4.980	8.993	2.790	5.054	18.730	8.724	2147
h325	4.005	-7.953	8.795	3.395	8.027	19.548	11.164	1733
h326	4.275	-7.977	8.895	3.610	8.003	18.457	10.964	2465
h327	5.116	-19.499	14.915	4.858	15.162	22.422	18.205	3700

Table 7.1: *Statistical analysis of vibration without shock absorber***WITH SHOCK ABSORBER**

File	Average vib	Peaks Eliminated			Peaks			Feed
		Min	Max	Mean	Min	Max	Mean	
h411	2.932	-5.971	2.973	1.711	3.023	27.650	11.385	4532
h412	2.099	-4.782	2.973	1.244	3.047	28.170	10.230	5039
h413	3.541	-5.847	2.998	1.972	3.023	31.044	13.934	5077
h414	3.927	-7.977	0.892	2.308	1.016	29.781	11.817	4356
h415	4.323	-9.167	1.882	2.549	2.007	30.871	14.518	3912
h416	4.395	-11.050	0.991	2.545	1.016	29.632	13.041	4291
h417	1.735	-6.392	1.487	1.038	1.536	27.502	7.487	4859
h418	1.232	-4.335	1.164	0.680	1.313	28.121	5.984	5169
h419	1.267	-3.742	0.991	0.692	1.016	27.650	6.161	3392
h4110	2.008	-6.937	0.991	1.105	1.040	27.947	8.204	3602
h4111	2.461	-5.302	0.942	1.378	1.016	27.402	8.544	3945

Table 7.2: *Statistical analysis of vibration data with shock absorber*

7.4 Determination of Natural Frequency and Damping

The Natural frequency of any a system is the frequency at which that system will oscillate without any external interference. The shock absorber's natural frequency is estimated in this section using two different methods: System Identification and Graphical Approximation.

7.4.1 System Identification

The shock absorber consists of a spring and mass assembly which can easily be modelled as second order system. The standard least-squares system identification method to calculate the model parameters has been used here. The transfer function of a standard second order system can be described as:

$$C(s) = \frac{G\omega_n^2}{s^2 + 2\zeta\omega_n s + \omega_n^2} \quad (7.1)$$

The denominator of this transfer function is called the characteristic equation of the system, and contains the term ω_n which is called the natural frequency of the second order system.

To apply the system identification algorithm a portion of vibration data was selected, and is shown in Figure 7.7. This selected data is the response of the shock absorber system to the hammer blows. The input of this system is the hammer blows themselves, which can be approximated by a train of impulses. Since the input signal (hammer blow energy) was not recorded, an arbitrary impulse train of the same frequency as that of output signal is generated to simulate the input signal. This is shown in Figure 7.8. Notice that the height of each impulse is proportional to the peak value of its respective output since an arbitrary constant gain is assumed.

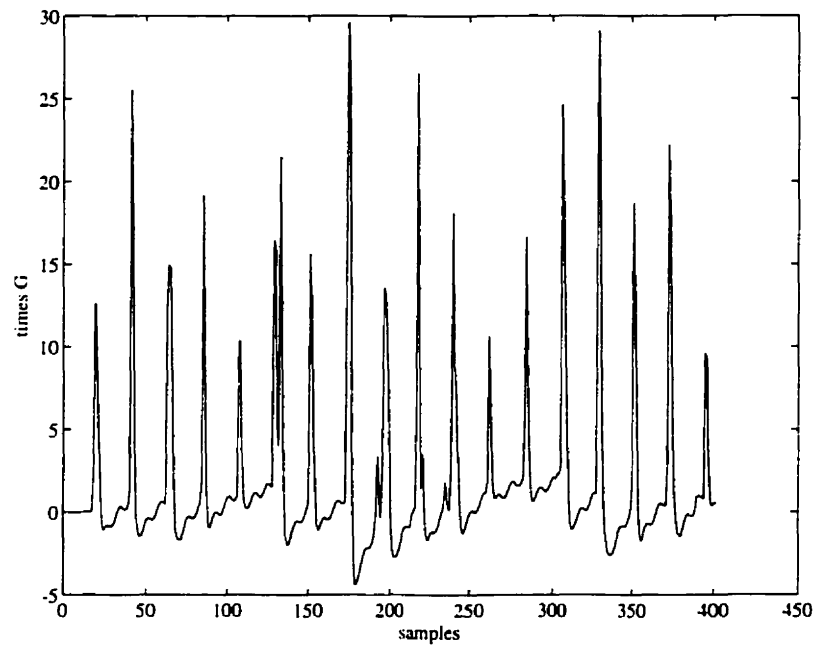


Figure 7.7: A portion of data selected for output of the shock absorber for system identification

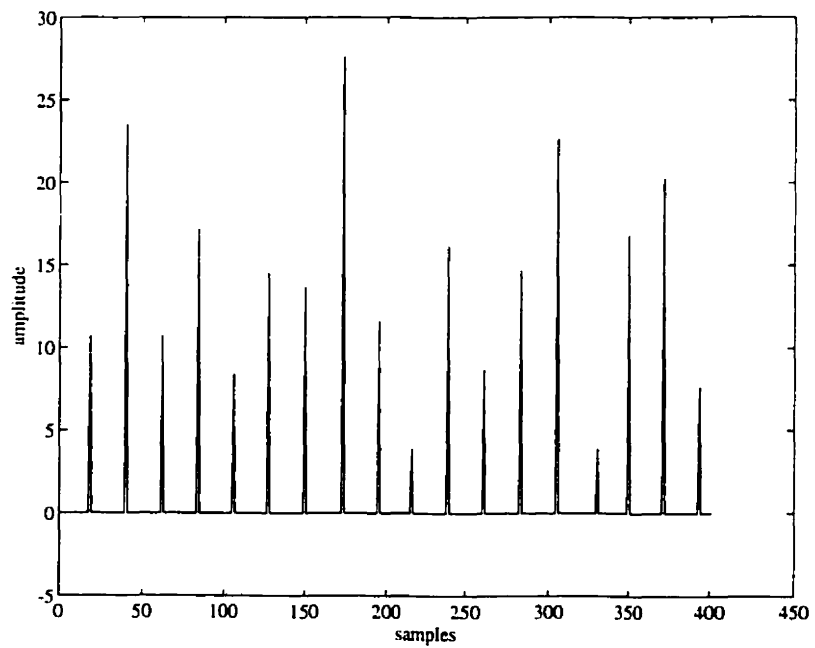


Figure 7.8: Impulse train has been generated which is used as an input to the shock absorber system for identification purposes

This input-output data set was used to estimate the parameters of a second-order ARX model [40]. The estimated model, in discrete-time, is given by the following equation.

$$C(z) = \frac{0.1974}{1 - 0.8909z^{-1} + 0.2962z^{-2}} \quad (7.2)$$

The continuous-time equivalent is given by

$$C(s) = \frac{-1.1619 \times 10^2 s + 9.0678 \times 10^4}{s^2 + 6.0839 \times 10^2 s + 1.8617 \times 10^5} \quad (7.3)$$

The denominator represents the characteristic equation of the system. Comparing this equation with the standard form, natural frequency of the system is estimated as:

$$\begin{aligned} \omega_n &= \frac{\sqrt{1.8617 \times 10^5}}{2\pi} \\ &= 431.47 \text{ rad.} \\ &= 68.670 \text{ Hz} \end{aligned}$$

The estimated frequency is close to an integer multiple of the hammer percussive frequency 22Hz (i.e. $22 \times 3 = 66$). Taking into account the factor of error, it is quite possible that the actual frequency is even nearer to 66 Hz.

For a second order system, natural damped frequency ω_d , otherwise known as the resonant frequency, is given by:

$$\omega_d = \omega_n \sqrt{1 - \zeta^2}$$

Comparing the characteristic equations of the systems 4.1 and 4.3 ζ is calculated as:

$$\begin{aligned} \zeta &= \frac{6.0839 \times 10^2}{2\omega_n} \\ &= 0.71 \end{aligned}$$

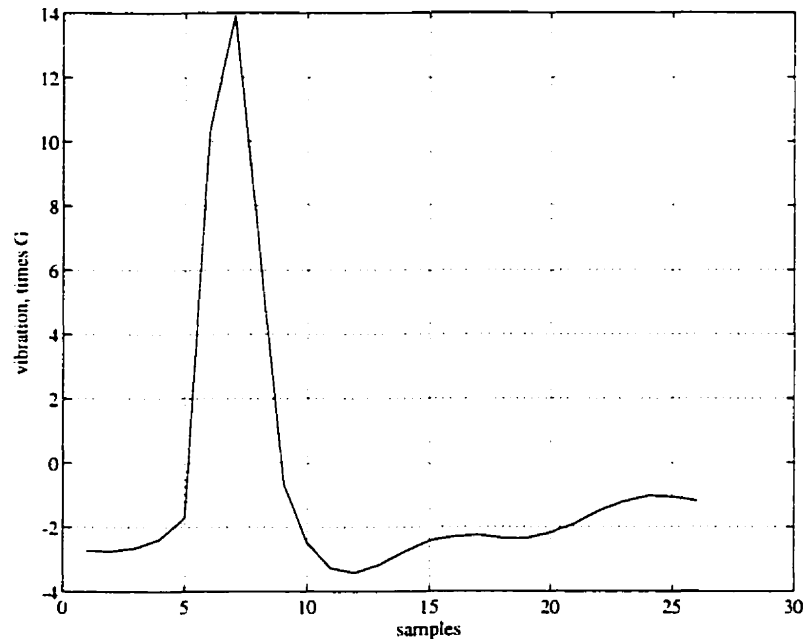


Figure 7.9: *Vibration at head. Only one cycle of the signal is shown. It is response of shock absorber to hammer impulse stroke*

and hence the resonant frequency of the system is:

$$\begin{aligned}\omega_d &= 68.67\sqrt{1-0.71} \\ &= 48.70 \text{ Hz}\end{aligned}$$

This frequency corresponds to the highest amplitude component of the signal in Figure 7.2.

7.4.2 Natural Frequency by Graphical Method

Alternatively, the natural frequency of a second order system can also be calculated graphically from its impulse response. We can use the same output signal as in the previous section. Response to a single impulse is plotted in Figure 7.9.

The time required to reach at maximum value of the step response is called the

peak time t_p . In the case of Impulse responses it is the time between the first two zero crossings. In the impulse response shown in the figure this time is measured graphically and is almost equal to 3.8 samples. This plot is negative biased with a value of -1.71. This value is considered as the zero when measuring the peak time.

Therefore

$$\begin{aligned}t_p &= 3.8 \times T_s \\ &= 0.0076 \text{ sec.}\end{aligned}$$

Where T_s is sampling period which is 0.002 seconds in this case. Natural frequency is given by:

$$\begin{aligned}\omega_n &= \frac{\pi}{t_p} \\ \omega_n &= 413.36 \text{ rad.} \\ &= 65.79 \text{ Hz}\end{aligned}$$

This results confirm that the actual natural frequency would be in between 65 and 69 Hz.

7.5 Static Test

The plot of force vs displacement is shown in Figure 7.10. The displacement represents the axial movement of the upper part of the shock absorber with respect to the lower part.

The maximum displacement of the shock absorber is 1 inch. This is obtained at a feed force of 14000 lbs. By observation of the curve it can be noticed that the relationship is approximately linear in the range from 0 to 7000 lbs. This is the actual working range of the machine. This range was never exceeded throughout the dynamic tests. A straight-line fit for the range of 0-7000 lbs, has been estimated using

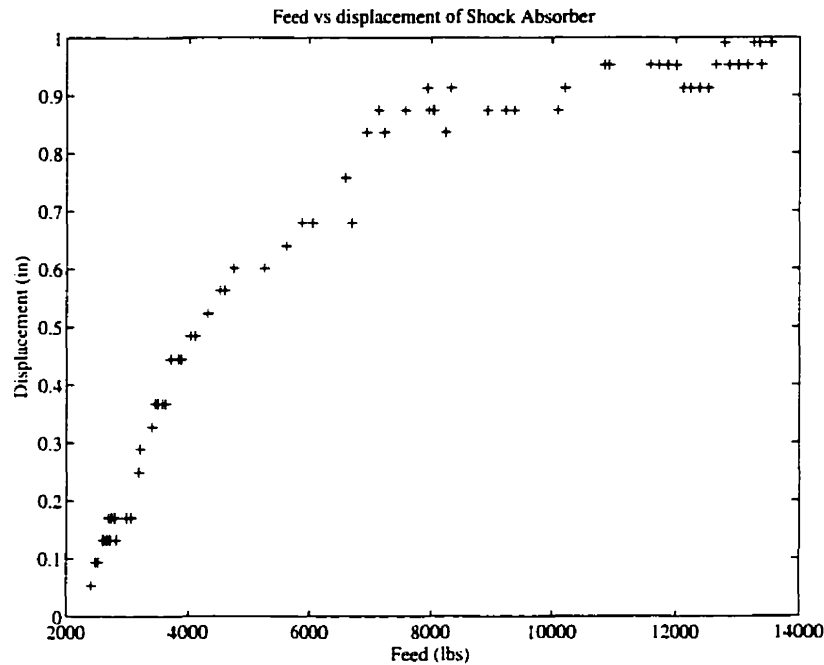


Figure 7.10: Response of shock absorber displacement against the applied feed force linear regression and is shown in Figure 7.11. This straight line can be represented by the following polynomial equation.

$$D = a_1F + a_2 \quad (7.4)$$

Where D is the displacement in inches. F is the applied Feed. a_1 and a_2 are the coefficients of the linear equations. For this straight line equation the values of the estimated parameters are:

$$a_1 = 1.98 \times 10^{-4}$$

$$a_2 = -3.7632 \times 10^{-1}$$

For the full range of movement of the shock absorber, the best polynomial fit is obtained using a third order equation given by:

$$D = a_1F^3 + a_2F^2 + a_3F + a_4$$

The estimated parameter values are:

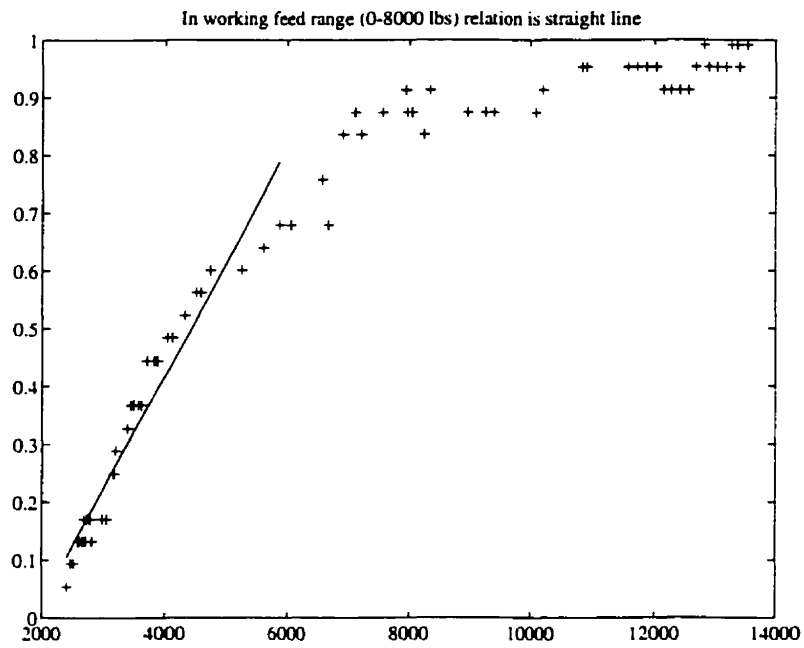


Figure 7.11: Working range straight line fit for feed vs displacement

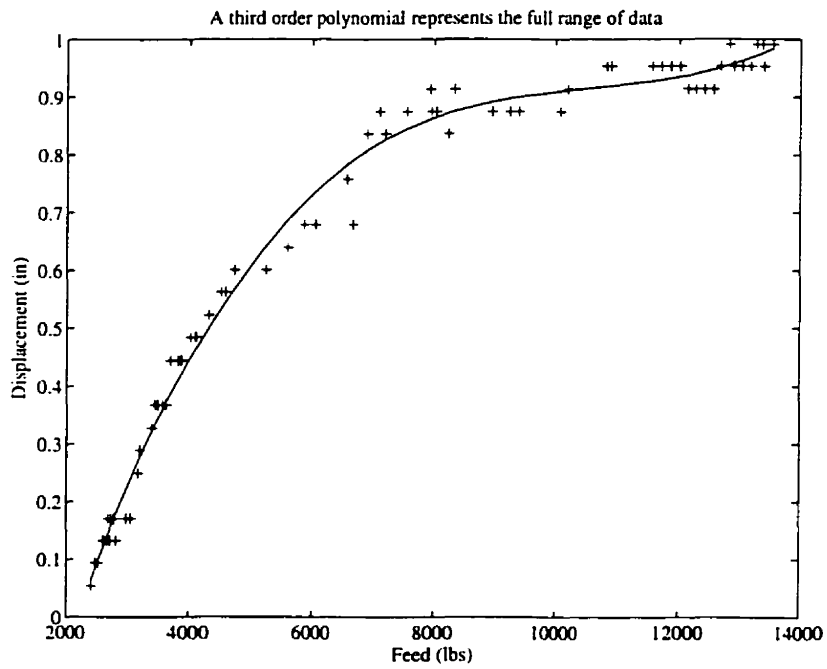


Figure 7.12: Full range curve fit for feed vs displacement of shock absorber

$$a_1 = 1.4113 \times 10^{-12}$$

$$a_2 = -4.4753 \times 10^{-8}$$

$$a_3 = 4.8374 \times 10^{-4}$$

$$a_4 = -8.6456 \times 10^{-1}$$

This fitted curve is shown in Figure 7.12.

7.5.1 Implication of Static Test Results for Shock Absorber

From the point of view of minimizing shock and vibration with this particular shock absorber, the optimal feed force seems to be 5000 lbs., as at this force the shock absorber is displaced 0.5 inch (half of its total movement) and stays in the centre of its range and hence will be able to equally absorb motions in both directions.

The drilling experiments were performed while keeping the feed force in the range of 1500-5000 lbs. The average feed force maintained on the machine during the experiments was in the range of 3500 lbs. which results in a nominal shock absorber displacement of less than 0.35 inch. At such a displacement, a severe shock in the forward direction will not be absorbed to the full capacity of the shock absorber, due to its reaching at the end of its travel.

To corroborate this, it can be noted that high frequency signals with low amplitudes were easily absorbed by the absorber. However, larger amplitude signals at lower frequencies were not properly absorbed.

7.6 Conclusions and Recommendations

1. The analysis reveals that the shock absorber is successfully damping a larger range of vibration frequencies. However, the shock absorber appears to amplify vibrations at the blow rate frequency.
2. The overall system damping, natural frequency, and resonant frequency, have been calculated using two different methods. In the first method, the system has been modelled as a second order system and then its characteristic equation has been used to calculate its natural frequency and resonant frequency. The second method calculates it from a “peak time” value obtained graphically.
3. The natural frequency calculated from both methods is close to the integer multiple of hammer frequency. The calculated resonant frequency is in close agreement with the observed resonance near 50 Hz.
4. Static testing indicates that a feed force of 5000 lbs. is most suitable for this shock absorber, as it displaces the absorber 0.5 inch and thus maximizes the range of movement of the shock absorber in both directions.

Recommendations for Design Change:

1. It is recommended that the shock absorber is modified such that it is at its mid range displacement at the optimal feed value.
2. The resonance frequency of the shock absorber should be set such that it should neither be close to the integer multiple of hammer blow frequency and its harmonics nor close to the rods resonant frequencies.

Chapter 8

Investigation of Machine Dependent Hole Deviation

8.1 Introduction

Deviation in blast holes adversely affects the fragmentation process which ultimately results in poor mining efficiency. It is therefore important to address deviation control in the evolution of automatic percussive drill automation. The control system developed in chapter 6 improves machine performance in the terms of drilling rate. The problem of hole deviation was not considered in that design. In the next few chapters we will address the problem of hole deviation in percussive drilling and suggest suitable strategies to control it. We start with the investigation of drilling deviation from the available field data and then propose some modifications in the design of existing drilling machines in order to achieve control of the hole deviation.

In this chapter data analysis in order to investigate the hole deviation is presented. Deviation can be classified based on its sources as: machine dependent hole deviation and the rock dependent hole deviation. The data collected from the field represents

the status of the machine only which can be employed to investigate the machine dependent hole deviation. A very limited rock information is available. It is therefore difficult to identify the rock structures which were responsible for the hole deviation. We have, therefore limited this investigation process to the machine dependent hole deviation.

Actual trajectories of the test holes are calculated using hole orientation data. These trajectories are then compared with the ideal trajectories to measure the deviation occurred in those holes. This information is also employed to distinguish between deviation caused by misalignment of the machine and the deviation caused by bit-rock interaction only. Study of correlation between the machine parameters and the deviation parameters is then presented.

8.1.1 Deviation in the Blast Hole

It is important to define the term “deviation” in the blast holes before any further analysis is presented. Blast hole are designed in such a way that a maximum fragmentation through blasting is achieved. These hole are generally drilled in a straight trajectory. The deviation in these holes is the measure of departure of the drilled holes from the desired straight paths. For this application the deviation is stated as the horizontal distance between the desired destination and the actual destination of the drilled hole.

The deviation control system to be developed for this application aims to improve the straightness of the holes.

The deviation can be classified based on its sources as shown in the Figure 8.1. The initial setup of the machine is among the most common errors responsible for hole deviation. The bit-rock interaction depends on machine variables as well as the rock variables. The deviation caused by the machine setup and the machine related

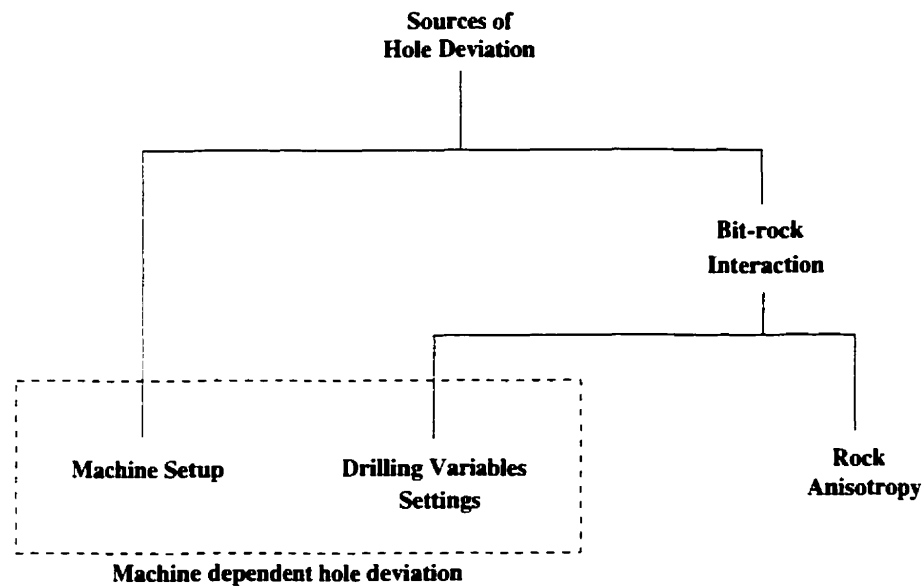


Figure 8.1: *Sources of hole deviation*

drilling variables is defined as machine depended hole deviations. This chapter presents an analysis of machine dependent hole deviation.

8.2 Hole Trajectory and Deviation Analysis

Orientation data acquired through geophysical survey of the test holes was employed to measure the deviation. The services of IFG Corporation and Sperry-Sun Drilling Services were hired for this survey. The IFG corporation survey used fluxgate magnetometers for hole orientation measurements whereas mechanical gyroscopic technology was employed by the Sperry-Sun Drilling Services for their measurements. An average value of the two orientation data sets is used in the following analysis.

This data gives three parameters related to hole orientation: the dip angle, the azimuth angle and the depth of the hole. The dip angle is the angle from vertical downwards and has positive values in counter clockwise direction. The azimuth angle is the angle of rotation from North in clockwise direction.

These three variables can be used to calculate the three dimensional trajectory of the hole. For a visible comparison, the trajectory for each hole is plotted in two dimensional plots showing two side views (x-z and y-z views) and a plan view (x-y view). These trajectory plots of all the test holes are given in appendix C, two of them are also plotted here in Figures 8.2 to 8.5. In these plots positive values of x, y and z represent East, North and Vertical downward directions respectively.

Each side view plot, e.g. of Figure 8.2, shows three trajectories drawn with different line styles. The dashed line represents the desired trajectory of the hole. The centre line represents the straight line on which the machine should have drilled after first alignment of the machine and the solid line represents the actual trajectory.

The plan view of each trajectory is plotted and scaled in such a way that the deviation could be seen clearly (e.g. see Figure 8.3). The origin of this figure is the desired destination of the hole and is marked as "o". The destination of the expected straight hole after initial alignment of the machine is marked as "+", and the destination of actual hole is marked as "*". The distance between origin and "+" is the measure of expected deviation due to misalignment. The distance between "+" and "*" is the measure of deviation caused by bit rock interaction only and the distance of "*" from the origin is the actual deviation occurred in the hole.

From the trajectory plot of Figure 8.2, by comparing the dashed line and the centre line (desired trajectory and the expected trajectory after initial misalignment), it can be noticed that the hole direction was not set in a desired direction properly which is a result of misalignment of the machine. This has resulted in drilling at a different angle. Planned angle of inclination for this hole was 82 degree whereas it was set at 81.6 degree and hence is a major factor causing the hole deviation in this hole.

From these trajectory plots it can be noticed that the first change in the direction of the actual hole (solid line) is at the depth of 70Ft. This change in the direction

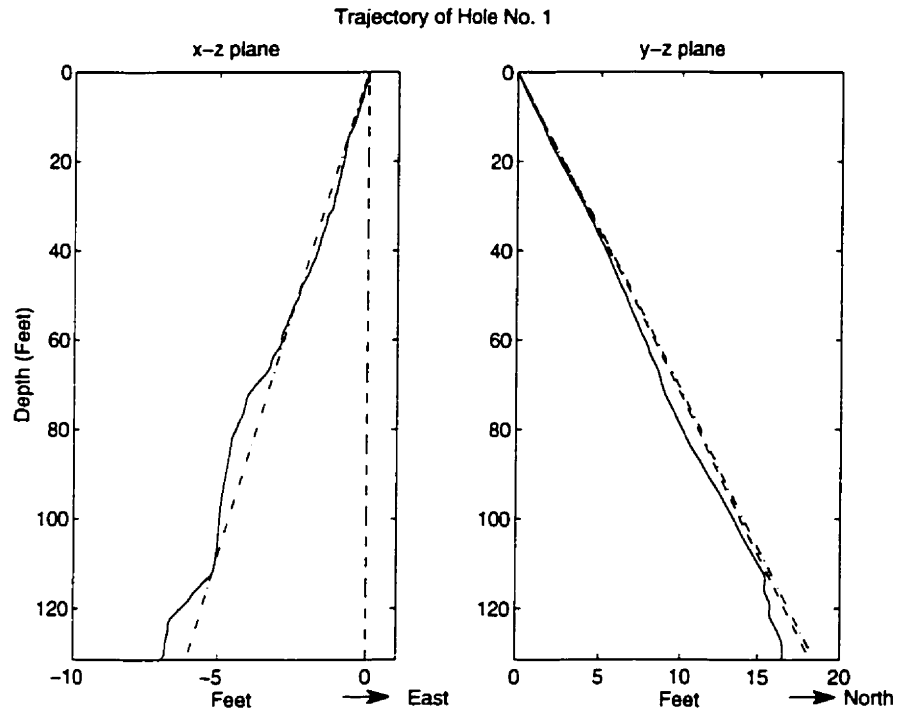


Figure 8.2: Trajectory of hole 1

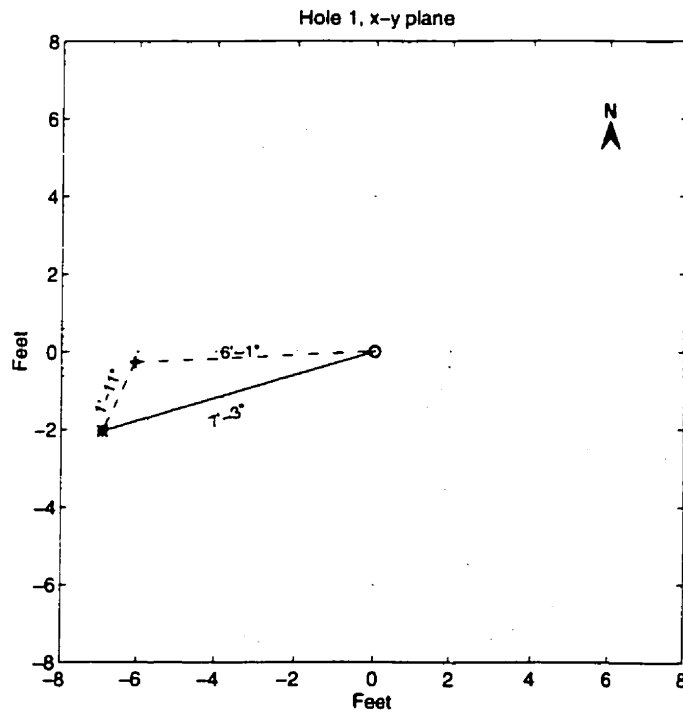


Figure 8.3: Deviation in hole 1

in xz-plane is not towards vertical, whereas in yz-plane it is towards vertical. This means the deviation does not seem to happen under the influence of hammer weight only but due to some other reason related to rock e.g. change in rock strength or lamination etc. At this point we don't have rock structure information at each specific depth, so it is not possible to make any argument. However in the next section we will present a study to relate the effect of change in drilling parameter on corresponding variation in bit direction.

It can be noticed from the Figure 8.3 that the deviation occurred due to misalignment of the machine is 6Ft. 1 inch. Where as deviation due to bit-rock interaction is 1 Ft. 11 inches only. This results in an overall deviation of 7 Ft. 3 inches.

Next two figures Figure 8.4 and 8.5 shows similar plots for hole 5. The desired dip angle for this hole was 72 degree where as it was set by operator at 73.76 degree, a misalignment of 1.76 degree. The trajectory shows a change in the direction at the depth between 30 and 40 Ft. This direction change is towards vertical. This mean the bending in the trajectory happened under the influence of hammer weight probably due to softer rock.

The deviation occurred in this hole can be seen in the Figure 8.5. There is 10Ft 5in. of deviation under the misalignment whereas under the bit-rock interaction it is only 3Ft. 5in. This results in total deviation of 13Ft.

Table 8.1 gives an overview of deviation measurements for all test holes. From this table it should be noticed that there were small deviations occurred in the test holes under bit-rock interaction as compared to the deviation occurred due to misalignment of the machine.

Trajectory plots for all the test holes are given in appendix C. From observation of all these trajectories it can be concluded that a major part of deviation occurred in the test holes are due to misalignment of the machine. Some of the deviation seemed under the influence of hammer weight since they are bending towards verti-

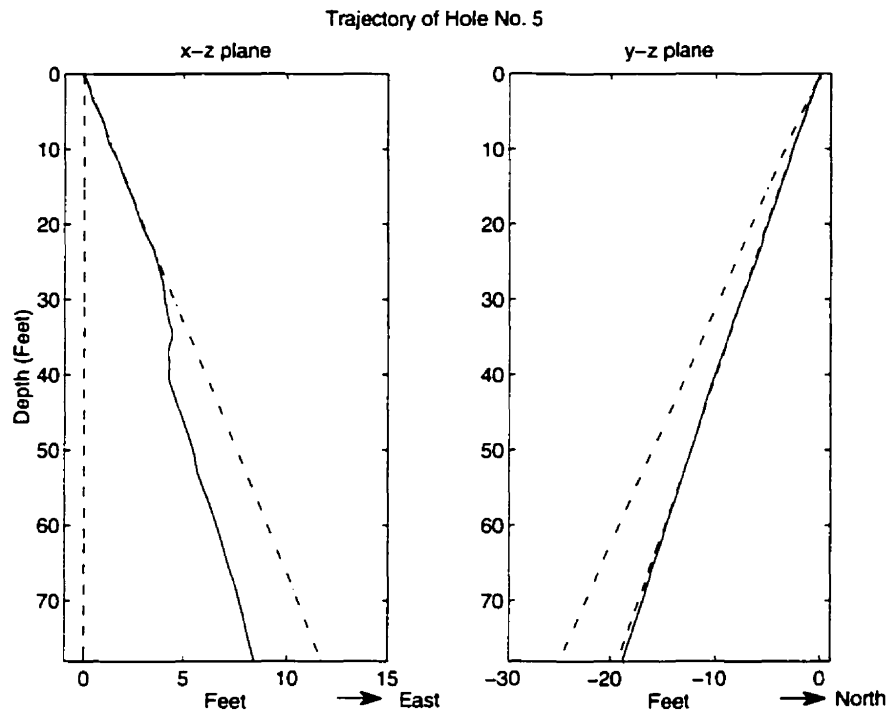


Figure 8.4: Trajectory of hole 5

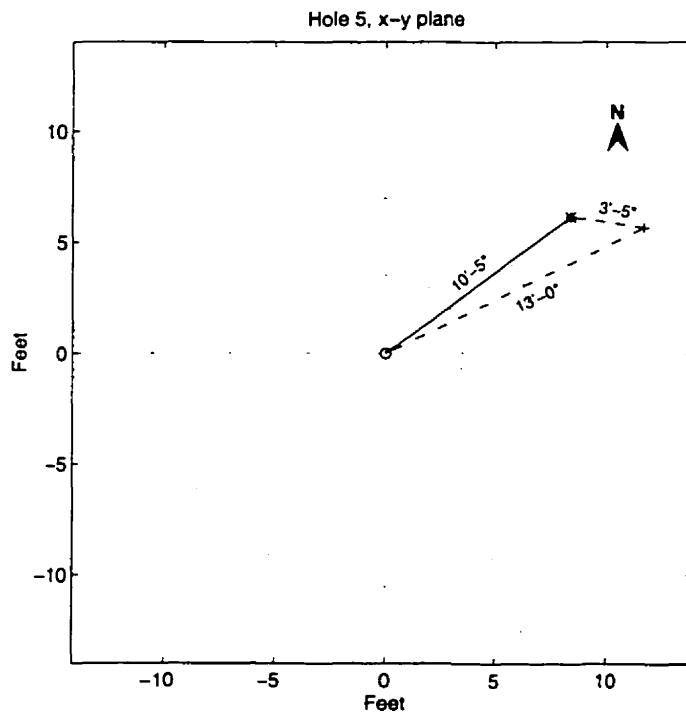


Figure 8.5: Deviation in hole 5

Hole No	Length	Dip angle		Deviation		
		Planned	Actual	due to Misalignment	due to Rock/Machine	Net
	(feet)	(deg)	(deg)	(feet)	(feet)	(feet)
1 (R6H15)	137.88	82.000	81.69	6.080	1.964	7.216
2 (R5H15)	140.32	82.000	82.3	7.369	1.430	7.897
3 (R5H16)	140.31	88.000	89.800	4.352	6.843	3.096
4 (R5H17)	120.69	84.000	84.055	3.873	1.132	3.798
5 (R5H18)	88.88	72.000	73.766	13.039	3.375	10.397
7 (R5H19)	68.58	56.000	55.440	3.523	2.598	6.008
8 (R6H14)	225.26	77.000	79.420	20.656	2.965	22.427
9 (R6H12)	67.26	67.000	66.428	17.617	3.222	17.637

Table 8.1: Table to compare the two types of deviations due to misalignment and machine/rock

cal. However most of the deviation did not occur downwards under the influence of hammer weight. For example hole no 1,2, 4 are partially bending downwards under the influence of hammer weight whereas most part their deviation are away from vertical. Hole 3, 7, 8 did not deviate towards vertical at all. However hole 5 seems to have deviated under the influence of hammer weight only.

It was also noticed during the experiments that the machine could not stabilize on its originally aligned position. Some times it was re-aligned when operator noticed its misalignment. It is therefore strongly recommended that a more precise alignment system be adopted for the alignment of the machine instead of the existing manual method used with CD90B.

8.3 Study of Correlation between Deviation and Machine Parameters

From the hole trajectory shown in previous section it is possible to distinguish between the deviation occurred due to misalignment of the machine and the deviation that occurred due to bit-rock interaction. In this section an analysis of drilling variables to identify their effects of on bit-rock interaction in regards to hole deviation is presented.

Machine data is analyzed to study the correlation between drilling parameters and deviation. This study is done by observing the variation in the deviation parameter and correlating it with corresponding variation in the machine parameters. The deviation parameter used for this study is dip angle and the machine parameters used are feed force, bit torque and head vibration.

Figure 8.6 shows four of these parameters included in the study for hole 5. Plot *a* is the dip angle, *b* is applied feed force, *c* is bit torque and the plot *d* is corresponding

vibration along the depth of the hole. Intended angle of inclination for this hole was 72 degree but due to misalignment it was set at an angle of 73.76 degree. During the drilling of this hole the value of the applied feed force and other parameter was kept almost constant. The variation in the dip angle can be noticed from 73.25 to 76.60 degrees. This variation seems independent of any variation in the drilling parameters shown in the Figure 8.6.

8.3.1 Applied Feed Force and Drill Deviation

In order to investigate for a possible correlation between feed force and the dip angle, all possible values of feed force from the available data were observed and related to the corresponding variation in the dip angle. They do not seem correlated. In the support of this argument two plots are given in the Figure 8.7 and 8.8. These are the plots of feed force and the corresponding dip angle taken from the data of the hole no. 1 and 3 respectively.

In the Figure 8.7 there is a variation in the feed force at different depths. At 650th inch of depth feed value is reduced from 2100 to 1260 lbs. A corresponding variation in dip angle is very slight. Similarly at the depth of 900 inches and 940 inches there are sudden increase in feed value to 2600 and 6000 lbs the dip angle seems insensitive to these high variations as nominal variation in dip is observed. However there is an increase in the dip angle at 1130th inch of depth when dip angle increase from 79.35 degree to 81 degree in response to feed variation from 6000 lbs to 1000 lbs. This only corresponding variation does not confirm that there exist any correlation between the two quantities.

The second Figure 8.8 confirms the insensitivity of the dip angle to feed force variations. In this figure dip angle continues to drops over a large span of the depth (from 100th inch to 300th inch) without any variation in the feed. Furthermore when a sudden change in the value of the feed is introduced it does not effect the slope of

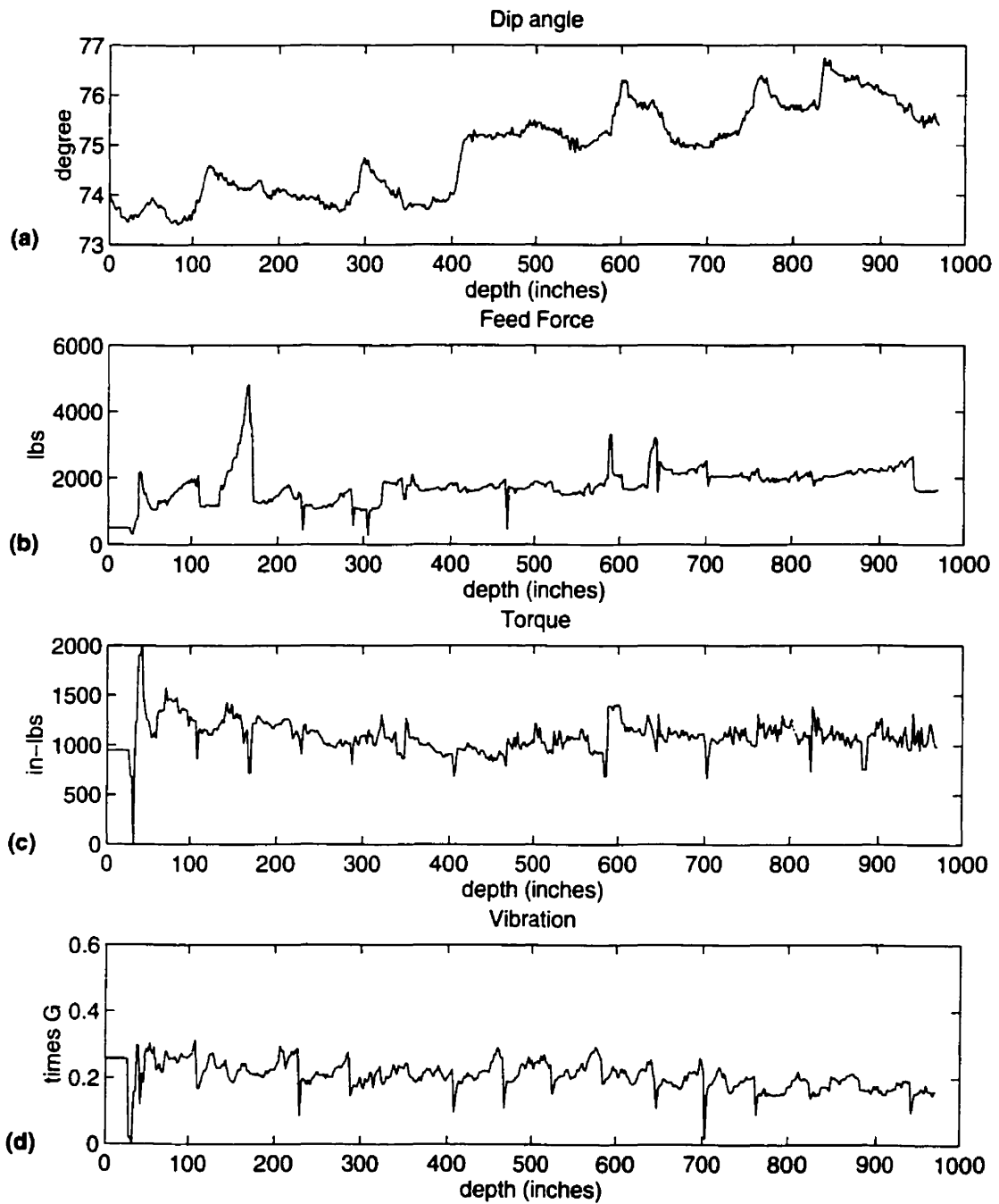


Figure 8.6: Deviation and drilling data for hole 5 (a) Dip angle (b) Feed force (c) Torque and (d) Vibration

the dip angle.

Conclusively, it seems that there does not exist a definite relationship between the two parameters. It is, therefore not possible to establish any such empirical or analytical relationship between two parameters from the available data which could be used in deviation controller design.

8.3.2 Study of Torque at Bit Direction Change

Bit torque is a variable that directly relates to applied feed force. It also varies with the change in the formation strength and hole cleaning condition as discussed in the chapter 4. Due to its dependency on the rock formation it is important to study the effects of this parameter on hole deviation. Figure 8.9 and 8.10 are the plots of dip angle and the corresponding bit torque. In the first Figure 8.9 it seems that there exists some dependency of dip angle on the bit torque, as each time bit torque switches to higher value a corresponding variation in the dip angle can be seen. However it is not very clear. Figure 8.10 does not show similar behaviour of dip angle in response to torque variations. In this figure there are larger variation in the dip angle even at the constant torque values. However in this case the torque value is at its lower level and never exceeded from 2300 in-lbs. From this result we can only conclude that there is a possibility of deviation at higher values of the torque. Similar conclusions were also drawn by Sinkala [80].

8.3.3 Observation of Vibration at Bit Direction Change

Plots shown in the Figure 8.11 and 8.12 show the dip angle and corresponding vibration taken from the hole no. 1 and 4. In the first figure, a change in the dip angle can be noticed at a sudden increase in the vibration level at the depth of 180th inch. Whereas the increase in vibration did not have much effect on the dip

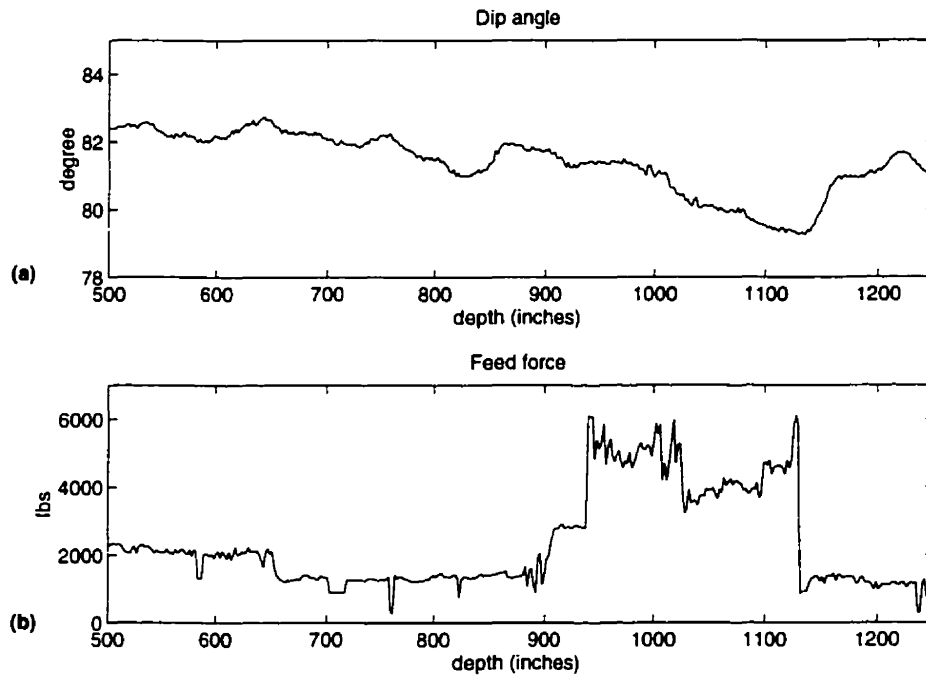


Figure 8.7: Dip angle and feed force from hole 1

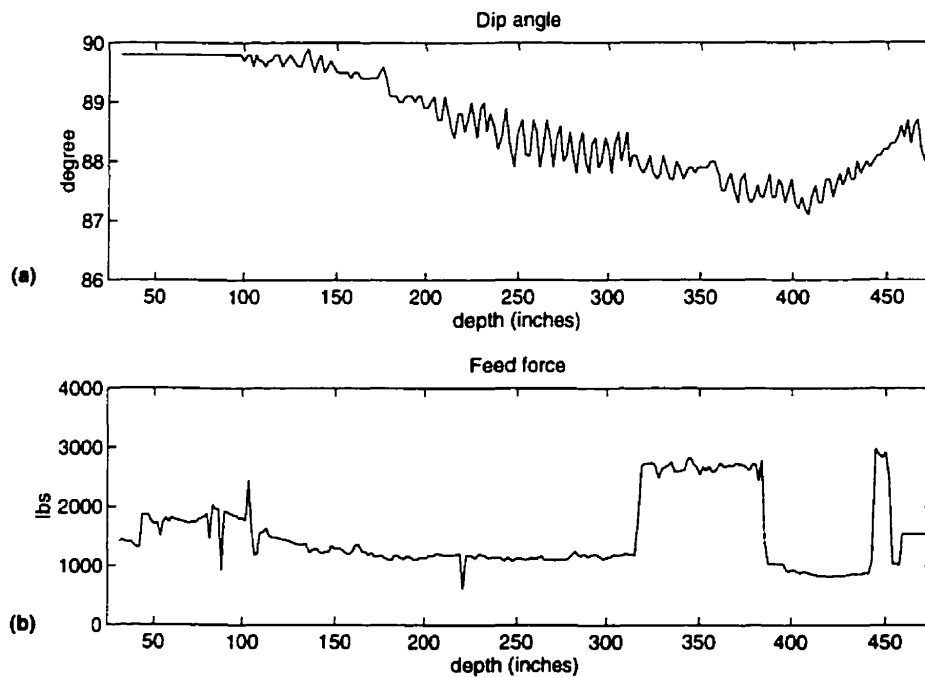


Figure 8.8: Dip angle and feed force from hole 3

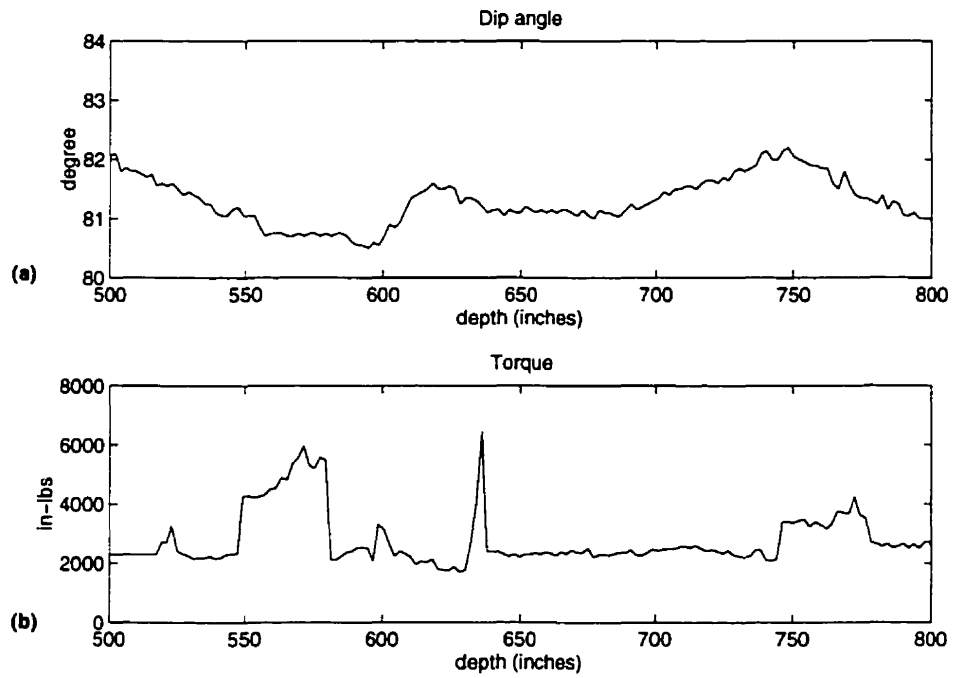


Figure 8.9: Dip angle and Torque at bit from hole 2

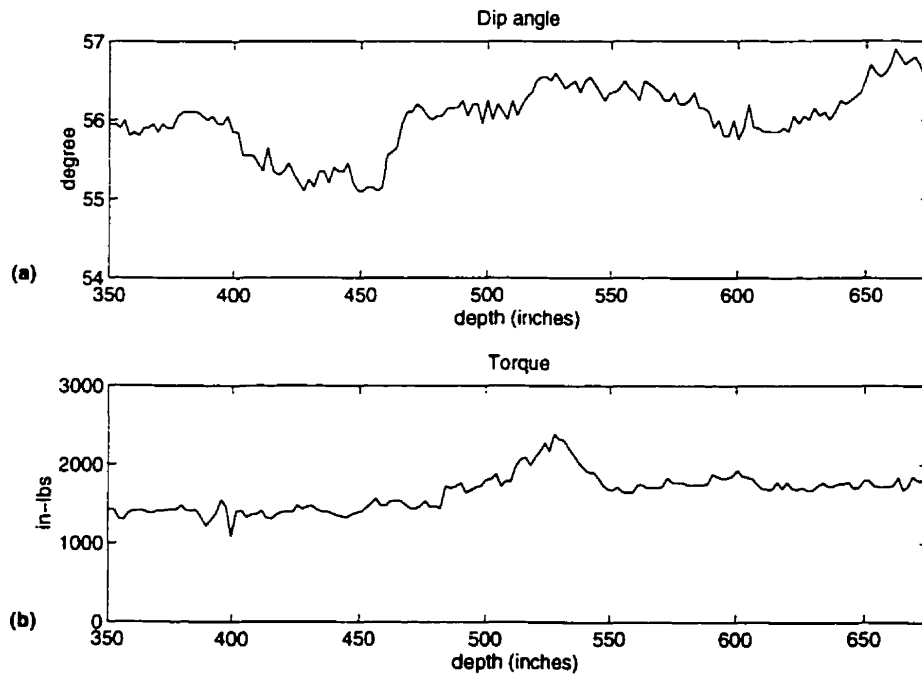


Figure 8.10: Dip angle and bit Torque from hole 7

angle at the depth of 475 inches. Similarly, in the Figure 8.12 a higher variation in dip angle can be seen even at lower level of vibration. Conclusively, if there is any correlation between the two parameters it is too poor to establish any mathematical relationship.

8.4 Quantitative Correlation between Deviation and Machine Variables

Analysis presented in the above section shows that the dip angle is poorly correlated with machine parameters. The level of correlation between these variables can be determined by correlation coefficient. The correlation coefficient is an statistical parameter that measures the correlation between two random variables.

By definition Correlation Coefficient is a measure of linear relationship between two variables.

The value of correlation coefficient equal to +1 implies a perfect linear relationship with a positive slope, while a value of correlation coefficient equal to -1 results from a perfect linear relationship with a negative slope. It might be said then that sample estimates of correlation coefficient close to unity in magnitude imply good correlation or linear association between the two variables, while values near zero indicate little or no linear relationship.

It is calculated as:

$$r_{xy} = \frac{S_{xy}}{\sqrt{S_{xx}S_{yy}}} \quad (8.1)$$

Where S_{xx} and S_{yy} are autocorrection of x and y respectively given by:

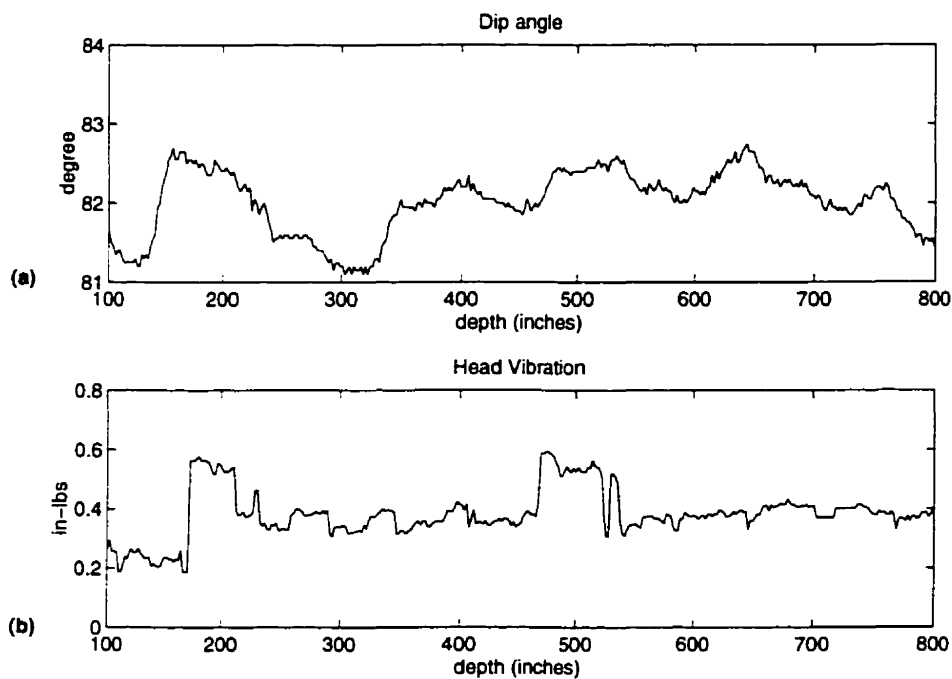


Figure 8.11: *Dip angle and head vibration from hole 1*

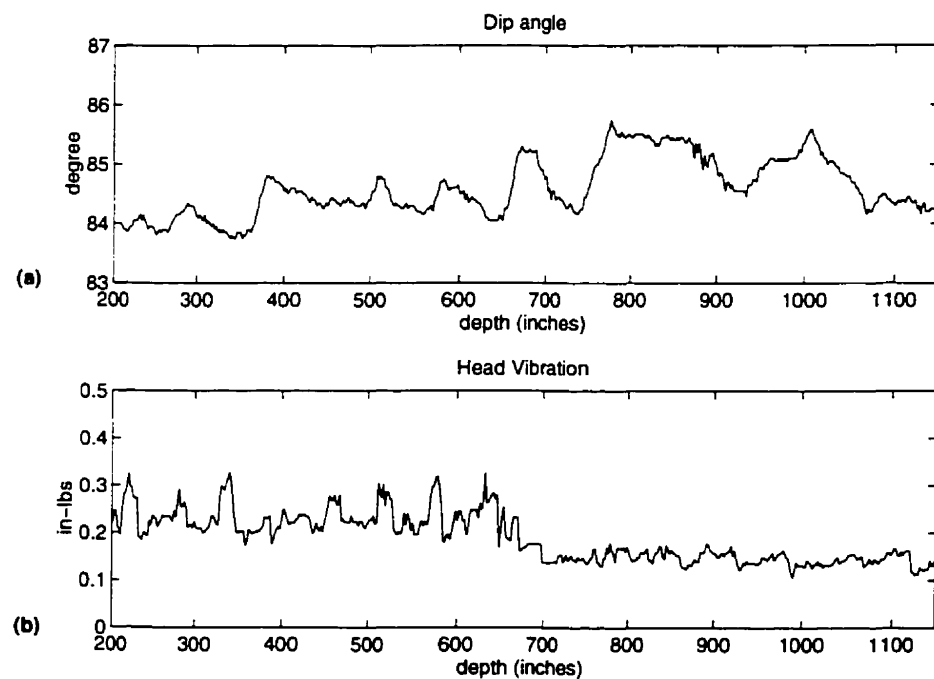


Figure 8.12: *Dip angle and head vibration from hole 4*

Hole No	Coefficient of Correlation between Dip angle and		
	Feed force	Bit Torque	Vibration
1 (R6H15)	0.0434	0.0053	0.1003
2 (R5H15)	0.1635	0.0117	0.1119
3 (R5H16)	0.1097	0.1087	0.2195
4 (R5H17)	0.0588	0.2320	0.4143
5 (R5H18)	0.2929	0.0894	0.3808
7 (R5H19)	0.2794	0.2271	0.4826
8 (R6H14)	0.2158	0.3173	0.4183
9 (R6H12)	0.4180	0.3639	0.2673
Mean	0.1977	0.1694	0.2994

Table 8.2: Coefficient of correlation between dip angle of the different machine parameters

$$S_{xx} = \sum_{i=1}^n (x_i - \bar{x})^2 \tag{8.2}$$

and

$$S_{yy} = \sum_{i=1}^n (y_i - \bar{y})^2 \tag{8.3}$$

Similarly S_{xy} is cross correlation between x and y given by:

$$S_{xy} = \sum_{i=1}^n (x_i - \bar{x})(y_i - \bar{y}) \tag{8.4}$$

Table 8.2 lists the values of correlation coefficient calculated for all holes. It can be seen that the value of the coefficient is quite small and varies between 0.0053 to 0.4826. The mean value of the coefficient of correlation between feed and dip angle is 0.1977. It is 0.1694 for correlation between bit torque and the dip angle

and 0.2994 for correlation coefficient between vibration and dip angle. These results support the results of previous section of poor correlation between machine data and the orientation data.

8.5 Conclusions

Analysis of the field data to investigate the machine dependent hole deviation was presented in this chapter. Following conclusions can be drawn from this analysis:

- The hole trajectory shows that deviation occurred not only due to bit-rock interaction but also due to misalignment of the drill rig.
- Majority of the deviation was due to misalignment of the machine. Smaller deviations were due to bit-rock interaction. Therefore more accurate means of machine alignment should be adopted for CD90B drill rig.
- A smaller portion of hole deviation appears to occur due to drill string weight.
- There is very poor correlation between the drilling machine parameters and the deviation parameters. This means that the most of the deviation due to bit-rock interaction is dependent on rock anisotropy and not on the machine input variables. Hence it is not possible to control the hole deviation by the adjustments of the machine parameters only.

Chapter 9

Design Concept for an ITH Guided Drill

9.1 Introduction

Field data analyzed in the previous chapter shows poor correlation between the drilling machine variables and hole deviation. Rather, the deviation relates to a number of uncontrollable parameters of the rock. It is therefore not possible to control the deviation by manipulating the machine variables alone. Alternatively, the concept of guided drilling can be applied to control the hole deviation.

This chapter discusses the design concept of a novel guided drilling system for ITH percussive drills. There are certain problems which need to be tackled for the development of guided drilling for this type of system, such as bit location measurement and the drill steering mechanism. Some techniques for bit location measurement have been presented. This chapter places emphasis on a novel hammer mechanism to add a steerability to the conventional drilling system. Modelling and simulation of this mechanism to analyze its steerability will be presented in the next chapter.

9.2 Guided Drilling System

Guided drilling can be defined in different ways depending on its application. One scenario is drilling a hole to reach the desired target regardless of the trajectory as, for example, when drilling a number of holes into a submarine reservoir from a single on-shore location. The second type is drilling a hole in a desired trajectory or in a desired rock type, an example of this is coal in-seam drilling. The third type is drilling a hole in a straight line as, for example, in blast hole drilling. The latter definition is the type of guided drilling which our conceptual design will focus on.

The guided drilling system, like a conventional closed loop feed back system, consists of three basic components.

- Bit location measurement
- Control Algorithm
- Actuation (Steering)

A block diagram of the guided closed loop system is shown in Figure 9.1, the bit position is assumed measured by employing a suitable sensor. This measurement is with respect to a reference point in three dimensions at an instant of time. The controller compares this position with the desired position to calculate the error. A command signal is then issued to the actuator based on the error signal. The actuator follows the command signal and sets the direction of drilling to minimize the error.

The controller uses an algorithm to calculate the command signal: this could be a linear PID type of controller or a LQG optimal controller. The algorithm is selected based on the type of application and can only be designed if the two other parts, the sensing and the actuation system, are available. In the remaining part of this

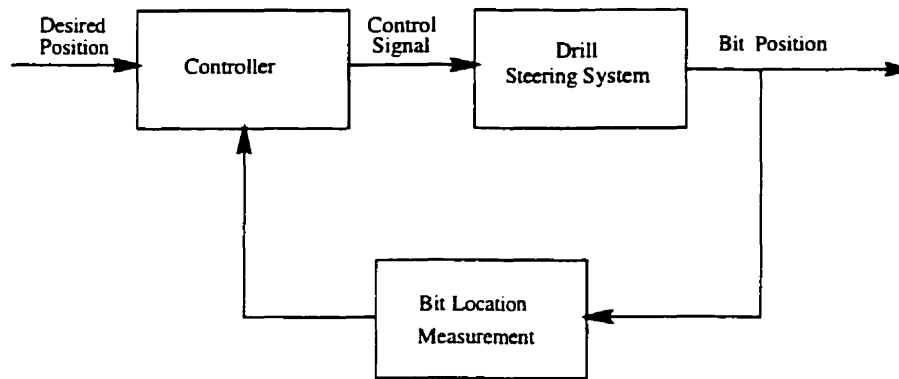


Figure 9.1: Block diagram for a close loop guided system

chapter we will therefore, concentrate on the design of the sensing and actuation parts of the guided system.

9.3 Bit Location Measurement

Bit position and orientation in three dimensions can be represented in polar coordinates as shown in the Figure 9.2. This is represented by the triplet $(R, \theta_{dp}, \theta_{az})$, where (R) is the distance of the bit from the origin, θ_{dp} is the dip angle and θ_{az} is the azimuth angle.

Since the bit rotates constantly during drilling, the rotation angle of the bit is also required to be measured in addition to the orientation angles $(\theta_{az}, \theta_{at})$ and is denoted by ϕ in the figure. The rotation angle is employed by the drill steering actuator mechanism, to be described later in this chapter, to change the drilling direction, i. e. achieve steering. Usage of the rotation angle by the actuator mechanism will be discussed in more detail in the next chapter.

There are several ways that can be applied to measure the position of the bit. These methods can be classified broadly as local sensing and remote sensing. The bit position can be measured locally by installing a down hole sensor close to the

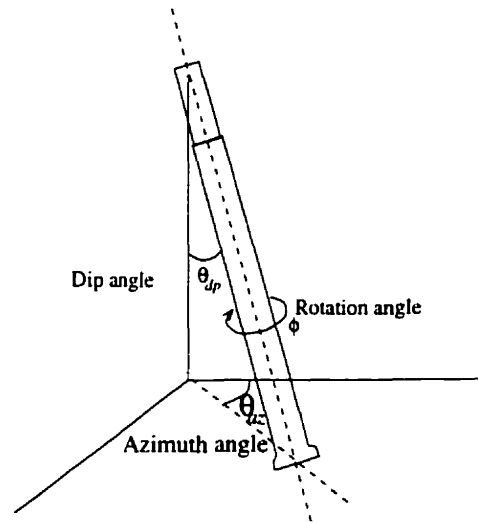


Figure 9.2: Three angles required to be measured to find the position of the drill bit

bit. It can also be sensed remotely from the surface. Both methods have advantages over each other: the choice between them for an ITH percussive system is a trade off between accuracy and survival of the sensor.

9.3.1 Bit Location Measurement by Down-Hole Sensor

Conventional gyroscopic methods can be used to measure bit position. It is a very accurate method and requires installation of a gyroscope assembly at the bottom of the hole. Three main problem associated with down hole sensor must be tackled for efficient operation of the sensing system: signal conditioning, communication and survival.

Several wire-line communication system have been developed for the oil industry [54], these methods tend to be cumbersome and expensive: a wireless telemetry system is much to be preferred. A wireless telemetry system using a microwave link between down hole assembly and the top hole assembly was proposed [64]. A technique involving electro-magnetic waves travelling along the outside of the drill

string used by [86] can also be considered for signal communication.

The percussive ITH hammer itself is a source of severe vibrations. Hence it is very important to consider survival of the sensor to be installed at the bottom of the hole and its capability of withstanding extreme vibration and shock levels. The concept given by [64] of installing the sensor in a special package above the hammer inside the rod assembly could be a good choice.

In summary, there are several problems associated with bit location measurement using down-hole sensors. It therefore does not seem feasible to use this approach in ITH percussive guided drilling.

9.3.2 Bit Location Measurement with Top-Hole Sensor

An alternative to the down hole installation of a sensor is to determine bit position from the surface. Acoustic hydro-phones can be used for this purpose. This approach seems more feasible since sensor survival and signal communication problems do not need to be considered.

Acoustic Emission (AE) source location techniques are successfully used in earth science to monitor the dynamic behaviour of subsurface fractures and can be applied to ITH percussive drills to locate bit position.

Percussive drills in operation can be viewed as a source of acoustic waves with frequency equal to blow rate of the hammer. This acoustic wave can be precisely located by employing acoustic source location techniques from the surface.

There are two types of source location methods which have been applied to subsurface AE measurements. One approach is the single component transducer array, where travel time differences for AE waves to the elements of the array are analyzed. The other approach is the triaxial hodogram method, where arrival direction and arrival time delay of two consecutive waves are measured from a signal recorded by

a triaxial detector [52] [58] [59]

The triaxial hodogram method makes it possible to determine AE source location by using a single sensor unit. It can readily be applied to bit location measurement. The accuracy of this has been further improved by use of spectral matrix analysis [52]. The measurement error for this method has been reported to be as low as 0.6% in distance and the 2.5 degrees per 100 meters in direction. Hence there is a good potential of these methods to be applied to bit location measurement.

Layout of the proposed set up for bit location measurement with a triaxial detector is shown in Figure 9.3. The triaxial detector should be placed at a shallow depth in an adjacent hole to avoid surface distortions [57]. The block diagram in the same figure shows the signal processing for the setup which uses triaxial hodogram analysis to calculate the depth, the dip angle and the azimuth angle for the bit location.

9.4 Steering Concept

Once the bit location is precisely measured, the error in the hole trajectory can be calculated. The actuator corrects this error in hole trajectory in accordance with the control signal. As mentioned previously, it is not desirable to install any instrument close to the ITH hammer due to severe vibrations. Any steering technique which involves installation of down-hole instruments would therefore not be acceptable.

One way to achieve such a robust steering system is similar to one which was developed in Britain by the National Coal Board, Mining Research and Development Establishment (MRDE) [71] in early eighties for rotary drilling. It involved the use of a down-hole motor (DHM) driven by the drilling fluid. The drill string in this case did not rotate and consequently could be used for a variety of steering devices. A commonly used device, the kick-off-sub, was employed as steering device, which

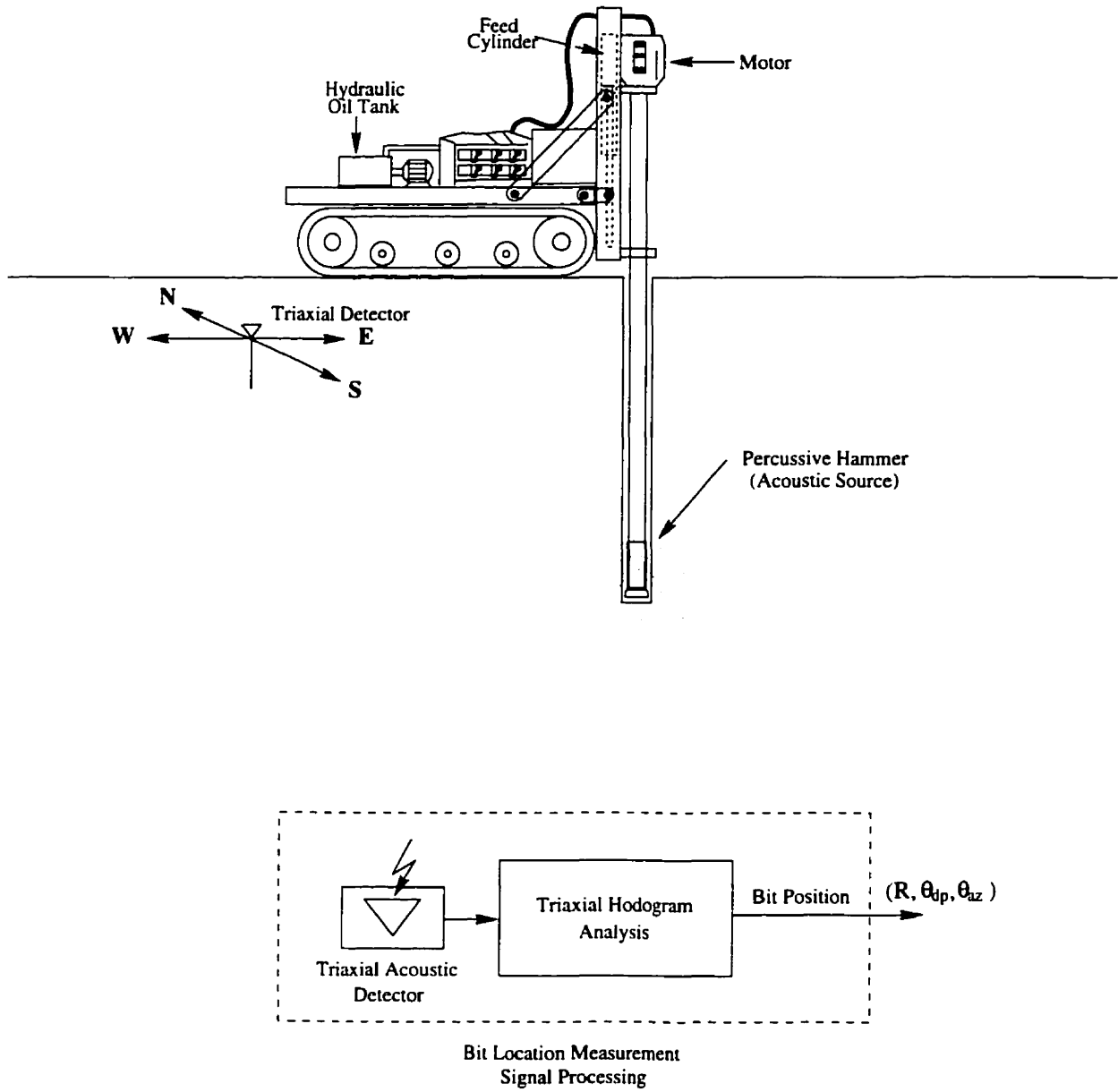


Figure 9.3: Proposed layout of Bit location measurement technique by triaxial detector, and signal processing diagram

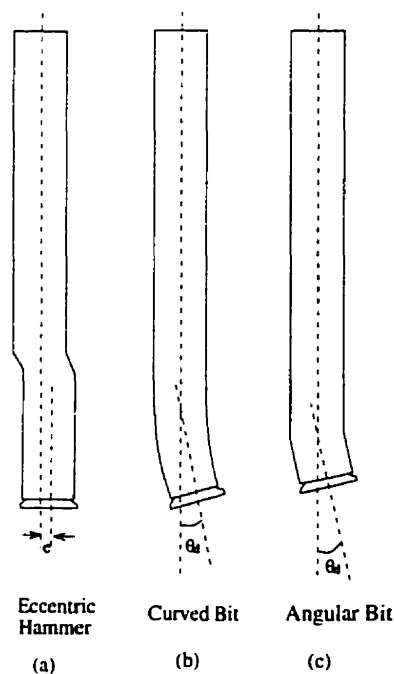


Figure 9.4: *Some possible hammer/bit configurations for angular drilling*

was used to offset the bit slightly from the axis of the drill string. Obviously the important feature of this technique is that steering direction can be changed easily by merely rotating the drill string. In this case (DHM) the drill string was not constantly in rotation but it was turned only for steering purpose.

In ITH percussive drilling the string is continuously rotated to provide indexing to the bit. In this case a permanent offset can be introduced between the bit axis and the axis of drill string as shown in the Figure 9.4a. This simple modification would make the hammer drill in a curved shape (provided it is not being rotated). However, if it is constantly rotated, as in normal operation, it will drill in the same direction as it was drilling without this modification except that the diameter will be slightly larger. This is shown in Figure 9.5. Figure 9.5a shows the expected shape of the drill string when it is not rotated whereas the Figure 9.5b shows the expected straight line trajectory when modified system is rotated at constant speed.

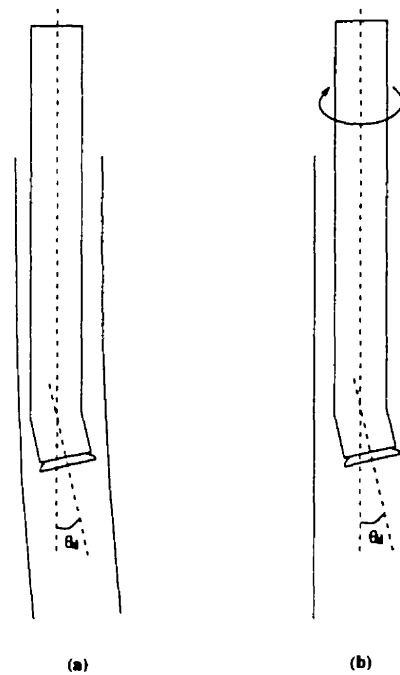


Figure 9.5: *Hole trajectory by CRE-Hammer (a) expected trajectory when bit is not rotated and (b) expected trajectory when hammer is rotated at constant speed.*

The design concept proposed here uses a minor modification in the conventional hammer. Some possible bit/hammer configurations are shown in Figure 9.4.

In the modified hammer with no rotation, the attack of the bit on the rock is coaxial with the axis of the hole but is displaced by an eccentricity e (or at an angle θ_d). Therefore, the bit impacts partially to the side of the wall of the hole hence, instead of drilling in a straight line it will deviate towards the side of the wall being hit. Continuous drilling in this fashion would result in a curved hole. In the case of constant rotation, bit impacts to the side walls are symmetrical on all sides of the hole, which results in a straight line trajectory.

By varying angular speed along the circumference of the hole, the eccentric hammer can be forced to work more on one side of the hole, by slowing down the angular speed, and less on other side, by increasing angular speed. Thus generating a lateral

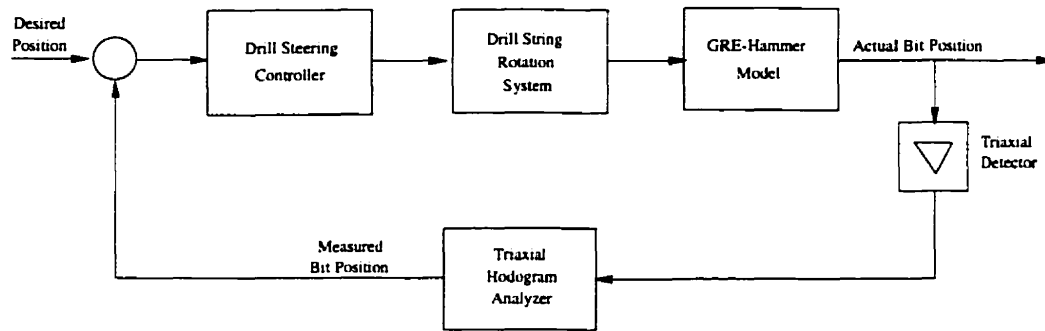


Figure 9.6: *Closed-loop Guided system using Triaxial acoustic detector and CRE-Hammer*

force imbalance around the bit, causing the string to deviate away from a straight line. This adds the steering feature to the eccentric hammer.

A two speed motor could be sufficient to add this feature in the system. The necessary characteristics required for such a motor are high torque, and short transient response.

Hence, through speed control it is possible to steer the modified drill in a desired trajectory. This proposed mechanism is referred to as the “Controlled Rotation Eccentric Hammer Mechanisms” or CRE-Hammer Mechanism.

In the next chapter we will develop a kinematic model of this system to analyze the steerability of the CRE-Hammer.

9.5 The Closed-loop Guided System

Successful development of bit orientation measurement and the proposed CRE-Hammer steering mechanism would enable the system to drill in the desired trajectory. Thus guidance could be achieved without installation of any down-hole instrumentation. This feature of the proposed system makes it unique and easily implementable.

The block diagram of this close-loop guided system which employs a Triaxial detector for bit position measurement and CRE-Hammer for steering the bit is shown in Figure 9.6. As can be seen from the block diagram, the drill steering is achieved through control of the bit rotation system. The bit rotation system can be switched from a one speed to other at any desired rotation angle with a small transition time. The steering controller calculates the switching phase angle based on the error signal and issues the command signal to the rotation system. Hence, it distributes the number of blows per unit of the rotation angle along the circumference of the hole wall in a desired manner. This results in the steering of the drill bit in a desired direction. The control algorithm will be described in detail in the next chapter.

9.6 Conclusion

This chapter discussed the design concept of development a guided drilling system for ITH percussive drilling.

- To add guidance to the existing drilling machine, some minor modifications are proposed which can easily be implemented at minimum cost. The proposed guided system does not require any installation of down-hole instrumentation.
- For bit location measurement a remote sensing technique which employs acoustic source location, using the triaxial hodogram method, is proposed.
- For steering actuation, a Controlled Rotation Eccentric Hammer Mechanism (CRE-Hammer Mechanism) is proposed. In this mechanism the rotation of the bit is controlled along the rotation angle of the bit of an eccentric hammer to achieve steering.

Chapter 10

Modelling and Simulation of Proposed Hammer Mechanism

10.1 Introduction

This chapter develops a kinematic model of the CRE-Hammer mechanism. The steerability of the system is analyzed through simulation of the mechanism.

The model is formulated by employing basic kinematic principles. It first calculates the bit position at each blow of the percussive hammer and then integrates the position vector along the depth of the hole. For simplicity a uniform rock formation is assumed. The model is simulated for constant rotation and dual rotation speed. Steering through dual rotation speeds is successfully demonstrated.

10.2 Trajectory of Hole drilled with Conventional ITH Percussive Hammer

Consider a conventional percussive in-the-hole (ITH) drill (the schematic of this hammer is shown in the Figure 1.2). During the normal operation of the percussive drill, a compressed-air or a hydraulically operated piston reciprocates inside a cylinder. In the power stroke (downward stroke) the piston impacts the bit and, this impacting action transfers the potential energy of the compressed air or the hydraulic fluid into kinetic energy. The bit moves and strikes on the facing rock, and rock breaking phenomenon of crushing and chipping takes place. In conventional hammers, the line of attack of the bit on the rock is along the axis of the drill string. The bit therefore penetrates in a straight line along the axis of the drill string.

Let the blow rate (the percussion rate) of the hammer be b_r blow/sec. If uniform geological formation is assumed then each blow will cause the hammer to penetrate $v(t)$ inch. $v(t)$ is constant for uniform rock formation. However it is a random variable in real situations because of rock anisotropy. Therefore, for a uniform rock formation the penetration rate is given by:

$$P_r = b_r v(t) \quad \text{inch/sec.} \quad (10.1)$$

Hole trajectory can be obtained by integrating the effects of the blow vectors along the drilling depth. We employ vector theory to calculate the trajectory. Let us denote a position vector by $P(t)$, which represent the position of the bit at time t in three dimensions with respect to the some reference point $O(x(0), y(0), z(0)) = (0, 0, 0)$. At a certain time instant this position vector is defined as $P(t) = P(x(t), y(t), z(t))$.

At each blow of the hammer the bit position is calculated by adding the vector $v(t)$

to the position vector $P(t)$. i.e.

$$P(x(t), y(t), z(t)) = P(x(t - \Delta t), y(t - \Delta t), z(t - \Delta t)) + v(x(t), y(t), z(t)) \quad (10.2)$$

In this equation the indices x , y and z represent the three mutually orthogonal components of the position vector. The Δt is the time interval between two consecutive blows. If we assume that the blow rate of the hammer is constant throughout the drilling, the time interval Δt can be assumed as a constant quantity.

The drill bit undergoes a constant rotation. The rotation has a little effect on the breakage process, however it does improve the drilling process by indexing the bit attack on the rock and enables it to cut in an efficient way. The penetration caused by the rotation only is therefore assumed to be zero.

10.3 Trajectory of Hole drilled with CRE-Hammer with no rotation

The proposed design of CRE-Hammer mechanism, described in the previous chapter, suggests a minor modification in the conventional hammer. The hammer is modified in such a way that there is a slight offset between the axis of hammer and the bit percussion line, or there is some angle, say θ_d , between them such as shown in the figure 9.4.

As defined above, $v(t)$ is the vector of penetration due to a single blow at time t . The direction of this vector is not co-axial with the CRE-Hammer axis but is at an angle θ_d as illustrated in Figure 10.1.

Let us assume a unit vector along the vertical line (z -axis) representing the unit length of penetration along z -axis. The direction of deviation of this vector can be obtained by rotating this unit vector by an angle θ_d and the length by multiplying

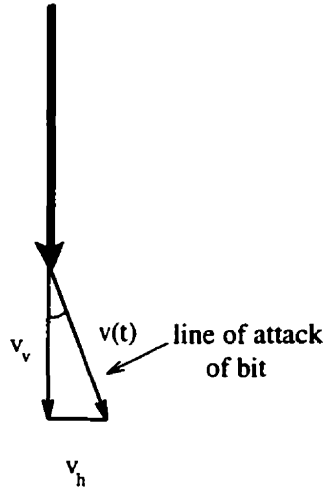


Figure 10.1: Penetration cause by a single blow vector $v(t)$ which is at an angle of θ_d with hammer axial line

with penetration $p(t)$ (penetration obtained by the blow at time t). Hence the increment vector $p_z(t)$ along z-axis would be

$$p_z(t) = \mathcal{R}_p p(t) u_z \quad (10.3)$$

Where

$$u_z = [0 \ 0 \ 1]^T$$

\mathcal{R}_p denotes the rotational operator, which rotates the vector $p(t)u_z$ around the y-axis by an angle θ_d (Since the drill string is not in rotation, it is assumed to be positioned such that the bit is offset along x-axis and causing deviation in x direction as shown in Figure 10.1). \mathcal{R}_p is therefore defined as a rotational matrix about the y-axis.

$$\mathcal{R}_p = R_y(\theta_d) \quad (10.4)$$

$$(10.5)$$

$$R_y(\theta_d) = \begin{pmatrix} \cos(\theta_d) & 0 & \sin(\theta_d) \\ 0 & 1 & 0 \\ -\sin(\theta_d) & 0 & \cos(\theta_d) \end{pmatrix} \quad (10.6)$$

Since the bit is not rotating the vector $p_z(t)$ can be added to the bit position vector $P(t)$ without applying any further rotation operation provided that it is drilling in the vertical direction (along z-axis). i.e.

$$v(t) = p_z(t) \quad (10.7)$$

For non vertical drilling the vector $p_z(t)$ is required to be reoriented in the direction of drilling before it is equated to the vector $v(t)$, to update the position $P(t)$. Therefore:

$$v(t) = \mathcal{R}_s p_z(t) \quad (10.8)$$

Where \mathcal{R}_s is the drill string orientation operator. It adjusts the position of a given vertical (along z-axis) vector along the direction of advancement of drill string. So it is defined as the product of two rotation matrices.

$$\mathcal{R}_s = R_y(\theta_{dp})R_z(\theta_{az}) \quad (10.9)$$

Where $R_y(\theta_{dp})$ and $R_z(\theta_{az})$ are rotational operators about the y-axis and the z-axis respectively similar to $R_y(\theta_d)$ in equation 10.6.

$$R_y(\theta_{dp}) = \begin{pmatrix} \cos(\theta_{dp}) & 0 & \sin(\theta_{dp}) \\ 0 & 1 & 0 \\ -\sin(\theta_{dp}) & 0 & \cos(\theta_{dp}) \end{pmatrix} \quad (10.10)$$

$$(10.11)$$

$$R_z(\theta_{az}) = \begin{pmatrix} \cos(\theta_{az}) & \sin(\theta_{az}) & 0 \\ -\sin(\theta_{az}) & \cos(\theta_{az}) & 0 \\ 0 & 0 & 1 \end{pmatrix} \quad (10.12)$$

The two angles θ_{az} and θ_{dp} are the dip and the azimuth angle respectively and represent the current drilling direction of the hammer.

Combining equation 10.3 and equation 10.8 we have:

$$v(t) = \mathcal{R}_s \mathcal{R}_p p_z(t) \quad (10.13)$$

The position vector at time t is updated by addition of the blow vector $v(t)$. Equation 10.14 gives this relationship.

$$P(x(t), y(t), z(t)) = P(x(t - \Delta t), y(t - \Delta t), z(t - \Delta t)) + v(x(t), y(t), z(t)) \quad (10.14)$$

Substituting the value of $v(t)$ from equation 10.13, we get:

$$P(x(t), y(t), z(t)) = P(x(t - \Delta t), y(t - \Delta t), z(t - \Delta t)) + p(t) \mathcal{R}_s \mathcal{R}_p u_z \quad (10.15)$$

Addition of the $v(x(t), y(t), z(t))$ vector which is deviated by an angle of θ_d with respect to the drilling line will also affect the orientation of the drill string. The new orientation angles θ_{az} and θ_{dp} of the hammer are calculated as follows:

A vector, V_h , along the drill string of length equal to the length of the hammer L_h , is used to find the orientation angles of the drill string, given by:

$$V_h(t) = P(t) - P(t - i_L) \quad (10.16)$$

Where i_L is an index to the position vector, which defines the rear of hammer so that the length of V_h is equal to L_h . This can be obtained by adding all the previous blow vectors till the sum is equal to L_h i.e.

$$i_L = \arg \min_n (|L_h - \sum_{i=0}^n v(t - \Delta t_i)|) \quad (10.17)$$

The hammer orientation angles θ_{dp} and θ_{az} are calculated as:

$$\theta_{dp}(t) = \tan^{-1} \left(\frac{|V_h(x, y)|}{V_h(z)} \right)$$

$$\theta_{az}(t) = \tan^{-1}\left(\frac{V_h(y)}{V_h(x)}\right)$$

The above mentioned mathematical model gives position of the bit when drilling in a uniform rock in the absence of rotation. The model was simulated in MATLAB. The value of bit blow rate used in simulation was 24 blow/sec. A penetration rate, P_r , value of 15 in/min (0.25 in/sec) was used to calculate penetration per blow $p(t)$. Diameter of the bit is 8 inches.

The result of this simulation is shown in the Figure 10.2 and 10.3. In the Figure 10.2 the bit angle θ_d is assumed as 0.0167 radians (0.96°) whereas in the other figure it is assumed as 0.0083 radian (0.47°). The deviation caused by the hammer itself is 250 inches (20 Ft.) and 125 inches (10 Ft.) over the drilling of 1000 in (83 Ft) respectively. The trajectory of the hole is as expected compared with the figure 9.5. A turning rate of 0.123in/in is achieved for θ_d equal to .0083 radian whereas it is 0.250in/in for θ_d equal to 0.0167 radians. These are the maximum value of the turning rate that can be achieved with the respective bit angles.

10.4 Addition of Rotation

In the case of a rotating drill, the bit-offset moves about the drill string axis and hits the side wall all around the hole. This situation is like a vector rotating around the other vector which is at an angle θ_d as shown in Figure 10.4.

At each blow the bit will hit on the side of the hole at a different angular position depending on angle ϕ (the rotation angle). The vector p_z in this case undergoes another rotation by an angle ϕ around the z-axis before it is operated on by \mathcal{R}_s . Thus equation 10.8 is modified as:

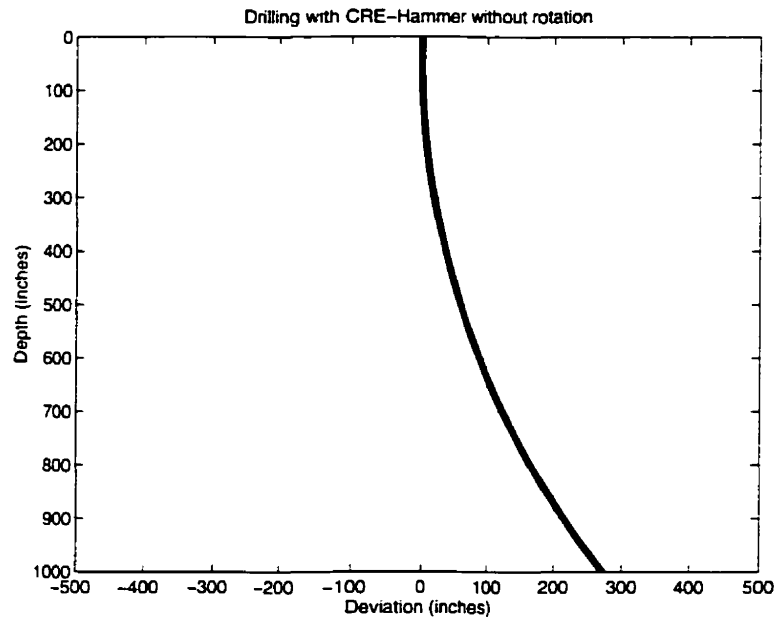


Figure 10.2: Result of simulation run for the model of CRE-Hammer mechanism when drill is not rotating. Assumed value of θ_d is 0.96°

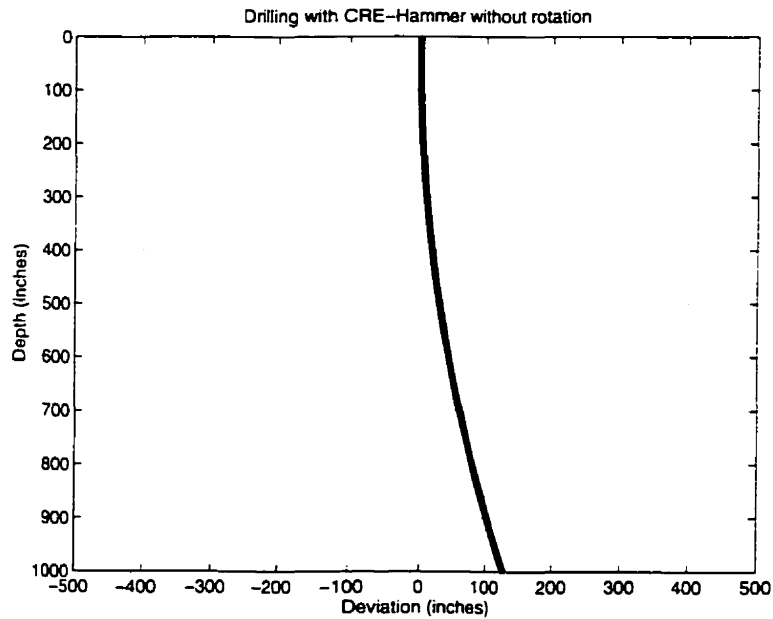


Figure 10.3: Result of simulation run for the model of CRE-Hammer Mechanism when drill is not rotating. Assumed value of θ_d used for this simulation is 0.47°

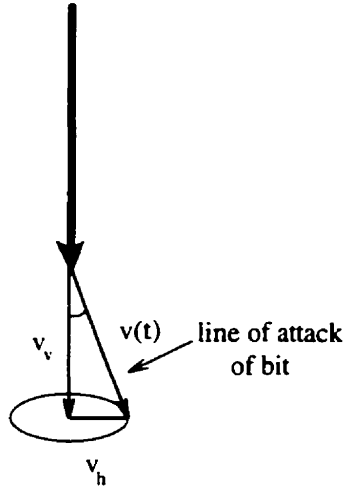


Figure 10.4: *Vector rotation around a centerline represents the effect of rotation when added to CRE-Hammer*

$$v(t) = \mathcal{R}_s \mathcal{R}_r p_z(t) \quad (10.18)$$

where

$$\mathcal{R}_r = R_z(\phi)$$

For constant rotation, it will equally impact on all sides of the hole causing an increase in the radius of the hole by $p_z \sin(\theta_d)$. As it is cutting equally on all sides of the hole, widening of the hole diameter would be smooth and a straight line trajectory would be obtained.

For simulation, the bit rotation circle was divided in n_s segments. The phase angle ϕ , therefore, varies between 0 to 2π with an increment of $2\pi/n_s$ radians. Let us assume that rotation speed is given by N RPM and the blow rate by b_r blows/sec. The angular velocity ω is

$$\omega = \frac{2\pi N}{60} \quad \text{rad/sec.} \quad (10.19)$$

The number of blows per radian of rotation are therefore:

$$b_{ra} = \frac{b_r}{\omega} = \frac{60b_r}{2\pi N} \quad (10.20)$$

The number of blows for each rotation angle ϕ increment are:

$$b_{rs} = b_{ra} \frac{2\pi}{n_s} \quad \text{blows} \quad (10.21)$$

The value of n_s used in simulations is 48. Simulation results for a constant rotation of the drill string are shown in the Figure 10.5 and 10.6. These two simulations were run at a different constant motor speeds of 15 RPM and 30 RPM. Figure 10.5 show the results of simulation when the drill is rotating at lower speed whereas Figure 10.6 is for simulation when the motor is rotating at higher speed. Plot *a* of each of these two figures shows three dimensional trajectory where as plot *b* shows two dimensional view of the trajectory. Initial drilling direction for figure 10.5 is along vertical and that of figure 10.6 is at an angle 0.1 radians (5.7°) with vertical. Both plots shows a straight line trajectory of the holes as expected. Since the CRE-Hammer bit hits to side walls of the holes, there is an expected increase in the diameter of the hole.

Increase in diameter δd can be calculated by multiplying horizontal components of $p_z(t) \sin(\theta_d)$ with number of blows per segment.

$$\delta d = 2p_z(t) \sin(\theta_d) b_{rs} \quad (10.22)$$

The diameter of the hole is given by:

$$d(t) = d_c + \delta d \quad (10.23)$$

Whereas d_c is the drill bit diameter which is the expected diameter of hole in absence of rotation.

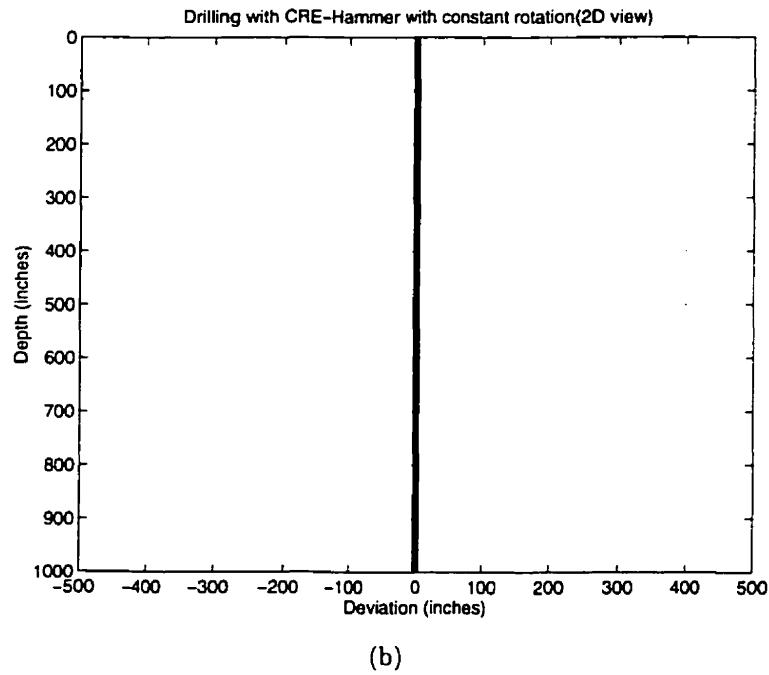
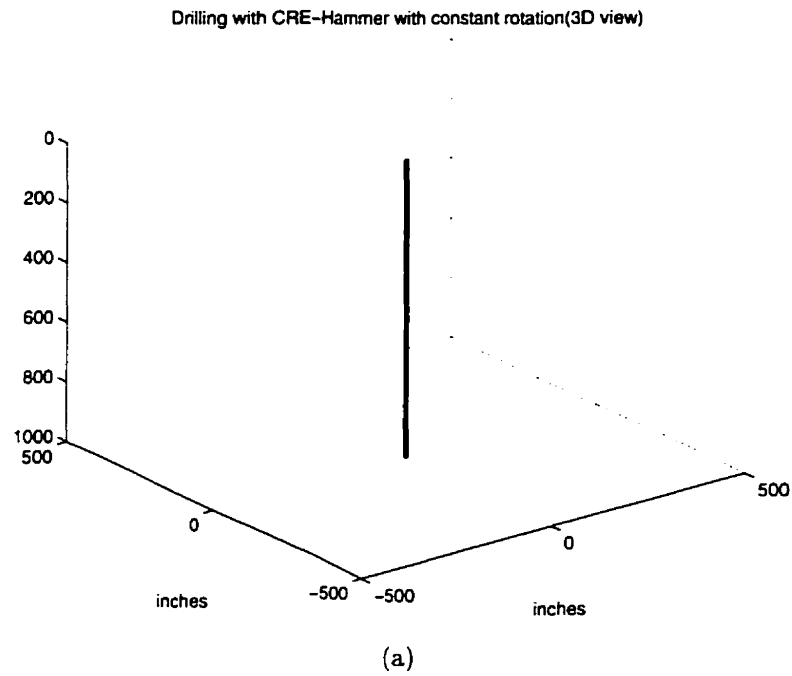
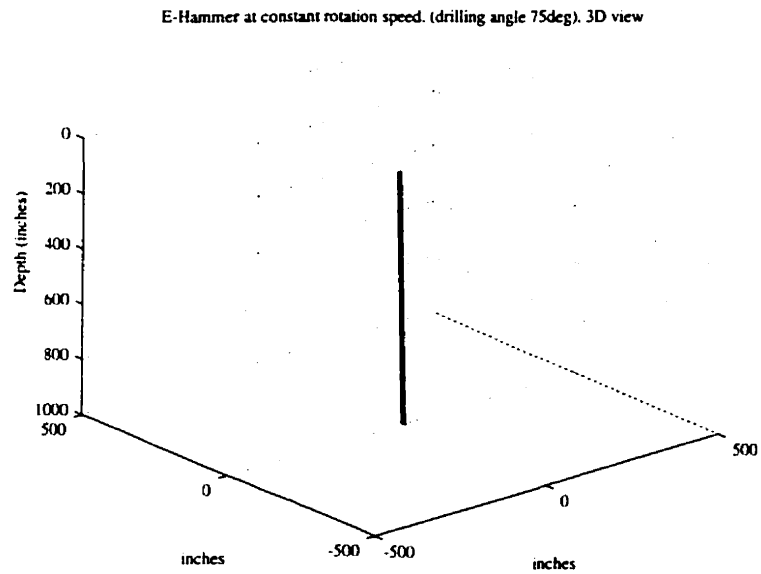
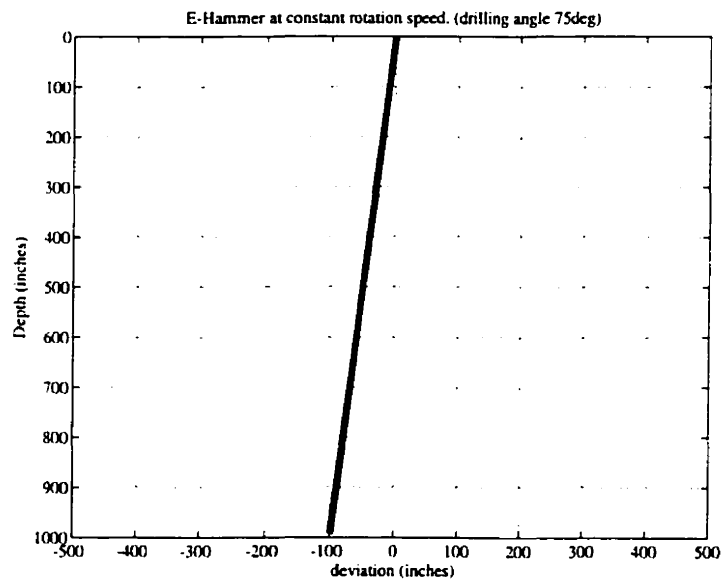


Figure 10.5: *Trajectory of hole drilled with CRE-Hammer when it is rotated at constant speed for vertical drilling (a) 3D view and (b) 2D view*



(a)



(b)

Figure 10.6: Trajectory of hole drilled with CRE-Hammer when it is rotated at constant speed for inclined drilling (a) 3D view and (b) 2D view

Increased hole diameter might increase the chances of drill string buckling. Hence a trade-off between the this diameter and the bit angle of attack should be the best choice in design of CRE-Hammer. The calculated values of δd were always less than the 0.01% of the bit diameter for all value of θ_d used in the simulations.

10.5 Steering the CRE-Hammer through Speed Control

It has been demonstrated by simulations that if the CRE-Hammer is used to drill without rotation it will deviate in a specific direction, i.e in the direction of offset in the bit. However, the drill trajectory is a straight line if a constant rotation is added to the CRE-Hammer and it will cause an increase in the diameter of the hole depending on the bit angle θ_d and the speed of the rotation.

At constant speed the number of bit strokes (blows) per unit angle of the rotation, b_{rs} , are also constant. However, if b_{rs} varies along the rotation angle, then depths of side cuts would not be equally divided all around the hole. It would be deeper on lower blow rate side and shallower on other side. For example if the blow rate during the rotation angle $0 \rightarrow \pi$ is half of the rate of blow during the angle $\pi \rightarrow 2\pi$, the horizontal components of the vector $p_z(t)$ for angle $0 \rightarrow \pi$ would be double in length as compared to the components for angle $\pi \rightarrow 2\pi$. The centre point of the hole will move toward the angle between $0 \rightarrow \pi$ which is $\pi/2$, hence a forced deviation will be achieved. Continuous drilling in such a pattern would obviously deviate the hole in the direction of the lower-blow rate side.

This means a controlled value of b_{rs} would be required to achieve control on drill steering. Two values of b_{rs} and switching from one value to other at some predetermined angles would suffice to achieve this capability. A fast switching would,

however, be the essential requirement for this system.

Variations in b_{rs} can be achieved by varying rotation speed of the drill string. A hydraulic motor is generally employed for such systems. A variable speed motor with a fast transient response can be used for this purpose. In the simulations we assume that such a motor is employed by the drilling system and that control over the speed at any desired rotation angle ϕ is also available.

Deviation caused by a single blow is $v(t) \sin(\theta_d)$. This deviation vector exists in the plane facing the drill bit. In case of vertical drilling it would be in the xy-plane, the direction angle of this vector is the same as the current value of the rotational angle ϕ . Vector $p_z(t)$ can be used to calculate the net deviation occurred during a complete rotation of drill bit. Since the deviation component of this vector is in the xy-plane, the sum of all the components of the $p_z(t)$ vector in this plane would be the net vector of deviation.

Net deviation in one rotation is the horizontal component of the vector D given by:

$$\mathbf{D} = \sum_{i=1}^{n_s} p_z(t_i) b_{rs}(i) \quad i = 1 \quad . \quad . \quad . \quad n_s \quad (10.24)$$

Where t_i represents the time in a one rotation of drill string such that $0 \leq \phi(t_i) \leq 2\pi$. In case of constant rotation when no deviation is expected, D would be a vertical vector i.e all of its component in horizontal plane would be zero. ($D \sin \theta_D = 0$).

However for an uneven distribution of b_{rs} along the circumference of bit rotation the horizontal component of this vector is non zero with the direction angle ϕ_D in xy-plane given by:

$$\phi_D = \tan^{-1} \left(\frac{D(x)}{D(y)} \right) \quad (10.25)$$

For the proposed system, two speeds of the motor are employed to achieve steering.

In this case, b_{rs} will have only two values, high and low, and therefore divides each rotation in two half circles such that b_{rs} switches its value from a to b at angle ϕ_{sw1} (switching angle 1) and return back to a at angle $\phi_{sw2} = \phi_{sw1} + \pi$ (switching angle 2). Now if $a < b$, during half circle travel from angle ϕ_{sw1} to ϕ_{sw2} the bit will have more chance to dig more in this area and causing deviation in this direction. The deviation angle ϕ_D , is given by:

$$\begin{aligned}\phi_D &= \frac{\phi_{sw2} - \phi_{sw1}}{2} + \phi_{sw1} \\ &= \frac{\phi_{sw1} + \pi - \phi_{sw1}}{2} + \phi_{sw1} \\ &= \phi_{sw1} + \frac{\pi}{2}\end{aligned}\tag{10.26}$$

Conversely for any required deviation angle ϕ_D it would be possible to find switching angles given by:

$$\phi_{sw1} = \phi_D - \frac{\pi}{2}\tag{10.27}$$

and

$$\begin{aligned}\phi_{sw2} &= \phi_{sw1} + \pi \\ &= \phi_D + \frac{\pi}{2}\end{aligned}\tag{10.28}$$

Change in switching angle can therefore be applied to vary the direction of steering. The controller calculates the switching angles based on the desired steering direction as given above. Figure 10.7 to 10.10 shows the result of simulation when the speed control was applied to the CRE-Hammer.

For Figure 10.7 the bit angle θ_d used is 0.47° . Speed switching angle for steering purpose used in this simulation are used are: $\phi_{sw1} = -45^\circ$ and $\phi_{sw2} = 135^\circ$. Clearly

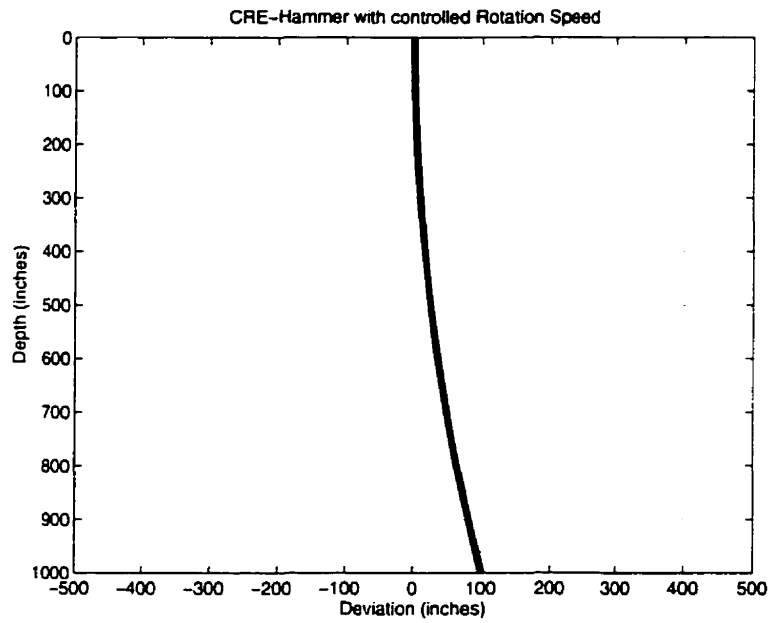


Figure 10.7: Result of simulation when CRE-Hammer with speed control was used. The bit angle θ_d used in the simulation is 0.47° .

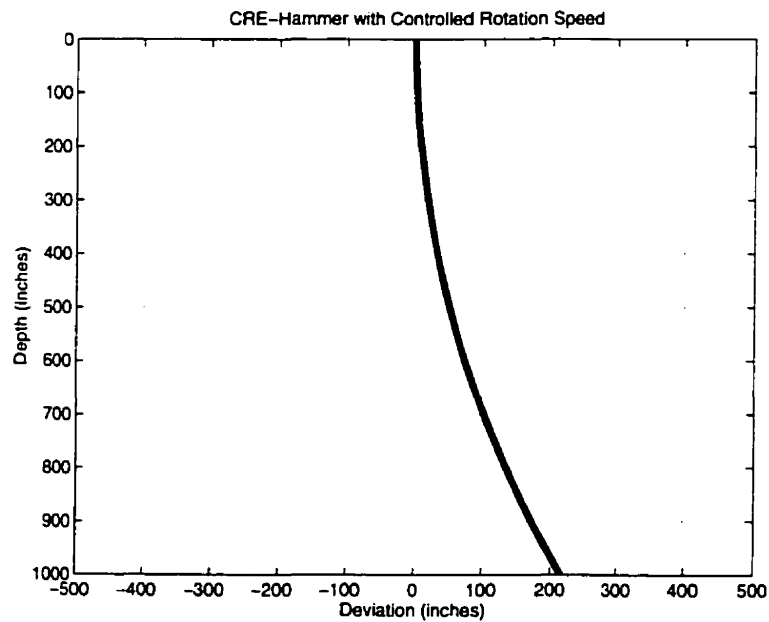


Figure 10.8: Result of simulation when CRE-Hammer with speed control was used. The bit angle θ_d used in the simulation is 0.96° .

a deviation from straight line is achieved which gives a turning rate of 0.1in/in. Similar values of switching angles were used for the simulation shown in Figure 10.8 but the bit angle was 0.96° . In this case a large deviation is achieved. The turning rate calculated for this case is 0.22in/in. The choice of the angle θ_d should be made based on field experiments of such a and desired steerability of the CRE-Hammer.

In Figures 10.9 and 10.10 two steering activities are simulated. The bit moves vertically in the first few inches. The speed of rotation during this length of drilling was kept constant. At the 100th inch the speed switching is started. During the drilling from 100 inches to 300 inches in figure 10.9 the ϕ_{sw1} is at phase angle of -45 degree where as ϕ_{sw2} is at phase angle of 135 degrees. It can clearly be seen that the drill has deviated towards the intended direction. At a depth of 300 inches the angle of deviation is changed by setting ϕ_{sw1} to 135 and ϕ_{sw2} equal to -45. This causes reverse steering and the drill starts deviating back to the vertical. The bit angle θ_d for the simulation of figure 10.9 was 0.96° The bit angle used for simulation of the figure 10.10 was 1.35° .

These results demonstrate the steering capability of the proposed drilling system.

10.6 Compensation for Torsional Twist in the Drill String

In the simulation of CRE-Hammer mechanism presented in this chapter the bit rotation angle ϕ was assumed to be precisely known. This angle is supposed to be measured by a sensor installed near rotary motor at the top of the hole. Hence the measured value gives the rotation angle of the drill string near the sensor. This value may not be representing true rotation angle of the bit due to a possible twist in the drill string caused by its torsional loading. This torsional loading is due to

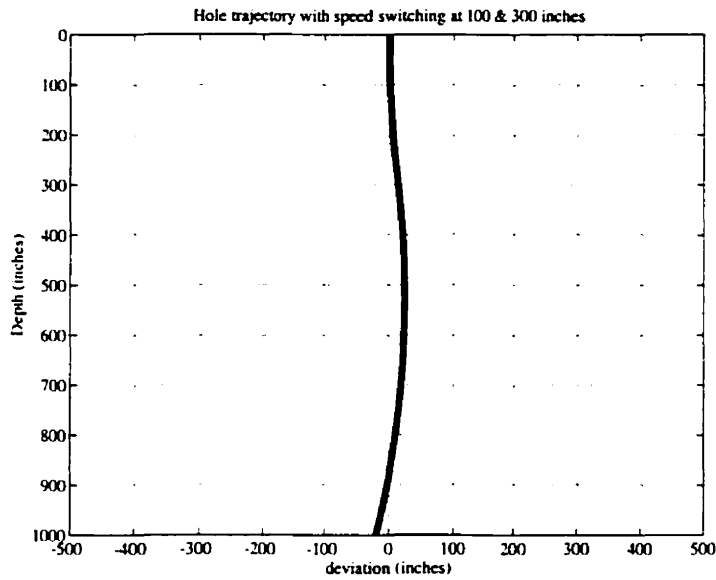


Figure 10.9: Result of simulation of CRE-Hammer, when it has two rotation speeds. Speed control angles were changed at 100 in and then 300 in. This cause a change in direction of bending of hole trajectory.

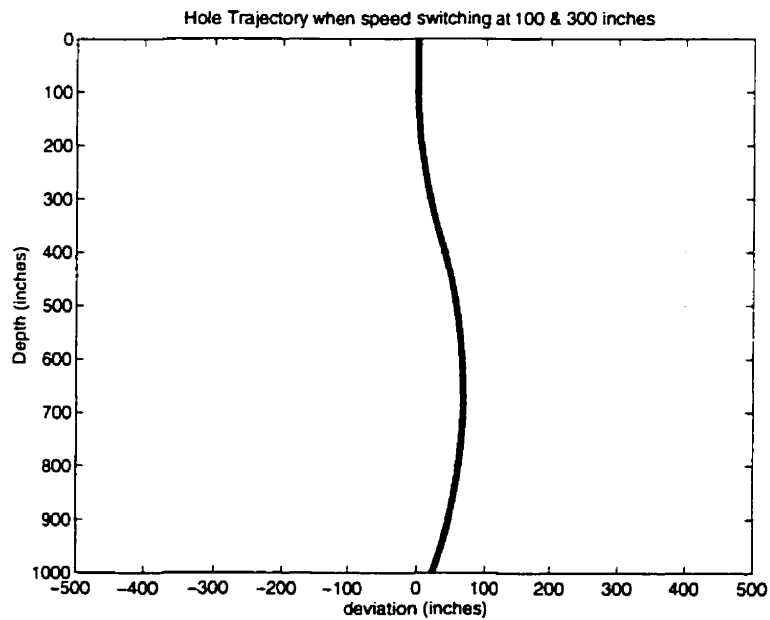


Figure 10.10: Result of simulation of CRE-Hammer, when it has two rotation speeds. Speed control angles were changed at 100 in and then 300 in. This cause a change in direction of bending of hole trajectory.

the torque applied by the rotary motor.

Since steering of the CRE-Hammer mechanism depends on the rotary motor speed switching along the circumference of the bit rotation, the error in the bit rotation angle may affect the accuracy of the steering direction. It is therefore important to compensate for the measurement error of bit rotation angle. There are two possible ways to compensate for the twist in the drill string. First, it can be compensated analytically, by calculating the twist angle of the drill string using the principles of mechanics and then adjusting the measured value of the drill string rotation angle accordingly. Second, it can also be compensated by the steering controller of the proposed guided drilling system.

10.6.1 Analytical Compensation

The drill string when in rotation at a certain speed is subject to the torsional loading. The rotation force is applied at the one end of the string whereas the friction in rotation is at the other end of the string i.e. at the bit. Which is a case for a hollow cylinder under torsional loading. The twist in the drill string can therefore be calculated if the value of the applied torque and the length of the cylinder is know [67]. Once twist angle is computed the measured value of the drill string rotation angle, ϕ_{bit} , can be corrected to calculate true value the bit rotation angle. The speed switching angle can then be adjusted accordingly.

The angle of twist of a cylinder under a torsion loading is given in [67] as follows:

$$\phi_{twist} = \int_0^L \frac{T(x)dx}{I_p(x)G} \quad (10.29)$$

Where:

$T(x)$ is the internal torque of the motor

$I_p(x)$ is the polar moment of inertia

L is the length of the cylinder

G is the shearing modulus of elasticity or modulus of rigidity.

It is constant for a material.

In the case of drill string it can be assumed that a constant torque is being transmitted through the drill string which is equal to applied motor torque T . $I_p(x)$ is also a constant for uniform cross-sectional area. Therefore the equation 10.29 is simplified as:

$$\phi_{twist} = \frac{TL}{I_p G} \quad (10.30)$$

The bit lags behind the string by an angle ϕ_{twist} . The bit rotation angle ϕ_{bit} is therefore adjusted as:

$$\phi_{bit} = \phi_s - \phi_{twist} \quad (10.31)$$

Where ϕ_s is denoted for the drill string rotation angle measured by the sensor. The rotational angles ϕ_D , ϕ_{sw1} , ϕ_{sw2} of equation 10.26, 10.27, 10.28 respectively can be compensated using above equation.

10.6.2 Compensation by Closed-loop System

The error in the direction of steering caused by the twist in the drill string is automatically compensated when the CRE-Hammer is combined with the bit location measurement system to form a closed-loop guided drilling system.

In the closed loop case the controller sets the switching angles according to desired

steering direction based on the error in the hole trajectory. The bit location measurement system indicates the change in the direction as a result of this control action. This change in the steering action when compared with the command signal will give an error proportion to the twist angle. The controller can be programmed to calculate the new switching angles taking into consideration of twist in the drill string.

One disadvantage of this technique is that on each control action the controller have to check for the twist error and compensate for it. This slows down the controller response to the trajectory errors and the error convergence time. A combined approach using both techniques for this compensation can be used for an efficient operation.

10.7 Conclusions

In this chapter a mathematical model of the proposed CRE-Hammer mechanism has been developed and simulated in Matlab in order to analyze the steerability of the mechanism. The results of the simulation have shown that the mechanism can be employed to steer the hole trajectory for guided ITH percussive drilling.

Steering of the drill bit in CRE-Hammer mechanism is achieved through speed control of the drill string rotation system. The control algorithm for the rotation system employs two state speed switching of the rotary motor along the rotation angle. A sharp transition response in speed switching is an essential required characteristic of the rotary motor.

The model was simulated for several values of the bit angle θ_d . Simulation results have shown different turning rate for each bit angle. It is therefore important that this parameter should be chosen carefully during the design of the mechanism. The selection criteria should be based on the desired turning rate, the accuracy of the bit location measurement system and the allowable variation in the hole deviation.

The hammer model developed in this chapter assumes a uniform rock formation. That is the penetration per blow, $p(t)$, was assumed constant. In real situations this value varies randomly due to variation in rock formation along the drilling length. The model can be further improved by randomly varying this parameter. Since the purpose of present work was just to demonstrate the steering capability of the proposed mechanism. Further improvement of the model is, therefore, left for future work.

Chapter 11

Conclusions

This thesis presented an experimental and analytical study of an ITH percussive drill with the objective of investigating the potential for automatic control of this type of drilling process. The research was focused in two areas: the enhancement of machine productivity, and the control of hole deviation. The research methodology involved field data acquisition, analysis of the experimental data, development of a control strategy, design, and simulation of the control system.

The first section of this chapter summarizes the original contributions to knowledge and technological innovations resulting from the research. The second section discusses the practical relevance and implications of these results. Finally, the last section lists suggested areas for further research.

11.1 Original Contributions

Feed Force: A Key Control Variable in ITH Percussive Drilling

The relationships of feed with torque, penetration rate and vibration were studied. This revealed that there exists a correlation between the input variable (feed) and

the output variables (penetration rate, torque, and vibration).

It has been concluded that the feed force is a useful variable for controlling the percussive drilling process. It can be manipulated to control all key output variables and an optimal feed value can be obtained for an efficient operation of the drilling process.

This is first time that the feed is used as an input control variable to compensate for variations in rock hardness to achieve maximum penetration rate in percussive drilling. This variable was also used previously by Changming and Sinkala [11] to control the drilling process. In their design the feed was adjusted only to limit the observed value of the torque. Variation of the rock hardness was not considered in their design.

Specific Fracture Energy of Rock: A Key Parameter for Drilling Rate Control

A detailed analysis was conducted to correlate the specific energy of the rock with the drilling process variables. It was found that there exists a feed value for each value of specific energy of the rock where a maximum penetration rate can be achieved. An empirical model to calculate the optimal feed value was also developed.

Drilling Rate Controller Design and Simulation

A passive control algorithm to improve productivity and quality of long holes was developed. This controller employs the specific energy of the rock being drilled to estimate the appropriate control signal. Empirical model obtained from the data analysis was employed to compute an optimal value of the control signal.

A drilling rate simulator was developed for validation of the passive control algorithm. To implement this simulator, models of all relevant components of the percussive drill were developed. These included analytical models of the feed system

and percussive hammer, and an empirical torque model for bit-rock interaction.

The results of simulations have shown that the productivity of the percussive drilling process can be significantly improved with this type of controller. An average 26% improvement in the productivity has been achieved.

Correlation Analysis of Deviation Data

Correlation analysis between drilling data and the hole orientation data for ITH percussive drilling was performed. This analysis concluded that deviation in the blast holes depends on two factors: machine misalignment and bit-rock interaction. The major source of the deviations was found to be due to misalignment of the machine. Relatively minor deviations were found to be due to bit-rock interaction. More accurate means of machine alignment should therefore be designed for ITH drill rigs.

There is little correlation between the drilling variables and deviation. Deviation due to bit-rock interaction is primarily dependent on rock anisotropy, and not on the machine variables. Hence it is not possible to fully control the hole deviation by the adjustments of the machine parameters alone.

It is therefore recommended that the deviation control problem should be tackled through Guided Drilling.

Guided Drilling for Deviation Control

Since guided drilling is an alternative approach to control the hole deviation, an innovative type of guided drilling system was also developed. This included selection and development of appropriate techniques for bit location measurement and drill steering mechanisms that could potentially be applied to ITH percussive drilling.

A novel mechanism to add steerability to a conventional ITH machine through rotation control was developed. This mechanism, referred to as the CRE-Hammer

mechanism, requires only minor modifications to the conventional drill rig. A simulation model of the CRE-Hammer mechanism was developed and steerability of the mechanism was analyzed through simulations.

For bit location measurement, an acoustic source location approach was proposed.

Vibration Control through Improved Shock-absorber Design

Data analysis has shown that there exists a correlation between vibrations transmitted from the percussive hammer via a shock-absorber and applied feed force. Hence feed force can be used to control vibrations. However, the vibrations are only weakly correlated to the applied feed force.

Hence, if feed is used to control vibration, in addition to controlling of other parameters such as drilling rate, it will be difficult to find an optimal value of the feed for both desired outputs. It is therefore not recommended to include vibrations as controllable parameter in such a multi-variable control. Instead, vibrations should be controlled locally through an improved design of the shock-absorber.

11.2 Practical Relevance and Implications

11.2.1 Usage

Guidelines for the Operators

The data base of specific energy curves can be used to prepare a SE vs. Feed table as an operating guideline for drill operators. The operator can calculate the specific energy at any time during the drilling using the parameter values available from the control panel of the machine and the current drilling rate. He can then follow the table to select the optimal value of the feed force.

Implementation of Drilling Rate Controller

The drilling rate controller designed and simulated in this thesis can be implemented on a CD90B ITH percussive drill without any major modification in the machine. The following recommendations can be used as guidelines in this regard:

- The instrumentation used for data acquisition must be sufficient for on line calculation of the specific energy of the rock.
- The existing feed system of the CD90B is not very sensitive or accurate. It should therefore be replaced with an advance electro-hydraulic servo valve and controller.
- The drilling rate controller designed in SIMULINK can be used in real time with minor modifications. The Matlab C code generator can be used to prepare source code for the controller for implementation purposes.

Improved Design of the Shock-absorber

The shock-absorber test results and analysis presented in Chapter 7 can be used as guidelines for design improvement of the shock-absorber.

11.2.2 Limitations

Portability of the SE Model

The Specific Energy model presented in chapter 4 of this thesis was developed from the data acquired at one mine site. It might predict a less accurate optimal value of the feed at a different mining site, or under significantly different geological conditions. However, the versatility of the model can be improved with more extensive experimental data acquired from a variety of different mine sites.

Control of drilling rate through specific energy uses the empirical model developed in the thesis. This model can only be applied to the machine used in the experiments. The reason for this limitation is that the calculated value of specific energy varies with the design and efficiency of machine. However, a similar model can be developed for other machines.

Limited Steering Rate of CRE-Hammer Mechanism

The steering design of CRE-Hammer mechanism is intended to control the straightness of holes. The mechanism can also be applied to drill a hole in a trajectory which requires small steering rates. However, it is not suitable for drilling along a trajectory which requires a large steering rate. The reason for this limited steerability is the stiffness of the drill string.

11.3 Future Work

Theoretical and experimental analysis of the innovative approach for guided drilling can be extended towards the implementation of a Guided Drilling system. Issues which merit further attention in this regard include:

Improvement of the Hammer Model

The hammer model, developed in chapter 11 assumes a uniform rock formation. The value of penetration per blow, $p(t)$, was assumed constant. It therefore does not take into account the variation in the rock hardness. The model should be further improved by randomly varying this parameter.

This model of the CRE-Hammer mechanism should further be improved by including dynamics of the mechanism. This would include drill string dynamics and dynamics of the rotation system. Frequency domain analysis of the model should then be

conducted to investigate for bandwidth and stability of the system.

Controller Design and Analysis

After improvement of the hammer model the deviation controller should be designed. The closed-loop system can be analyzed through simulations.

Development of Bit Location Measurement

Bit location measurement is an important requirement for the closed-loop Guided Drilling System. The Guided System cannot be implemented unless location of the bit is properly measured. The proposed measurement approach using AE source location techniques should be developed initially at the laboratory level and then extended to field experiments.

Real Time Implementation

After successful computer analysis and simulation of the CRE-Hammer and implementation of the bit location measurement system, the CRE-Hammer mechanism can be implemented to complete the Guided Drilling design. This should include the following steps:

- Mechanical design and fabrication of CRE-Hammer.
- Development of dual-speed high-torque rotation motor with fast transient response
- Field testing of CRE-Hammer, with and without rotation
- Controller design and implementation
- Field testing of the closed-loop system

Bibliography

- [1] G. Almgren. Economic Aspects in Hole Deviation in Sub-level Stopping. In *AIME Conference*, pages 559–572, Denver, June 1981.
- [2] W. R. Anderson. *Controlling Electrohydraulic Systems*. Marcel Dekker, Inc, New York, 1988.
- [3] Anon. Drilling and Cutting Systems. In *Colliery Guardian*, number 4 in 234, April 1986.
- [4] Anon. “Son of Flowmole” Gets Thumbs up from BG Southern Region Trails. In *Gas World*, volume 191, October. 1986.
- [5] K. J. Astrom and B. Wittenmark. *Digital Control System Design*. Prentice-Hall, 1984.
- [6] I. Auranen. Modern Blast Hole Drilling – Vertical or Inclined Blast Holes? In *Mine and Quarry*, volume 15-9, pages 17-19, September 1986.
- [7] D. B. Bogy and P. R. Paslay. Buckling of Drill Pipe in an Inclined Hole,. In *Transactions of the ASME, Journal of Industry*, pages 214–220, May 1964.
- [8] E. T. Brown, S. J. Green, and K. P. Sinha. The influence of Rock Anistrophy on Hole Deviation in Rotary Drilling — A Review. In *International Journal of Rock Mechanics, Mining Science and Geomechanic Abstracts*, volume 18 (5), pages 387–401, October 1981.

- [9] N. P. Callas. Deviation Control for Bored-raise Pilot Hole. Technical report, Report for USBM contract NO. J0285005, 1999.
- [10] C. Catlin. *Petroleum Engineering: Drilling and Well Completion*,. Prentice Hall, 1960.
- [11] W. Changming and T. Sinkala. Thrust—A key Parameter in Automatic Control of Percussive Drilling. In *Proceedings of International Symposium on Mining Mechanization and Automation*, volume II, pages 8–11 to 8–20, June 1991.
- [12] B. G. Clark. Principles of Rock Drilling and Bit Wear. In *Quart. Jour.*, number 1 in 77. Colorado School of Mines, 1982.
- [13] R. A. Cunningham. Calculation of Torque and Horsepower. In *Trans. of Technical Session of the Rotary Drilling Committee, American Assn. of Oilwell Drilling Contractors*, pages 16–17, Houston, Feb. 1967.
- [14] R. A. Cunningham. An Empirical Approach For Relationg Drilling Parameters. In *Journal of Petroleum Technology*, pages 991–987, July 1978.
- [15] K. Dahl. Computer Control Comes to Hard Rock Drilling. In *Tunnels and Tunnelling*, pages 12–15, May 1981.
- [16] G. Deguchi, S. Matsunaga, K. Takahashi, and H. Nakai. Development of Continuous Directional Surveying Tool for Horizontal Long-Hole Using Three Components Optical Fiber Gyroscopes. In *Proceedings of International Symposium on Mining Mechanization and Automation*, volume II, pages 8–21 to 8–30, June 1991.
- [17] R. Desbrandes. *Encyclopedia of Well Logging*. Gulf Publishing company, 1985.
- [18] N. R. Draper. *Applied Regression Analysis, Second Edition*,. John Wiley and Sons, 1981.

- [19] A. E. Dunstan. *The Science of Petroleum*. Oxford University Press, 1938.
- [20] E. Easterling. A measuring technique for rock dependent hole deviations - a field study on smooth blasted holes. Master's thesis, Lulea Technical University, Sweden.
- [21] H. C. Fischer. On Longitudinal Impact I-VI. In *The Hague Martinus Nijhoff*, volume I-VI, 1960.
- [22] S. Granholm, N. Vagenas, and J. Morris. The Robotized Mine - a Utopia ?. In *Proc. of the 2nd Inter. Conf. on Innovative Mining System*, pages 124-134, Pennsylvania State University USA, 1986.
- [23] S. J. Green. Hydro-mechanical Borehole Deviation Sensing and Control Device. Technical report, National Science Foundation Contract DAR-7820994, December 1979.
- [24] G. P. Hancke. Electronic Fine Feed Control on Diesel Hydraulic Deep Hole Diamond Drill. In *IFAC Conference on Automation in Mining Mineral and Metal Processing*, pages 103-107, Buenos Aires Argentina, 1989.
- [25] H. L. Hartman. Basic Studies of Percussion Drilling. In *Mining Engineering*, volume 11 (1), pages 68-75, January 1959.
- [26] C. Y. Ho and Y. Jianchi. Design of automated Jumbo Drilling Robot Manipulator,. In *IFAC Conference on Automation in Mining Mineral and Metal Processing, Tokyo 1986*, volume 10, pages 59-66, 1987.
- [27] D. F. Howarth and J. C. Rowlands. Quantitative Assessment of Rock Texture and Correlation with Drillability and Strength Properties. In *Rock Mech. and Rock Eng.*, volume 20, pages 57-85. Springer-Verlag, 1987.
- [28] W. Hustrulid. *Theoretical and Experimental Study of Percussive Drilling of Rock*. PhD thesis, University of Minnesota, 1968.

- [29] W. Hustrulid. The Percussive Drilling of Quartzite. In *Journal of the South African Institute of Mining and Metallurgy*, pages 245–268, July 1971.
- [30] W. Hustrulid and C. Fairhurst. A Theoretical and Experimental Study of the Percussive Drilling of Rock. In *Inter. Jour. Rock Mech. Min. Sci.*, volume 8, pages 311–356, 1971.
- [31] J. Jaeger and N. Cook. *Fundamentals of Rock Mechanics*, 3rd ed. Chapman and Hall Publishers, London, 1979.
- [32] D. Jiao. *Analysis of Variables Affecting the Performance of a Hydraulic Rotary Percussive Drill*. PhD thesis, University of Newcastle, Tyne, England, 1989.
- [33] D. Jiao, L. Daneshmend, M. Amjad, M. Jian, and J. Peck. CD-90B ITH Drilling Project Reports. Technical Report Volume I-V, CCARM McGill University, Montreal., January 1993.
- [34] M. G. Karfakis and J. F. Evers. Technical Note – Effects of Rock Lamination Anisotropy on Drilling Penetration and Deviation. In *Inter. Journal of Rock Mechanics, Mining Science and Geomechanic Abstracts*, volume 24, pages 371–374, Dec 1987.
- [35] L. G. Karlsson, B. Lundberg, and K. G. Sundin. Experimental Study of a Percussive Process for Rock Fragmentation. In *International Journal of Rock Mechanics and Mining Sciences*, volume 26, pages 45–50, January 1989.
- [36] S. R. Knapp. Are we missing the cheapest solution to our crooked hole problem? In *Oil and Gas Journal*, volume 59, pages 103–108, 1961.
- [37] S. R. Knapp. New bit concept helps control hole deviation. In *World. Oil*, volume 160, pages 113–116, 1965.
- [38] S. R. Kramer. Guided Piercing Tool. In *Pipeline and Gas Journal*, number 8 in 212, pages 45–47, August 1985.

- [39] P.-E. Lindvall. Sources of Error in Long Hole Drilling – Their Consequences and How to Avoid Them. In *First International Symposium on ROCK FRAGMENTATION BY BLASTING*, pages 739–751, Lulea, Sweden, August 1983.
- [40] L. Ljung. *System Identification, Theory for the user*. Prentice-Hall Pub, 1987.
- [41] A. Lubinski and H. B. Woods. Factors affecting the angle of inclination and dog-legging in rotary bore holes. In *Drilling and Production Practice*, pages 222–242, New York, 1953. American Petroleum Institute.
- [42] B. Lundberg. *Some Basic Problems in Percussive rock Destruction*. PhD thesis, Chalmers University of Technology, Gothenberg, Sweden, 1971.
- [43] B. Lundberg. Microcomputer simulation of longitudinal impact between nonuniform elastic rods. In *International Journal of Mechanical Engineering Education*, volume 9-4, pages 301–315, 1981.
- [44] B. Lundberg. Microcomputer Simulation of Stress Wave Energy Transfer to Rock in Percussive Drilling. In *International Journal of Rock Mechanics, Mining Science and Geomechanic Abstracts*, volume 19, pages 229–239, 1982.
- [45] B. Lundberg. Computer Simulation of Percussive Drilling a Basis for Tomorrow's Products. In *Future Trends in rock excavation. Documentation on Sandvik Rock Tools ROCK DRILLING DAY*, September 16-18 1987.
- [46] B. Lundberg and L. G. Karlsson. Influence of Geometrical Design on the Efficiency of a Simple Down-the-hole Percussive Drill. In *International Journal of Rock Mechanics, Mining Science and Geomechanic Abstracts*, volume 23, pages 281–287, 1986.
- [47] W. C. Maurer. The Perfect Cleaning Theory of Rotary Drilling. In *Journal of Petroleum Technology, Trans. of AIME*, volume 225, pages 1270–74, November 1962.

- [48] R. T. McLamore. The Role of Rock Strength Anisotropy in Natural Hole Deviation. In *Journal of Petroleum Technology*, pages 1313–1321, November 1971.
- [49] A. Medda. The precision of long hole drilling with modern machines in mining operation. In *1st Inter. Symp. on Rock Frag. by Blasting*, Lulea, Sweden, 1983.
- [50] M. Mellor. Normalization of Specific Energy (Technical Note). In *International Journal of Rock Mechanics and Mining Science*, volume 9, pages 661–663, 1972.
- [51] J. E. Mercer. Guided Microtunnelling Equipment for Small-Diameter Utility Installation. In *Tunnelling and Underground Space Technology*, volume 4, pages 207–213, 1989.
- [52] H. Moriya, K. Nigano, and H. Niitsuma. Precise source location of AE doublets by spectral matrix analysis of triaxial hodogram. In *Geophysics*, volume 59, pages 36–45, January 1994.
- [53] A. H. Morris and D. H. Rees. Guided Longhole Drilling. Technical report, European Communities Commission Internal Report on ECSC no. 7220-AF/810, 1985.
- [54] A. H. Morris and J. S. Wykes. Guided Longhole Drilling and Instrumentation. In *Mining Engineer*, pages 445–451, London, March 1984.
- [55] A. A. Mostafa. *Study of Bit Rock Interaction and Their Effects on Hole Deviation Trends*. PhD thesis, University of Texas at Austin, 1975.
- [56] C. E. Murphey and J. B. Cheatham. Hole Deviation and Drill String Behavior. In *Soc. Petrol. Engrs J.*, volume 6, 1966.
- [57] H. Niitsuma. Resource Engineering, Faculty of Engineering, Tohoku University, Japan. Personal Communications.

- [58] H. Niitsuma, K. Nakatsuka, N. Chubachi, H. Yokayamma, and M. Takanohishi. Downhole AE measurement of a Geothermal Reservoir and its Application to Reservoir Control. In *Fourth Conference on Acoustic Emission/Microseismic Activity in Geological Structure and Materials*, pages 47–60, Pennsylvania State University, October 22-24 1985.
- [59] H. Niitsuma and H. Saito. Evaluation of the three-dimensional configuration of a subsurface artificial fracture by triaxial sheer shadow method. In *Geophysics*, volume 56, pages 2118–2128, December 1991.
- [60] E. Nordlund. The Effect of Thrust on the Performance of Percussive Rock Drills. In *International Journal of Rock Mechanics, Mining Science and Geomechanic Abstracts*, volume 26, January 1988.
- [61] A. G. Paithanker and G. B. Misra. A critical appraisal of the Protodyakonov index. In *International Journal of Rock Mechanics, Mining Science and Geomechanic Abstracts*, volume 13, pages 249–251, 1976.
- [62] A. G. Paithanker and G. B. Misra. Drillability of Rocks in Percussive Drilling from ‘Energy per Unit Volume’ as Determined with a Micro Bit. In *Mining Engineering*, Sept. 1980.
- [63] W. G. Pariseau. Wedge Indentation of Anisotropic Geologic Media. In *Dynamic Rock Mechanics, Proceeding of 12th AIME Symposium on Rock Mechanics*, pages 529–546, New York, U. S., 1971. (Edited by Clark G.B.).
- [64] J. Pathak and M. F. Dias. Microprocessor-Controlled Down-The-Hole Drill for Enhancing Productivity and Accuracy in Underground Hardrock Bulk Mining Methods. In *IEEE Transactions on Industry Applications*, volume 23 (6), pages 1099–1104, Nov/Dec. 1987.
- [65] G. Pearse. Hydraulic Rock Drills. In *Mining Magazine*, pages 220–231, March 1985.

- [66] J. Poane, D. Madson, and W. E. Bruce. Drillability studies — laboratory percussive drilling. Technical Report of investigations 7300, U. S. Bureau of Mines., 1969.
- [67] E. P. Popov, S. Nagarajan, and Z. A. Lu. *Mechanics of Materials*. Prentice-Hall, Inc., Englewood Cliffs, New Jersey, 1978.
- [68] H. Rabia. Specific Energy as a Criterion for Drill Performance Prediction. In *Internal Journal of Rock Mechanics, Mining Science and Geomechanic Abstracts*, volume 19, pages 39–42, 1982.
- [69] H. Rabia. A Unified Prediction Model for Percussive and Rotary Drilling. In *Mining Science and Technology*, volume 2, pages 207–216, 1985.
- [70] H. Rabia and N. Brook. The Effects of Apparatus Size and Surface Area of Charge on the Impact Strength of Rock. In *Internal Journal of Rock Mechanics, Mining Science and Geomechanic Abstracts*, volume 18, pages 211–219, 1981.
- [71] D. H. Rees. Guided Longhole Drilling. In *GULECKAOF FONSHUNGSH*, volume 48 (2), April 1987.
- [72] H. M. Rollins. Are 3° and 8° holes worth their cost? In *Oil Gas J.*, volume 57, pages 163–171, 1959.
- [73] H. Schunnesson. Towards Automated Drilling in Sweden. In *1st IFAC Workshop on Advances in Automation of Underground Hard Rock Mining*, Montreal, Quebec, September 1988.
- [74] H. Schunnesson. Drill Process Monitoring in Percussive Drilling, A Multivariate Approach to Data Analysis,. Master's thesis, Lulea University of Technology, Sweden, 1990.
- [75] R. Simon. Discussion of a Laboratory Study of Rock Breakage by Rotary Drilling. In *Journal of Petroleum Technology*, pages 78A–80, December 1959.

- [76] R. Simon. Energy Balance in Rock Drilling. In *paper SPE 499 presented at SPE Conference on Drilling and Rock Mechanics*, pages 23–24, Austin, TX, Jan. 1963.
- [77] R. Simon. Transfer of the Stress Wave Energy in the Drill Steel of Percussive Drill to the Rock. In *International Journal of Rock Mechanics, Mining Science and Geomechanic Abstracts*, volume 1, pages 397–411, 1964.
- [78] T. Sinkala. Phenomena of Rock Dependent Drill Hole Deviations- A Field Study. Master's thesis, Lulea University of Technology Sweden, 1986.
- [79] T. Sinkala. Rock and hole pattern influences on percussion hole deviation: a field study. In *Inter. Conf. DRILLEX'87*, Stoneleigh, Warwickshire, England, April 1987.
- [80] T. Sinkala. *Hole Deviations in Percussion Drilling and Control Measures*,. PhD thesis, Lulea University of Technonogy, Sweden, 1989.
- [81] W. H. Somerton. A Laboratory Study of Rock Breakage by Rotary Drilling. In *In Transaction of AIME*, volume 216, pages 92–97, 1959.
- [82] B. Suntanov and G. Shandalov. Effects of geological conditions on well deviations. (in russian). In *Izv, vyssh, ucheb. Zaved, Geol. razved*, number 106 in 3, 1961.
- [83] TAMROCK. Handbook of Underground Drilling. TAMROCK Drills SF-33310 Tampere, Finland.
- [84] R. Teale. The Concept of Specific Energy in Rock Drilling. In *Internal Journal of Rock Mechanics and Mining Science*, volume 2, pages 57–73, 1965.
- [85] H. F. Unger and R. R. Fumanti. Percussive Drilling With Independent Rotation. Technical Report of investigations 7692, U. S. Bureau of Mines.

- [86] J. R. Wait and D. A. Hill. Remote Sensing. In *IEEE Transactions on Geo-Science Electronics*, volume 17, pages 21–24, 1979.
- [87] B. H. Walker and M. B. Friedman. Three-dimensional Force and Deflection Analysis of a Variable Cross Section Drill String. In *Journal of Pressure Vessel Technology*, pages 367–373., May 1977.
- [88] T. M. Warren. Factors Affecting Torque for Roller Bits. In *Journal of Petroleum Technology*, pages 1500–8, September 1984.
- [89] K. Whitworth, editor. *Blast Hole Drilling*, volume 234, No. 4, April 1986.
- [90] G. Wijk. Some Stamp Test Results for Lemunda Sandstone, Ekeberg Marble and Bohus Granite. In *SveDeFo Report DS 1984: 9*, volume 9, Stockholm, Sweden, 1984.
- [91] P. J. E. Woods and R. J. Hopley. Horizontal Long Hole Drilling Underground at Boulby Mine, Cleveland Potash Ltd. In *The Mining Engineer*, pages 585–91, January 1980.
- [92] J. S. Wykes and A. H. Morris. Instrument Development: Guided Longhole Drilling. In *Colliery Guardian*, number 8 in 233, pages 386–398, Aug. 1985.

Appendix A

Modelling of Electro-Hydraulic Servo Valve

Model of the nozzle-flapper type electro hydraulic valve used in the simulator for chapter 6 is described in the following. A major part of this model is taken from Anderson [2].

Figure A.1 shows schematic of the nozzle-flapper type electro-hydraulic servo-valve. There are two stages in the valve, the pilot stage and the boost stage. The pilot consists of a magnetic circuit and the hydraulic circuit. This stage provides a differential pressure at small flow rates. The boost stage becomes a power amplifier in that it will reproduce the pilot pressures at much higher flow rate than the pilot stage alone could produce.

The magnetic circuit of the pilot stage provides movement of the flapper at the nozzles, in order to activate the hydraulic circuit for a given electrical input signal. It provides a torque on the armature to move it against the effective spring of the pivot. The resulting movement on the armature is reflected on the flapper through the pivot. This flapper movement, with respect to the nozzle, is the valve input to be

according to

$$T = K_{tm}I + K_m\alpha \quad (\text{A.2})$$

where

K_{tm} = main torque motor gain (in-lbs/mA)

K_m = magnetic decentring spring rate (in-lbs/rad)

I = input current (mA)

α = angular position of armature.

The torque motor's influence on the system takes place inside the close loop. The net torque is therefore given by:

$$\begin{aligned} \Sigma T = J\alpha &= J\ddot{\theta} \\ J\ddot{\theta} &= -f\dot{\theta} - K_p\theta - T_o + T_m + (T_i - T_{fb}) \\ &= -f\dot{\theta} - K_p\theta - K_oL_o^2\theta + K_m\theta + (T_i + T_{fb}) \\ &= -f\dot{\theta} - (K_p - K_m + K_oL_o^2)\theta + T_i - T_{fb} \\ &= -f\dot{\theta} - K_x\theta + (T_i - T_{fb}) \\ J\ddot{\theta} + f\dot{\theta} + K_x\theta &= (T_i - T_{fb}) = T_e \end{aligned} \quad (\text{A.3})$$

Taking Laplace transform

$$\begin{aligned} Js^2\theta(s) + fs\theta(s) + K_x\theta(s) + T_e(s) \\ \theta(s)[Js^2 + fs + K_x] &= T_e(s) \\ \frac{\theta(s)}{T_e} &= \frac{1}{Js^2 + fs + K_x} \end{aligned} \quad (\text{A.4})$$

where

θ = armature and flapper rotation

J = polar inertia of armature and flapper

f = velocity coefficient of friction

$$K_x = K_p - K_m + K_o L_o^2$$

K_p = stiffness of the torque armature pivot (i.-lb/rad)

K_m = magnetic decentering stiffness (in.-lb/rad)

$K_o L_o^2$ = effective stiffness of the oil in this chamber.

L_o = length of linkage

Angular movement θ caused by the torque will move the flapper by X_e :

$$X_e = L_o \sin(\theta) \approx L_o \theta \quad \text{for small } \theta \quad (\text{A.5})$$

The hydraulic circuit of the servo-valve uses the position created by the electro-magnetic circuit to create an unbalance. At neutral position (no input armature movement), there are equal exit areas at the nozzles. With an orifice between the supply pressure and each output control port, and ambient pressure exists which is less than the supply pressure and greater than the tank pressure.

For a given input-position change of the flapper, say to the right, the flow Q_4 will decrease because the orifice becomes smaller. This causes restriction to flow causing the control port pressure P_2 to increase. Correspondingly, the drain flow Q_2 is less restricted, this lowers the left control port pressure P_1 . The output load flow equations are:

$$Q_a = Q_1 - Q_2 = C_{d0} A_0 \sqrt{(2/\rho)(P_s - P_1)} - C_{dn} \pi D_n (X_0 - X_e) \sqrt{(2/\rho) P_1}$$

$$Q_b = Q_3 - Q_4 = C_{d0} A_0 \sqrt{(2/\rho)(P_s - P_2)} - C_{dn} \pi D_n (X_0 - X_e) \sqrt{(2/\rho) P_2}$$

If the output control ports (C_a and C_b) are blocked,

$$Q_a = Q_b = 0 \quad (\text{A.6})$$

Which reduces to

$$Q_1 = Q_2 \quad (\text{A.7})$$

$$C_{d0}A_{01}\sqrt{(2/\rho)(P_s - P_1)} = C_{dn}\pi D_n(X_0 - X_e)\sqrt{2/\rho}P_1$$

$$\frac{P_s - P_1}{P_1} = \left[\frac{C_{dn}\pi D_n(X_0 + X_e)}{C_{d0}A_{01}} \right]^2 = \frac{P_s}{P_1} - 1$$

$$P_1 = \frac{P_s}{1 + \left[\frac{C_{dn}\pi D_n(X_0 + X_e)}{C_{d0}A_{01}} \right]^2}$$

where:

X_0 = null distance between flapper and nozzle

X_e = stroke of flapper at nozzle

Also,

$$Q_3 - Q_4 = 0$$

$$C_{d0}A_{02}\sqrt{(2/\rho)(P_s - P_2)} = C_{dn}\pi D_n(X_0 - X_e)\sqrt{2/\rho}P_2$$

$$P_2 = \frac{P_s}{1 + \left[\frac{C_{dn}\pi D_n(X_0 + X_e)}{C_{d0}A_{02}} \right]^2}$$

At null ($X_e=0$), the pressures P_1 and P_2 are equal to the resulting ambient pressure at both control ports:

$$P_1 = P_2 = P_{null} = \frac{P_s}{1 + [C_{dn}\pi D_n X_0 / C_{d0}A_0]^2} \quad (\text{A.8})$$

where

D = diameter

A_0 = area of orifice at the nozzle

o = orifice

C_d = discharge coefficient

n = nozzle

e = working stroke at the nozzle

The primary objective of the pilot stage is to provide flow as its output. The resulting flow produces an output differential pressure proportional to the pilot input. The flow gain for the pilot is the output flow created by the nozzles for a given flapper deflection X_e :

$$K_q = \frac{Q_1}{X_e} \quad (\text{A.9})$$

The decentering effects of differential pressure controller is designed such that the it counter balances the mechanical stiffness of the flapper. This causes K_p cancels K_m which results in K_x becoming dependent only on the hydraulic circuit and its related stiffness.

$$K_x = K_p - K_m + K_o L_o K_x = K_o L_o \quad (\text{A.10})$$

This nozzle-flapper design becomes a closed-loop device, modulated by the differential pressure from the nozzle. The nozzles in such setup is feedback mechanism for maintaining a differential pressure, ΔP , across the pilot-stage output ports. The differential pressure across the output ports when pilot stage driving a load (the boost stage is treated a load. This load is defined as hydraulic capacitance (C_h) is proportional to the net nozzle flow Q , given by:

$$\Delta P = \frac{1}{C_h s} Q \quad (\text{A.11})$$

Figure A.2 is the block diagram of the pilot stage driving the boost stage load. The hydraulic capacitance of the load is defined by:

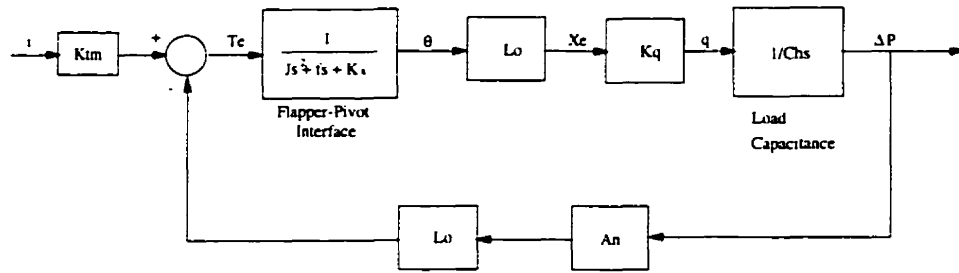


Figure A.2: Block diagram of electro hydraulic differential pressure control valve for controlling the feed pressure across the feed cylinder

$$C_h = \frac{V}{\beta} \tag{A.12}$$

where

V = volume of oil between the pilot and load.

β = bulk modulus of the oil.

Combining Equations A.5, A.9 and A.11 gives the transfer function of the hydraulic circuit of the pilot stage.

$$\Delta P = \frac{L_o K_q}{C_h s} \theta \tag{A.13}$$

The feedback torque (T_{fb}) applied on flapper by nozzles is proportional differential oil flow ($Q_1 - Q_2$) across the flapper is given by:

$$T_{fb} = L_o A_n \tag{A.14}$$

Net torque applied on the flapper is the torque cause by input current minus the feed back torque:

$$T_e = I K_{tm} - T_{fb} \tag{A.15}$$

Parameter	Values	Units
K_{tm}	13.82	<i>in. - lb/mA</i>
J	3.8007e-04	<i>in. - lb/rad</i>
f	0.0423	
K_x	0.45	<i>in. - lb/rad</i>
L_o	0.01	<i>inch</i>
K_q	100	<i>in²/sec.</i>
A_n	0.0552	<i>inch</i>
C_h	0.0024	<i>in³/psi</i>

Table A.1: Parameter value for the electro-hydraulic control valve use in the simulation

Equations A.15, A.4 and A.13 represents the dynamics of the servo valve. Combining these equations gives the transfer function, given by:

$$\frac{\Delta P(s)}{I(s)} = \frac{K_q L_o}{C_h s^3 + C_h f s^2 + K_x C_h s + K_q L_o^2 A_n} \quad (\text{A.16})$$

Control input current I for the servo valve is supplied by a separate power control circuit that takes voltage as inputs. Assuming G_{op} is gain of the circuit:

$$\frac{\Delta P(s)}{V(s)} = \frac{G_{op} K_q L_o}{C_h s^3 + C_h f s^2 + K_x C_h s + K_q L_o^2 A_n} \quad (\text{A.17})$$

This input-output transfer function take voltage V as input and the differential press ΔP across the power cylinder.

The parameter values used in the simulation of this model are listed in the table A.1.

Appendix B

SIMULINK Programs for drilling process simulator

B.1 Introduction

All the simulations and data analysis presented in this thesis were performed in the Matlab environment. The matlab is a specially designed software for simulations of dynamic systems. The SIMULINK is a block oriented toolbox runs in Matlab environment.

The drilling process simulator developed in the chapter 4 was simulated in the SIMULINK. In this appendix the circuit diagrams developed for this purpose using SIMLINK block library functions have been presented.

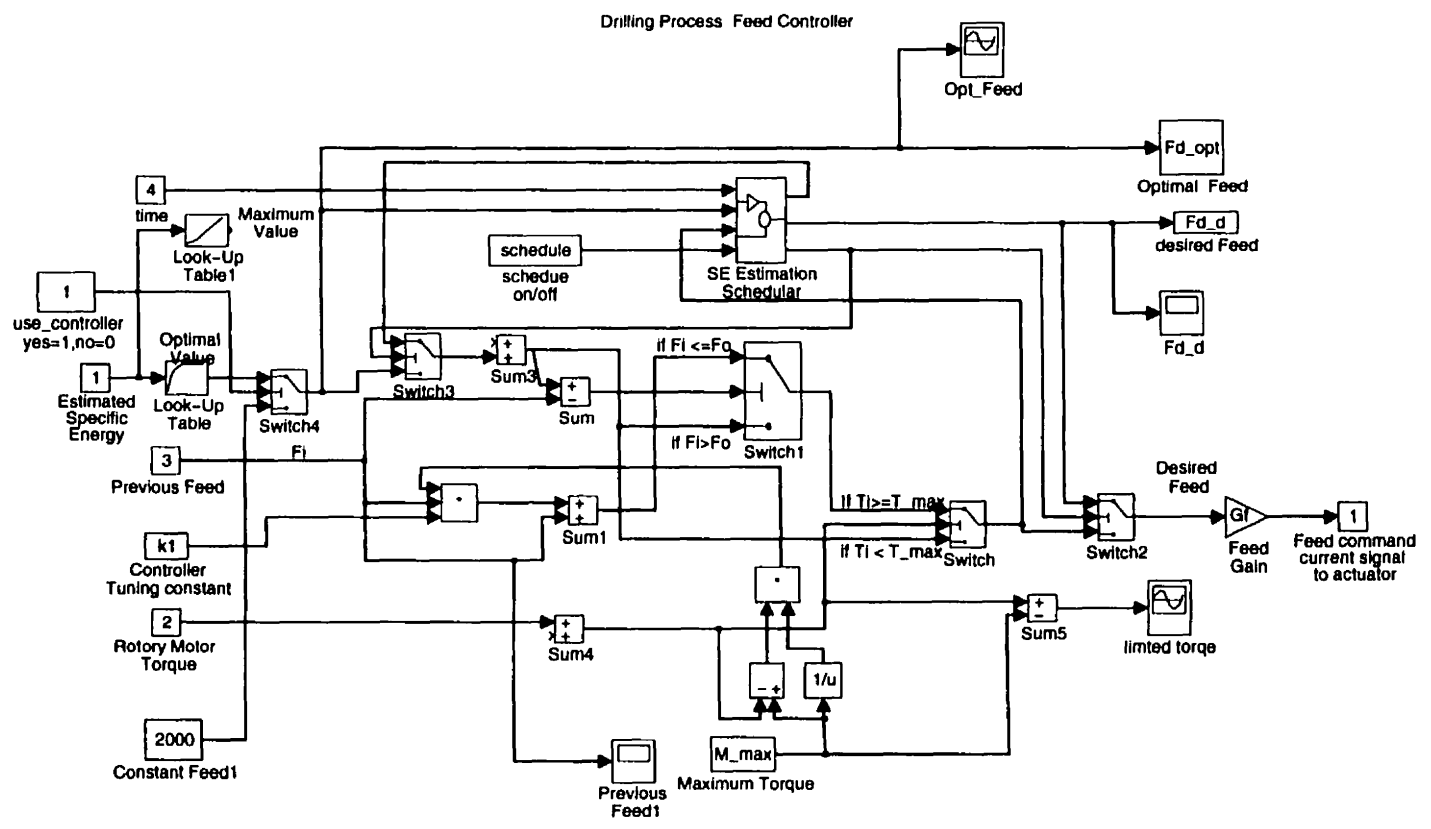


Figure B.2: Drilling Process Controller

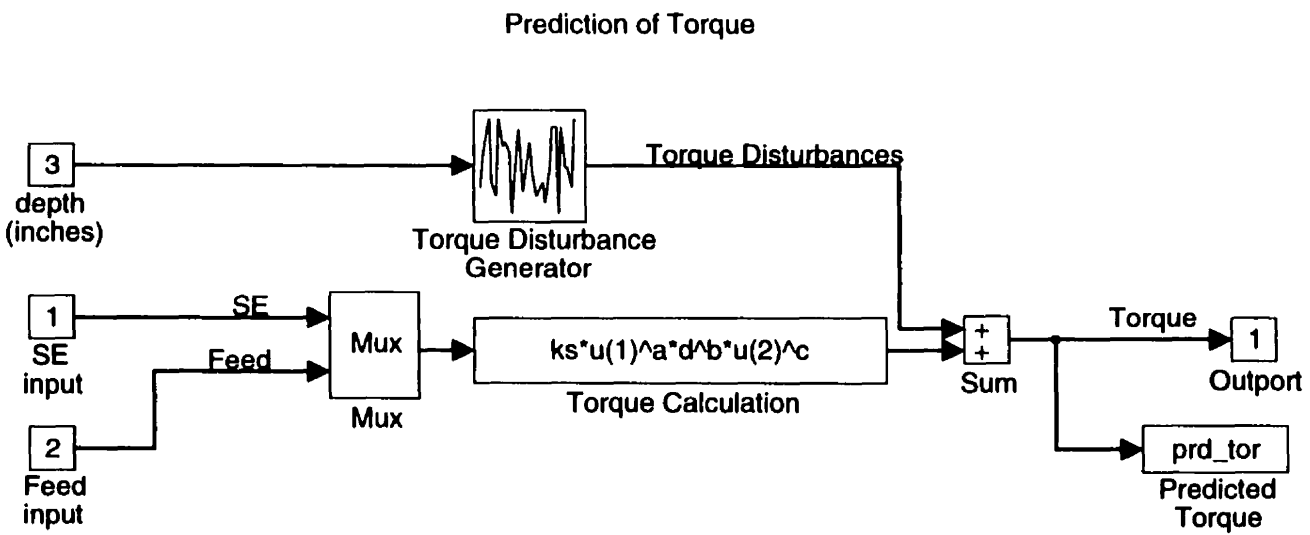


Figure B.5: Simulink block for torque prediction

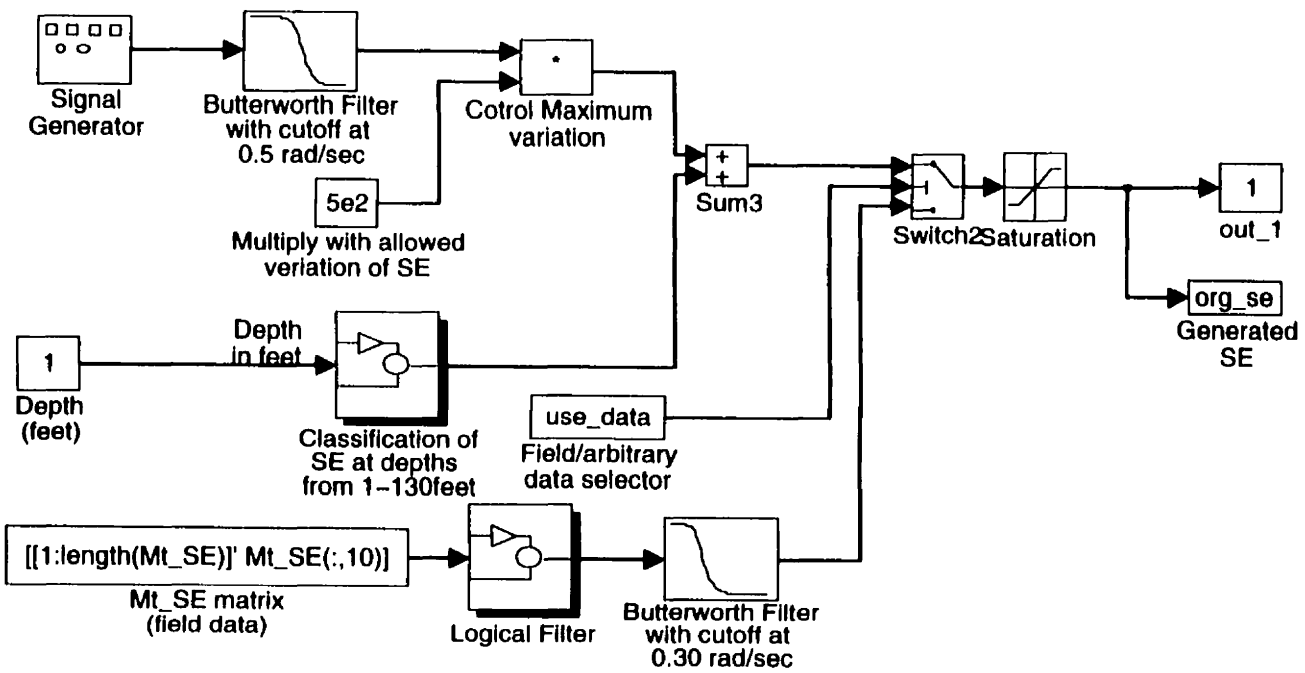


Figure B.6: Simulink block for randomly varying rock property generator

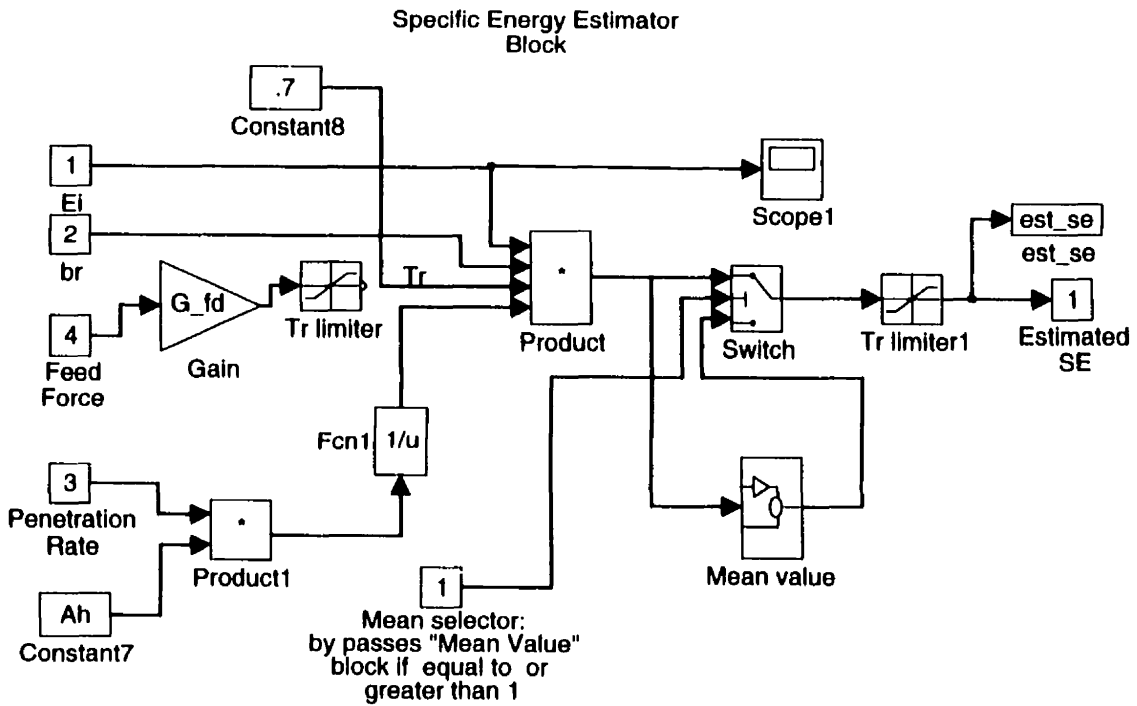


Figure B.7: Simulink block for SE estimator

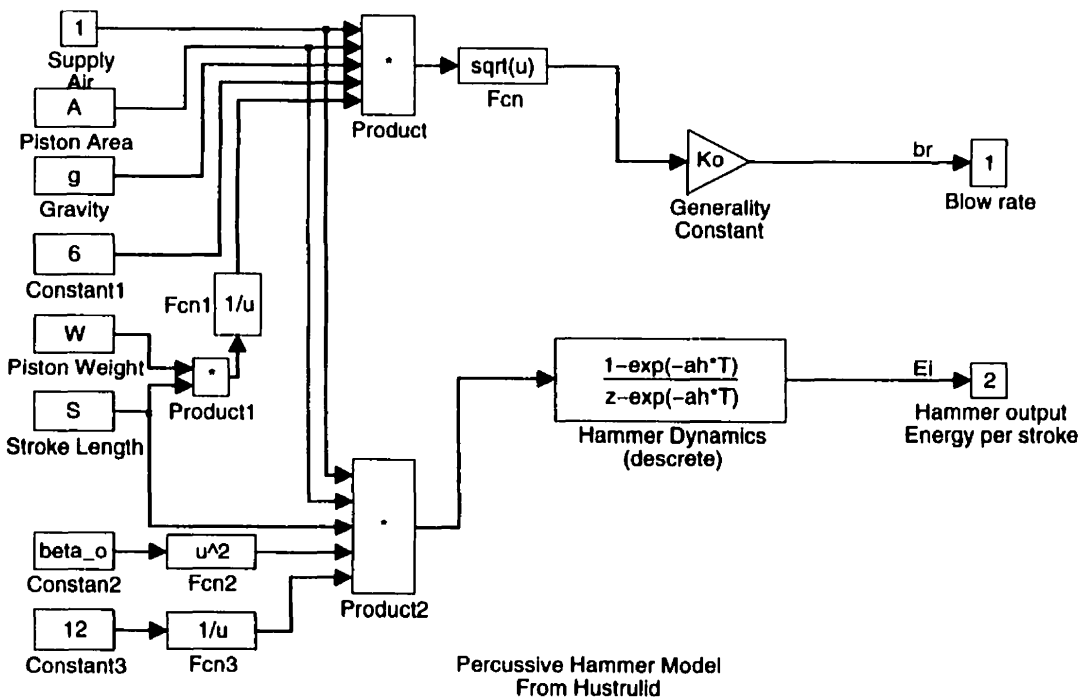


Figure B.8: Simulink block Percussive Hammer Model

Appendix C

Test Hole Trajectories and Deviation

In this appendix trajectories of all the test holes are given. Orientation data is employed to plot these trajectories.

This data can be used to calculate three dimensional trajectory of the hole. However for a visible comparison, the trajectory for each hole is plotted in two dimensional plots showing two side views (x-z and y-z views) and a plan view (x-y view). The positive values of x, y and z represent East, North and Vertical directions respectively.

Each side view plot, e.g. of Figure C.1, shows three trajectories drawn with different line styles. The dashed line represents the desired trajectory of the hole, the centre line represents the straight line one which the machine should have drilled in a straight line after first alignment of the machine and the solid line represents the actual trajectory.

The plan view of each trajectory is plotted and scaled in such a way that a deviation could be seen clearly (e.g. see Figure C.2). The origin of this figure is the desired

destination of the hole and is marked as “o” the destination of the expected straight hole after initial alignment of the machine is marked as “+” and the destination of actual hole is marked as “*”. The distance between origin and “+” is the measure of expected deviation due to misalignment. The distance between “+” and “*” is the measure of deviation caused by bit rock interaction only and the distance of “*” from the origin is the actual deviation occurred in the hole.

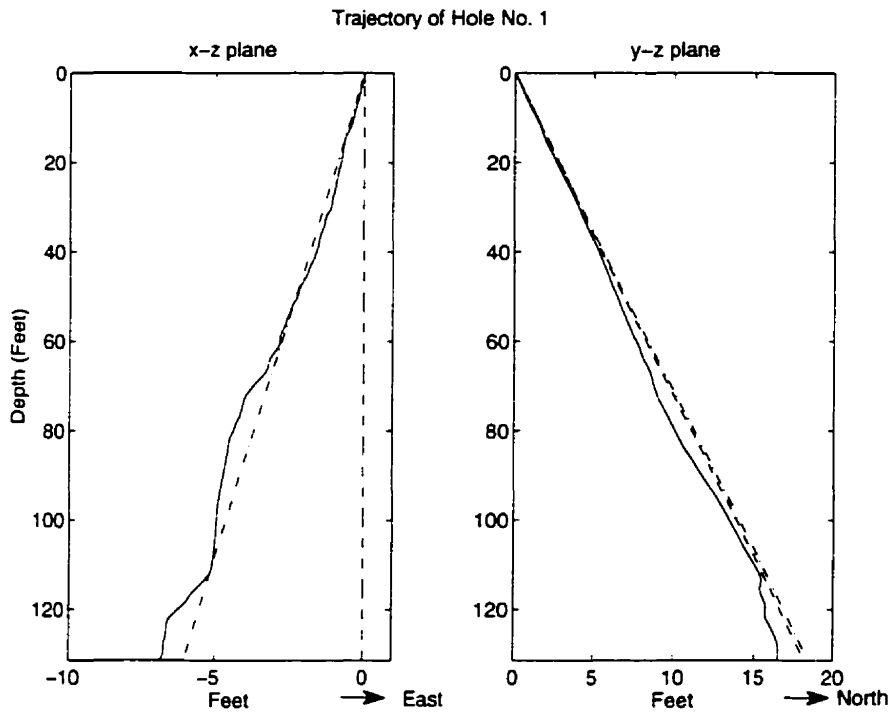


Figure C.1: Trajectory of hole no. 1

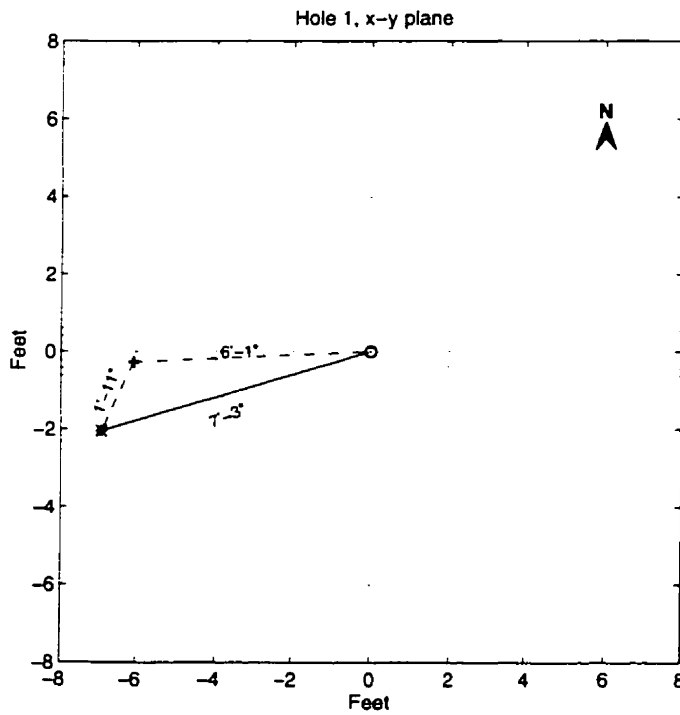


Figure C.2: Deviations occurred in hole no. 1

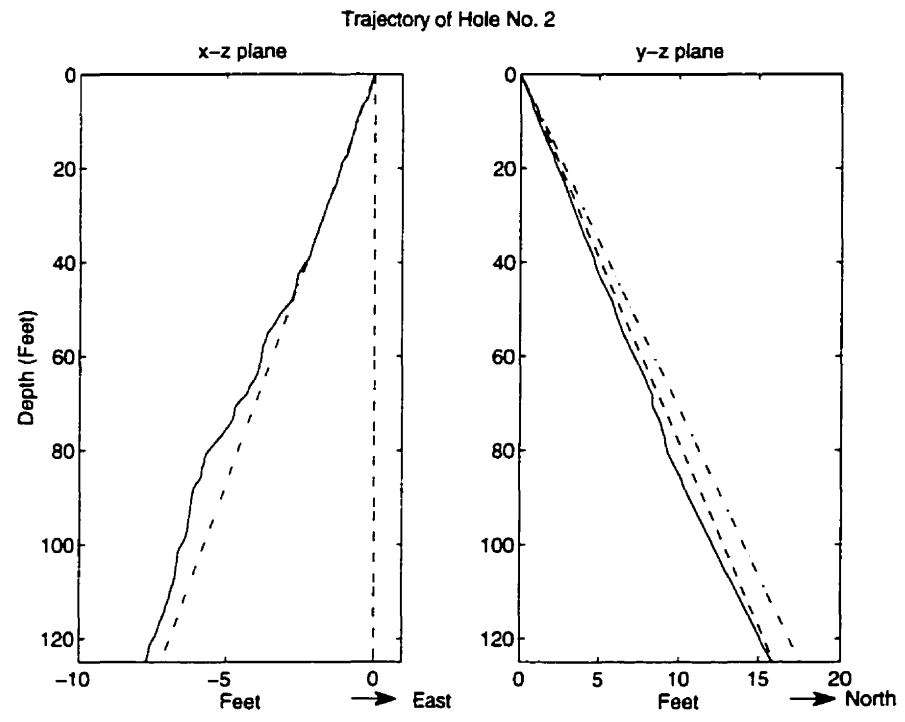


Figure C.3: Trajectory of hole no. 2

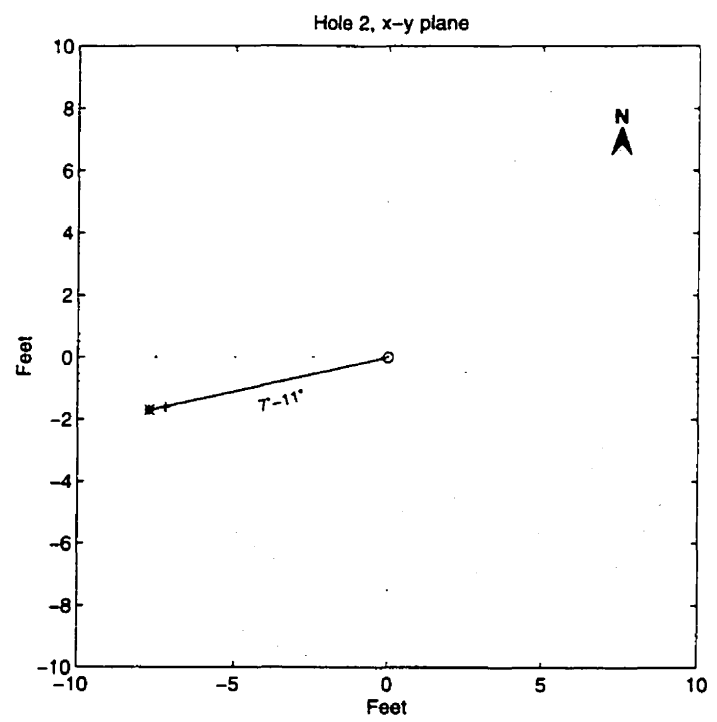


Figure C.4: Deviation occurred in hole no. 2

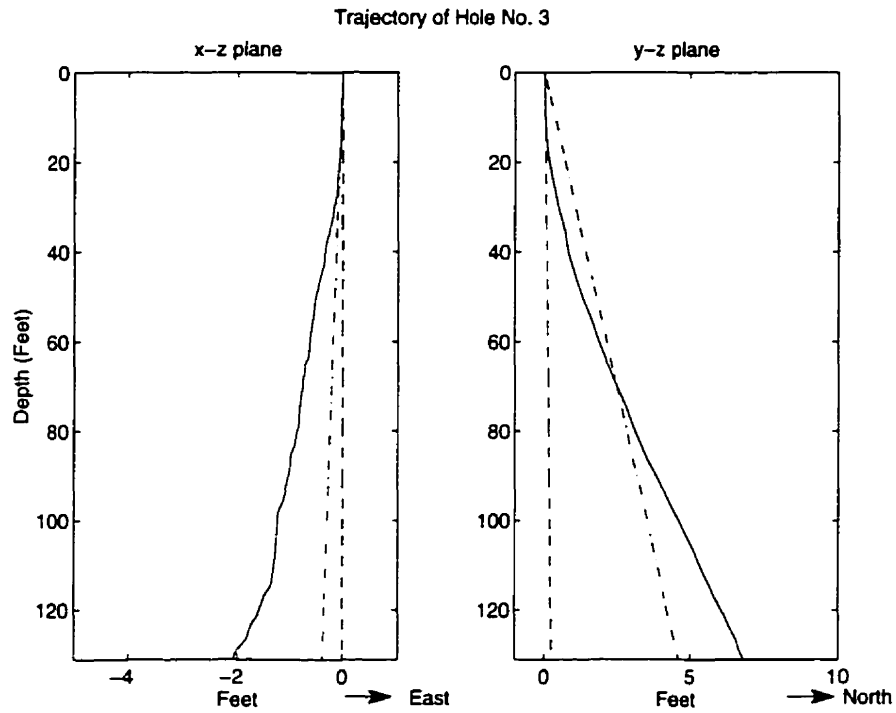


Figure C.5: Trajectory of hole no. 3

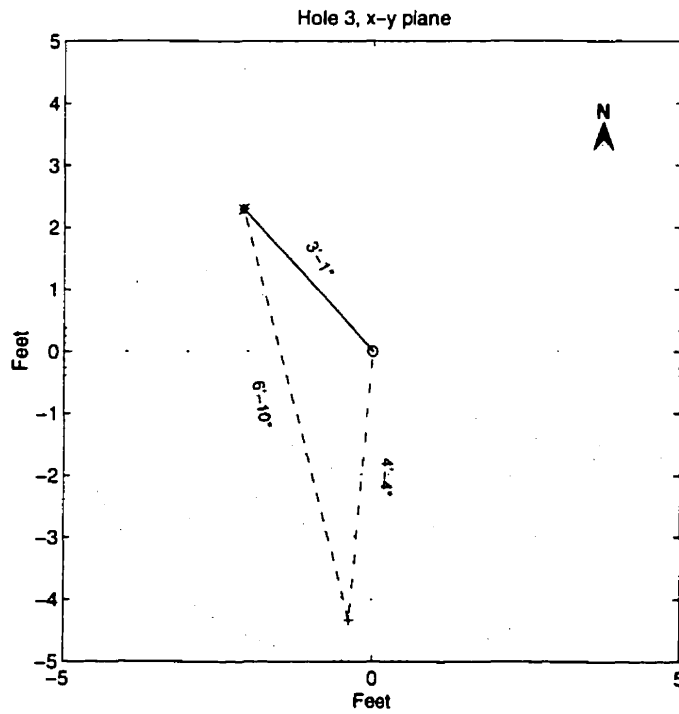


Figure C.6: Deviation occurred in hole no. 3

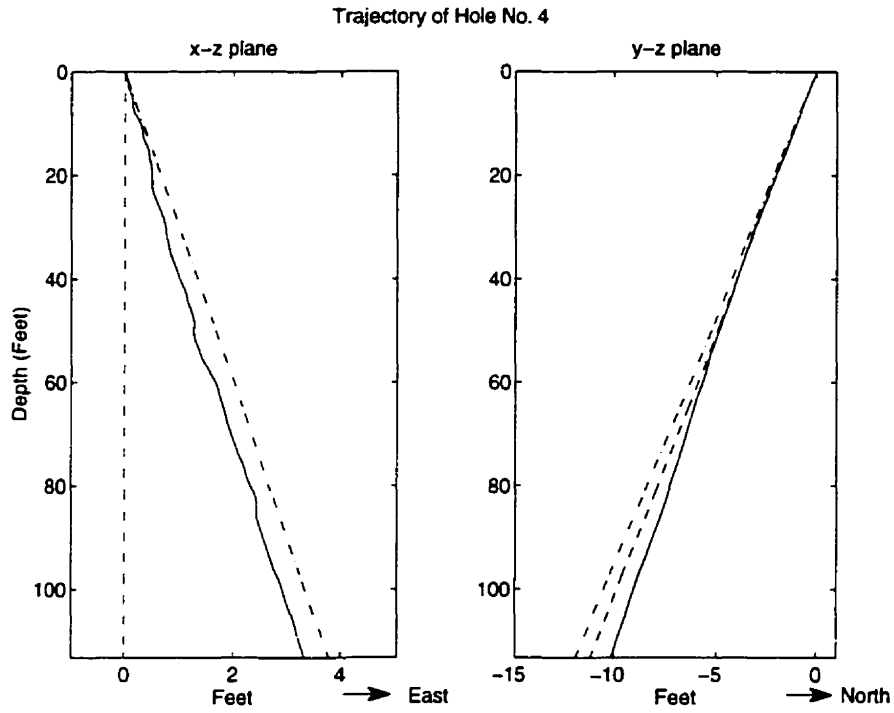


Figure C.7: Trajectory of hole no. 4

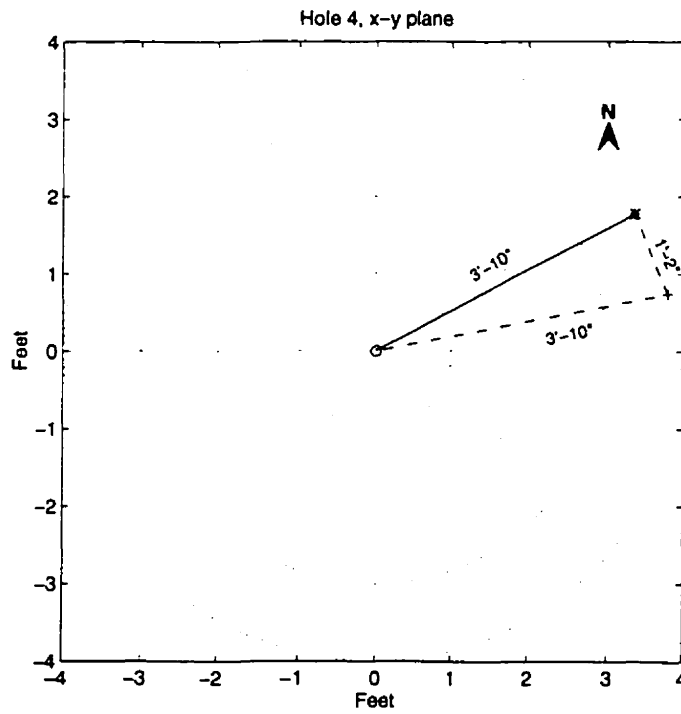


Figure C.8: Deviation occurred in hole no. 4

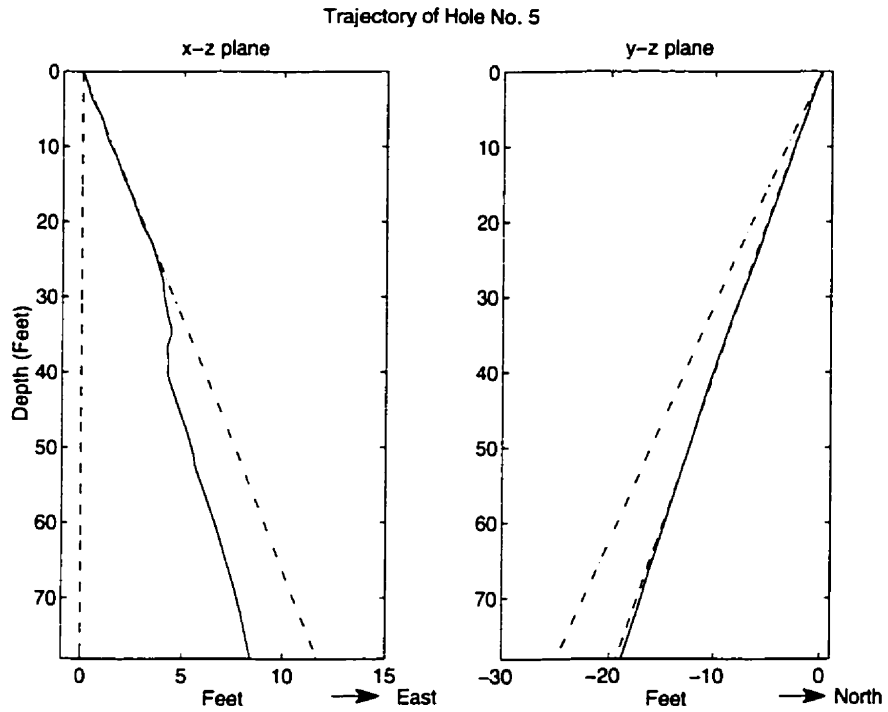


Figure C.9: Trajectory of hole no. 5

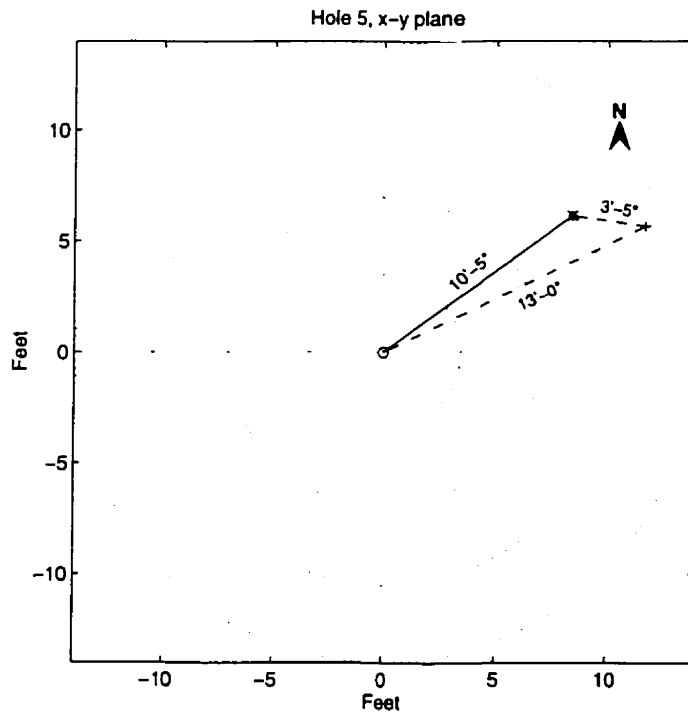


Figure C.10: Deviation occurred in hole no. 5

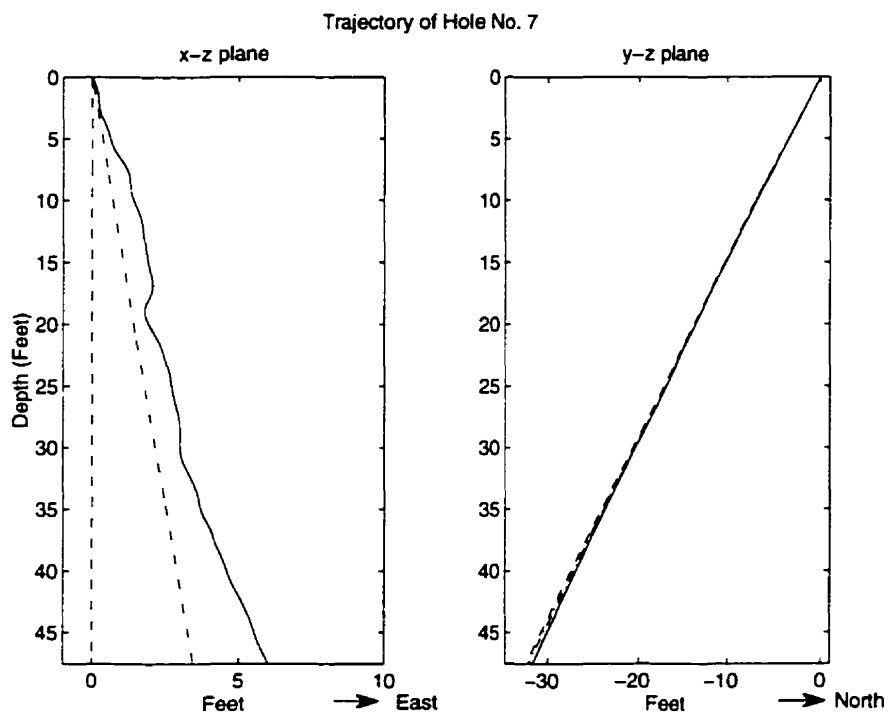


Figure C.11: Trajectory of hole no. 7

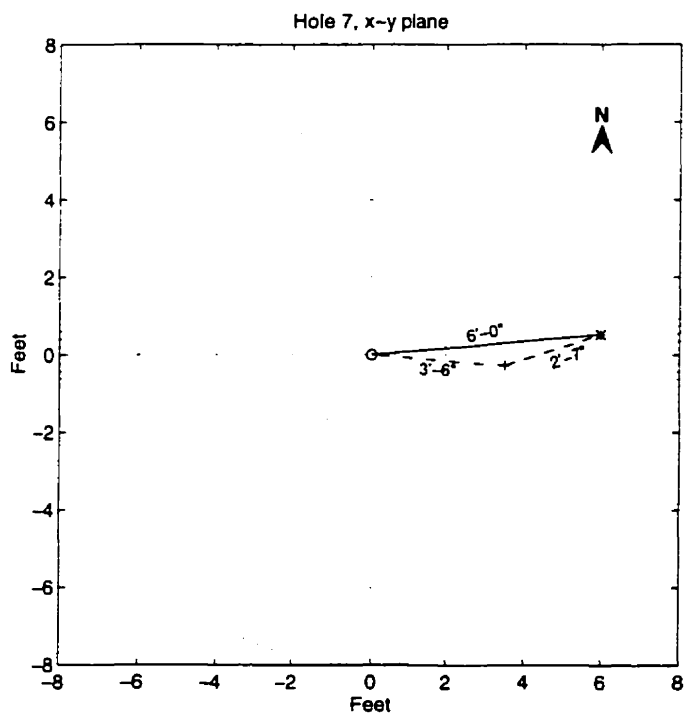


Figure C.12: Deviation occurred in hole no. 7

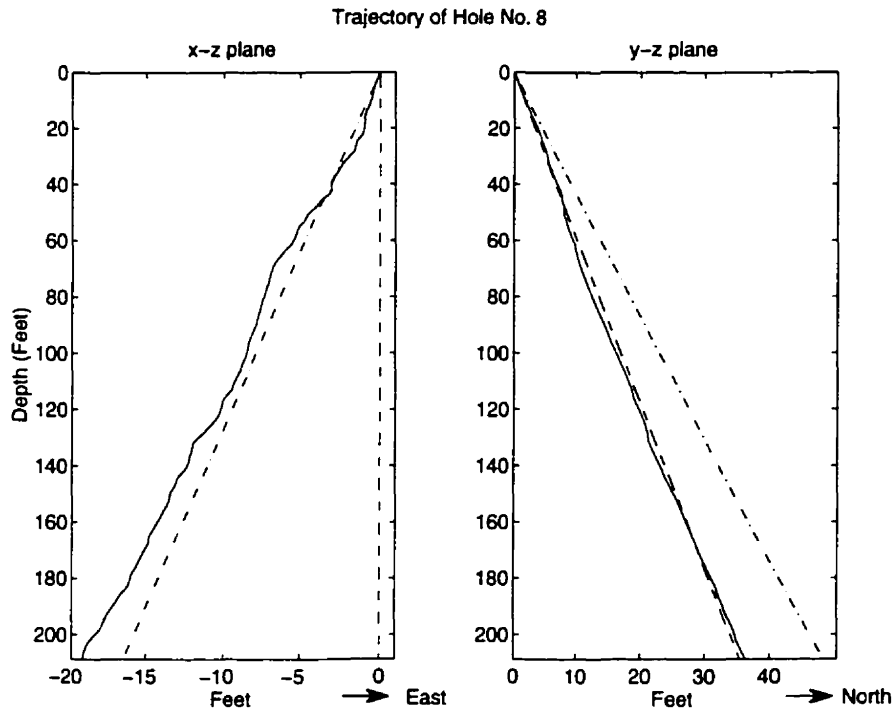


Figure C.13: *Trajectory of hole no. 8*

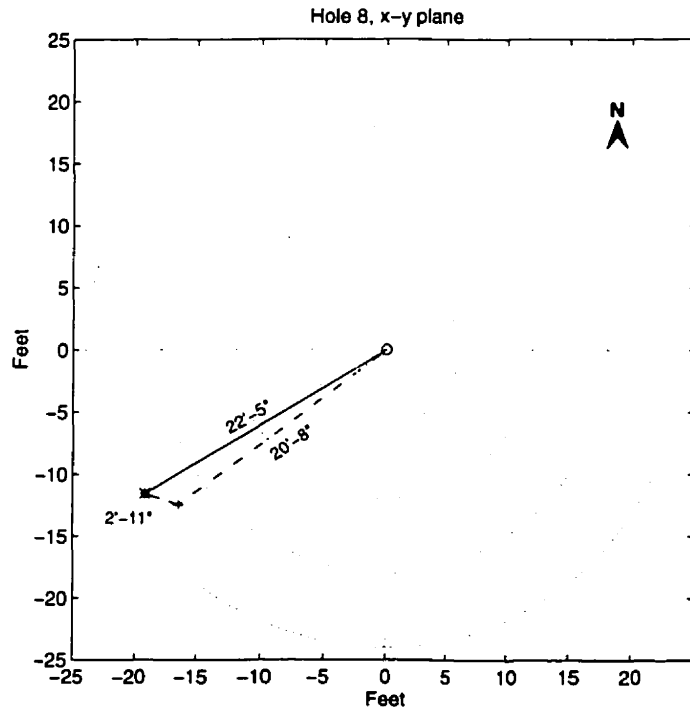


Figure C.14: *Deviation occurred in hole no. 8*

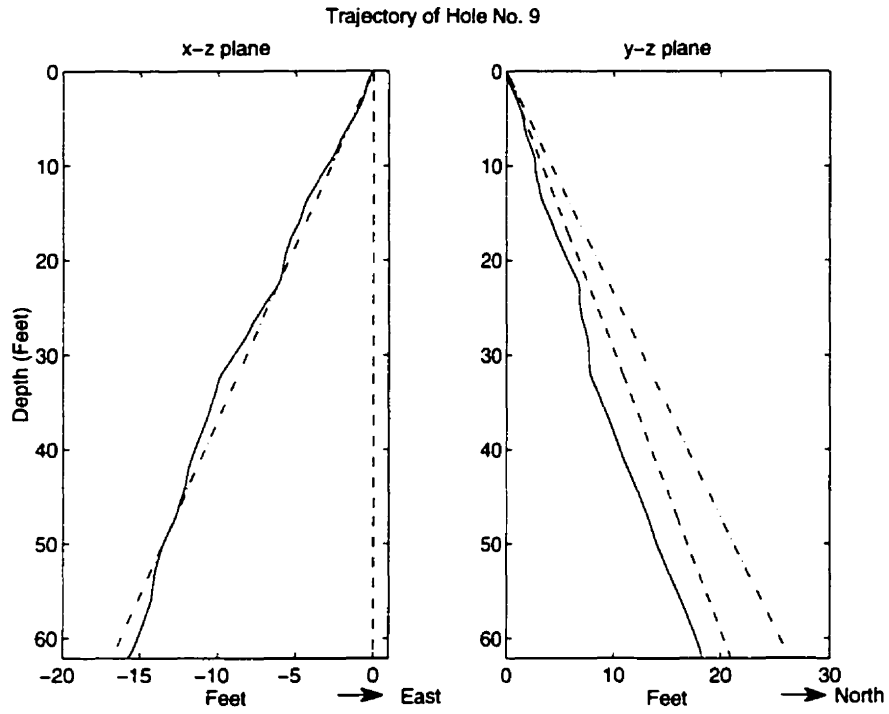


Figure C.15: *Trajectory of hole no. 9*

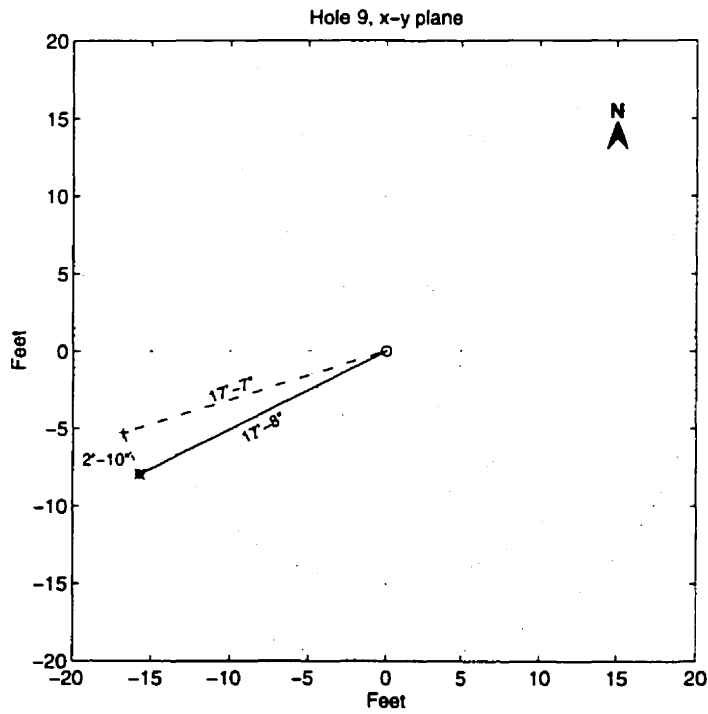


Figure C.16: *Deviation occurred in hole no. 9*

Appendix D

Table of Conversion

In this thesis imperial units were used in data analysis and simulations. There are two reasons for using these units. Firstly all the instrumentations of the percussive drill, CD90B which was used for data acquisition, are calibrated in imperial units. Secondly these are the most commonly used units by INCO technical and research staff and easily understood to the operators. Since SI units have become an international standard in science and technology, a conversion table is provided in this appendix. The table gives SI equivalents of only those quantities which are used in the thesis.

Conversion Table

Quantity	Imperial Units	Equivalent in SI Units
Length	inch	= 2.54 centimeter
	foot	= 0.3048 meter
Area	inch ²	= 6.451×10^{-4} meter ²
Volume	inch ³	= 1.638×10^{-5} meter ³
Mass	pound	= 3.732×10^{-1} kilogram
Force	pound	= 4.448 newton
Velocity	inch/minute	= 2.540×10^{-2} meter/minute
Acceleration	inch/minute ²	= 7.056×10^{-6} meter/second ²
Pressure	pound/inch ²	= 7.031×10^{-2} kilogram/centimeter ²
	pound/inch ²	= 6.895×10^3 newton/meter ²